Title

Genetic Targeting of Small-molecules in Drosophila melanogaster.

Author

Kirk, Molly Jane

Publication Date

2021

Peer reviewed|Thesis/dissertation

Genetic Targeting of Small-molecules in *Drosophila melanogaster*.

By

Molly Jane Kirk

A dissertation submitted in partial satisfaction of the

requirements for the degree of

Doctor of Philosophy

in
Molecular and Cellular Biology

in the

Graduate Division

of the

University of California Berkeley

Committee in charge:

Professor Evan W. Miller, Chair
Professor Kristin Scott
Professor Christopher J. Chang
Professor Marla Feller

Fall 2021

Genetic Targeting of Small-molecules in *Drosophila melanogaster*.

By Molly Jane Kirk

Abstract

Genetic Targeting of Small-molecules in *Drosophila melanogaster*.

By

Molly Jane Kirk

Doctor of Philosophy in Molecular and Cellular Biology
University of California, Berkeley
Professor Evan W.
Miller, Chair

Small-molecule synthetic tools are immensely useful in biological experimentation. However, these small molecules are not inherently targeted to genetically defined cell populations, thus hindering their use in complex living tissues. In my dissertation work, I adapted and developed two novel genetic constructs that traffic small molecule tethering proteins HaloTag[1] and $SNAP_f$ [2] to the extracellular surface in cell lines and *Drosophila* brain tissue. I then applied these novel targeting systems toward two distinct applications: functional voltage imaging in live *Drosophila* brains using synthetic voltage-sensitive dyes and registration of live-fly brains to standard anatomical templates for comparison with existing databases.

Voltage imaging in intact brains offers the tantalizing promise of watching, in real-time, the electrical changes that underlie physiology. To enable voltage imaging in *Drosophila melanogaster*, we combined a chemically synthesized rhodamine voltage reporter (RhoVR) with a genetically encoded, self-labeling enzyme, HaloTag. We generated a *Drosophila* reporter line that expressed the HaloTag enzyme on the extracellular surface. We validated the voltage sensitivity of this approach in cell culture before driving expression of HaloTag in specific neurons in flies. We showed that selective labeling of synapses, cells, and brain regions can be achieved with RhoVR-Halo in larval neuromuscular junction (NMJ) and whole adult brains. We validated the voltage sensitivity of RhoVR-Halo in fly tissue via dual-electrode/imaging at the NMJ, showing the efficacy of this approach for measuring synaptic excitatory post-synaptic potentials (EPSPs) in muscle cells, and performed voltage imaging of carbachol-evoked depolarizations and osmolarity-evoked hyperpolarizations in projection neurons and in interoceptive suboesophageal zone neurons in fly brain explants following *in vivo* labeling. The turn-on response to depolarizations, fast response kinetics, and two-photon compatibility of chemical indicators, coupled with the cellular and synaptic specificity of genetically-encoded enzymes will make RhoVR-Halo a powerful complement to neurobiological imaging in *Drosophila*.

The *Drosophila* neurobiology community has developed a multitude of open-source neuron anatomy databases for comparative analysis of anatomy across samples. Unfortunately, fixation and permeabilization of the sample are often required which precludes their use in live tissue. Our novel extracellularly targeted tethering platforms comprised of $SNAP_f$ and HaloTag fusion proteins allowed for multispectral, *in vivo*

anatomical analysis at the single-cell and whole-brain levels. We labeled the neuronal expression patterns of various Gal4 driver lines in live *Drosophila* brains recapitulating histological staining. Expressing $SNAP_f$ pan-neuronally, we registered brains to an existing anatomical template. From directly registered live brain tissue, we performed bridging registrations and a neuronal morphology similarity search (NBLAST)[4]. We predict that these extracellular platforms will become a valuable complement to existing anatomical methods and prove useful for future genetic targeting of other small molecule probes, drugs, and actuators.

Dedicated to Gregory Bithell
a loving uncle who is dearly missed

157
Table of Contents

Acknowledgments:

There are so many people I would like to thank for their support and guidance throughout my graduate work. First and foremost, I would like to thank my fiancée Mahyar who has been with me and by my side through some of the hardest portions of this Ph.D. process. He was there for the excitements and the lowest of the lows (which were often quite confusing, as he will tell you). I am so grateful to have a partner like him who always reminds me that there is more to life than just what I see in front of me and brightness and optimism all around us. His optimism and willingness to listen often kept me going through the rough patches of my Ph.D. I will always be glad to come home to find him singing to the cats or hatching some new trail run/ski trip/backpacking or climbing adventure for us to go on that weekend!

Secondly, I would like to thank my two advisors Evan Miller and Kristin Scott. First off, Evan is an amazing scientist and mentor. When I joined the lab, I threw us both in the deep end, asking him to mentor a project in a model organism neither of us had ever worked with and in a field that was not his primary training. Still, Evan rose to the occasion, becoming an expert in *Drosophila* neurobiology right alongside me, exploring a completely new world. I cannot thank him enough for giving me the freedom to try out my wacky ideas and the guidance to make sure they worked out. I am also very grateful to have had the opportunity to work with Kristin. She is not only an amazing person and scientist but is truly a wonderful example of how to be a kick-ass woman in science! I am grateful for all her support and clear, kind, and honest guidance over my tenure I to thank Brittany, Vince, Nels, Xinxi, Maggie, Ellie, Salil, Steven, and all the other members of both my labs. They have been amazing, supportive, and just plain good fun to work with since day one.

Finally, I would like to thank my friends and family, but as my mother always said, “family first! I am so grateful for the support of my parents, especially my mom, throughout this process. As a teenager, I got to watch my mom do a Ph.D. in Biogeochemistry while running a business and raising two kids. Having done a Ph.D. now, I can honestly say that my mother is the strongest person I know. She set an amazing example of how to be a scientist while simultaneously balancing all of life’s other joys. Both she and my father were available for the after-work phone calls, the dilemmas. They were supportive of me throughout my entire graduate work. I cannot thank them enough for telling me to keep going and telling me to take a break occasionally. I would also like to thank my sister, who just graduated with her doctorate as a Family Nurse Practitioner; it has been amazing to have a buddy to do this with! As for friends, I would like to thank my dear friends Meg Baker and Kent Davis, whose spiritual guidance and personal guidance have shown me how to live a life I could have never dreamed of. Ultimately thank you to everyone who helped me get to this point in my life; I am forever grateful for you and your support.

Chapter 1: Voltage-imaging in *Drosophila melanogaster:* bridging the gap between tool development and functional application

Abstract:

Changes in transmembrane potential are a key signaling mechanism for the brain. To interpret these electrical phenomena and understand in a fundamental way how they drive behavior, we turn to vertebrate and invertebrate model organisms. The Fruit Fly, *Drosophila melanogaster,* has been uniquely valuable due to its small nervous system, genetic tractability, and complex behavioral patterns. To measure these electrical phenomena, it would be ideal to directly monitor these electrical events across large populations of neurons within the awake, behaving fly. This has only recently become possible with the development of voltage imaging platforms that allow for action potential and subthreshold event detection in *Drosophila melanogaster*. Although many different voltage imaging platforms have been developed, few have been applied in *Drosophila*, and the *Drosophila* community has utilized even fewer of these applications to any great extent. This review of voltage imaging techniques and applications is targeted explicitly to *Drosophila* researchers and serves to bridge the gap between tool development and functional application of voltage indicators in *Drosophila.*

Introduction:

Electrical activity is a critical signal in the brain. The simultaneous monitoring of neuronal electrical activity and animal behavior allows us to derive neural circuit encoding principles crucial to understanding brain function. To derive these principles, we turn to invertebrate and vertebrate model organisms. Here, *Drosophila melanogaster,* a common invertebrate model organism, has made significant contributions. Due to its unique repertoire of complex behavioral phenotypes, relatively small nervous system, and available genetic tools for circuit dissection, *Drosophila* offers a robust platform for linking neuronal activity to behavior outcomes[1]. However, to establish this link, we must accurately monitor electrical activity in the brain. Here we present an overview of current activity reporting techniques in *Drosophila melanogaster* and a review of voltage-imaging techniques and specific applications in the fly.

One technique for reporting neuronal activity is electrophysiology[2]. Here a glass electrode is attached to a neuron and directly accesses the cell interior to monitor and control transmembrane potentials[3] (**Figure 1-1a**). This technique is the gold standard for electrical reporting as it gives the most direct measurement of transmembrane potential. It shows the best temporal resolution of any available method for recording activity. However, electrophysiology is invasive, limited to measuring transmembrane potentials at the soma and extremely difficult to perform. This difficulty decreases the throughput and spatial resolution as only a few cells can be recorded at one time[4]. It almost entirely precludes the recording of activity across multicell circuits in the brain. In *Drosophila,* it is particularly challenging as the neurons of this animal are extremely small and surrounded by a difficult to penetrate glial sheath, which significantly impacts the throughput and sometimes feasibility of electrophysiology in *Drosophila*[5].

Due to this difficulty, optical probes of neuronal activity such as calcium indicators (**Figure 1-1b**) have become a widely accepted method for monitoring neuronal activity. GCaMPs[6–

[12], the most prominent indicators of this class, use a calcium chelating protein calmodulin kinase coupled to a circularly permutated GFP molecule to sense calcium influx into the cell. This calcium influx is highly correlated to neuronal activity [8,10,13–15] and can even be used to determine the number of low-frequency action potential events in a specific neuron[16]. The advent of calcium imaging revolutionized the *Drosophila* field allowing for genetically specific recordings from many neurons simultaneously[17]. Their application covers the breadth of *Drosophila* neurobiology ranging from whole-brain calcium imaging of pan-neuronal activity[18] to single synapse recording in the neuromuscular junction[12]. These methods have been previously reviewed in detail. [17] Although these tools have significantly impacted the field, there are some drawbacks. Namely, these indicators lack temporal resolution as they report a secondary response to neuronal activity that occurs an order of magnitude slower than action potentials themselves[19,20]. They are also hindered by the fact that calcium recording does not directly measure transmembrane potential. Though these two signals are highly correlated[8,13–15] the intracellular calcium concentrations could be affected by calcium release from internal stores or other non-activity related calcium signaling events[21].

Another optical method to monitor neuronal activity in vivo is voltage imaging[22,23](**Figure 1-1c**). Here the voltage is directly detected by a voltage-sensitive protein or synthetic molecule, which ultimately translates the transmembrane potential into fluorescence changes in a fluorophore. An ideal voltage imaging probe marries the spatial resolution and high-throughput nature of an imaging technique with direct, sub-millisecond visualization of transmembrane potentials. This technique surmounts the limitations of electrophysiology and even permits the imaging of voltage changes in neuronal processes, which is not possible using electrophysiology alone. Many voltage sensors have been created over several decades of probe development[23–25], yet very few are optimized for application in *Drosophila*. The *Drosophila* community has utilized even fewer of these applications to any great extent. For this reason, we sought to produce a review of voltage imaging techniques and applications targeted explicitly to *Drosophila* researchers.

History of voltage sensors

Invertebrates have been at the heart of voltage sensor development, with many probes being explored using the squid giant axon[26]. The first voltage sensors were voltage-sensitive dyes, purely synthetic molecules whose properties allow them to report transmembrane potential via shifts in their optical properties. Fast voltage-sensitive dyes or electrochromic voltage-sensitive dyes directly interact with the electrical field shifting their excitation and emission spectra based on the polarization of the membrane. This direct interaction with the transmembrane field produces submillisecond changes in fluorescence intensity but suffers from low fractional changes in fluorescence (~10% per 100 mV, on average). The second class of voltage-sensitive dyes rely on the voltage-dependent, slow diffusion of a molecule through the plasma membrane.

These probes can produce much larger fractional changes in fluorescence ~80% per 100 mV. However, these probes exhibit high levels of capacitive loading, which can

dramatically affect cell physiology[25,27]. A thorough review of the voltage-sensitive dye class is out of the scope of this chapter but can be found in (Loew, 2015)[25].

Due to the high capacitive load of slow voltage-sensitive dyes, many of the pioneering insect studies relied on fast electrochromic voltage-sensitive dyes. Here, RH795 [28–30] and RH414[31,32] (**Table 1-1)** voltage-sensitive dyes were used to explore neuronal activity in the antennal lobe of both honeybees and hawkmoths. Exclusively performed in the antennal lobe, these experiments monitored a high level of activity resulting from the many incident axons and dendrites within the glomerular fields of the antennal lobe[33]. Even with this averaging of large activity changes, the probe produced minimal changes in fluorescence intensity (0.4% F/F), requiring multi-trial averaging to identify[30](**Table 1-2).** Another issue these studies had was voltage-sensitive dyes indiscriminately label all membranes and lack targeting to any genetically defined populations. This pan-neuronal labeling significantly diminishes their signal-to-noise in complex tissues and makes it difficult to genetically identify responding neurons in vivo [34] Due to these difficulties in targeting, genetically encoded protein-based voltage sensors became a major aim of the voltage imaging community.

Voltage-sensitive domain fluorescent protein (VSD-FP) based probes

ArcLight:

The first of Voltage-sensitive domain fluorescent protein (VSD-FP) indicators to be expressed in *Drosophila* was ArcLight (**Figure 1-2a**), which employs a super ecliptic pHluorin attached to the VSD from *Ciona intestinalis*. This probe shows -35% F/F per 100 mV in HEK293T cells and has relatively slow two-component kinetics (10 ms -fast and 50 ms -slow). ArcLight was the first genetically encoded probe to resolve single action potentials and subthreshold events in cultured mammalian cells[35],and as a result, its in vitro characterization is a benchmark for other probes[36,37]. The original characterization of ArcLight in *Drosophila* was performed by Cao et al., 2013. Here, ArcLight was expressed in genetically defined populations of both olfactory sensory neurons and olfactory projection neurons, revealing odor-evoked depolarizations and hyperpolarizations. ArcLight reported neuronal activity with an order of magnitude larger fluorescence intensity changes than voltage-sensitive dyes (-4% F/F). When expressed in lateral ventral circadian clock neurons while performing simultaneous patch-clamp electrophysiology, ArcLight revealed single-trial recordings of action potentials and subthreshold events[38].

ArcLight has become a staple of voltage imaging in *Drosophila*. It has been used to monitor hyperpolarizations[39–41] depolarizations [42–50], dendritic activity[36,51,52], and even whole-brain voltage imaging[53]. Its application has spanned many experimental systems, from larval to adult flies. Although ArcLight is a powerful tool, there is still much room for improvement. First, the kinetics of this probe is still an order of magnitude too slow to resolve high-frequency neuronal activity, which occurs on the order of 1-2 ms per action potential[54]. Following Nyquist sampling theory, the temporal resolution required to detect action potentials accurately is on the order of 0.25 to 0.5 ms. Second, the negative-going

nature, or the decreased fluorescence intensity in response to depolarization, of this probe may make optical monitoring of depolarizing activity challenging to monitor in high noise recordings[55]. On the other hand, this facilitates detection of hyperpolarizations, which can be an asset. Ultimately, Arclight is a robust probe for detecting neuronal activity, but suffers from slow kinetics.

ASAPs

ASAP or Accelerated Sensor of Action Potentials (**Figure 1-2b**) adapted the VSD-FP motif using a voltage-sensing domain from *Gallus gallus* and fusing that to a circularly permutated GFP molecule, centering the cpGFP molecule directly in the middle of the voltage-sensitive domain, coupled the movement of the voltage-sensitive S4 domain with the fluorescence of the GFP molecule. The original ASAP1 showed an approximately -20% F/F per 100 mV and relatively fast kinetics compared to ArcLight with on 2.1 ms and off 2.0 ms [56]. Further developing this probe resulted in two variants, one with faster kinetics (ASAP2f)[57] and one with higher sensitivity (ASAP2s)[36]. ASAP2s identified a single point mutation in the S4 domain, which increased the voltage-sensitivity to -38% F/F per 100 mV and slowed the kinetics of the probe to 7.0 ms -on and 16.7 ms -off[36]. ASAP2f showed a slight increase in F/F with (- 25% per 100mV) while maintaining similar kinetics seen in ASAP1 (on was 2.8 and off 2.4 ms)[57]. Finally, ASAP3 was developed through mechanism-based evolution of the original ASAP2s protein, which resulted in a -51 % F/F per 100 mV and had similar yet slightly faster kinetics when compared ASAP2s at temperatures relevant to *Drosophila* research. on 3.7 and off 16.0 ms[58]. Uniquely, these probes show a strong non-linearity at hyperpolarizing potentials meaning that these probes may be ideal for reporting hyperpolarization events in vivo[56]. This series of probes increased the kinetics and sensitivity of genetically encoded voltage sensors resulting in tracking of higher frequency activity invitro.

Only ASAP2s, ASAP2f, and ASAP1 have been characterized in *Drosophila melanogaster*. ASAP3 did not improve voltage signal reporting in *Drosophila* and thus was not reported (communication with Francois St. Pierre). These probes were characterized in the *Drosophila* visual system, reporting graded hyperpolarizations and depolarizations in L1 neurons in response to light and dark conditions. Using ASAP2f revealed higher intensity signaling in vivo than ASAP1 and maintained its fast kinetics. Comparing the kinetics and voltage-sensitivity of ASAP2s alongside many other voltage sensors under two-photon excitation revealed ASAP2s[36] and ASAP2f[59] were more voltage-sensitive under two-photon excitation than other available probes with a -5% F/F response to a graded depolarizing potential.

Unfortunately, ASAPs have not been used extensively in the *Drosophila* field, potentially due to the lack of action potential resolution in *Drosophila*. However, current characterization data strongly suggests that these probes should report low-frequency action potential activity with high fidelity in *Drosophila,* this has yet to be reported in part due to the difficulty in patching L1 neurons while simultaneously recording in the away behaving fly. A study comparing the voltage-sensitivity of these GEVI systems while simultaneously patch-clamping neurons in vivo would be highly informative concerning

the utility of these probes. The other drawbacks to this methodology are that signal responses are minimal, and the kinetics are too slow to report action potential activity accurately in vivo. Improvement on these characteristics of ASAPs would greatly improve their applications in *Drosophila*.

Rhodopsin-based probes

Rhodopsin-based probes consist of seven transmembrane domain rhodopsin molecules, which traffic to the membrane when expressed in cells. Like the electrochromic voltage-sensitive dyes, these rhodopsin molecules directly sense the transmembrane potential and alter their emission and excitation profiles in response to an electric field[60,61]. This class of sensors is rapid and reports neuronal activity with high signal-to-noise ratios (SNR) in vitro and in vivo.

Purely rhodopsin-based

The first of the rhodopsin-based indicators to be explored in *Drosophila* was Arch (**Figure 1-2c**). Arch is a microbial rhodopsin, which shows large fractional changes in fluorescence, nearly 100% F/F per 100 mV, and rapid submillisecond kinetics (0.5 ms -on and -off). Arch also reports neuronal activity with high fidelity in primary neuronal culture with a 10.6 SNR for spike detection[62]. *Drosophila* motor neurons expressing Arch at the neuromuscular junction revealed action potential waveforms in vivo, while simultaneous loose patch recordings confirmed the activity seen in the Arch signal. Arch showed a 150 %F/F per action potential in vivo and monitored action potential waveform alterations, such as broadening under various conditions in vivo using high temporal resolution confocal point imaging, where a confocal point in the sample is excited and recorded from limiting the frame rate to the pixel dwell time of the system[63].

However, Arch has rarely been used in *Drosophila,* which may be due to some of the probe's weaknesses. First, Arch maintains its hyperpolarizing photocurrent, which may dramatically impact neuronal physiology as it hyperpolarizes the cell by ~10 mV upon rhodopsin activation. This photocurrent is avoidable using a non-conducting Arch D95N mutant which abolishes the photocurrent but decreases the kinetics of the probe to about 40 ms (on)[62]. Second, Arch and all other rhodopsin-based methods are incapable of two-photon excitation due to their unique photocatalytic cycle[61]. Finally, this probe exhibits extremely low fluorescence output due to the very low brightness of the rhodopsin molecule. This low fluorescence intensity requires high-intensity light power, which can be phototoxic and create local heat, impacting physiology[64].

Protein-based electrochromic FRET molecules

Citing the dimness of Arch, developers sought to increase fluorescence intensity by coupling rhodopsins to a second fluorophore and reporting voltage via FRET[22]. The first probe of this class to be expressed in *Drosophila* was Ace2N-2AA-mNeon (**Figure 1-2d)**, which couples fast, voltage-sensitive rhodopsin Ace to the fluorescence of fluorescent protein mNeonGreen[65] This reporter shows approximately -25 % F/F per 100 mV with

fast kinetics in the submillisecond range (0.42 ± 0.07 ms on and 0.52 ± 0.07 ms off.) Importantly, the addition of mNeonGreen increases quantum yield of the probe decreasing the light intensity required to image single action potential events[64] Unfortunately, the voltage sensitivity of these rhodopsin-based probes decreases significantly in the eFRET sensor class. In the *Drosophila,* Ace2N-2AA-mNeon was expressed in the antennal lobe local and projection neuron populations, revealing fractional changes in fluorescence on the order of -3% F/F per action potential but showed high single-spike detection fidelity. This probe detected natural odorant presentation in the dendritic branches of the projection neurons and allows for the visualization of spike propagation across the antennal lobe. Ace2N-2aa-mNeon was further characterized in a foundational study that allowed for long-term imaging of mushroom body neurons expressing Ace2N-2aa-mNeon through a chronic cuticle window[66].

Having resolved the issue of fluorescence intensity, the field turned toward red-shifting these probes to allow for deeper imaging in the brain. Here, site-directed saturating mutagenesis of Ace-mRuby, a red-shifted Ace-2N-mNeon derivative, revealed mutations that increased the sensitivity of Ace-mRuby by 2-fold, they called the resulting probe Varnam. Varnam reports a F/F of -14% per 120 mV while maintaining the submillisecond kinetics of its predecessors[67]. When characterized in *Drosophila*, Varnam was expressed in PPL1- mushroom body neurons. Imaging in their axonal compartment in the mushroom body, Varnam reported single action potential events in vivo. It reported single neuron responses to olfactory stimulation in the mushroom body. Finally, leveraging the red-shifted nature of these probes, Varnam allowed for the simultaneous recording of Ace2N-mNeon and Varnam in the mushroom body circuit. Simultaneously reporting activity from PPL1- and MBON- with correlated neuronal responses to odorant presentation[67]. As this probe is relatively new, it has not been fully explored or adopted into the *Drosophila* community; however, they show great promise in reporting voltage responses in vivo.

Chemi-genetic hybrid probes

Voltron

Another method proposed to enhance the brightness of electrochromic rhodopsins is the FRET coupling of bright, photostable small molecule dyes to voltage-sensitive rhodopsins. Here, an Ace rhodopsin molecule is fused to a covalent small molecule tethering protein HaloTag[68,69] When a reactive dye is applied to the sample, it will form a stable covalent bond with HaloTag and permit FRET-based voltage-sensing at the membrane. Ace2::HaloTag combined with high quantum yield Janelia Fluors [70]results in a voltage sensor termed Voltron (**Figure 1-2e**). Voltron is sensitive (-23 % F/F per 100 mV) and has rapid kinetics (0.88 ± 0.13 ms on 0.80 ± 0.44 ms off). Voltron offers spectral flexibility in that one can rapidly change the spectra of the sensor by switching dye loaded onto the sample. This probe reports action potentials in vitro with fractional changes >-10% F/F. Voltron expressed in the PPL1- mushroom body neurons reported action potential events on the order of -5% F/F from dendritic, axonal, contralateral axonal, and somatic compartments of the cell, reporting high fidelity detection of action potential events as confirmed by simultaneous loose patch electrophysiology.

Rhodopsin-based molecules have the best signal-to-noise ratios and spike detection of any probes used in *Drosophila melanogaster.* They offer spectral flexibility, high sensitivity, and fast kinetics all in one sensor. However, there is one major drawback to these tools; they cannot perform under multiphoton excitation. This drawback is due to the rhodopsin molecule's complex photophysical properties, making it impossible to excite with multiphoton light sources to any great extent[61]. This photophysical issue limits imaging to single-photon excitation, or the first approximately 100 µm of depth in a tissue sample. Although, in *Drosophila,* this issue is often avoidable with careful experimental design, it greatly impacts our ability to image deep structures in the brain. Finally, although these probes greatly improved signal-to-noise ratios the voltage responses are still in the single-digit percentiles which could be improved to increase spike detection.

Photo-induced electron transfer (PeT) voltage-sensitive dyes

PeT voltage-sensitive dyes are the final voltage-sensing mechanism employed in *Drosophila*. They are hypothesized to function via intermolecular electron transfer. At rest, PeT holds a fluorophore in a quenched state, but upon depolarization, the rate of electron transfer is diminished, and the fluorophore becomes bright. This results in an increased fluorescence in response to neuronal activity[24,27]. These probes show relatively high fractional changes in fluorescence ranging from VoltageFluor 2.1.Cl [27](25 %F/F) to RhoVR1[19] (48% F/F per 100mV). These voltage-sensitive dyes[71] can be tethered to genetically defined neuronal populations via the expression of extracellularly trafficked small molecule tethering proteins HaloTag[68] and $SNAP_f$[72]. However, when targeted, these probes lose some of their voltage sensitivity, ranging from 14%-25% F/F per 100 mV[71,73]. The kinetics of these dyes are on the nanosecond time scale, an order of magnitude faster than other genetically encoded probes[74]. Finally, these probes are two-photon sensitive, with RhoVR-Halo showing a 2-fold higher cross-section than GFP at its peak excitation[75].

When applied in *Drosophila,* HaloTag and $SNAP_f$ were fused to a transmembrane domain which readily trafficked the tethering proteins to the extracellular surface. These extracellularly trafficked proteins covalently tethered bath applied voltage-sensitive dyes RhoVR-Halo or mSNAP2. Both RhoVR-Halo (**Figure 1-2f**) and mSNAP2, when tethered to olfactory projection neurons and stimulated with acetylcholine mimic carbachol, revealed large fractional changes in fluorescence (31 %F/F, RhoVR-Halo and ~25 %F/F, mSNAP2). Finally, when applied to neuromuscular junction (NMJ) in *Drosophila* larvae, they maintained their 15% F/F per 100 mV, rapid kinetics, and linear voltage-fluorescence relationship. Finally, RhovR-Halo was also used to monitor single-trial excitatory post-synaptic potentials at the neuromuscular junction, suggesting that RhoVR-Halo may be capable of tracking single action potential events in vivo[75].

Although these probes show great promise with their linear voltage responses and rapid kinetics, there are some drawbacks as currently employed. First, the kinetics of these PeT voltage-sensitive dyes have not been fully exploited in vivo. Thus, their kinetics and voltage sensitivity to single-action potential events have not been reported. Second, these probes are significantly dimmer than other voltage sensors owing to a combination of a) lower intrinsic quantum yield for PeT voltage-sensitive dyes compared to other sensors

and b) lower solubility for the PeT voltage-sensitive indicators which impact their ability to label brain tissue. Finally, the function of these probes under multiphoton excitation in vivo has not been reported in *Drosophila*, suggesting that further exploration should be applied to these sensors in the fly brain.

Considerations for voltage imaging experimentation

Voltage imaging has been a long-standing goal in the neuroscience community yet has remained difficult to implement compared to techniques such as calcium imaging. This is in part due to the complex challenges of acquiring, detecting, and processing voltage imaging data. The following section will directly address the challenges often encountered when using this technique and demonstrate how to resolve them in functional imaging studies.

Probe Selection

As previously shown, voltage sensors each have benefits and drawbacks so selecting an optimal probe for the specific experiment highly important. When selecting a probe, three features should be considered 1) the need for 2-photon excitation, 2) the time course, magnitude, and direction of the expected response, and 3) the optical needs of the experiment. First, the rhodopsin-based probes do not function under multiphoton excitation; as a result, they will not be useful for a functional imaging experiment which requires two-photon illumination. If the experiment does require two-photon, the best options are to use a VSD-FP based probe or genetically tethered PeT voltage-sensitive dye. Second, it is important to consider the expected kinetics, magnitude, and direction of the expected voltage response. Few of the existing voltage sensors have fast enough kinetics to track high-frequency action potentials in vivo; thus, if the experiment requires the recording of action potential frequency, it will be best to use probes that have shown single event detection as well as have submillisecond kinetics. However, if the experiment does not call for single spike detection but rather overall voltage changes, one can often be more flexible on the kinetics of the probe. The magnitude of the voltage response is also of importance because probe must be sensitive enough to detect the voltage change of interest. Also, the direction of the probe should be positive-going in the direction of the voltage response to facilitate activity identification (i.e., for a hyperpolarization, it would be useful to use Arclight or another negative-going probe). Finally, if the experiment calls for a red-shifted voltage sensor, which could occur when the experiment calls for deep imaging or red-shifting to avoid unwanted cross-talk between other probes or actuators. We have generated a flow chart to assist in the selection of a probe (**Figure 1-3**)

Data Acquisition

A critical challenge in applying voltage imaging is obtaining sufficient temporal resolution to detect action potentials while simultaneously collecting enough photons to resolve signals from noise. This balancing act depends strongly on the type of experiments in question, but some overarching principles can be helpful for determining the optimal

sampling rate. Nyquist sampling suggests that to report events within a signal accurately, one must sample at a rate 2.5-fold faster than the fastest event[76]. This would require at least 2 kHz resolution to reliably report action potentials with their characteristic 1-2 ms duration. However, it is often difficult to drive data collection at these high acquisition rates without impacting the signal-to-noise ratio. For this reason, many under-sample their optical recording data to 500 Hz; the increased integration time improves the spike detection by greatly impacting the signal-to-noise ratio (SNR). Although under-sampling is acceptable for spike detection the data shows mild aliasing, which can result in variations in spike height. For this reason, if the aim is to collect data concerning spike amplitude, rise and decay tau, it is advisable to obtain data using Nyquist sampling rates or higher.

Detector Selection

Many current functional imaging techniques rely on laser raster scanning to record from live samples. However, for voltage imaging, raster scanning is often far too slow due to the pixel dwell times and laser timing which greatly diminish temporal resolution. Spinning disk microscopy and swept field microscopy can reach speeds close to those required to obtain voltage transients, however in application, these techniques often result in a significant loss of light, eroding the SNR to the point where reliable spike detection is no longer possible. Recent advancements in microscopy technology have developed mechanisms to overcome the issue of light loss, exciting local volumes at kilo-Hertz frame rates[77,78] however these novel tools have not yet been applied to *Drosophila* preparations. Due to these limitations, the current standard for imaging of voltage transients in *Drosophila* is wide-field epifluorescence. This is often performed using a cooled fast EMCCD or CMOS camera. The use of ultrafast cameras allows for rapid acquisition of data at kHz frequency while permitting the collection of all photons emitted from a sample.

Conclusion:

In summary, we have presented an overview of current studies and applications of voltage imaging in *Drosophila melanogaster.* We compared the kinetics, sensitivities, and functional characterization in vitro and in vivo of available voltage sensing probes for application in *Drosophila*. Furthermore, we have outlined the functional applications of the probes in the field of *Drosophila* neurobiology, showing where each probe has been applied to address neurobiological questions. Finally, we have discussed the process of designing experiments and acquiring data for functional voltage imaging experiments. Ultimately, we hope this review will be helpful to the adoption of these powerful voltage imaging tools into mainstream *Drosophila* neurobiology experimentation pipelines.

Figures.

Figure 1-1.

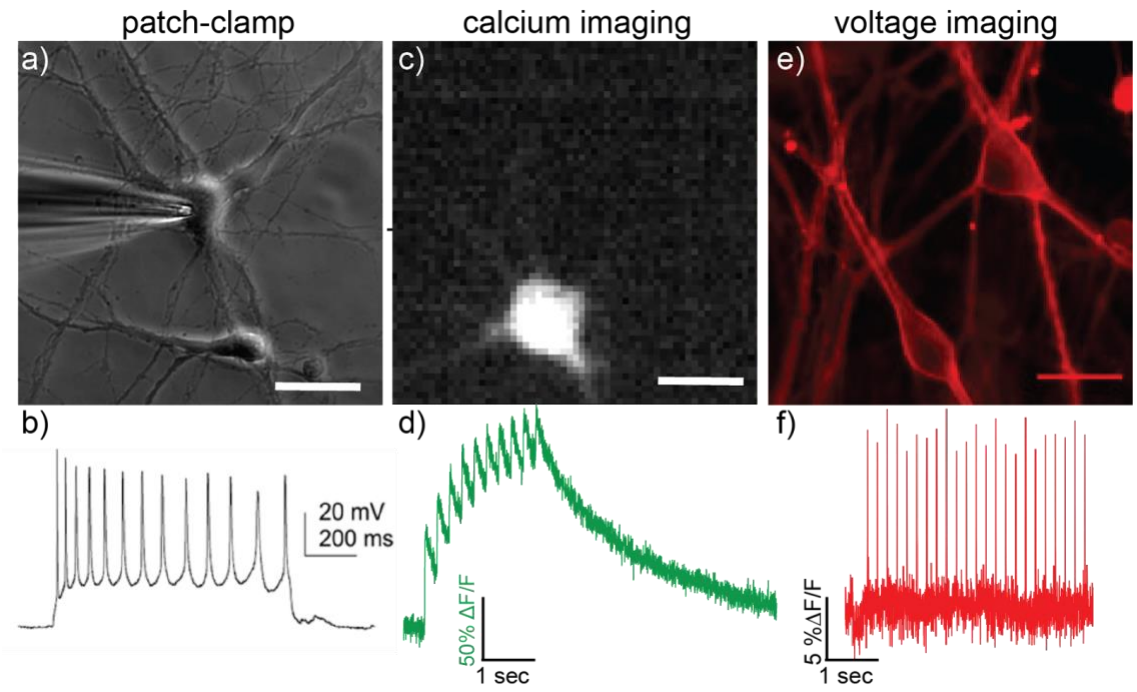

Figure 1-1. Activity monitoring methods for in vivo application. DIC image of HEK Cell undergoing patch-clamp electrophysiology **(a)**. **b)** example trace of neuronal activity as reported by patch-clamp electrophysiology. **c)** epifluorescence microscopy image of a neuron labeled with Oregon Green BAPTA fluorescent calcium sensor with trace of neuronal activity reported in panel **(d)**. **e)** epifluorescence micrograph of neuron labeled with voltage-sensitive dye RhoVR1 and the resulting trace from electrically evoked action potentials in cultured rat hippocampal neurons **(f)**. Scale on all images is 20 µm. Panel a and b are modified from Molleman, 2003 [79] and Bario-Alonso et.al.,2018 [80] respectively. Panel c and d are modified from Gonzalez et.al., 2021[20]

Figure 1-2.

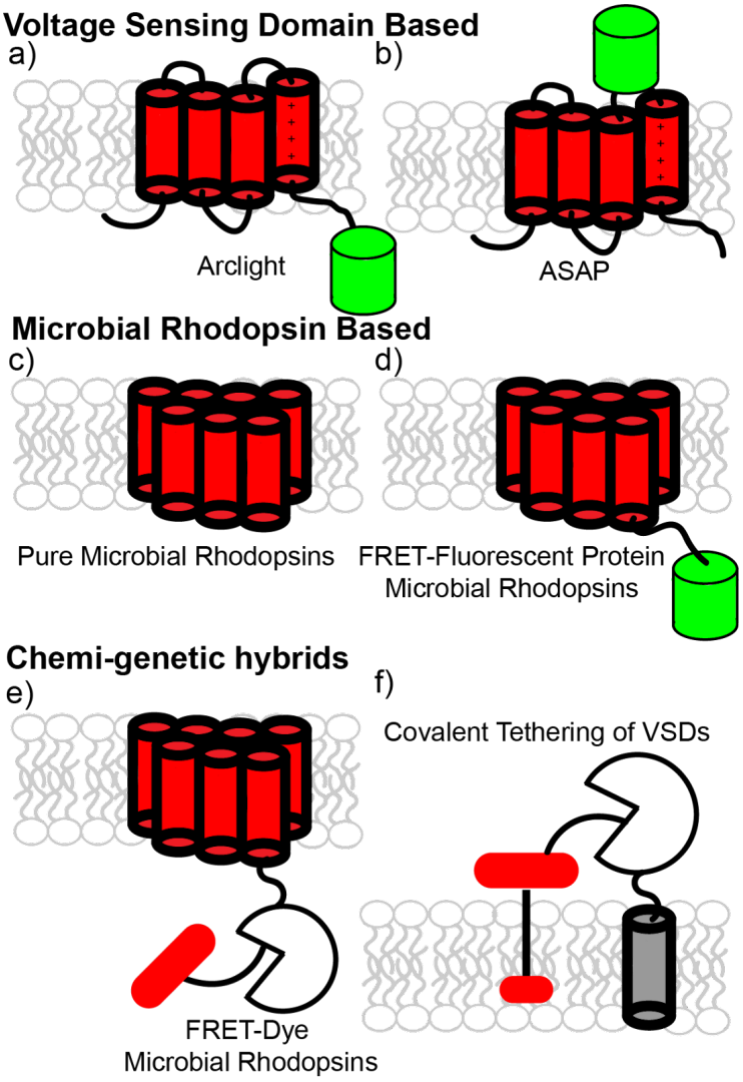

Figure 1-2. Voltage imaging platforms for application in *Drosophila melanogaster*. Voltage-sensitive domain-based probes, Arclight **(a)** and ASAP**(b)** which couple four TM domain-based voltage-sensitive phosphatases to the fluorescence of a GFP based fluorophore. **c)** electrochromic rhodopsin-based voltage sensors which monitor electrical potential via shifts in the emission profile of a voltage-sensitive rhodopsin molecule or electrochromic FRET**(d)** between the rhodopsin molecule and a fluorescent protein. Chemigenetic hybrids which use either voltage-sensitive rhodopsins **(e)** or voltage-sensitive dyes **(f)** to monitor neuronal activity, via a covalent tethering protein HaloTag or $SNAP_f$

Figure 1-3.

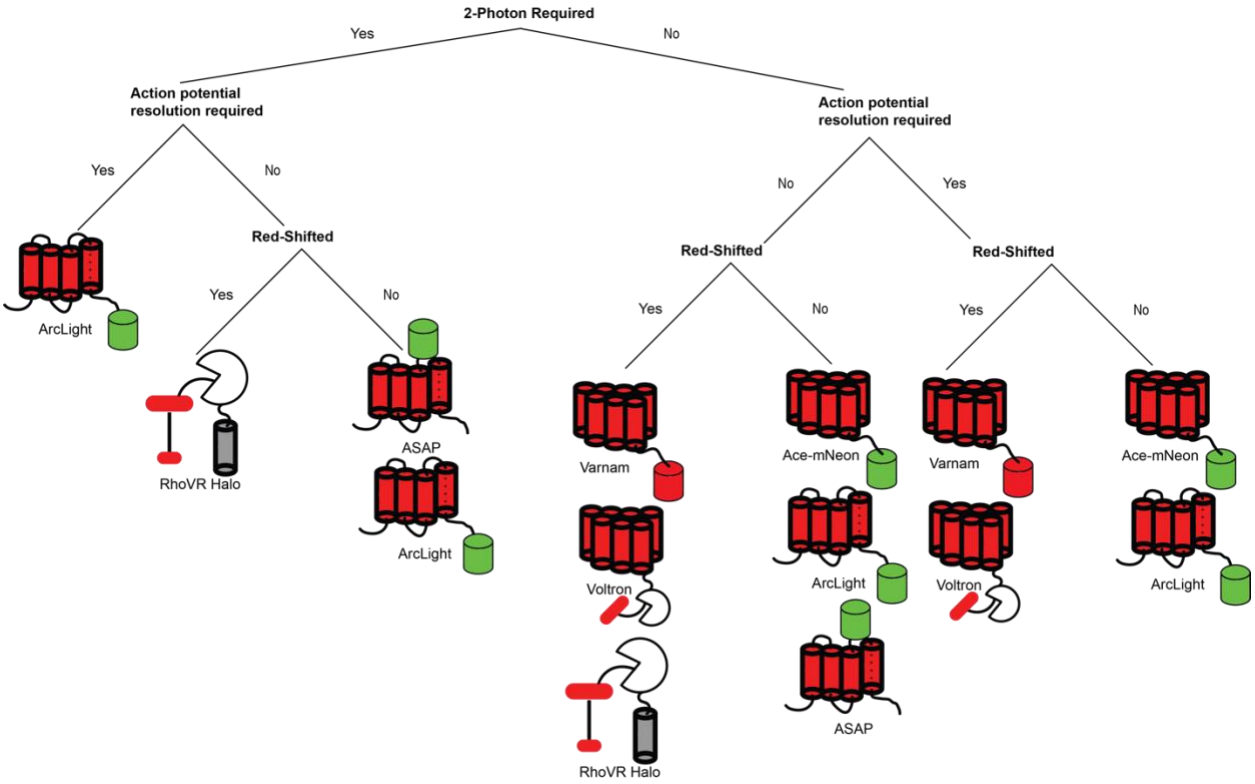

Figure 1-3. Flow chart for probe selection. Chart of two-photon sensitivity, single event detection in *Drosophila* and color spectrum for all available genetically targeted voltage-sensitive probes for in vivo application in *Drosophila*.

Table 1-1: In vitro characterization of voltage sensors

Sensor	% F/F per 100mV	tau fast on (ms)	tau slow on (ms)	% fast	tau fast off (ms)	tau slow off (ms)	% fast	peak emission (nm)
RH795	N/A	pico to femto seconds	N/A	100 %		N/A	100%	686
RH414	N/A	pico to femto seconds	N/A	100 %		N/A	100%	716
ArcLight	-35	28	271	39	104	283	61	509[35]
ASAP1	–23.3 ± 1.1%	2.9 +/- 0.3	161 +/- 33	74 +/- 5	2.3 +/- 0.4	177 +/- 38	63 +/- 6	509[56]
ASAP2s	–38.7 ± 1.1%	5.2 +/- 0.4	63 +/- 11	56 +/- 7	24 +/- 7	106 +/- 47	49 +/- 17	509[36]
ASAP2f	N/A	2.8+/- 0.1	135 ± 16	81 ± 2	2.4 ± 0.2	155 ± 16	71 ± 3	509[57]
ASAP3	-51 ± 1	3.7 ± 0.1	48 ± 4	81 ± 1 79	16.0 ± 0.3 ms	102 ± 2	81 ± 1	509[58]
Arch	100	0.5 ms	N/A	N/A	N/A	N/A	N/A	687[62]
Ace2N-2AA-mNeon	-9	0.42 ± 0.07	3.0 ± 0.9	62 ± 7	0.52 ± 0.07	4.5 ± 0.9	69 ± 7	517[64]
Varnam	-5	0.88 ± 0.13	5.2 ± 0.5	N/A	0.80 ± 0.44	4.7 ± 0.3	N/A	592[67]
Voltron	varies	0.64 ± 0.09	4.1 ± 0.6	61 ± 4	0.78 ±0.12	3.9 ± 0.2	55 ±7	Varies[81]
RhoVR-Halo	15	nanoseconds	N/A	100 %	nanoseconds	N/A	100%	588[19,75]
mSNAP2	21	nanoseconds	N/A	100 %	nanoseconds	N/A	100%	540

Table 1-2: In vivo parameters of voltage sensors in insects

Sensor	single trial event detection	applications in *Drosophila*
RH795	No	Antennal lobe (bulk recording)
RH414	No	Antennal lobe (bulk recording)
ArcLight	Yes	Antennal lobe, clock neurons[38]
ASAP1	No	L1 visual neurons[56]
ASAP2s	No	L1 visual neurons[36]
ASAP2f	No	L2 visual neurons[67]
Arch	Yes	Larval NMJ motor neuron [63]
Ace2N-2AA-mNeon	Yes	Antennal lobe (LN and PN)[83]
Varnam	Yes	PPL1- [82]
Voltron	Yes	PPL1- [69]
RhoVR-Halo	Yes	Larval NMJ, SEZ, Antennal lobe (bulk recording) [75]
mSNAP2	N/A	Antennal lobe (bulk recording) (unpublished)

References

1. Brand, A. H. & Perrimon, N. Targeted gene expression as a means of altering cell fates and generating dominant phenotypes. *Development* **118**, 289–295 (1993).
2. Hamill, O. P., Marty, A., Neher, E., Sakmann, B. & Sigworth, F. J. Improved patch-clamp techniques for high-resolution current recording from cells and cell-free membrane patches. *Pflügers Arch. Eur. J. Physiol.* **391**, 85–100 (1981).
3. Penner, R. A Practical Guide to Patch Clamping. *Single-Channel Rec.* 3–30 (1995). doi:10.1007/978-1-4419-1229-9_1
4. Kodandaramaiah, S. B. *et al.* Multi-neuron intracellular recording in vivo via interacting autopatching robots. *Elife* **7**, 1–19 (2018).
5. Ryglewski, S. & Duch, C. Preparation of Drosophila central neurons for in situ patch clamping. *J. Vis. Exp.* 1–9 (2012). doi:10.3791/4264
6. Nakai, J., Ohkura, M. & Imoto, K. R ES EAR C H AR TIC LES A high signal-to-noise Ca 2 + probe composed of a single green fluorescent protein. **3**, 137–141 (2001).
7. Tallini, Y. M. *et al.* Imaging cellular signals in the heart in vivo: Cardiac expression of the high-signal Ca2+ indicator GCaMP2. *Proc. Natl. Acad. Sci. U. S. A.* **103**, 4753–4758 (2006).
8. Tian, L. *et al.* Imaging neural activity in worms, flies and mice with improved GCaMP calcium indicators. *Nat. Methods* **6**, 875–881 (2009).
9. Akerboom, J. *et al.* Optimization of a GCaMP calcium indicator for neural

activity imaging. *J. Neurosci.* **32**, 13819–13840 (2012).
10. Chen, T. W. *et al.* Ultrasensitive fluorescent proteins for imaging neuronal activity. *Nature* **499**, 295–300 (2013).
11. Dana, H. *et al.* Sensitive red protein calcium indicators for imaging neural activity. *Elife* (2016). doi:10.7554/eLife.12727
12. Dana, H. *et al.* High-performance calcium sensors for imaging activity in neuronal populations and microcompartments. *Nat. Methods* **16**, 649–657 (2019).
13. Wallace, D. J. *et al.* Single-spike detection in vitro and in vivo with a genetic Ca2+sensor. *Nat. Methods* (2008). doi:10.1038/nmeth.1242
14. Kerr, J. N. D., Greenberg, D. & Helmchen, F. Imaging input and output of neocortical networks in vivo. *Proc. Natl. Acad. Sci. U. S. A.* **102**, 14063–14068 (2005).
15. Kwan, A. C. & Dan, Y. Dissection of cortical microcircuits by single-neuron stimulation in vivo. *Curr. Biol.* **22**, 1459–1467 (2012).
16. Kwan, A. C. What can population calcium imaging tell us about neural circuits? *J. Neurophysiol.* **100**, 2977–2980 (2008).
17. Simpson, J. H. & Looger, L. L. Functional imaging and optogenetics in drosophila. *Genetics* **208**, 1291–1309 (2018).
18. Mann, K., Deny, S., Ganguli, S. & Clandinin, T. R. Coupling of activity, metabolism and behaviour across the Drosophila brain. *Nature* **593**, 244–248 (2021).
19. Deal, P. E., Kulkarni, R. U., Al-Abdullatif, S. H. & Miller, E. W. Isomerically Pure Tetramethylrhodamine Voltage Reporters. *J. Am. Chem. Soc.* **138**, 9085–9088 (2016).
20. Gonzalez, M. A. *et al.* Voltage Imaging with a NIR-Absorbing Phosphine Oxide Rhodamine Voltage Reporter. *J. Am. Chem. Soc.* **143**, 2304–2314 (2021).
21. Grienberger, C. & Konnerth, A. Imaging calcium in neurons. *Neuron* (2012). doi:10.1016/j.neuron.2012.02.011
22. Shen, Y., Nasu, Y., Shkolnikov, I., Kim, A. & Campbell, R. E. Engineering genetically encoded fluorescent indicators for imaging of neuronal activity: Progress and prospects. *Neurosci. Res.* **152**, 3–14 (2020).
23. Bando, Y., Grimm, C., Cornejo, V. H. & Yuste, R. Genetic voltage indicators. *BMC Biol.* **17**, 1–12 (2019).
24. Liu, P. & Miller, E. W. Electrophysiology, Unplugged: Imaging Membrane Potential with Fluorescent Indicators. *Acc. Chem. Res.* **53**, 11–19 (2020).
25. Loew, L. M. Design and use of organic voltage sensitive dyes. *Membr. Potential Imaging Nerv. Syst. Hear.* (2015). doi:10.1007/978-3-319-17641-3_2
26. Cohen, L. B. *et al.* Changes in axon fluorescence during activity: Molecular probes of membrane potential. *J. Membr. Biol.* **19**, 1–36 (1974).
27. Miller, E. W. *et al.* Optically monitoring voltage in neurons by photo-induced electron transfer through molecular wires. *Proc. Natl. Acad. Sci.* **109**, 2114 LP – 2119 (2012).
28. Grinvald, A., Lieke, E. E., Frostig, R. D. & Hildesheim, R. Cortical point-spread function and long-range lateral interactions revealed by real-time optical imaging of macaque monkey primary visual cortex. *J. Neurosci.* **14**, 2545–2568 (1994).

29. Galizia, C. G., Joerges, J., Küttner, A., Faber, T. & Menzel, R. A semi-in-vivo preparation for optical recording of the insect brain. *J. Neurosci. Methods* **76**, 61–69 (1997).
30. Galizia, C. G., Küttner, A., Joerges, J. & Menzel, R. Odour representation in honeybee olfactory glomeruli shows slow temporal dynamics: An optical recording study using a voltage-sensitive dye. *J. Insect Physiol.* **46**, 877–886 (2000).
31. Grinvald, A., Hildesheim, R., Farber, I. C. & Anglister, L. Improved fluorescent probes for the measurement of rapid changes in membrane potential. *Biophys. J.* **39**, 301–308 (1982).
32. Okada, K., Kanzaki, R. & Kawachi, K. High-speed voltage-sensitive dye imaging of an in vivo insect brain. *Neurosci. Lett.* **209**, 197–200 (1996).
33. Jefferis, G. S. X. E. Insect Olfaction: A Map of Smell in the Brain. *Curr. Biol.* **15**, R668–R670 (2005).
34. Peterka, D. S., Takahashi, H. & Yuste, R. Imaging Voltage in Neurons. *Neuron* (2011). doi:10.1016/j.neuron.2010.12.010
35. Jin, L. *et al.* Single Action Potentials and Subthreshold Electrical Events Imaged in Neurons with a Fluorescent Protein Voltage Probe. *Neuron* **75**, 779–785 (2012).
36. Chamberland, S. *et al.* Fast two-photon imaging of subcellular voltage dynamics in neuronal tissue with genetically encoded indicators. *eLifewi* **6**, 1–35 (2017).
37. Bando, Y., Sakamoto, M., Kim, S., Ayzenshtat, I. & Yuste, R. Comparative Evaluation of Genetically Encoded Voltage Indicators. *Cell Rep.* **26**, (2019).
38. Cao, G. *et al.* Genetically targeted optical electrophysiology in intact neural circuits. *Cell* **154**, 904–913 (2013).
39. Kallman, B. R., Kim, H. & Scott, K. Excitation and inhibition onto central courtship neurons biases drosophila mate choice. *Elife* **4**, 1–18 (2015).
40. Jourjine, N., Mullaney, B. C., Mann, K. & Scott, K. Coupled Sensing of Hunger and Thirst Signals Balances Sugar and Water Consumption. *Cell* (2016). doi:10.1016/j.cell.2016.06.046
41. Sampson, M. M. *et al. Serotonergic modulation of visual neurons in Drosophila melanogaster*. *PLoS Genetics* **16**, (2020).
42. Haynes, P. R., Christmann, B. L. & Griffith, L. C. A single pair of neurons links sleep to memory consolidation in Drosophila melanogaster. *Elife* **4**, 1–24 (2015).
43. Akin, O., Bajar, B. T., Keles, M. F., Frye, M. A. & Zipursky, S. L. Cell-type-Specific Patterned Stimulus-Independent Neuronal Activity in the Drosophila Visual System during Synapse Formation. *Neuron* **101**, 894-904.e5 (2019).
44. Azevedo, A. W. & Wilson, R. I. in central mechanosensory neurons. **96**, 446–460 (2018).
45. Klein, M. *et al.* Sensory determinants of behavioral dynamics in Drosophila thermotaxis. *Proc. Natl. Acad. Sci. U. S. A.* **112**, E220–E229 (2015).
46. Knecht, Z. A. *et al.* Distinct combinations of variant ionotropic glutamate receptors mediate thermosensation and hygrosensation in drosophila. *Elife* **5**, 1–15 (2016).

47. Knöpfel, T., Tomita, K., Shimazaki, R. & Sakai, R. Optical recordings of membrane potential using genetically targeted voltage-sensitive fluorescent proteins. *Methods* (2003). doi:10.1016/S1046-2023(03)00006-9
48. Kay, A. R. *et al.* Goggatomy: A method for opening small cuticular compartments in arthropods for physiological experiments. *Front. Physiol.* **7**, (2016).
49. Sharma, A. & Hasan, G. Modulation of flight and feeding behaviours requires presynaptic IP3 RS in dopaminergic neurons. *Elife* **9**, 1–25 (2020).
50. Aguilar, J. I. *et al.* Neuronal Depolarization Drives Increased Dopamine Synaptic Vesicle Loading via VGLUT. *Neuron* **95**, 1074-1088.e7 (2017).
51. Kunst, M. *et al.* Calcitonin gene-related peptide neurons mediate sleep-specific circadian output in Drosophila. *Curr. Biol.* **24**, 2652–2664 (2014).
52. Sitaraman, D. *et al.* Propagation of Homeostatic Sleep Signals by Segregated Synaptic Microcircuits of the Drosophila Mushroom Body. *Curr. Biol.* **25**, 2915–2927 (2015).
53. Aimon, S. *et al. Fast near-whole-brain imaging in adult drosophila during responses to stimuli and behavior*. *PLoS Biology* **17**, (2019).
54. NYQUIST, H. Certain Topics in Telegraph Transmission Theory. *Trans. Am. Inst. Electr. Eng.* **47**, 617–644 (1928).
55. Abdelfattah, A. S. *et al.* A general approach to engineer positive-going {eFRET} voltage indicators. *bioRxiv* **14**, 690925 (2019).
56. St-Pierre, F. *et al.* High-fidelity optical reporting of neuronal electrical activity with an ultrafast fluorescent voltage sensor. *Nat. Neurosci.* **17**, 884–889 (2014).
57. Yang, H. H. H. *et al.* Subcellular Imaging of Voltage and Calcium Signals Reveals Neural Processing In Vivo. *Cell* **166**, 245–257 (2016).
58. Villette, V. *et al.* Ultrafast Two-Photon Imaging of a High-Gain Voltage Indicator in Awake Behaving Mice. *Cell* **179**, 1590-1608.e23 (2019).
59. Yang, H. H. H. *et al.* Subcellular Imaging of Voltage and Calcium Signals Reveals Neural Processing In Vivo. *Cell* (2016).
60. Grindley, J. *et al.* Electrical Spiking in Escherichia coli. **333**, 345–349 (2017).
61. Maclaurin, D., Venkatachalam, V., Lee, H. & Cohen, A. E. Mechanism of voltage-sensitive fluorescence in a microbial rhodopsin. *Proc. Natl. Acad. Sci. U. S. A.* **110**, 5939–5944 (2013).
62. Kralj, J. M., Douglass, A. D., Hochbaum, D. R., MacLaurin, D. & Cohen, A. E. Optical recording of action potentials in mammalian neurons using a microbial rhodopsin. *Nat. Methods* **9**, 90–95 (2012).
63. Ford, K. J. & Davis, G. W. Archaerhodopsin voltage imaging: Synaptic calcium and BK channels stabilize action potential repolarization at the Drosophila neuromuscular junction. *J. Neurosci.* **34**, 14517–14525 (2014).
64. Gong, Y. *et al.* High-speed recording of neural spikes in awake mice and flies with a fluorescent voltage sensor. *Science (80-.).* **350**, 1361–1366 (2015).
65. Shaner, N. C. *et al.* A bright monomeric green fluorescent protein derived from Branchiostoma lanceolatum. *Nat. Methods* **10**, 407–409 (2013).
66. Huang, C. *et al.* Long-term optical brain imaging in live adult fruit flies /631/1647/245/2186 /631/1647/328/2236 /631/378/2624 /14/69 /14/35 /14/56

/64/24 article. *Nat. Commun.* **9**, 1–10 (2018).
67. Kannan, M. *et al.* Fast, in vivo voltage imaging using a red fluorescent indicator. *Nat. Methods* **15**, 1108–1116 (2018).
68. Los, G. V. *et al.* HaloTag: A novel protein labeling technology for cell imaging and protein analysis. *ACS Chem. Biol.* **3**, 373–382 (2008).
69. Abdelfattah, A. S. *et al.* Bright and photostable chemigenetic indicators for extended in vivo voltage imaging. *Science (80-.).* **365**, 699–704 (2019).
70. Grimm, J. B., Brown, T. A., English, B. P., Lionnet, T. & Lavis, L. D. Synthesis of Janelia Fluor HaloTag and SNAP-tag ligands and their use in cellular imaging experiments. in *Methods in Molecular Biology* (2017). doi:10.1007/978-1-4939-7265-4_15
71. Deal, P. E. *et al.* Covalently Tethered Rhodamine Voltage Reporters for High Speed Functional Imaging in Brain Tissue. *J. Am. Chem. Soc.* **142**, 614–622 (2020).
72. Sun, X. *et al.* Development of SNAP-tag fluorogenic probes for wash-free fluorescence imaging. *ChemBioChem* **12**, 2217–2226 (2011).
73. Ortiz, G. *et al.* A silicon-rhodamine chemical-genetic hybrid for far red voltage imaging from defined neurons in brain slice. *ChemRxiv* **8**, (2020).
74. Beier, H. T., Roth, C. C., Bixler, J. N., Sedelnikova, A. V & Ibey, B. L. Visualization of Dynamic Sub-microsecond Changes in Membrane Potential. *Biophys. J.* **116**, 120–126 (2019).
75. Kirk, M. J. *et al.* Voltage imaging in Drosophila using a hybrid chemical-genetic rhodamine voltage reporter. (2021).
76. Craven, D., McGinley, B., Kilmartin, L., Glavin, M. & Jones, E. Compressed sensing for bioelectric signals: A review. *IEEE J. Biomed. Heal. Informatics* **19**, 529–540 (2015).
77. Wu, J. *et al.* Kilohertz two-photon fluorescence microscopy imaging of neural activity in vivo. *Nat. Methods* **17**, 287–290 (2020).
78. Villette, V. *et al.* Ultrafast Two-Photon Imaging of a High-Gain Voltage Indicator in Awake Behaving Mice. *Cell* **179**, 1590-1608.e23 (2019).
79. Molleman, A. Patch Clamping: An Introductory Guide to Patch Clamp Electrophysiology. *Wiley* 186 (2003). doi:10.1002/0470856521
80. Barrio-Alonso, E., Hernández-Vivanco, A., Walton, C. C., Perea, G. & Frade, J. M. Cell cycle reentry triggers hyperploidization and synaptic dysfunction followed by delayed cell death in differentiated cortical neurons. *Sci. Rep.* **8**, 1–15 (2018).
81. Abdelfattah, A. S. *et al.* Bright and photostable chemigenetic indicators for extended in vivo voltage imaging. *Science (80-.).* **365**, 699–704 (2019).
82. Yang, H. H. H. *et al.* Subcellular Imaging of Voltage and Calcium Signals Reveals Neural Processing In Vivo. *Cell* (2016). doi:10.1016/j.cell.2016.05.031
83. Gong, Y. *et al.* High-speed recording of neural spikes in awake mice and flies with a fluorescent voltage sensor. *Science (80-.).* **350**, 1361–1366 (2015).

Chapter 2: Voltage imaging in *Drosophila* using a hybrid chemical-genetic rhodamine voltage reporter

Portions of this work have been published in Kirk, et al. *Front Neurosci*, **2021**, *15*, 754027

Portions of this work were completed in collaboration with others: HEK cell patch-clamp electrophysiology was performed by Brittany R. Benlian, in vivo patch-clamp electrophysiology was performed by Yifu Han, Mikhail Drobizhev took the multiphoton spectra and technical support was given by Arya Gold and Ashvin Ravi.

Abstract

We combine a chemically-synthesized, voltage-sensitive fluorophore with a genetically encoded, self-labeling enzyme to enable voltage imaging in *Drosophila melanogaster*. Previously, we showed that a rhodamine voltage reporter (RhoVR) combined with the HaloTag self-labeling enzyme could be used to monitor membrane potential changes from mammalian neurons in culture and brain slice. Here, we apply this hybrid RhoVR-Halo approach *in vivo* to achieve selective neuron labeling in intact fly brains. We generate a *Drosophila* UAS-HaloTag reporter line in which the HaloTag enzyme is expressed on the surface of cells. We validate the voltage sensitivity of this new construct in cell culture before driving expression of HaloTag in specific brain neurons in flies. We show that selective labeling of synapses, cells, and brain regions can be achieved with RhoVR-Halo in either larval neuromuscular junction (NMJ) or in whole adult brains. Finally, we validate the voltage sensitivity of RhoVR-Halo in fly tissue via dual-electrode/imaging at the NMJ, show the efficacy of this approach for measuring synaptic excitatory post-synaptic potentials (EPSPs) in muscle cells, and perform voltage imaging of carbachol-evoked depolarization and osmolarity-evoked hyperpolarization in projection neurons and in interoceptive suboesophageal zone neurons in fly brain explants following *in vivo* labeling. We envision the turn-on response to depolarizations, fast response kinetics, and two-photon compatibility of chemical indicators, coupled with the cellular and synaptic specificity of genetically-encoded enzymes, will make RhoVR-Halo a powerful complement to neurobiological imaging in *Drosophila*.

Introduction

Voltage imaging in intact brains offers the tantalizing promise to watch, in real time, the electrical changes that underlie physiology. Approaches for voltage imaging rely on fluorescent indicators, either chemically synthesized, genetically encoded, or combinations of the two. Chemically-synthesized indicators have a storied past, but suffer from combinations of low sensitivity, slow response kinetics, and the inability to localize to defined neurons. More recently, genetically-encoded indicators of voltage changes circumvent problems of localization to specific neurons. However, genetically encoded indicators also face problems of localization at the cellular membrane, slow response kinetics, low brightness, turn-off or non-linear responses to voltage changes, and incompatibility with two-photon (2P) illumination.

Our group has focused on the development of chemically-synthesized voltage-sensitive fluorophores that respond to changes in membrane potential via a photoinduced electron transfer (PeT) based mechanism. At hyperpolarizing potentials, the voltage across the membrane accelerates PeT from one side of the molecule to the other, short-circuiting, and quenching fluorescence.[1] At depolarized potentials, PeT is slowed, and the quantum yield of the dye increases. This configuration allows fast,[2] linear, turn-on responses to depolarizations (with corresponding fluorescence decreases for hyperpolarization), good signal to noise, and compatibility with 2P excitation.[3-4] However, attempts to deploy voltage-sensitive fluorophores in brain tissues resulted in comprehensive staining of all

neuronal membranes, making it difficult to visualize clear boundaries between cells or regions of the brain.[3, 5] Therefore, there is strong interest in developing hybrid systems in which voltage-sensitive dyes are directed to cells of interest, either via expression of exogenous enzymes[6-8] or via targeting of native ligands.[9] Other strategies involve targeting synthetic fluorophores to genetically-encoded voltage-sensitive proteins, whether opsins[10-11] or voltage-sensing domains.[12]

We recently reported a chemical-genetic hybrid, in which a chemically-synthesized rhodamine-based voltage reporter (RhoVR)[13] attached to a flexible polyethylene glycol (PEG) linker terminating with a chloroalkane forms a covalent bond with a cell-expressed HaloTag (**Figure 2-1**), enabling voltage imaging from defined neurons, in mouse cortical brain slices.[14] This approach, RhoVR-Halo, takes advantage of the fast kinetics, linear turn-on response, and 2P compatibility of RhoVR-type indicators,[3-4] and pairs it with the ability to target specific cells using traditional genetic methods.

The wealth of genetic tools, small brain size for optical imaging, and short generation time make *Drosophila melanogaster* an attractive model organism.[15-17] Genetically encoded indicators have been previously deployed in *Drosophila* and fall into two broad classes: 1) fluorescent protein (FP) fusions with voltage-sensing domains and 2) electrochromic FRET indicators (eFRET) that couple voltage-dependent changes in opsin absorbance with FRET to a fluorescent protein. FP-VSD fusions like ArcLight[18-20] or ASAP,[21-22] have been used in multiple *Drosophila* contexts and show negative-going responses to membrane depolarizations, use “GFP”-like excitation and emission, and display non-linear response kinetics across the entire physiological range. Electrochromic-FRET indicators[23] like Ace2N-mNeon[24] or Varnam[25] (and their chemigenetic relative, Voltron, which replaces the FP with a HaloTag)[10] have also been used in *Drosophila* and provide fast, negative-going responses to depolarizations. These types of indicators are not compatible with 2P excitation, likely owing to the complex photocycle involved in opsin-based voltage sensitivity.[26]

Therefore, to expand the RhoVR-Halo methodology beyond vertebrate systems, we developed a stable transgenic UAS reporter line in *Drosophila* to express HaloTag on the extracellular surface of neurons, enabling the selective staining of defined neuronal populations when crossed with existing GAL4 driver lines. When paired with voltage-sensitive RhoVR-Halo,[14] HaloTag-expressing flies allow cell type-specific labeling *in vivo*, and voltage imaging in a variety of contexts, including synaptic imaging at the neuromuscular junction (NMJ) and across multiple neurons in fly brain explants.

Results

Generation of HaloTag constructs for expression in flies

Although HaloTag and other self-labeling enzymes have been successfully expressed in transgenic flies, the reported lines localize HaloTag intracelluarly.[10, 27-28] Our first task was to generate a HaloTag that expressed on the extracellular face of membranes. Previous

chemical-genetic hybrids deployed in mammalian cells used a transmembrane domain from the platelet-derived growth factor receptor (PDGFR) to localize HaloTag to the cell surface and a secretion signal peptide from immunoglobulin K (IgK) to enhance export of the construct.[14] To adapt HaloTag-directed chemical-genetic hybrids for voltage imaging in *Drosophila*, we selected CD4 as a transmembrane anchor, on account of its good membrane association in *Drosophila* neurons,[29] fusing it to the C-terminus of the HaloTag. We sub-cloned this construct into different vectors for expression in mammalian (pcDNA3.1) and insect cells (pJFRC7).[30]

HaloTag-CD4 shows good expression on cell surfaces. In mammalian cells, CD4 localizes to the cell surface by anti-CD4 immunocytochemistry (**Figure 2-2**). Inclusion of the self-labeling enzyme, HaloTag, affords the opportunity to confirm not only localization, but activity of the expressed enzyme by delivering HaloTag substrates. HEK cells expressing HaloTag-CD4 and treated with RhoVR-Halo (100 nM) show good membrane localization (**Figure 2-3a**), while cells that do not express HaloTag-CD4 show approximately 3.5-fold lower fluorescence levels (**Figure 2-3b-c**). RhoVR-Halo survives fixation: following live-cell imaging, cells can be fixed and retain their RhoVR-Halo staining, which serves as a useful counterstain to the anti-CD4 immunocytochemistry (**Figure 2-2**). Live cells labeled with RhoVR-Halo and subsequently fixed, permeabilized with detergent and assayed for CD4 via immunochemistry reveal the majority of CD4 is found intracellularly, however RhoVR-Halo primarily localizes to cell membranes (**Figure 2-3b**). HEK cells expressing HaloTag-CD4 and labeled with TMR-Halo show approximately 15-fold greater fluorescence than cells that do not express HaloTag-CD4 (**Figure 2-4**).

In S2 cells, an immortalized *Drosophila* cell line, we also observe cell surface localization of HaloTag-CD4, as visualized by anti-CD4 immunocytochemistry (**Figure 2-5**). S2 cells show similar HaloTag-CD4 dependent staining with TMR-Halo (100 nM, **Figure 2-6, Figure 2-5a-b**) with a 20-fold enhancement in fluorescence intensity in HaloTag-CD4 expressing cells compared to non-expressing cells (**Figure 2-6c**). TMR-Halo staining in S2 cells is also retained post-fixation (**Figure 2-5**).

We evaluated the voltage sensitivity of RhoVR-Halo in HaloTag-CD4 expressing HEK293T cells (**Figure 2-7**). After loading cells with RhoVR-Halo (500 nM), cells were subjected to whole-cell, patch-clamp electrophysiology. The voltage sensitivity of RhoVR-Halo in HaloTag-CD4 expressing HEK293T cells is approximately 14% per 100 mV (±2%, SEM n = 7 cells). This is approximately 70% of the value we obtained when HaloTag is targeted with previously developed[14] HaloTag-pDisplay (**Figure 2-8**).

Validation of HaloTag-expressing Flies

To evaluate the performance of cell surface-expressed HaloTag-CD4 in intact flies, we generated transgenic flies (BestGene Inc.) and crossed the resulting UAS-HaloTag-CD4 line with a pan-neuronal driver line, neuronal synaptobrevin-GAL4 (nSyb-GAL4),[31] which was used to drive HaloTag-CD4 expression in all neurons, (**Figure 2-9a**). Brains of nSyb-

GAL4>HaloTag-CD4 flies show strong CD4 expression (**Figure 2-9a-c**). The pattern of anti-CD4 fluorescence indicates good localization to the plasma membrane (**Figure 2-9d-e**).

To evaluate the specificity of labeling, we expressed UAS-HaloTag-CD4 in a subset of neurons. We crossed UAS-HaloTag-CD4 flies with GH146-GAL4 flies[32-33] to drive expression in a subpopulation of olfactory projection neurons (PNs) in the antennal lobe, a key olfactory relay. Immunohistochemistry reveals strong CD4 staining, localized to the antennal lobe in transgenic GH146-GAL4>HaloTag-CD4 flies (**Figure 2-9f-h**). These neurons also showed good extracellular staining (**Figure 2-9i-l**).
HaloTag remains functional when expressed on the cell surface of *Drosophila* neurons, enabling a range of brain regions and neurons to be labeled with small molecules. We delivered TMR-Halo (1 μM) to live flies via application of a solution of TMR-Halo in artificial hemolymph (AHL) to flies with their cuticle removed[34] (see **Methods** for dissection details). We then imaged via confocal microscopy to establish the extent of labeling (**Figure 2-10**). In GH146-GAL4>HaloTag flies (PN labeling) treated with TMR-Halo, we observe strong fluorescence localized to the antennal lobe **(Figure 2-10a**). Non-transgenic fly controls show low fluorescence levels in the brain and antennal lobe (GH146-GAL alone, **Figure 2-10b**). TMR-Halo in combination with HaloTag-CD4 can be used to label single cells. VT011155-GAL4>HaloTag-CD4 fly brains drive expression in single interoceptive suboesophageal zone neurons (ISNs),[19] and treatment with TMR-Halo results in bright fluorescence localized to these neurons (**Figure 2-10c**). Similar staining profiles can be achieved with the voltage-sensitive RhoVR-Halo, which clearly labels PNs of the antennal lobe (**Figure 2-10d**, GH146-GAL4). High magnification examination of labeled projection neurons reveals membrane-localized staining (**Figure 2-10e and g**, red) alongside Hoechst 33342 nuclear staining (**Figure 2-10f and h, blue**). RhoVR-Halo can also label smaller sub-sets of neurons cells; treatment of Nan-GAL4>HaloTag-CD4 brains with RhoVR-Halo results in labeling of ISNs (**Figure 2-10i**).

We used the same live-animal staining procedure to optimize the loading of RhoVR-Halo (**Figure 2-11**). We find that 2 μM RhoVR-Halo provides good staining in the antenna lobes of GH146-GAL4>HaloTag-CD4 crosses (**Figure 2-11**). Fluorescence from RhoVR-Halo is localized to the periphery of cell bodies, again supporting the extracellular expression of HaloTag-CD4 (**Figure 2-10e-h**). Compared to regions of the brain that do not express HaloTag-CD4, RhoVR-Halo fluorescence is approximately 3 times higher (**Figure 2-11b-c**). We find homozygous flies for GH146-GAL4>HaloTag-CD4 have slightly higher fluorescence levels compared to levels of heterozygous flies, when stained with the same concentration of RhoVR-Halo (**Figure 2-11h-j**). However, because the difference in fluorescence intensity in homozygous flies was not significantly larger than heterozygotes, we used heterozygous flies for subsequent experiments.

Functional Imaging

We established the voltage sensitivity of RhoVR-Halo in fly tissue expressing HaloTag-CD4 using two different approaches. First, we performed electrophysiology using dual

two-electrode voltage-clamp combined with fluorescence imaging at the larval *Drosophila* neuromuscular junction (NMJ). We used the motor neuron driver OK6-GAL4 to drive pre-synaptic expression of HaloTag-CD4 (**Figure 2-12a-f**) or the muscle driver G14-GAL4 to express HaloTag-CD4 in the post-synaptic muscle (**Figure 2-12g-l**). In live 3rd instar larval NMJ preparations, RhoVR-Halo (2 μM) clearly stains pre-synaptic neuronal compartments when HaloTag-CD4 expression is targeted in motor neurons (red, **Figure 2-12d**), co-localizing with the neuronal plasma membrane marker horseradish peroxidase (HRP, grey, **Figure 2-12e-f**). In a complementary fashion, when HaloTag-CD4 is expressed in post-synaptic muscle cells, RhoVR-Halo fluorescence (red, **Figure 2-12j**) accumulates at NMJs outside of the neuronal membrane outlined by HRP (grey, **Figure 2-12k-l**). RhoVR-Halo readily detects excitatory post-synaptic potentials (EPSPs) in muscle cells, confirmed by simultaneous optical imaging and sharp electrode recordings (**Figure 2-12m-o**). Importantly, we next used two-electrode voltage-clamp recordings in a semi-dissected larval preparation with muscle HaloTag-CD4 expression (G14-GAL4>HaloTag-CD4, **Figure 2-12p**). This approach demonstrated that depolarizing potentials result in an increase in RhoVR-Halo signal (m6, **Figure 2-12q-s**) with an overall voltage sensitivity of approximately 12% ΔF/F per 100 mV (± 0.2%, n = 8), in reasonably close agreement to the value determined in HEK293T cells (14%, **Figure 2-7**). Analysis of electrode (**Figure 2-12r**) and optical recordings (**Figure 2-12s**) show good correspondence. In contrast, no change in fluorescence signals was observed in an adjacent unclamped/unstimulated muscle cell (m7, **Figure 2-12q**, grey).

As a second confirmation of voltage sensitivity in fly tissues, we developed a stereotyped stimulation protocol for imaging in fly brain explants. We generated flies that express both HaloTag and the voltage-sensitive fluorescent protein, ArcLight, in PNs (GH146 GAL4, HaloTag/CyO; ArcLight/TM2) for use as an internal positive control. The use of RhoVR-Halo, with excitation and emission profiles in the green/orange region of the visible spectrum, allows for the simultaneous deployment of GFP-based indicators,[13-14] like ArcLight.[18] *Drosophila* antennal lobe projection neurons receive input from the olfactory receptor neurons (ORNs) in the antennae.[35] As these projection neurons primarily receive cholinergic input from the ORNs,[36] we hypothesized that PNs could be readily stimulated with carbachol (CCH), a non-hydrolysable acetylcholine mimic. We treated ArcLight/HaloTag-CD4 expressing fly brain explants with carbachol (100 μM) and observed robust fluorescence decreases timed to carbachol treatment, indicating a depolarizing membrane potential response to this neurotransmitter analog (**Figure 2-13a-d**).

Using this robust stimulation protocol in fly brain explants, we next performed two-color voltage imaging with RhoVR-Halo and ArcLight. As before, we loaded RhoVR-Halo (2 μM) in live flies, removed the brains, and imaged the brain explants using epifluorescence microscopy. Excitation provided alternately with blue (475 nm) or green (542 nm) light to excite ArcLight or RhoVR-Halo, respectively, revealed robust fluorescence responses to carbachol (100 μM) treatment (**Figure 2-14**). RhoVR-Halo fluorescence increases with carbachol stimulation (**Figure 2-14a-d**), corresponding to membrane voltage depolarization and the turn-on response of RhoVR-type indicators.[13-14] In contrast, ArcLight fluorescence decreases with carbachol stimulation (**Figure 2-14e**), showing a

fluorescence decrease in response to depolarization, consistent with the turn-off response to depolarization for ArcLight indicators.[18] Importantly, neither RhoVR-Halo nor ArcLight responds to a control experiment that omits carbachol from the perfusion solution (**Figure 2-14c and f**). Finally, the chemical-genetic hybrid approach of RhoVR-Halo enables additional controls to be carried out using the same transgenic flies. When HaloTag/ArcLight expressing flies are treated with TMR-Halo and then stimulated with carbachol, there is no response from the voltage-insensitive TMR-Halo (**Figure 2-14c and g**), but ArcLight still responds (**Figure 2-14g**). Using a "functionally dead" rhodamine dye in this experiment allows for control experiments to be run in the same transgenic animals as the experiments. Similar experiments with inactive mutants of genetically-encoded indicators/actuators (like ArcLight or GCaMP) would require the generation of separate transgenic animals with the inactivating mutation.

To evaluate the ability of RhoVR-Halo to report on physiological stimuli, we probed the response of RhoVR-Halo in ISNs, cells that respond dynamically to changes in osmolarity. Previous studies demonstrated that increases in osmolarity (240 mOsm to 440 mOsm) evoke hyperpolarizing responses in ISNs.[19] Consistent with this, we find that ISNs expressing HaloTag-CD4 (Nanchung-GAL4) and labeled with RhoVR-Halo hyperpolarize upon an increase in osmolarity, as indicated by decreases in RhoVR fluorescence (**Figure 2-15a-c**). In fly brains labeled with voltage-insensitive TMR-Halo, we observe no change in fluorescence (**Figure 2-15a-c**). In contrast, flies expressing ArcLight in ISNs show fluorescence increases in response to increased osmolarity (**Figure 2-16**). Two-color voltage imaging alongside ArcLight in flies that express both HaloTag-CD4 and ArcLight in ISNs (Nanchung-GAL4, UAS-HaloTag-CD4/CyO; UAS-ArcLight/TM2) reveals osmolarity-induced decreases in RhoVR fluorescence coupled with increases in ArcLight fluorescence (**Figure 2-15d-f**), while control experiments at constant osmolarity show no responses in either ArcLight or RhoVR fluorescence (**Figure 2-15g**). Heterozygous flies expressing HaloTag in ISNs and labeled with RhoVR-Halo also respond to changes in osmolarity (**Figure 2-17**). Taken together, these data establish the utility of RhoVR-Halo for monitoring sensory-induced changes to membrane potential.

Discussion

In summary, we show that RhoVR-Halo indicators can be used for direct visualization of membrane potential changes in synapses and brains of flies. We show, for the first time, that RhoVR-Halo dyes can label specific neurons *in vivo* and that voltage changes can be visualized using epifluorescence microscopy at synapses in the NMJ and whole-brain explants. The hybrid chemical-genetic strategy employed here features a turn-on response to membrane depolarization and affords the opportunity to "plug-and-play" different fluorescent dyes to enable imaging in different colors[37] or to run critical control experiments using a non-voltage-sensitive fluorophore in the same genetic background (**Figure 2-14g-i**). We envision that RhoVR-Halos, with their high two-photon (2P) cross-section (93 GM at 840 nm, **Figure 2-18**), can be combined with high-speed 2P imaging methods to provide fast voltage imaging in the brain.

Despite these advances, several drawbacks are associated with this methodology at present. First, in the imaging data presented here, we do not take full advantage of the response kinetics of PeT-based indicators like RhoVR, which should have nanosecond responses times based on the mechanism of voltage sensing.[2, 38-39] Secondly, we do not take full advantage of the high 2P excitation cross-section of RhoVR dyes. Especially notable is the substantial cross-section at ~1030-1040[4] nm (**Figure 2-18**), which allows for the use of high-powered 2P illumination in emerging fast 2P methods.[4, 40] Third, in fly brains, RhoVR-Halo voltage-sensitive indicators are not as bright as their fluorophore-only counterparts. This is likely a result of combinations of a) lower intrinsic quantum yield for RhoVR-Halo compared to TMR-Halo (since the presence of a molecular wire quenches the dyes) and b) lower solubility for the rather greasy RhoVR-Halo indicators compared to the smaller, more compact TMR-Halo dyes. The former can be addressed by using published methods to generate brighter fluorophores. The latter can be addressed by the use of new chemistries to attach HaloTag ligands, freeing up other sites for solubilizing groups. Even with these limitations, we envision that chemical-genetic hybrids like RhoVR-Halo will be an important complement to the expanding set of methods for visualizing membrane potential changes in living systems, especially in contexts where turn-on response to depolarization, fast kinetics, and 2P compatibility are required.

Methods

Plasmid construction.

We included a secretion signal derived from the signal peptide of the *Caenorhabditis elegans* β-integrin PAT-3[41] at the N-terminus of HaloTag, with the 5' UTR from *heat shock protein 70* (*hsp70*) and the 3'UTR and polyA tail from SV40 early genes, as described previously.[29]

For expression in HEK cells, we subcloned HaloTag via restriction digest (NheI, SalI) and subsequent Gibson Assembly into pCDNA3.1 vector containing a cytomegalovirus (CMV) promoter, a 5' PAT3 secretion signal, and a 3' CD4 transmembrane domain. For expression in S2 cells and transgenic generation, the insert Pat3-HaloTag-CD4 was assembled into pJFRC7[30] backbone via restriction digest (CD8::GFP was removed by XhoI and XbaI) and Gibson assembly (Addgene). All constructs were sequence confirmed by the UCB Sequencing Facility. Sequences used for all constructs can be found in the attached electronic construct maps.

Scheme 1-1. Plasmid maps

pcDNA3.1-PAT3-Halo-CD4 (6679 bp)

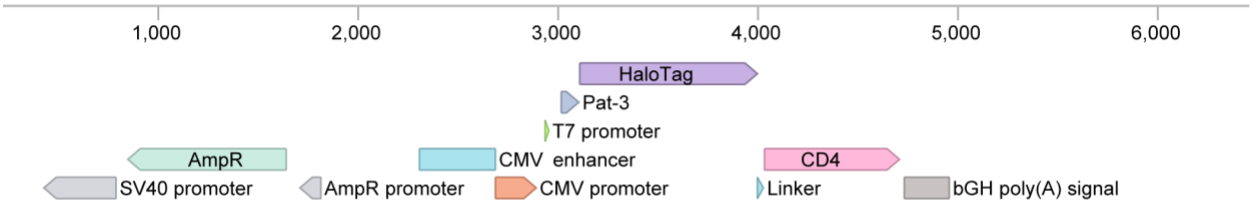

pJFRC7-PAT3-Halo-CD4 (9839 bp)

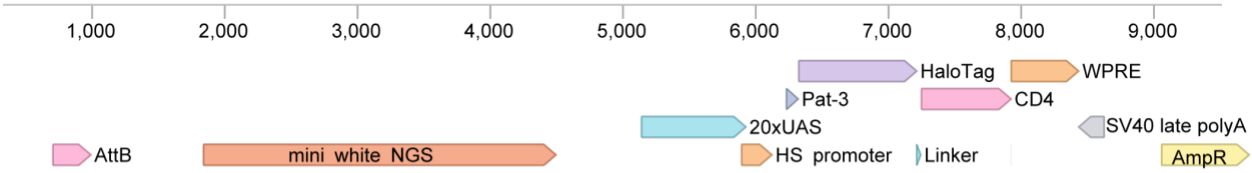

pJFRC19-PAT3-Halo-CD4 (9718 bp)

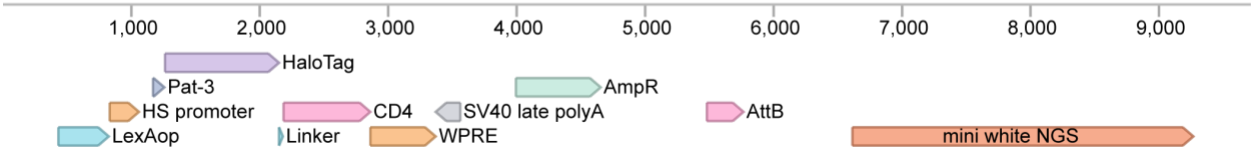

Cell culture and transfection.

We obtained all cell lines from the UCB Cell Culture Facility. Human embryonic kidney 293T (HEK) cells were maintained in Dulbecco's modified eagle medium (DMEM) supplemented with 1 g/L D-glucose, 10% fetal bovine serum (FBS; Thermo Scientific), and 1% GlutaMax (Invitrogen) at 37 °C in a humidified incubator with 5 % CO2. Cells were passaged and plated in DMEM (as above) at a density of 50,000 cells onto 12 mm coverslips pre-treated with Poly-D-lysine (PDL;1mg/ml; Sigma-Aldrich). Transfection of plasmids was carried out using Lipofectamine 3000 (Invitrogen) 12 hours after plating. Imaging was performed 36 hours after plating.

S2 Cells were maintained in Schneider's Drosophila media (Thermo Fisher Scientific) supplemented with 10% FBS at 28°C in a non-humidified incubator under atmospheric conditions. Cells were passaged and plated at 500,000 cells per well in a 24 well plate. Six hours after plating, promotor Tubulin Gal4 pCaSper (Addgene #17747)[42] was cotransfected with pJFRC7 constructs using a modified Lipofectamine 3000 (Life Technologies) protocol. This protocol included a 20-minute preincubation of lipofectamine and DNA in Opti-MEM (Life Technologies) and no p3000 reagent. Forty-eight hours after transfection, S2 cells were transferred onto PDL-treated (1 mg/mL) 12 mm coverslips and allowed to adhere for 30 minutes before dye loading and imaging.

Dye loading.

We maintained DMSO stock solutions (100 µM) of all dyes at -80 °C in single-use aliquots. Aliquots were further diluted to a working concentration of 100 nM in HBSS and incubated on cells for 30 minutes at 37 °C for HEK cells and room temperature for S2 cells. We then replaced all dye-containing HBSS with fresh HBSS and imaged in HBSS at room temperature.

Epifluorescence microscopy.

Imaging was performed on an AxioExaminer Z-1 (Zeiss) equipped with a Spectra-X Light engine LED light (Lumencor), controlled with Slidebook (v6, Intelligent Imaging Innovations). Images were acquired with a W-Plan-Apo 20x/1.0 water objective (20x; Zeiss) and focused onto an OrcaFlash4.0 sCMOS camera (sCMOS; Hamamatsu). The optical setup for imaging with each dye is described below.

Table 1-1. Optical filter sets for epifluorescence microscopy

Dye	Excitation	Emission	Dichroic
HT-RhoVR1	525-560nm	593/40 BP	562 LP
HT-TMR	525-560nm	593/40 BP	562 LP
A488	455-495nm	430/32, 508/14, 586/30, 708/98 BP	432/38, 509/22, 586/40, 654 nm LP
Hoechst 33342	375-400nm	405/40 BP	415 LP

Epifluorescent image analysis.

For fluorescence intensity measurements, regions of interest were drawn around cell bodies, and fluorescence was calculated in ImageJ (FIJI), NIH). We identified transfected cells by setting a threshold that excluded all cells in the non-transfected controls. We calculated the fold change between non-transfected and transfected cells by taking the ratio of transfected cells fluorescence and non-transfected cell fluorescence. For each condition, at least 100 cells were circled across three to five individual coverslips.

Immunocytochemistry.

Immediately following live-cell dye loading experiments, cells were fixed for 20 minutes at room temperature with 4% formaldehyde in PBS. Cells were then washed in PBS (3x 5-minute washes) and treated with either 0.3% Triton X-100 in PBS for the permeabilized condition or PBS for the nonpermeabilized condition. Cells were again washed in PBS and blocked for at least 45 minutes in 0.1% NGS in PBS. Cells were then incubated overnight at 4 °C with 1:500 mouse anti CD4 (OKT4; Thermo Fisher Scientific). We then washed each sample in PBS and stained with a spectrally compatible mouse secondary Goat anti-Mouse A488 (Life Technologies) or Goat anti-Mouse A647 (Life Technologies)

1:1000 in 0.1%NGS for 2hrs at room temperature. We added Hoechst 33342 (10mg/mL -20 stock) 1:1000 for the last 15 minutes of this incubation period. Cells were then washed (3 x 5-minute washes) in PBS and mounted onto glass slides using Fluoromount Mounting Media (VWR International) before imaging.

Transgenic generation.

pJFRC7-Pat3-HaloTag-CD4 were sent to Best Gene Inc. for injection into the following genomic sites via phi-C31 integration.

Table 2-2. Injection phi C31 site and stock line

Construct	Injection Site	Injection Stock
pJFRC7-Pat3-HaloTag-CD4	VIE260B	VDRC#60100

Immunohistochemistry.

Fly brains were dissected in calcium-magnesium free artificial hemolymph (AHL-/-; NaCl 108.0 mM, KCl 5.0 mM, $NaHCO_3$ 4.0 mM, $NaH_2PO_4 \cdot H_2O$ 1.0 mM, Trehalose· 2 H_2O 5.0 mM, Sucrose 10.0 mM, HEPES 5.0 mM and adjusted to pH 7.5 with NaOH) and fixed for 20 minutes in 4% formaldehyde in PBS. Brains were then washed in PBS (3x 5-minute washes) and treated with either 0.3% Triton x -100 in PBS for the permeabilized condition or PBS for the nonpermeabilized condition. Brains were again washed in PBS and blocked for at least 45 minutes in 0.1% NGS in PBS. Cells were incubated overnight in block containing 1:50 RT anti HA (Sigma Aldrich) or 1:100 or 1:200 mouse anti CD4 at 4 °C for 48 hours. Brains were then washed in PBS (3 x 5-minute washes) and stained with Goat anti-Rat A488 (Life Technologies) 1:1000 and Goat anti-Mouse A594 (Life Technologies) in block for 4 hours at room temperature shaking. We added Hoechst 33342 (10 mg/mL) 1:1000 for the last 15 minutes of this incubation. Brains were then washed and mounted onto glass slides using Vectashield mounting media (Vector Laboratories) before imaging using confocal microscopy.

Live-fly brain dye loading with HT-TMR and voltage-sensitive dyes.

Live-fly preparations were performed in the following way: 10-40 day old flies were briefly anesthetized on ice and placed into a small slit on a custom-built plastic mount at the cervix so that the head was isolated from the rest of the body. The head was then immobilized using clear nail polish, which was allowed to set for 15 minutes. The head cuticle was then removed using sharp forceps in calcium-magnesium free Artificial Hemolymph solution (AHL-/-)[43], and the esophagus was cut to eliminate autofluorescence. The AHL was then replaced with calcium-magnesium free AHL containing 0.2% Pluronic F127, and either 2 µM RhoVR-Halo or 1 µM TMR-Halo (for functional imaging experiments, this was lowered to 100 nM TMR-Halo to match fluorescence intensity with RhoVR-Halo), and the glial sheath was punctured manually over the optic lobes to permit dye access. DMSO concentrations were maintained below 3% vol/vol in the dye loading solutions. Following a 15-minute loading period in the dark

at room temperature, the brains were removed and then imaged via confocal or epifluorescent microscopy. When imaged under confocal microscopy, brains were mounted onto glass coverslips with spacers to prevent sample loss and deformation. When imaged under epifluorescent microscopy, brains were adhered to PDL- (Poly-D-Lysine), or PLL- treated (Poly-L-Lysine) coverslips and bathed in AHL.

Confocal Microscopy.

We performed confocal imaging using an LSM710 upright confocal microscope maintained by the Biological Imaging Facility at UC Berkeley. Images were acquired under 543 nm laser illumination focused on the sample using a 20x air objective and collecting 548-685 nm wavelengths using a 54 µm pinhole. Brains were scanned in the z-direction beginning at the top of the brain for 15 planes with 3µm steps. Each image totals the first 45 µm of the brain tissue.

Table 2-3. Optical settings for confocal microscopy

Dye	Excitation	Emission
RhoVR-Halo	543 nm	548-685

Confocal imaging analysis.

Confocal stacks from live prep dye loading of voltage-sensitive dyes were collapsed into a summed z-projections using ImageJ (FIJI). Fluorescence intensity, represented as 8-bit mean pixel values, was measured for the antennal lobe and a region of non-labeled protocerebrum from each brain. The ratio of the AL region's intensity and the nontargeted protocerebrum was then calculated and displayed as fold change above background. No background subtraction was performed in these calculations.

Carbachol ArcLight functional imaging.

GH146-Gal4, HaloTag-CD4/CyO; Arclight/Tm2 brains were removed from the animal in AHL-/- and immediately loaded into a perfusion chamber where they were mounted onto a PDL-coated coverslip. Samples were incubated for 3 minutes at room temperature with constant perfusion of AHL+/+ (NaCl 108.0 mM, KCl 5.0 mM, $NaHCO_3$ 4.0 mM, $NaH_2PO_4 \cdot H_2O$ 1.0 mM, Trehalose 2 H_2O 5.0 mM, Sucrose 10.0 mM, HEPES 5.0 mM, $CaCl_2$ 2 H_2O 2.0 mM, $MgCl_2$ 6 H_2O 8.2 mM, perfused at 5 mL/min) before imaging was performed. Perfusion was maintained throughout the experiment. Imaging was performed on an AxioExaminer Z-1 (Zeiss) equipped with a Spectra-X Light engine LED light (Lumencor), controlled with Slidebook (v6, Intelligent Imaging Innovations). Images were acquired with a W-Plan-Apo 20x/1.0 water objective (20x; Zeiss) and focused onto an OrcaFlash4.0 sCMOS camera (sCMOS; Hamamatsu). The acquisition rate of 1 Hz for each experiment with 2 ms exposure times and light power (35 W/cm^2) were maintained across all experiments independent of acquisition frequency. A baseline was obtained for

one minute, and then brains were stimulated for 30 seconds, followed by a 5-minute recovery period between stimulations.

Dual Color Functional Imaging.

GH146-Gal4, HaloTag-CD4; Arclight/Tm2 flies had their cuticle removed as described in the section above and then loaded with 2 µM RhoVR-Halo or 100nM HT-TMR in the presence of 0.2% Pluronic F127 at room temperature for 15 minutes. Following loading, the brains were immediately removed and placed into a perfusion chamber where they were mounted onto PDL-coated coverslips. Samples were incubated for 3 minutes at room temperature with constant perfusion of AHL+/+ (perfused at 5 mL/min) before imaging was performed. Perfusion was maintained throughout the experiment. Imaging was performed on an AxioExaminer Z-1 (Zeiss) equipped with a Spectra-X Light engine LED light (Lumencor), controlled with Slidebook (v6, Intelligent Imaging Innovations). Images were acquired with a W-Plan-Apo 20x/1.0 water objective (20x; Zeiss) and focused onto an OrcaFlash4.0 sCMOS camera (sCMOS; Hamamatsu). The acquisition rate was 1.7 Hz with 125 ms exposure for RhoVR-Halo and 100ms exposure for Arclight. The light power of 13.1 mW/mm^2 (RhoVR-Halo) and 19.7 mW/mm^2 (Arclight) was maintained across all experiments. A baseline was obtained for one minute and then brains were stimulated in triplicate for 30 seconds followed by a 5-minute recovery period between stimulations.

Functional imaging data analysis.

We extracted fluorescence intensity values over time for the antennal lobe using an in-house MATLAB code, and background-subtracted these values. We then corrected the values for bleaching using an asymmetric least squares fit as described previously[44] and added back the baseline value, which was the average of the first 50 frames. Finally, we used the adjusted traces to calculate the % $\Delta F/F_0$, where F_0 was defined as the average of frames 2 to 50 from each video. These were then subsequently plotted and displayed using Prism Graph Pad as Mean and Standard Error of the Mean.

NMJ Imaging and Electrophysiology.

Third-instar larvae were dissected in ice-cold modified HL3 saline containing (in mM): 70 NaCl, 5 KCl, 10 $MgCl_2$, 10 $NaHCO_3$, 115 mM sucrose, 5 trehalose, and 5 4-(2-hydroxyethyl)-1-piperazineethanesulfonic acid (HEPES) at pH 7.2 as described.[45-46] Guts, trachea, and the ventral nerve cord were removed from the larval body wall. Dissected preparations were then bathed for 15 mins in ice-cold HL3 saline containing 2 µM HT-RhoVR and 0.2% Pluronic F127. The preparation was perfused three times with fresh HL3 saline. For sharp electrode and two-electrode voltage-clamp (TEVC) recordings, electrodes with resistances between 10-35 MΩ were inserted in muscle 6 of segment A2 and A3 in HL3 saline containing 0.4 mM $CaCl_2$. Experiments were conducted using a Zeiss Examiner A1 microscope equipped with a 63x/1.0NA water-dipping objective. Electrophysiological data were acquired using an Axoclamp 900A amplifier,

Digidata 1440A acquisition system, and pClamp 10.5 software (Molecular Devices). To elicit EPSPs, an ISO-Flex stimulus isolator (A.M.P.I.) was used to evoke 10 electrical stimulations at 1 Hz with 0.5 msec duration, using stimulus intensities set to avoid multiple EPSPs. To clamp muscles at multiple voltages, the muscle membrane potential was held at -70 mV using a TEVC configuration and clamped from -100 to 0 mV for 500 msec at 10 mV steps. Electrophysiological signals were digitized at 10 kHz and filtered at 1 kHz. Recordings were rejected with input resistances lower than 5 Ωohm or resting potentials more depolarized than -60 mV. Electrophysiology data were analyzed using Clampfit (Molecular Devices). Average holding data for each voltage was calculated for each muscle. Voltage imaging was performed simultaneously with electrophysiological recordings using a PCO sCMOS 4.2 camera at 67 fps (596 x 596 pixels). Voltage imaging was performed using a high-intensity LED (Thor Labs) at 8 individual NMJs during 120-second imaging sessions from two different larvae. Imaging data with severe muscle movements were rejected. Each ROI was manually selected using the outer edge of terminal Ib boutons observed by baseline RhoVR1 signals with ImageJ.[47-48] Fluorescence intensities were measured as the mean intensity of all pixels in each individual ROI. ΔF for an EPSP event or voltage-clamping was calculated by subtracting the baseline RhoVR1 fluorescence level F from the intensity of the RhoVR1 signal during each EPSP event or voltage-clamped at a particular ROI. Baseline RhoVR1 fluorescence of each ROI was defined as average fluorescence in the initial 50 msec of voltage holding or EPSP baseline. ΔF/F was calculated by normalizing ΔF to baseline signal F. The mean intensity at each voltage step was measured as the mean fluorescence intensity of 200 msec during the middle of each voltage step.

Two-photon cross-section measurements

The general methods and protocols used for two-photon characterization were published before.[49] Here, we briefly describe them, emphasizing specific details that are different from previously presented methods.

Two-photon excitation spectra and cross-sections.

All measurements were done for solutions in DPBS buffer pH 7.4 at concentrations of 10 μM (TMR), 1 μM (RhoVR 1).[50] Our experimental setup for two-photon spectral measurements includes a tunable femtosecond laser InSight DeepSee Dual (Spectra-Physics) coupled with a photon-counting spectrofluorimeter PC1 (ISS).[49] The two-photon fluorescence excitation (2PE) spectra were measured by automatically stepping laser wavelength and recording total fluorescence intensity at each step in the left emission channel of the PC1 spectrofluorimeter. To eliminate scattered laser light, a combination of short pass filters FF01-770/SP and SP01-633RU-25 (Semrock) was used for TMR and RhoVR 1 in the range 700 – 1300 nm. In all cases, the quadratic dependence of fluorescence signal on laser power was observed in these ranges of wavelengths.
The cross-section $_{2,A}$() was measured at 812, 840, and 1064 nm using relative method and well characterized reference standards. Rhodamine 6G in methanol was chosen for measurements at 812 and 840 nm, with $_{2,\mathrm{Rh6G}}$ = 75 and 43 GM, respectively. These

values are the average of two independent measurements[51-52] showing good correlation.[49] The measurement at 1064 nm was performed using Rhodamine B in alkaline ethanol as a reference standard. Its cross-section was published relatively to Rhodamine 6G in ethanol ($_{2,RhB}/_{2,Rh6G}$ = 1.109,[53] 1.000,[54] 1.091,[55] 1.083,[56-57] 1.053,[58] 1.095,[59] with the average $< _{2,RhB}/ _{2,Rh6G}>$ = 1.072 ± 0.017). Using this number together with the Rhodamine 6G cross-section in ethanol ($_{2,Rh6G}$) obtained after averaging of seven independent measurements: $< _{2,Rh6G}>$ = 12.4 ± 2.6 GM (see[11] Table 3), we calculate $_{2,RhB}$ = 13.3 ± 2.8 GM for Rhodamine B in ethanol at 1064 nm and use it as a reference

For the cross-section measurement, we first collected a total (without monochromator) two-photon excited fluorescence signal I as a function of laser power P for both the sample and reference solutions (samples were held in 3x3 mm cuvettes (Starna) with maximum optical density less than 0.1). For SiRho and BERST1, the fluorescence was collected at 90° to excitation laser beam through the FF01-770/SP, FF01-745/SP, and BLP02-561R-25 (Semrock) filters, using the left emission channel of a PC1 spectrofluorimeter working in photon counting mode. The power dependences of fluorescence were fit to a quadratic function $I = aP^2$, from which the coefficients a_S and a_R were obtained for the sample (index S) and reference (index R) solutions, respectively. Second, the one-photon excited fluorescence signals were measured for the same samples and in the same registration conditions. In this case, a strongly attenuated radiation of a Sapphire 561-50 CW CDRH (Coherent) laser at 561 nm was used for excitation. The fluorescence power dependences for the sample and reference were measured and fit to a linear function: $I = bP$, from which the coefficients b_S and b_R were obtained. The two-photon absorption cross-section was then calculated as follows:

Here, $_1$ is the wavelength used for one-photon excitation (561 nm), $_2$ is the wavelength used for two-photon excitation (812, 840, or 1064 nm), $_{R,S}(_1)$ are the corresponding extinction coefficients, measured at $_1$. This approach allows us to automatically correct for the laser beam properties (pulse duration and spatial intensity distribution), fluorescence collection efficiencies for one- and two-photon modes, PMT spectral sensitivity, differences in quantum yields, and concentrations between S and R solutions.

The extinction coefficients at 561 nm were measured by scaling the corrected fluorescence excitation spectra to the corresponding maximum values: 81,000 M^{-1} cm^{-1} for TMR (measured here at 10 µM), 87,000 M^{-1} cm^{-1} for RhoVR1,[13] 139,000 M^{-1} cm^{-1} (measured here at 10 µM), and then taking the signal value at 561 nm. This makes it possible to avoid errors due to the contribution of dimers and aggregates to optical density. Finally, the two-photon excitation spectra were scaled to the calculated $_2$ values with the scaling factor equal to an average scaling factors obtained at different wavelengths where the $_2$ was measured.

Figures.

Figure 2-1.

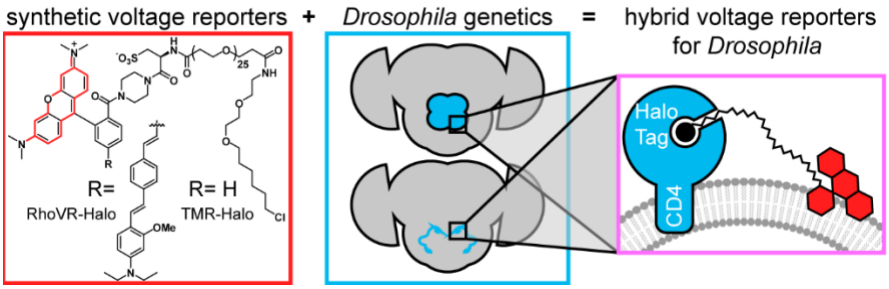

Figure 2-1. Chemical-genetic hybrids for voltage imaging in *Drosophila*. (Red box) Chemically synthesized rhodamines with chloroalkane ligands will form covalent adducts with HaloTag enzymes. When R = the indicated molecular wire, the resulting RhoVR-Halo is voltage-sensitive. When R = H, the tetramethyl rhodamine-Halo is not voltage-sensitive (TMR-Halo). (Teal box) The use of GAL4-UAS fly lines enables selective expression of HaloTag enzymes in defined populations of neurons. (Magenta box) When HaloTag is fused with CD4, expression on the cell surface of defined neurons allows *in vivo* labeling (with either TMR-Halo or RhoVR-Halo) followed by *ex vivo* voltage imaging (with RhoVR-Halo).

Figure 2-2.

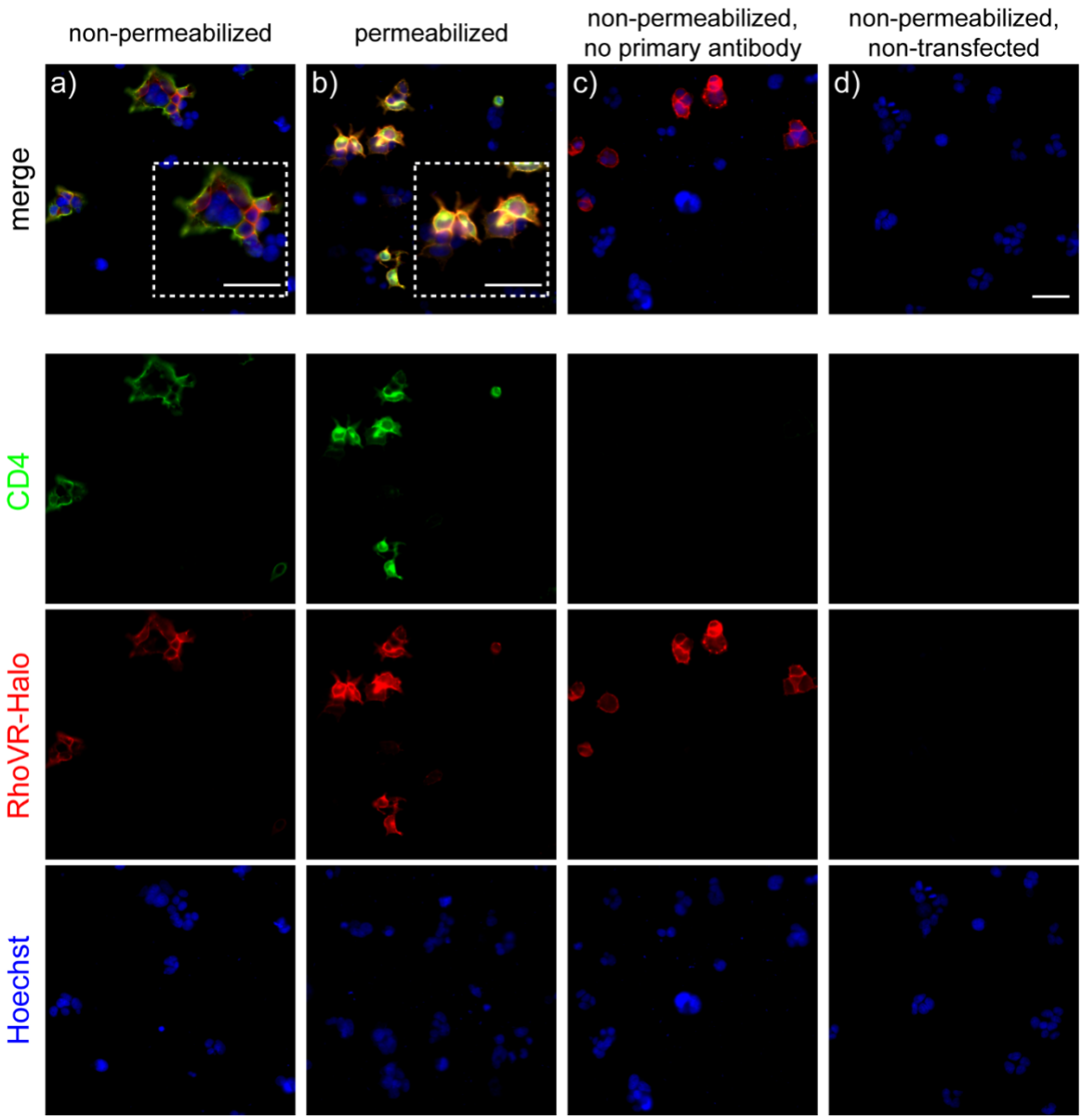

Figure 2-2. Immunocytochemistry of HaloTag-CD4 in HEK293T cells. Widefield epifluorescence images of *post hoc* immunocytochemistry of HEK293T cells expressing HaloTag-CD4, stained with RhoVR-Halo (100 nM) and then treated under **a)** non-permeabilizing conditions (no detergent) or **b)** permeabilizing conditions (0.3% Triton X-100) after fixation. Control cells were treated identically (under non-permeabilizing conditions) and lacked either **c)** primary anti-CD4 antibody or **d)** were not transfected. Green is CD4, red is RhoVR-Halo (100 nM, during live-cell imaging, prior to fixation), and blue is Hoechst 33342 (at a concentration of 10 µg/mL, equivalent to 16 µM). Scale bar is 50 µm. Insets in panels (**a**) and (**b**) show a zoomed-in region of cells in that panel. Scale bar is also 50 µm.

Figure 2-3.

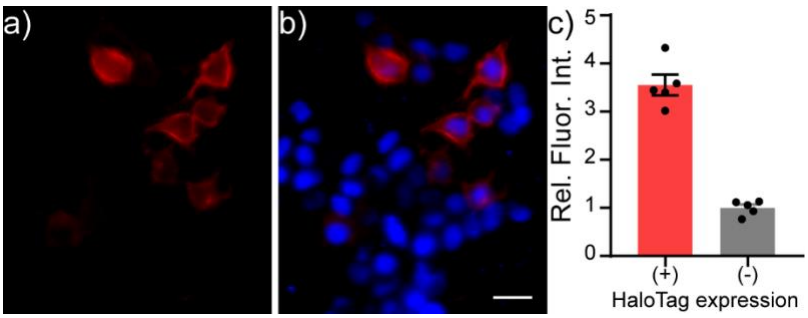

Figure 2-3. Live-cell staining of RhoVR-Halo in HEK293T cells expressing HaloTag-CD4. Epifluorescence images of HEK293T cells expressing HaloTag-CD4 (CMV promoter) and stained with **a)** RhoVR-Halo (100 nM, red) and **b)** Hoechst 33342 (1 µM, blue). Scale bar is 20 µm. **c)** Plot of relative fluorescence intensity in cells expressing HaloTag vs. cells that do not express HaloTag. HaloTag (+) cells were assigned based on a threshold obtained from a non-transfected control. Data are mean ± SEM for n = 5 different coverslips of cells. Data points represent average fluorescence intensities of 30 to 40 cells.

Figure 2-4.

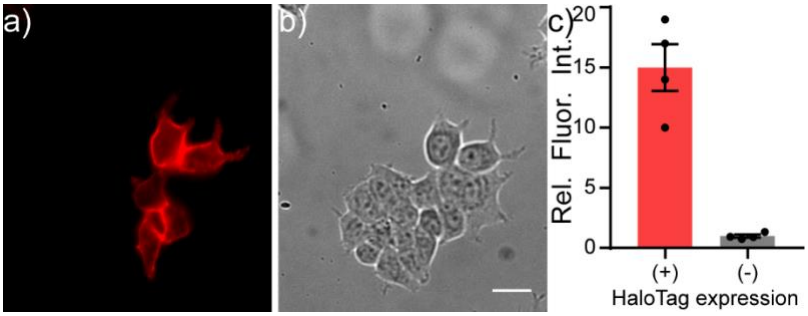

Figure 2-4. TMR-Halo staining in HEK293T cells. Live-cell staining of TMR-Halo in HEK293T cells expressing HaloTag-CD4. Epifluorescence images of HEK293T cells expressing HaloTag-CD4 (CMV promoter) and stained with **a)** TMR-Halo (100 nM, red) and **b)** DIC image of the area in panel **(a)** Scale bar is 20 µm. **c)** Plot of relative fluorescence intensity in cells expressing HaloTag vs. cells that do not express HaloTag. HaloTag-(+) cells were assigned based on a threshold obtained from a non-transfected control. Data are mean ± SEM for n = 4 different coverslips of cells. Data points represent average fluorescence intensities of 40 to 50 cells.

Figure 2-5.

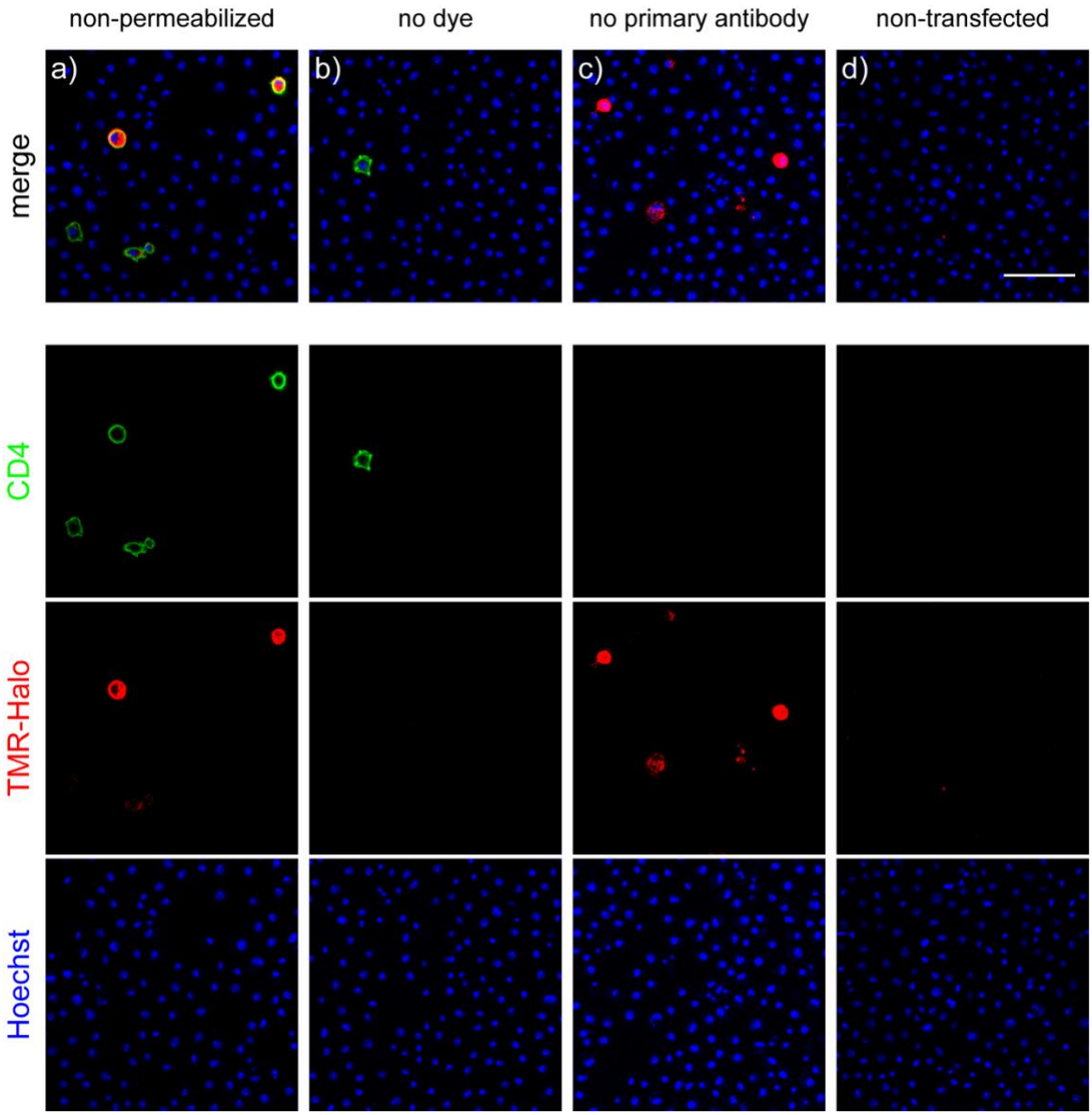

Figure 2-5. Immunocytochemistry in *Drosophila* S2 cells. Confocal images of *post hoc* immunocytochemistry of *Drosophila* S2 cells expressing HaloTag-CD4 (co-transfection with tubP-GAL4 and UAS-HaloTag-CD4), stained with TMR-Halo (100 nM, as in **Figure 3** in the main text), and fixed under **a)** non-permeabilizing conditions. Before fixation, control cells were treated either **b)** without TMR-Halo ("no dye"), **c)** with dye, but without primary anti-CD4 antibody, or **d)** with dye, but without transfection. Green is CD4, red is TMR-Halo (100 nM, during live-cell imaging, before fixation), and blue is Hoechst 33342 (at a concentration of 10 µg/mL, is equivalent to 16 µM). Scale bar for all images is 50 µm.

Figure 2-6.

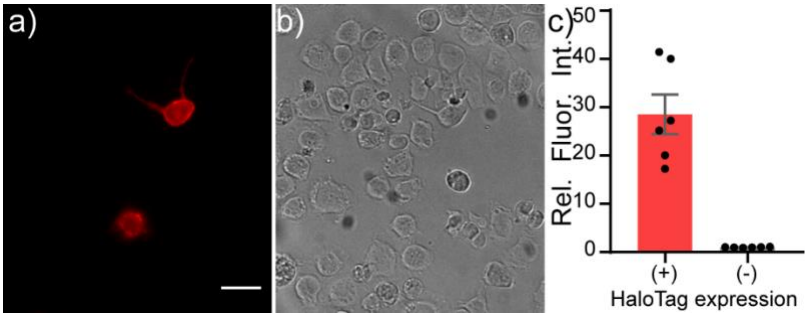

Figure 2-6. Live-cell staining of *Drosophila* S2 cells with TMR-Halo. Live-cell staining of TMR-Halo in *Drosophila* S2 cells expressing HaloTag-CD4. Epifluorescence images of *Drosophila* S2 cells transfected with tubP-GAL4 and HaloTag-CD4 UAS and **a)** stained with TMR-Halo (100 nM). **b)** Transmitted light image of cells in panel (**a**). Scale bar is 20 µm. **c)** Plot of relative fluorescence intensity in cells expressing HaloTag vs. cells that do not express HaloTag from the same cultures. HaloTag-(+) cells were assigned based on a threshold obtained from a non-transfected control. Data are mean ± SEM for n = 6 different coverslips.

Figure 2-7.

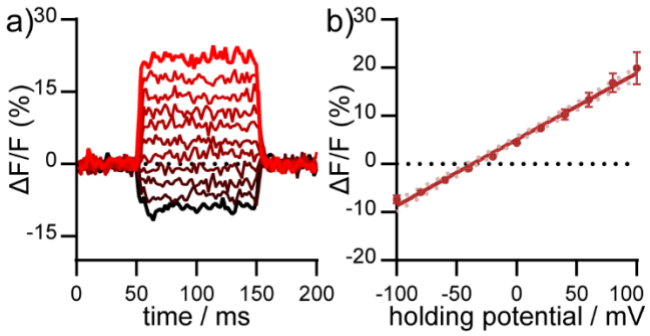

Figure 2-7. Voltage sensitivity of RhoVR-Halo in HEK293T cells expressing HaloTag-CD4. **a)** Plot of ΔF/F vs. time for a single HEK293T cell expressing HaloTag-CD4 and stained with RhoVR-Halo. The HEK293T cell was held at -60 mV and then stepped through hyperpolarizing and depolarizing potentials, in 20 mV increments, from -100 mV to +100 mV. **b)** Plot of ΔF/F vs. potential in mV. Data are mean ± standard error of the mean for n = 7 separate cells. Solid line is the line of best fit, and pink dots are 95% confidence interval.

Figure 2-8.

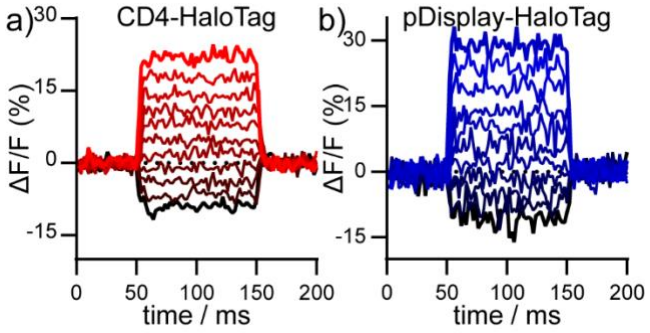

Figure 2-8. Comparison of voltage sensitivity of RhoVR-Halo with CD4-HaloTag and pDisplay-HaloTag. Voltage sensitivity of RhoVR-Halo in HEK293T cells expressing a) HaloTag-CD4 or b) pDisplay-HaloTag. Data are plots of ΔF/F vs. time for a single HEK293T cell expressing either **a)** HaloTag-CD4 (reproduced from Figure 4a in main text) or **b)** HaloTag-pDisplay and stained with RhoVR-Halo. The HEK293T cell was held at -60 mV and then stepped through hyperpolarizing and depolarizing potentials, in 20 mV increments, from -100 mV to +100 mV.

Figure 2-9.

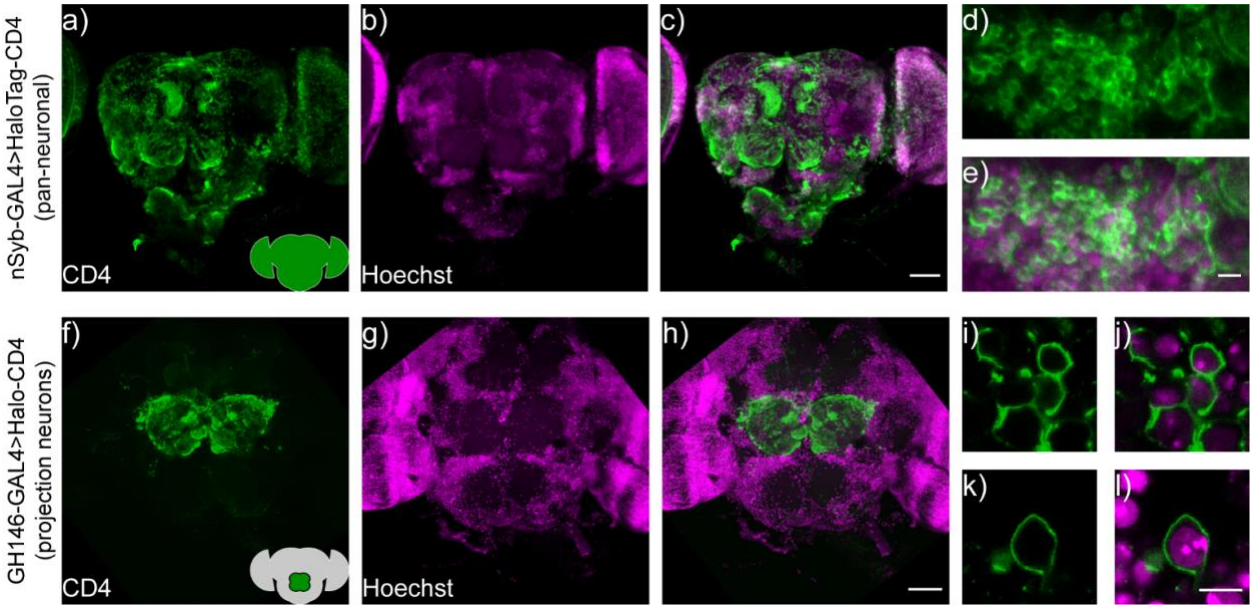

Figure 2-9. HaloTag-CD4 expression in transgenic *Drosophila*. **a)** nSyb-GAL4, HaloTag-CD4 brains express CD4 pan-neuronally. Maximum z-projection of a confocal fluorescence microscopy stack of brain explant from either **a-e)** nSyb-GAL4>HaloTag-CD4 or **f-l)** GH146-GAL4>HaloTag-CD4, fixed and stained for an extracellular epitope of the CD4 protein (OKT4, green) and counterstained for nuclei with Hoechst 33342 (16 µm or 10 µg/mL, magenta). Scale bar is 50 µm for whole-brain images (**a-c** and **f-h**) and 5 µm for zoomed-in regions (**d-e** and **i-l**). Insets on panels **a** and **f** show schematized brains with an approximate location of the staining for reference.

Figure 2-10.

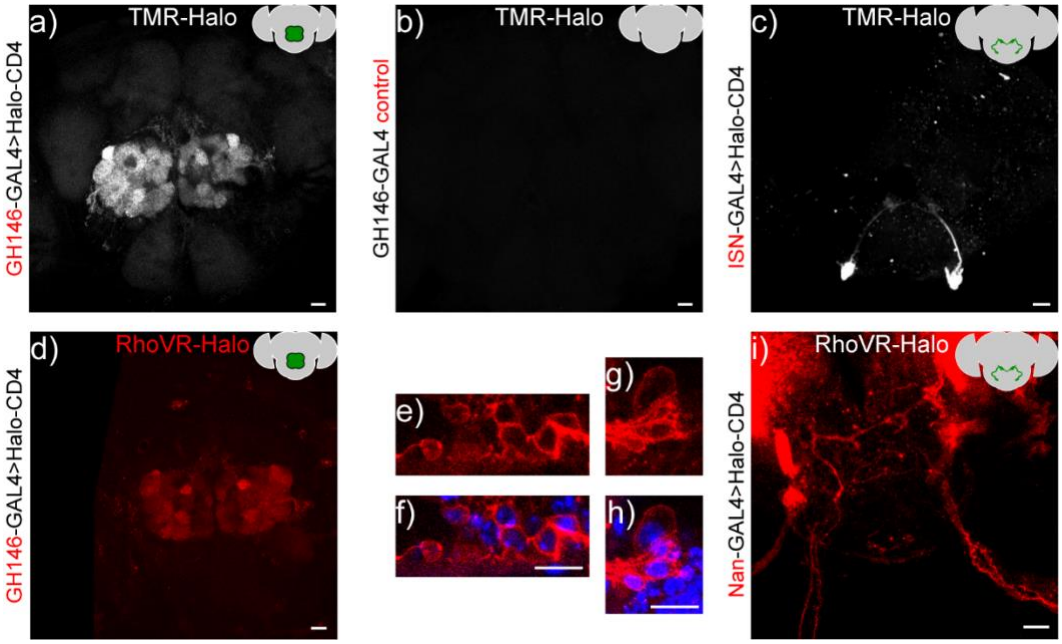

Figure 2-10. *In vivo* labeling of *Drosophila* neurons with TMR-Halo or RhoVR-Halo. Top row: Maximum z-projection of a confocal fluorescence microscopy stack of live brain explants labeled with voltage-*insensitive* TMR-Halo (1 μM) in an intact, live-fly before dissection and imaging. Crosses were either **a)** GH146-GAL4>HaloTag-CD4, **b)** GH146-only control, or **c)** VT011155-GAL4>HaloTag-CD4.
Bottom row. Maximum or sum z-projections of confocal fluorescence microscopy stack of live brain explants labeled with voltage-*sensitive* RhoVR-Halo (1 to 2 μM), labeling either **d-h)** projection neurons (GH146-GAL4>Halo-CD4, max projection) or **i)** ISNs (Nan-GAL4>Halo-CD4, sum projection). **e** and **g)** High magnification images of RhoVR-Halo staining in PNs (red), overlaid with **f** and **h)** Hoechst 33342 nuclear stain (blue). All scale bars are 20 μm.

Figure 2-11. Optimization of dye loading in live-fly brains using voltage-sensitive dye RhoVR-Halo.

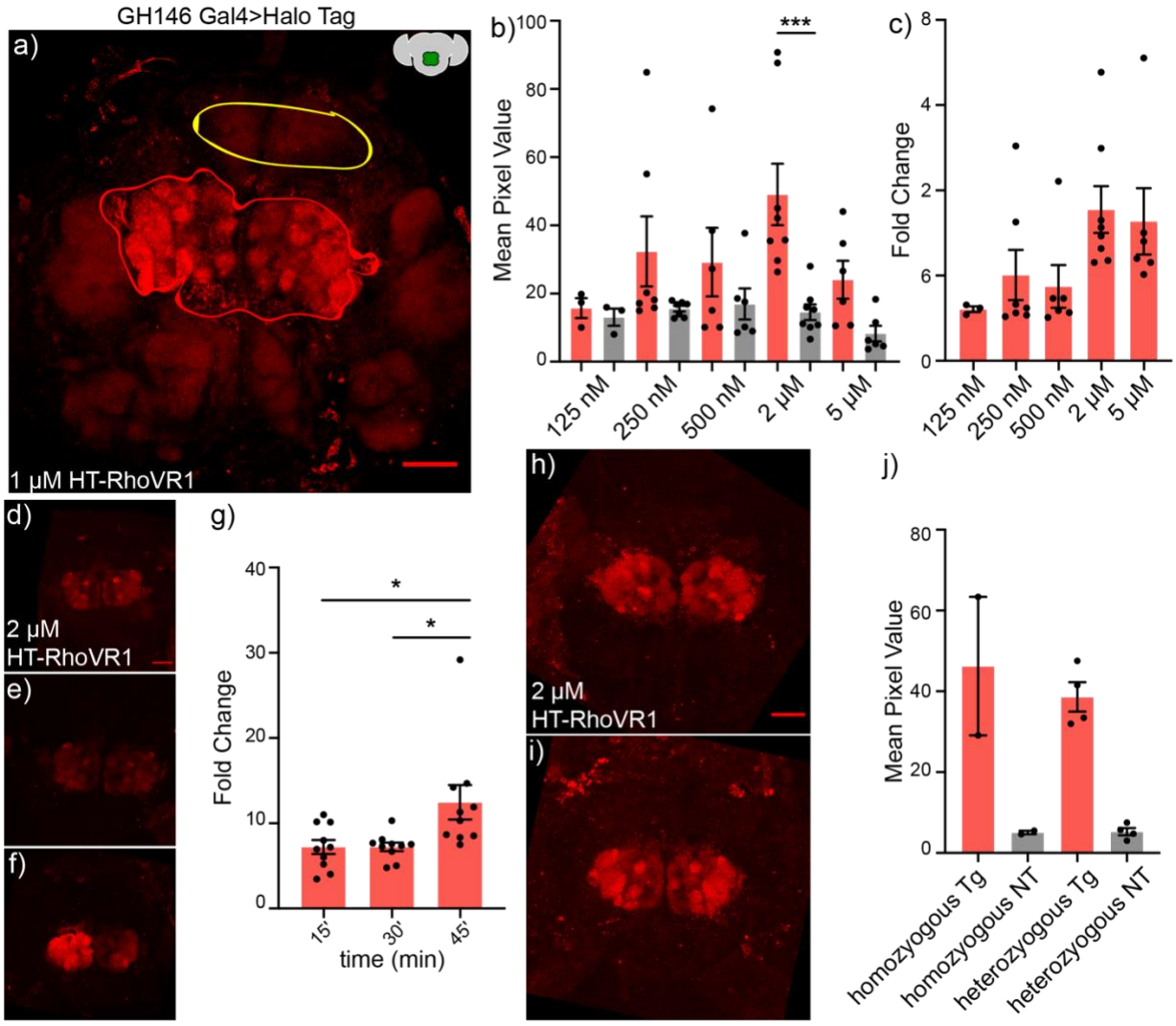

Figure 2-11. Optimization of dye loading in live-fly brains using voltage-sensitive dye RhoVR-Halo.

a) Maximum confocal z-projection 1 µM RhoVR-Halo loading in GH146 Gal4>HaloTag-CD4 in live explant tissue samples. Regions selected for quantification are circled in red, antennal lobe, and yellow, protocerebrum. Scale is 50 µm. **b)** Quantification of mean fluorescence intensity in GH146 Gal4> HaloTag-CD4 explant brains loaded with varying concentrations of RhoVR-Halo. Red depicts intensities taken from the antennal lobe, while grey depicts intensity taken from the protocerebrum. Data represents at least 6 individual brains per condition (***, p = 0.0006). **c)** Quantification of fold change in fluorescence intensity from targeted regions than non-targeted regions in live GH146-Gal4> HaloTag-CD4 loaded with varying concentrations of RhoVR-Halo. Data represent normalized data across at least 6 sample brains per condition. **d)** Maximum z-projection confocal stack of GH146-Gal4> HaloTag-CD4 live explant brain loaded with 2 µM RhoVR-Halo for 15 minutes at room temperature in a live imaging preparation. The scale is 50

µm. **e)** Maximum z-projection confocal stack of GH146-Gal4> HaloTag-CD4 live explant brains loaded with 2 µM RhoVR-Halo for 30 minutes at room temperature in a live imaging preparation. The scale is the same as d. **f)** Maximum z-projection confocal stack of GH146-Gal4> HaloTag-CD4 live explant brains loaded with 2 µM RhoVR-Halo for 45 minutes at room temperature in a live imaging preparation. The scale is the same as d. **g)** Quantification of fold fluorescence intensity change in GH146-Gal4>HaloTag-CD4 treated with 2 µM RhoVR-Halo for 15,30 or 45 minutes. Data represents normalized fluorescence intensity across at least 9 independent samples per condition. **h)** Maximum z projection of a confocal stack from RhoVR-Halo loaded GH146-Gal4> HaloTag-CD4 heterozygote live explant brains. The scale is 50 µm. **i)** Maximum z projection of a confocal stack from RhoVR-Halo loaded GH146-Gal4> HaloTag-CD4 homozygote live explant brains. The scale is the same as h. **j)** Quantification of fold intensity change in RhoVR-Halo loaded GH146-Gal4> HaloTag-CD4 heterozygotes and homozygotes.

Figure 2-12.

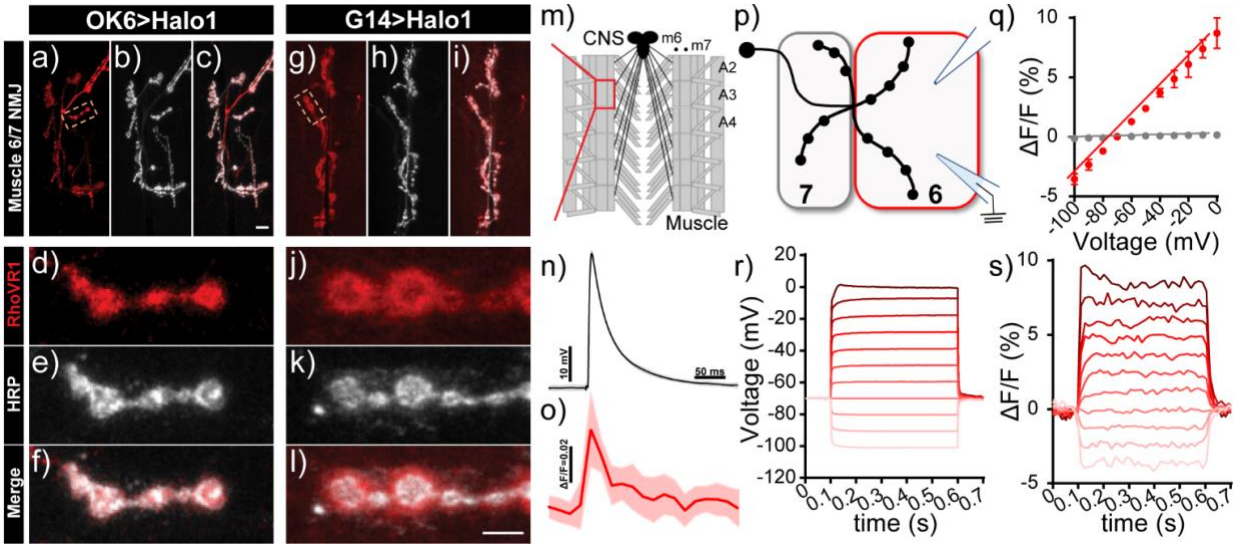

Figure 2-12. Voltage imaging with RhoVR-Halo using the *Drosophila* neuromuscular junction (NMJ). **a-l)** Confocal images of motor neurons labeled with RhoVR-Halo (2 µM) in NMJs of **a-f)** presynaptic neuron-labeled OK6-GAL4>Halo-CD4 flies or **g-l)** post-synaptic muscle-labeled G14-GAL4>Halo-CD4 flies. Red is RhoVR-Halo fluorescence; grey is HRP – a neuronal membrane marker. Scale bars are 10 µm (a-c, g-i) and 5 µm (d-f, j-l). **m)** Schematic of *Drosophila* NMJ. Excitatory post-synaptic potentials (EPSPs) recorded at NMJs of G14-GAL4>Halo-CD4 larvae stained with RhoVR-Halo (2 µM). Sharp electrode recordings of EPSPs are in **n)** grey, and **o)** optically recorded EPSPs are in red. Data are mean ± SEM of 8 replicates. **p)** Schematic of two-electrode measurements. Muscle cell 7 is unclamped, while the membrane potential of muscle cell 6 (m6) is clamped, held at -70 mV, and stepped to hyper- and depolarizing potentials ranging from -100 mV to 0 mV. **q)** Plot of ΔF/F vs. holding potential for m6 (clamped, red) or m7 (unclamped, grey) in G14-GAL4>Halo-CD4 flies stained with RhoVR-Halo. Data

are mean ± standard error of the mean for n = 8 independent determinations. Example plots of change in **r)** voltage or **s)** fluorescence (ΔF/F) vs. time for the clamped m6 cell.

Figure 2-13.

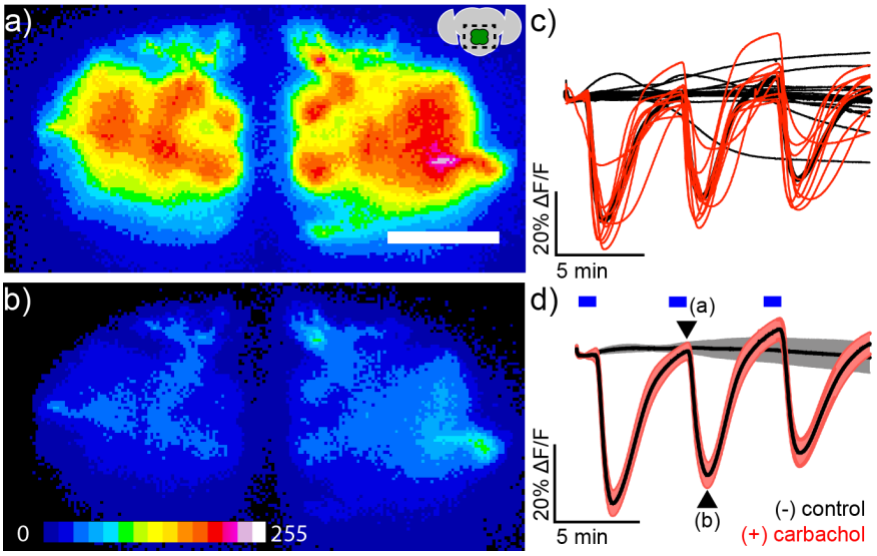

Figure 2-13. Imaging carbachol-induced depolarization in *Drosophila* projection neurons in live explants using ArcLight. Epifluorescence images of live explant *Drosophila* brain expressing ArcLight in antennal lobe projection neurons (GH146-GAL4,HaloTag-CD4/CyO>ArcLight/TM2) **a)** immediately before and **b)** 30 s after stimulation with 100 μM carbachol. Scale bar is 50 μm. Image is pseudo-colored, and the scale bar indicates 8-bit pixel grey values. **c)** Plot of ArcLight fluorescence (ΔF/F) vs. time for individual fly brains in response to three 100 μM carbachol stimulations (red, n = 10) and control (vehicle only) stimulations (black, n = 11). Each trace represents one individual brain. **d)** Plot of mean ArcLight fluorescence (ΔF/F). Data are mean ± SEM. Blue bars represent the addition of vehicle (control) or carbachol.

Figure 2-14.

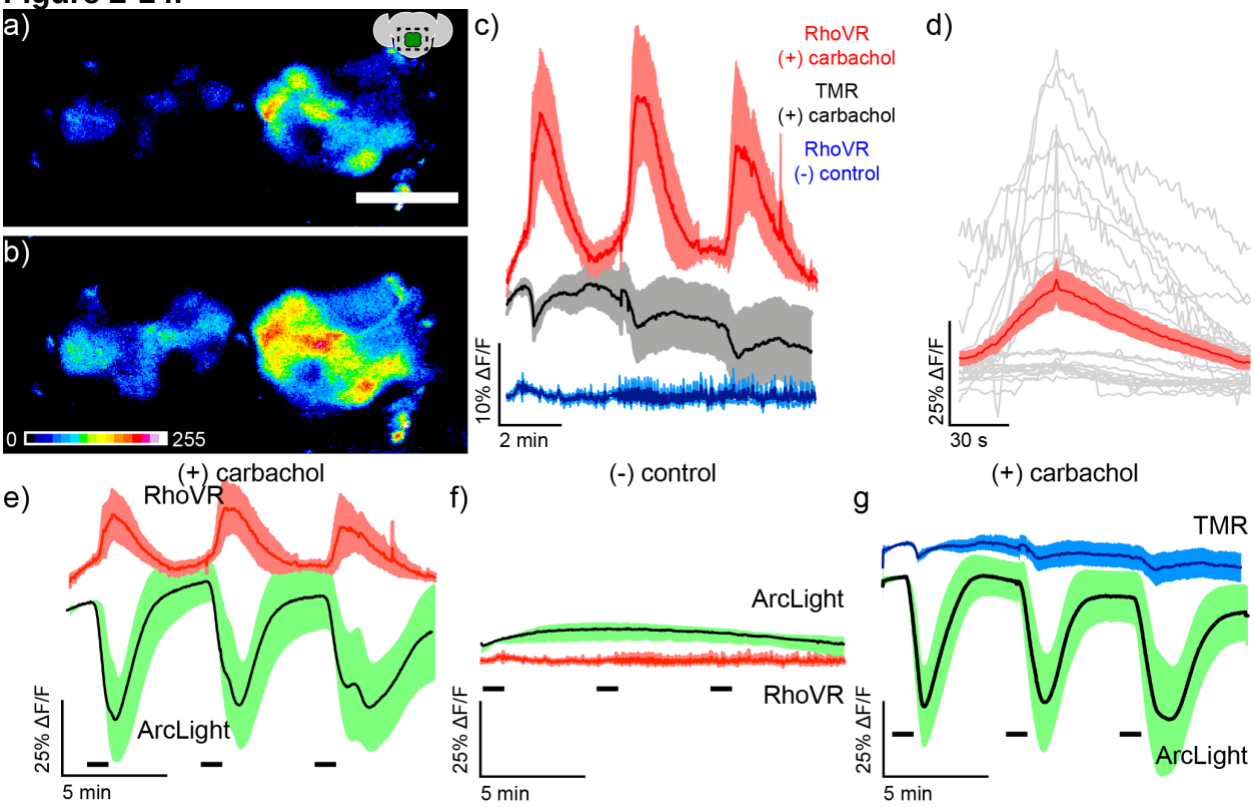

Figure 2-14. Simultaneous two-color visualization of carbachol-induced depolarization in projection neurons of live *Drosophila* brain explants with RhoVR-Halo and ArcLight. Epifluorescence images of live explant *Drosophila* brain expressing HaloTag-CD4 in antennal lobe projection neurons (GH146-GAL4, UAS-HaloTag-CD4/CyO; UAS-ArcLight/TM2) and labeled with RhoVR-Halo (2 μM) in live flies before dissection and explant imaging **a)** immediately before and **b)** 30 s after stimulation with 100 μM carbachol. Scale bar is 50 μm. **c)** Plots of average ΔF/F traces for *Drosophila* brains under the following conditions: stained with voltage-sensitive RhoVR-Halo (2 μM) and stimulated with 100 μM carbachol (red, n = 7 brains), stained with voltage-insensitive TMR-Halo (100 nM) and stimulated with 100 μM carbachol (grey, n = 7 brains), or stained with voltage-sensitive RhoVR-Halo (2 μM) and treated with vehicle control (blue, n = 6 brains). **d)** Plots of individual ΔF/F responses from RhoVR-Halo to carbachol stimuli (grey) and the average across all responses (red, SEM in light red). Traces of responses were aligned by peak response time and display 50 seconds before peak response and 150 seconds after peak response (grey). **e)** Plots of average ΔF/F traces for *Drosophila* brains stained with voltage-sensitive RhoVR-Halo (2 μM) and stimulated with 100 μM carbachol (red, n = 7 brains). ArcLight responses are recorded simultaneously (green, n = 7 brains). RhoVR traces are replicated from panel (**c**) for comparison with ArcLight. **f)** Plots of average ΔF/F traces for *Drosophila* brains stained with voltage-sensitive RhoVR-Halo (2 μM) and then treated with a vehicle control (red, n = 6 brains). ArcLight responses are recorded simultaneously (green, n = 6 brains).

RhoVR traces are replicated from panel (**c**) for comparison with ArcLight. **g)** Plots of average ΔF/F traces for *Drosophila* brains stained with voltage-*insensitive* TMR-Halo (100 nM) and stimulated with 100 µM carbachol (blue, n = 6 brains). ArcLight responses are recorded simultaneously (green, n = 6 brains). TMR traces are replicated from panel (**c**) for comparison with ArcLight. For all plots, data are mean ±SEM for the indicated number of samples. *Drosophila* brain explants were stimulated three times for 30 s with either 100 µM carbachol or vehicle. Stimulus (delivery of carbachol or vehicle) is depicted by small black bars immediately below the traces).

Figure 2-15.

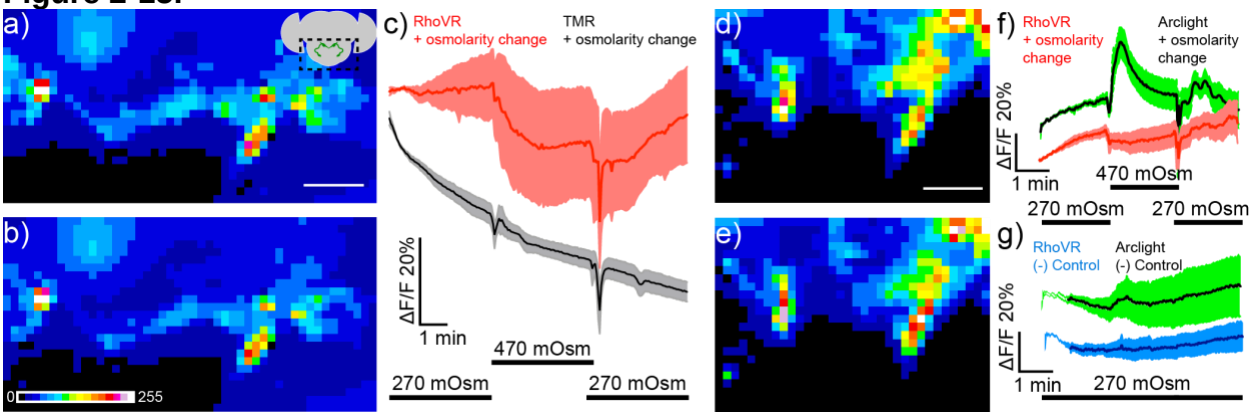

Figure 2-15. Imaging osmolarity induced hyperpolarizations in *Drosophila* interoceptive neurons in live explants using single color and dual-color imaging. Spinning disk confocal maximum z-projections of live explant *Drosophila* brain expressing HaloTag in ISNs (Nanchung-Gal4, UAS-HaloTag/Nanchung-Gal4, UAS-HaloTag; TM2/TM6B) **a)** before and **b)** after stimulation with high osmolarity hemolymph (470 mOsm). Scale bar is 50 µm. Image is pseudo-colored, and the scale bar indicates 8-bit pixel grey values. **c)** Plot mean of fluorescence (%ΔF/F) vs. time in response to one osmolarity simulation of either RhoVR-Halo (red, n = 5) or HT-TMR (black, n=5) loaded brains. Data are mean ± SEM Black bars below indicate the stimulation time course switching from 270 mOsm to 470 mOsm. Maximum z-projections of live explant *Drosophila* brain expressing HaloTag and Arclight in the ISNs (Nanchung-Gal4, UAS-HaloTag/UAS-Arclight; TM2/TM6B) **d)** before and **e)** after stimulation with high osmolarity hemolymph (470 mOsm). **f)** Plot mean of fluorescence (%ΔF/F) vs. time for simultaneously imaged Arclight (green) and RhoVR-Halo (red) in response to high osmolarity simulation (n=7) **g)** Plot mean of fluorescence (%ΔF/F) vs. time for simultaneously imaged Arclight (green) and RhoVR-Halo (red) in response a vehicle control (n=7).

Figure 2-16.

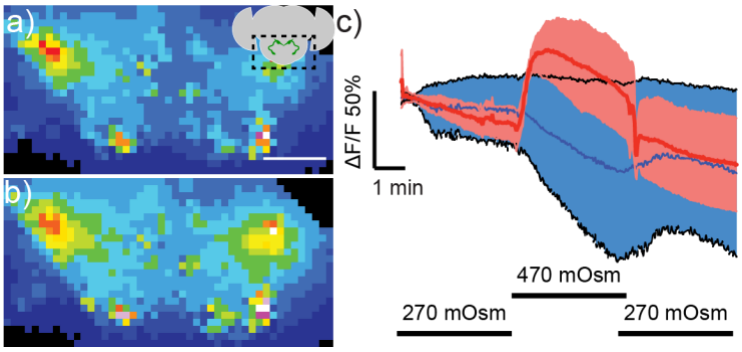

Figure 2-16. Imaging osmolarity-induced hyperpolarizations in ISNs in *Drosophila* using Arclight voltage indicator. Spinning disk confocal maximum z-projections of live explant *Drosophila* brain expressing Arclight in the ISNs (Nanchung-Gal4, UAS-HaloTag/ UAS-Arclight; TM2/TM6B) **a)** before and **b)** after stimulation with high osmolarity hemolymph (470 mOsm). Scale bar is 50 µm. Image is pseudo-colored, and the scale bar indicates 8-bit pixel grey values. **c)** Plot mean of fluorescence (%ΔF/F) vs. time in response to either a high osmolarity stimulation (red, n=8) or vehicle control (blue, n=8). Data are mean ± SEM Black bars below indicate the stimulation time course switching from 270 mOsm to 470 mOsm.

Figure 2-17.

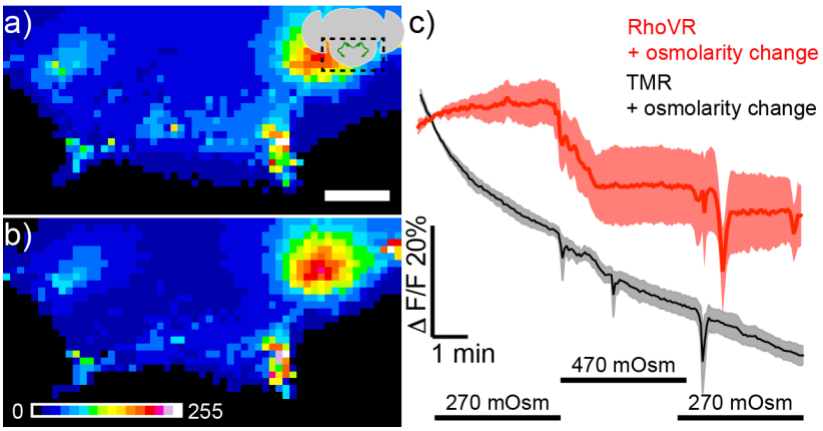

Figure 2-17. Imaging osmolarity-induced hyperpolarizations in ISNs in heterozygous transgenic *Drosophila* using RhoVR-Halo voltage indicator. Spinning disk confocal maximum z-projections of live explant *Drosophila* brain expressing HaloTag-CD4 in the ISNs (Nanchung-Gal4, UAS-HaloTag/CyO; TM2/TM6B) **a)** before and **b)** after stimulation with high osmolarity hemolymph. Scale bar is 50 µm. Image is pseudo-colored, and the scale bar indicates 8-bit pixel grey values. **c)** Plot mean of fluorescence (%ΔF/F) vs. time in response to one osmolarity simulation of either RhoVR-Halo (red, n = 5) or HT-TMR (black, n=5) loaded brains. Data are mean ± SEM Black bars below indicate the stimulation time course switching from 270 mOsm to 470 mOsm.

Figure 2-18

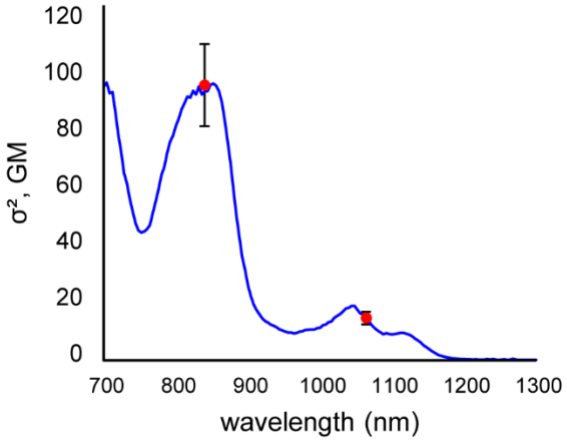

Figure 2-18. Two-photon cross excitation and absorption cross-section values of RhoVR 1. Plot of relative two-photon excitation spectra (solid blue line) and absolute two-photon absorption cross-section values at selected wavelengths (red dots) of RhoVR 1 (σ^2, in units of Göppert-Mayer, GM = 10^{-50} cm^4 s $molecules^{-1}$ $photons^{-1}$) vs. wavelength. Error bars are 15% error associated with the absolute absorption cross-section value. A machine-readable file (.csv) is included in the supplementary files.

References

1. Liu, P.; Miller, E. W., Electrophysiology, Unplugged: Imaging Membrane Potential with Fluorescent Indicators. *Accounts of Chemical Research* **2020,** *53* (1), 11-19.
2. Beier, H. T.; Roth, C. C.; Bixler, J. N.; Sedelnikova, A. V.; Ibey, B. L., Visualization of Dynamic Sub-microsecond Changes in Membrane Potential. *Biophysical Journal* **2019,** *116* (1), 120-126.
3. Kulkarni, R. U.; Vandenberghe, M.; Thunemann, M.; James, F.; Andreassen, O. A.; Djurovic, S.; Devor, A.; Miller, E. W., In Vivo Two-Photon Voltage Imaging with Sulfonated Rhodamine Dyes. *ACS Central Science* **2018,** *4* (10), 1371-1378.
4. Kazemipour, A.; Novak, O.; Flickinger, D.; Marvin, J. S.; Abdelfattah, A. S.; King, J.; Borden, P. M.; Kim, J. J.; Al-Abdullatif, S. H.; Deal, P. E.; Miller, E. W.; Schreiter, E. R.; Druckmann, S.; Svoboda, K.; Looger, L. L.; Podgorski, K., Kilohertz frame-rate two-photon tomography. *Nature methods* **2019,** *16* (8), 778-786.
5. Woodford, C. R.; Frady, E. P.; Smith, R. S.; Morey, B.; Canzi, G.; Palida, S. F.; Araneda, R. C.; Kristan, W. B.; Kubiak, C. P.; Miller, E. W.; Tsien, R. Y., Improved PeT Molecules for Optically Sensing Voltage in Neurons. *Journal of the American Chemical Society* **2015,** *137* (5), 1817-1824.
6. Ng, D. N.; Fromherz, P., Genetic Targeting of a Voltage-Sensitive Dye by Enzymatic Activation of Phosphonooxymethyl-ammonium Derivative. *ACS Chemical Biology* **2011,** *6* (5), 444-451.
7. Liu, P.; Grenier, V.; Hong, W.; Muller, V. R.; Miller, E. W., Fluorogenic Targeting of Voltage-Sensitive Dyes to Neurons. *Journal of the American Chemical Society* **2017,** *139* (48), 17334-17340.
8. Sundukova, M.; Prifti, E.; Bucci, A.; Kirillova, K.; Serrao, J.; Reymond, L.; Umebayashi, M.; Hovius, R.; Riezman, H.; Johnsson, K.; Heppenstall, P. A., A Chemogenetic Approach for the Optical Monitoring of Voltage in Neurons. *Angewandte Chemie (International ed. in English)* **2019,** *58* (8), 2341-2344.
9. Fiala, T.; Wang, J.; Dunn, M.; Šebej, P.; Choi, S. J.; Nwadibia, E. C.; Fialova, E.; Martinez, D. M.; Cheetham, C. E.; Fogle, K. J.; Palladino, M. J.; Freyberg, Z.; Sulzer, D.; Sames, D., Chemical Targeting of Voltage Sensitive Dyes to Specific Cells and Molecules in the Brain. *Journal of the American Chemical Society* **2020,** *142* (20), 9285-9301.
10. Abdelfattah, A. S.; Kawashima, T.; Singh, A.; Novak, O.; Liu, H.; Shuai, Y.; Huang, Y.-C.; Campagnola, L.; Seeman, S. C.; Yu, J.; Zheng, J.; Grimm, J. B.; Patel, R.; Friedrich, J.; Mensh, B. D.; Paninski, L.; Macklin, J. J.; Murphy, G. J.; Podgorski, K.; Lin, B.-J.; Chen, T.-W.; Turner, G. C.; Liu, Z.; Koyama, M.; Svoboda, K.; Ahrens, M. B.; Lavis, L. D.; Schreiter, E. R., Bright and photostable chemigenetic indicators for extended in vivo voltage imaging. *Science* **2019,** *365* (6454), 699-704.
11. Liu, S.; Lin, C.; Xu, Y.; Luo, H.; Peng, L.; Zeng, X.; Zheng, H.; Chen, P. R.; Zou, P., A far-red hybrid voltage indicator enabled by bioorthogonal engineering of rhodopsin on live neurons. *Nature Chemistry* **2021,** *13* (5), 472-479.
12. Deo, C.; Abdelfattah, A. S.; Bhargava, H. K.; Berro, A. J.; Falco, N.; Farrants, H.; Moeyaert, B.; Chupanova, M.; Lavis, L. D.; Schreiter, E. R., The HaloTag as a general scaffold for far-red tunable chemigenetic indicators. *Nature Chemical Biology* **2021,** *17* (6), 718-723.

13. Deal, P. E.; Kulkarni, R. U.; Al-Abdullatif, S. H.; Miller, E. W., Isomerically Pure Tetramethylrhodamine Voltage Reporters. *Journal of the American Chemical Society* **2016,** *138* (29), 9085-9088.
14. Deal, P. E.; Liu, P.; Al-Abdullatif, S. H.; Muller, V. R.; Shamardani, K.; Adesnik, H.; Miller, E. W., Covalently Tethered Rhodamine Voltage Reporters for High Speed Functional Imaging in Brain Tissue. *Journal of the American Chemical Society* **2020,** *142* (1), 614-622.
15. Simpson, J. H., Mapping and manipulating neural circuits in the fly brain. *Advances in genetics* **2009,** *65*, 79-143.
16. Caygill, E. E.; Brand, A. H., The GAL4 System: A Versatile System for the Manipulation and Analysis of Gene Expression. *Methods in molecular biology (Clifton, N.J.)* **2016,** *1478*, 33-52.
17. Simpson, J. H.; Looger, L. L., Functional Imaging and Optogenetics in Drosophila. *Genetics* **2018,** *208* (4), 1291-1309.
18. Jin, L.; Han, Z.; Platisa, J.; Wooltorton, J. R.; Cohen, L. B.; Pieribone, V. A., Single action potentials and subthreshold electrical events imaged in neurons with a fluorescent protein voltage probe. *Neuron* **2012,** *75* (5), 779-85.
19. Jourjine, N.; Mullaney, B. C.; Mann, K.; Scott, K., Coupled Sensing of Hunger and Thirst Signals Balances Sugar and Water Consumption. *Cell* **2016,** *166* (4), 855-866.
20. Chen, D.; Sitaraman, D.; Chen, N.; Jin, X.; Han, C.; Chen, J.; Sun, M.; Baker, B. S.; Nitabach, M. N.; Pan, Y., Genetic and neuronal mechanisms governing the sex-specific interaction between sleep and sexual behaviors in Drosophila. *Nature Communications* **2017,** *8* (1), 154.
21. Yang, H. H.; St-Pierre, F.; Sun, X.; Ding, X.; Lin, M. Z.; Clandinin, T. R., Subcellular Imaging of Voltage and Calcium Signals Reveals Neural Processing In Vivo. *Cell* **2016,** *166* (1), 245-57.
22. Chamberland, S.; Yang, H. H.; Pan, M. M.; Evans, S. W.; Guan, S.; Chavarha, M.; Yang, Y.; Salesse, C.; Wu, H.; Wu, J. C.; Clandinin, T. R.; Toth, K.; Lin, M. Z.; St-Pierre, F., Fast two-photon imaging of subcellular voltage dynamics in neuronal tissue with genetically encoded indicators. *eLife* **2017,** *6*, e25690.
23. Zou, P.; Zhao, Y.; Douglass, A. D.; Hochbaum, D. R.; Brinks, D.; Werley, C. A.; Harrison, D. J.; Campbell, R. E.; Cohen, A. E., Bright and fast multicoloured voltage reporters via electrochromic FRET. *Nature Communications* **2014,** *5* (1), 4625.
24. Gong, Y.; Huang, C.; Li, J. Z.; Grewe, B. F.; Zhang, Y.; Eismann, S.; Schnitzer, M. J., High-speed recording of neural spikes in awake mice and flies with a fluorescent voltage sensor. *Science* **2015,** *350* (6266), 1361-6.
25. Kannan, M.; Vasan, G.; Huang, C.; Haziza, S.; Li, J. Z.; Inan, H.; Schnitzer, M. J.; Pieribone, V. A., Fast, in vivo voltage imaging using a red fluorescent indicator. *Nature methods* **2018,** *15* (12), 1108-1116.
26. Maclaurin, D.; Venkatachalam, V.; Lee, H.; Cohen, A. E., Mechanism of voltage-sensitive fluorescence in a microbial rhodopsin. *Proceedings of the National Academy of Sciences* **2013,** *110* (15), 5939-5944.
27. Kohl, J.; Ng, J.; Cachero, S.; Ciabatti, E.; Dolan, M.-J.; Sutcliffe, B.; Tozer, A.; Ruehle, S.; Krueger, D.; Frechter, S.; Branco, T.; Tripodi, M.; Jefferis, G. S. X. E.,

Ultrafast tissue staining with chemical tags. *Proceedings of the National Academy of Sciences* **2014,** *111* (36), E3805-E3814.
28. Sutcliffe, B.; Ng, J.; Auer, T. O.; Pasche, M.; Benton, R.; Jefferis, G. S. X. E.; Cachero, S., Second-Generation Drosophila Chemical Tags: Sensitivity, Versatility, and Speed. *Genetics* **2017,** *205* (4), 1399-1408.
29. Han, C.; Jan, L. Y.; Jan, Y.-N., Enhancer-driven membrane markers for analysis of nonautonomous mechanisms reveal neuron–glia interactions in Drosophila. *Proceedings of the National Academy of Sciences* **2011,** *108* (23), 9673-9678.
30. Pfeiffer, B. D.; Ngo, T. T.; Hibbard, K. L.; Murphy, C.; Jenett, A.; Truman, J. W.; Rubin, G. M., Refinement of tools for targeted gene expression in Drosophila. *Genetics* **2010,** *186* (2), 735-55.
31. DiAntonio, A.; Burgess, R.; Chin, A.; Deitcher, D.; Scheller, R.; Schwarz, T., Identification and characterization of Drosophila genes for synaptic vesicle proteins. *The Journal of Neuroscience* **1993,** *13* (11), 4924-4935.
32. Stocker, R. F.; Heimbeck, G.; Gendre, N.; de Belle, J. S., Neuroblast ablation in Drosophila P[GAL4] lines reveals origins of olfactory interneurons. *Journal of Neurobiology* **1997,** *32* (5), 443-456.
33. Wilson, R. I.; Turner, G. C.; Laurent, G., Transformation of Olfactory Representations in the Drosophila Antennal Lobe. *Science* **2004,** *303* (5656), 366-370.
34. Harris, D. T.; Kallman, B. R.; Mullaney, B. C.; Scott, K., Representations of Taste Modality in the Drosophila Brain. *Neuron* **2015,** *86* (6), 1449-60.
35. Kazama, H.; Wilson, R. I., Homeostatic matching and nonlinear amplification at identified central synapses. *Neuron* **2008,** *58* (3), 401-13.
36. Restifo, L. L.; White, K., Molecular and Genetic Approaches to Neurotransmitter and Neuromodulator Systems in Drosophila. In *Advances in Insect Physiology*, Evans, P. D.; Wigglesworth, V. B., Eds. Academic Press: 1990; Vol. 22, pp 115-219.
37. Ortiz, G.; Liu, P.; Deal, P. E.; Nensel, A.; Martinez, K.; Shamardani, K.; Adesnik, H.; Miller, E. W., A Silicon-Rhodamine Chemical-Genetic Hybrid for Far Red Voltage Imaging from Defined Neurons in Brain Slice. *ChemRxiv* **2020**, 10.26434/chemrxiv.12760166.v1.
38. Lazzari-Dean, J. R.; Gest, A. M. M.; Miller, E. W., Optical estimation of absolute membrane potential using fluorescence lifetime imaging. *eLife* **2019,** *8*, e44522.
39. Milosevic, M. M.; Jang, J.; McKimm, E. J.; Zhu, M. H.; Antic, S. D., In Vitro Testing of Voltage Indicators: Archon1, ArcLightD, ASAP1, ASAP2s, ASAP3b, Bongwoori-Pos6, BeRST1, FlicR1, and Chi-VSFP-Butterfly. *eneuro* **2020,** *7* (5), ENEURO.0060-20.2020.
40. Wu, J.; Liang, Y.; Chen, S.; Hsu, C. L.; Chavarha, M.; Evans, S. W.; Shi, D.; Lin, M. Z.; Tsia, K. K.; Ji, N., Kilohertz two-photon fluorescence microscopy imaging of neural activity in vivo. *Nature methods* **2020,** *17* (3), 287-290.
41. Gettner, S. N.; Kenyon, C.; Reichardt, L. F., Characterization of beta pat-3 heterodimers, a family of essential integrin receptors in C. elegans. *The Journal of cell biology* **1995,** *129* (4), 1127-41.

42. Lee, T.; Luo, L., Mosaic Analysis with a Repressible Cell Marker for Studies of Gene Function in Neuronal Morphogenesis. *Neuron* **1999,** *22* (3), 451-461.
43. Wang, J. W.; Wong, A. M.; Flores, J.; Vosshall, L. B.; Axel, R., Two-Photon Calcium Imaging Reveals an Odor-Evoked Map of Activity in the Fly Brain. *Cell* **2003,** *112* (2), 271-282.
44. Peng, J.; Peng, S.; Jiang, A.; Wei, J.; Li, C.; Tan, J., Asymmetric least squares for multiple spectra baseline correction. *Analytica chimica acta* **2010,** *683* (1), 63-8.
45. Goel, P.; Dufour Bergeron, D.; Böhme, M. A.; Nunnelly, L.; Lehmann, M.; Buser, C.; Walter, A. M.; Sigrist, S. J.; Dickman, D., Homeostatic scaling of active zone scaffolds maintains global synaptic strength. *The Journal of cell biology* **2019,** *218* (5), 1706-1724.
46. Kiragasi, B.; Goel, P.; Perry, S.; Han, Y.; Li, X.; Dickman, D., The auxiliary glutamate receptor subunit dSol-1 promotes presynaptic neurotransmitter release and homeostatic potentiation. *Proceedings of the National Academy of Sciences* **2020,** *117* (41), 25830-25839.
47. Schindelin, J.; Arganda-Carreras, I.; Frise, E.; Kaynig, V.; Longair, M.; Pietzsch, T.; Preibisch, S.; Rueden, C.; Saalfeld, S.; Schmid, B.; Tinevez, J.-Y.; White, D. J.; Hartenstein, V.; Eliceiri, K.; Tomancak, P.; Cardona, A., Fiji: an open-source platform for biological-image analysis. *Nature methods* **2012,** *9* (7), 676-682.
48. Rueden, C. T.; Schindelin, J.; Hiner, M. C.; DeZonia, B. E.; Walter, A. E.; Arena, E. T.; Eliceiri, K. W., ImageJ2: ImageJ for the next generation of scientific image data. *BMC bioinformatics* **2017,** *18* (1), 529.
50. Drobizhev, M.; Molina, R. S.; Hughes, T. E., Characterizing the Two-photon Absorption Properties of Fluorescent Molecules in the 680-1300 nm Spectral Range. *Bio-protocol* **2020,** *10* (2), e3498.
51. Makarov, N. S.; Drobizhev, M.; Rebane, A., Two-photon absorption standards in the 550–1600 nm excitation wavelength range. *Opt. Express* **2008,** *16* (6), 4029-4047.
52. de Reguardati, S.; Pahapill, J.; Mikhailov, A.; Stepanenko, Y.; Rebane, A., High-accuracy reference standards for two-photon absorption in the 680–1050 nm wavelength range. *Opt. Express* **2016,** *24* (8), 9053-9066.
53. Hermann, J. P.; Ducuing, J., Dispersion of the two-photon cross section in rhodamine dyes. *Optics Communications* **1972,** *6* (2), 101-105.
54. Vsevolodov, N. N.; Kostikov, L. P.; Kaiushin, L. P.; Gorbatenkov, V. I., [2-photon absorption of laser radiation by chlorophyll a and organic dyes]. *Biofizika* **1973,** *18* (4), 755-7.
55. Li, S.; She, C. Y., Two-photon Absorption Cross-section Measurements in Common Laser Dyes at 1·06 μm. *Optica Acta: International Journal of Optics* **1982,** *29* (3), 281-287.
56. Catalano, I. M.; Cingolani, A., Absolute two-photo fluorescence with low-power cw lasers. *Applied Physics Letters* **1981,** *38* (10), 745-747.
57. Catalano, I. M.; Cingolani, A., Multiphoton cross-section measurements with low-power cw laser-induced luminescence. *Applied optics* **1982,** *21* (3), 477-80.
58. Rodríguez, L.; Echevarria, L.; Fernandez, A., I-scan thermal lens experiment in the pulse regime for measuring two-photon absorption coefficient. *Optics Communications* **2007,** *277* (1), 181-185.

59. Kaatz, P.; Shelton, D. P., Two-photon fluorescence cross-section measurements calibrated with hyper-Rayleigh scattering. *J. Opt. Soc. Am. B* **1999,** *16* (6), 998-1006.

Chapter 3: Genetic targeting of small molecule dyes in *Drosophila* to access neuronal morphology databases

Portions of this work were completed in collaboration with others: Gabriella Stern experimental design and neuronal segmentation.

Abstract

Visualizing neuronal anatomy often requires labor-intensive immunohistochemistry on fixed and dissected brains. To facilitate rapid anatomical staining in live brains, we developed an approach using genetically targeted membrane tethers that covalently link fluorescent dyes for in vivo neuronal labeling. We generated a series of extracellularly trafficked small molecule tethering proteins, HaloTag-CD4[1] and $SNAP_f$-CD4, which directly label transgene expressing cells with commercially available ligand substituted fluorescent dyes. We developed stable transgenic *Drosophila* reporter lines which express extracellular HaloTag-CD4 and $SNAP_f$-CD4 under both LexA and Gal4 drivers. Expressing these enzymes in live *Drosophila* brains, we labeled the neuronal expression patterns of various Gal4 driver lines recapitulating histological staining in live brain tissue. Expressing $SNAP_f$-CD4 pan-neuronally, we registered brains to an existing anatomical template. From directly registered live brain tissue, we performed bridging registrations and a neuronal morphology similarity search (NBLAST)[2]. We anticipate that these extracellular platforms will not only become a valuable complement to existing anatomical methods but will also prove useful for future genetic targeting of other small molecule probes, drugs, and actuators.

Introduction

Resolving the anatomical structure of the brain's neural circuits is foundational to studying neuronal computations and behavior. The expression of genetically encoded fluorescent proteins is the most common method to explore neuroanatomy in vivo. Although expression of fluorescent proteins is a valuable technique, a limitation of the approach is that fluorescent proteins are often spectrally incompatible with other fluorophores but cannot be readily changed without the generation of different transgenic organisms. For this reason, we sought to increase the flexibility of in vivo anatomical analysis. We proposed that an ideal system for in vivo anatomical analysis would 1) permit rapid and accurate staining of neuroanatomical structures in vivo, 2) facilitate changes in fluorescence spectra to readily pair with any available fluorophore, probe, or actuator, and 3) allow for temporal control of fluorescence activation. To increase the ease and flexibility of performing anatomical analysis in vivo, we have generated a series of extracellularly targeted small molecule tethering proteins that permit exploration of neuronal anatomy in both a rapid, accurate, and highly flexible manner.

Although an in vivo approach offers a higher through-put method for anatomical analysis, the gold standard of anatomical techniques is immunohistochemistry (IHC). Here, tissues are preserved in a fixative and stained with antibodies targeted to specific proteins or epitopes[3]. This technique allows for the multispectral labeling of multiple proteins and permits the highly detailed inspection of anatomical samples. However, this technique cannot be performed in vivo, as antibody access to intracellular epitopes requires permeabilization and fixation. This technique is often laborious, taking 2-3 weeks to achieve uniform staining in some preparations[4]. A similar method, Hybrid IHC, shortens the timeline significantly[4–6]. Hybrid IHC utilizes genetically encoded small molecule tethering systems, HaloTag[7], SNAP-Tag [8], and SNAPf [9], which traffic to the inner leaflet of the plasma membrane[4]. These tethering platforms are genetically encoded monomeric

enzymes that catalyze the formation of a stable covalent bond with ligand substituted fluorescent dyes[10]. When the reactive dye is added to fixed and permeabilized tissues, it readily labels structures expressing the covalent tethering protein, mimicking the results of standard IHC. Hybrid IHC labels low complexity structures such as live murine skin samples in vivo[11]. However, the intracellular location of the tethering proteins may limit dye binding in non-permeabilized tissues.

Expanding upon Hybrid IHC, we sought to develop an anatomical method that is genetically targeted, multispectral, and compatible with in vivo experimentation. We have developed a series of extracellularly targeted small molecule targeting enzymes HaloTag-CD4[1] and $SNAP_f$-CD4, which functionally tether water-soluble dyes in vitro (**Figure 3-1a)**. Further, leveraging the genetic flexibility, small nervous system, and plethora of anatomical tools, we generated stable transgenic *Drosophila* lines that express HaloTag-CD4 and $SNAP_f$-CD4 on the extracellular surface in genetically defined neuronal populations (**Figure 3-1b**). Due to the extracellular localization of the tethering proteins, our method does not require permeabilization or fixation to access the covalent tethers and is thus amenable to the exploration of neuronal anatomy in live brain tissues (**Figure 3-1c**).

Results

Generation of $SNAP_f$ constructs for extracellular expression in flies

Our group had previously developed a chemical-genetic hybrid voltage sensor that targets HaloTag to the extracellular surface using an N-terminus PAT-3 secretion signal *(*from *C. Elegans)* and CD4 transmembrane anchor. We showed that HaloTag-CD4 could target dyes to the extracellular surface both in vitro and in vivo[1]. Similarly adapting $SNAP_f$ for extracellular targeting, we generated a PAT-3-$SNAP_f$-HA-CD4($SNAP_f$-CD4) fusion protein for extracellular trafficking in *Drosophila*. We sub-cloned $SNAP_f$-CD4 into both mammalian (pcDNA3.1) and insect expression vectors (pJFRC7, pJFCR19) **(Scheme 3-1).** $SNAP_f$-CD4 shows good extracellular expression with the CD4 localizing to the cell surface by anti-CD4 immunocytochemistry when expressed in HEK 293T cells **(Figure 3-2).** The $SNAP_f$, self-labeling enzyme confirms not only localization but activity of the expressed enzyme by treating with Snap Tag reactive substrates. $SNAP_f$-CD4 treated with SS-A488 (100 nM) shows good membrane localization in HEK cells **(Figure 3-3a)**. Cells that do not express $SNAP_f$-CD4 show approximately 3.6-fold lower fluorescence levels (**Figure 3-3b and c)**. Following live-cell imaging, cells can be fixed and retain their SS-A488 staining, a valuable counterstain to the anti-CD4 immunocytochemistry **(Figure 3-2).**

We also observe cell surface localization of $SNAP_f$-CD4 in S2 *Drosophila* cell lines, as visualized by anti-CD4 immunocytochemistry **(Figure 3-4).** S2 cells show similar $SNAP_f$-CD4 dependent staining with SS-A488 (100 nM, **Figure 3-5, Figure 3-4a-b**), with a 37-fold enhancement in fluorescence intensity in $SNAP_f$-CD4 positive cells compared to non-expressing cells (**Figure 3-5c**). SS-A488 staining in S2 cells is also retained post-fixation **(Figure 3-4).**

Validation of UAS- SNAP$_f$-CD4 transgenic fly lines

To evaluate the performance of cell surface-expressed SNAP$_f$-CD4 in live brains, we generated transgenic flies for both Gal4/UAS (pJFRC7) and LexA/op (pJFRC19) **(Figure 3-6)** expression (Best Gene Inc.). Crossing the resulting UAS-SNAP$_f$-CD4 line with a pan-neuronal driver line, neuronal synaptobrevin-GAL4 (nSyb-GAL4) resulted in staining of all neurons in the *Drosophila* brain[12]. Brains of nSyb-GAL4>SNAP$_f$ -CD4 flies show robust CD4 and HA expression **(Figure 3-7a, Figure 3-8 a and d)**, unlike controls which do not express SNAP$_f$-CD4 **(Figure 3-7b, Figure 3-8 b and e)**. The anti-CD4 and anti-HA fluorescence pattern indicates good localization to the plasma membrane, as the immunofluorescence is isolated from the Hoechst nuclear counterstain in confocal optical sections **(Figure 3-7b).**

Development and assessment of live brain Hybrid IHC

In developing our dye loading protocol, we aimed to limit time required to perform the technique and number of tissue interactions. In **Figure 3-9a,** we schematize IHC and Hybrid IHC, highlighting each method in terms of these two aspects: time and tissue interactions. IHC takes up to 10-12 days and requires over 25 tissue interactions. Hybrid IHC dramatically decreases this time to approximately 1 hour with 10 tissue interactions. SNAP$_f$-CD4 and HaloTag-CD4 extracellular tether dye loading protocol requires only 1-2 tissue interactions and takes approximately 15 minutes in total. The short labeling time with SNAP$_f$-CD4 and HaloTag-CD4 may facilitate assessment of neuronal anatomy after functional imaging studies.

To evaluate the ability of SNAP$_f$-CD4 and HaloTag-CD4 to label a variety of Gal4 expression patterns with varying depth, complexity, and specificity, we expressed them under four commonly used Gal4 driver lines, GH146-Gal4 **(Figure 3-9b),** Nanchung-Gal4 **(Figure 3-9c)**, OK107-Gal4 **(Figure 3-9d),** and Fruitless-Gal4 **(Figure 3-9e)**. We loaded these live brains with either HT-TMR[1] or SS-549 (a highly soluble, red-shifted dye, 1 µM), respectively. We found that these dyes robustly labeled the expected neuronal populations for each line regardless of depth, complexity, or specificity and showed high-intensity staining with minimal background fluorescence.

SNAP$_f$-CD4 labeling of genetically defined cell populations is not only fast but also flexible, as it is compatible with a wide range of spectrally-tuned dyes **(Figure 3-10a).** To illustrate this, we loaded GH146-Gal4>SNAP$_f$-CD4 brains with SS-A488, a green dye **(Figure 3-10b)**, SS-549, a red-shifted dye **(Figure 3-10c)**, or SS-A647, a far red-shifted dye **(Figure 3-10d)**. These live brains show the expected expression pattern in the antennal lobe, labeling both cell bodies and dendritic fields with high intensity and minimal background staining. The “plug and play” feature of SNAP$_f$-CD4 and HaloTag-CD4, i.e., the ability to rapidly switch colors to suit the needs of a specific experiment, distinguishes our system from the expression of fluorescent proteins.

Live brain registration using SNAP$_f$-CD4.

We next sought to register live brains to an anatomical template brain to allow for direct comparisons of anatomy across different specimens. During the registration process, brain images are transformed via rigid, linear, and non-rigid, non-linear, transformations to match the coordinate space of an anatomical template brain[13,14]. Once transformed to template space, one can directly compare the expression patterns and single-cell projection patterns to existing anatomical databases such as FlyCircuit[15] using the similarity algorithm NBLAST[2]. Registration is most often performed using immunostaining for BRP (Brush pilot), a pan-neuronal marker for neuropil regions, which creates a strong counterstain for neuronal anatomy. Here, the BRP staining must be uniform and permeate evenly throughout the sample for the registration to properly align the samples.

To transition registration methodology for in vivo work, we first needed to label structures throughout the brain uniformly. This uniform labeling had previously been shown in fixed and permeabilized tissue using an intracellular $SNAP_f$::BRP fusion protein[16]. We thus took this opportunity to compare dye loading of intracellular proteins with that of our extracellular localized tags. Loading the original $SNAP_f$::BRP line with cell-permeable dye JF-546[17], the dye localized mainly to the superficial layers of the live brain and did not evenly label deep brain structures (**Figure 3-11a,c**). Pan-neuronally expressed nSyb-Gal4>$SNAP_f$-CD4 loaded with cell impermeant SS-A647 showed uniform and penetrant staining (**Figure 3-11b,d**).

Interestingly, pan-neuronal $SNAP_f$-CD4 labeled with SS-A647, **(Figure 3-12a)** closely recapitulated BRP immunohistochemistry, as shown in **(Figure 3-12b)**, which depicts the JFRC2010 template[14], a single female brain immunostained for BRP. We thus hypothesized that the pan-neuronal $SNAP_f$-CD4 could be used to register brains to template space directly. Testing this hypothesis, we loaded nSyb-Gal4>$SNAP_f$-CD4 with SS-A467 (10 µM) and found that we could readily register brains to the JFRC2010[14] template using the CMTK registration algorithm[18]. To assess the efficacy and accuracy of our staining, we generated a data set of 17 female and 11 male live-loaded brains, which we registered to JFRC2010 **(Figure 3-12a-c).** We had an approximately 50% success rate across all brains sampled (6/17 females and 8/11 males). We determined successful registrations by overlaying the registered live brain data **(Figure 3-12a)** with the template brain **(Figure 3-12b)** and qualitatively comparing the regional overlap of the various structures within the brain (See Methods) **(Figure 3-12c)**. Brains that failed often had poor alignment due to a poor imaging orientation or minor damage to tissue resulting from the dissection process.

We quantitatively evaluated the registration quality across 10 randomly selected brains (5 male, 5 female). using two independent measures: Dice Coefficient and Symmetric Euclidean Distance. Dice Coefficient **(Figure 3-12d)** measures the areal overlap between a registered brain region and its corresponding region on the template brain. To select the regions for comparison, we used the template-defined regions of interest determined by Ito et al. 2014[19] and compared those to experimenter-drawn regions of interest throughout each brain structure at 5 µm steps in the z-dimension **(Figure 3-12d, Figure 3-13)**. We chose four brain regions, Antennal lobe (AL), Antero ventrolateral

protocerebrum (AVLP), Mushroom body (MB), and Suboesophageal zone (SEZ), which vary in both depth and complexity throughout the brain. All four brain regions registered with over an 80% areal overlap at their best-registered z-plane **(Figure 3-12e, Figure 3-14).** We also calculated the average boundary as the mean symmetric Euclidean distance or the average of the shortest distance between the template ROI and the experimenter drawn ROI and the symmetric computation **(Figure 3-12f)**. Using this method, we found that the average boundary error was between 4-6 µm across all four brain regions **(Figure 3-12g)**. This resolution is approximately one order of magnitude larger than reported for immunostaining registration to template[23]. The average boundary error could be improved by generating a live template brain that can be bridging registered to the JFRC2010 template space. Further investigating boundary error, we calculated the error for each z-plane at 5 µm steps within the sample. We found that central portions of most brain regions showed low boundary error and that the extremes of structures tended to show the most dramatic boundary error, a trend also seen in the Dice Coefficient **(Figure 3-13)**.

To further assess the quality of registration using live staining and access anatomical databases via similarity searches, we performed an NBLAST search using live registered brains. We expressed GFP::CD8 under a sparse LexA driver line R34G02-LexA, which labels a single bilateral neuron pair in the suboesophageal zone called interoceptive neurons or ISNs[20]. We registered these brains using pan-neuronally expressed $SNAP_f$-CD4 labeled with SS-A647. Manually tracing the right projection pattern of the ISN produced the target neuron for our search (**Figure 3-15 a**). To create our query database, we seeded a database of 15,500 single neurons[15] and expression patterns[21] with a manually traced ISN neuron from an immunostained and registered brain (**Figure 3-15 b)**. We then performed an NBLAST search using our live registered brain and our seeded database. The immunostained ISN trace was the top hit with a mean normalized NBLAST score of 0.2. **Figure 3-15 c** shows an overlay of the top 5 hits, showing neurons with arbors that overlap with the ISNs.

Discussion

In summary, we show that extracellularly anchored small molecule tethers HaloTag-CD4 and $SNAP_f$-CD4 can be used to covalently label genetically defined populations of cells with commercially available dyes both in cultured cells and in live *Drosophila* brain tissue. We show that UAS-$SNAP_f$-CD4 can be used to directly register brains to template space with an approximately 4-6 µm error in registration. We also use live registered brains to access neuronal morphology databases using the similarity search NBLAST. The hybrid chemical-genetic nature of our system provides a high level of flexibility: a broad spectrum of dyes are available for immediate application and may be selected for use without the generation of a novel transgenic fly. This multiplexing of anatomical and physiological experimentation can be used simultaneously or sequentially within the same live sample.

Despite these advances, several drawbacks are associated with this technique at present. First, it is entirely Gal4/LexA dependent and thus may not yield satisfactory results in weaker expressing lines. This issue may be evaded in the future via the addition of tandem repeating small molecule targeting proteins, which can be secreted to the

extracellular surface[5]. This may also be mitigated by the expression of UAS-Gal4 or op-LexA reporter lines to increase the expression of the activator protein in positive cells. Secondly, we are only able to register the first half of the brain. This is a result of the lack of soluble Snap Tag reactive dyes with a large 2-photon cross-section [22], the generation of which would permit deeper light penetration and resolution throughout the entire brain. Our current methodology is not as accurate at registering brains or revealing fine neuronal arborizations as IHC [23] or Hybrid IHC[24] as shown by the larger boundary error and inability to visualize small neurites in the GFP labeled expression patterns. In specific situations, these issues may hinder its usefulness in neural identification. This is potentially due to the need for rapid acquisition (under 15 minutes) of images to prevent morphological changes to the brain structure in explant brains and could be mitigated by the application and imaging of the brain in the intact fly. Future endeavors should focus on optimizing the system for high-resolution microscopy in the intact fly and determining best practices for registration, including algorithm, sample preparation, and template selection. It is important to note that our study is not the first to register live brains to a template. Other groups have been able to do this by registering intracellularly expressed Td-Tomato imaged under two-photon excitation[25–27]. Although these tools can be used to register whole brain, they have not been used to perform morphology similarity searches in vivo, and are restricted to the use of TdTomato wavelengths. Our technique complements existing systems by offering spectral flexibility and rapid visualization.

Ultimately, we have generated a novel series of extracellular small molecule tethering proteins. We have shown that these tools offer a fast and flexible method for anatomical analysis both in cell culture and in live *Drosophila* brain tissues. These tools may be adopted for live brain staining as presented here as well as for genetic targeting of other small molecules such as drugs, actuators, and probes to the extracellular surface.

Methods

Plasmid construction.

We included a secretion signal derived from the signal peptide of the *Caenorhabditis elegans* β-integrin PAT-3 at the N-terminus of HaloTag, with the 5' UTR from heat shock protein 70 (hsp70) and the 3'UTR and polyA tail from SV40 early genes, as described previously.[27]
For expression in HEK cells, we subcloned HaloTag via restriction digest (NheI, SalI) and subsequent Gibson Assembly into pCDNA3.1 vector containing a cytomegalovirus (CMV) promoter, a 5' PAT3 secretion signal, and a 3' CD4 transmembrane domain. For expression in S2 cells and transgenic generation, the insert Pat3-HaloTag-CD4 was assembled into pJFRC7[29] backbone via restriction digest (XhoI and XbaI removed CD8::GFP) and Gibson assembly (Addgene). All constructs were sequence confirmed by the UCB Sequencing Facility. Sequences used for all constructs can be found in the attached electronic construct maps.

Scheme 3-1. Construct maps of mammalian and *Drosophila* constructs

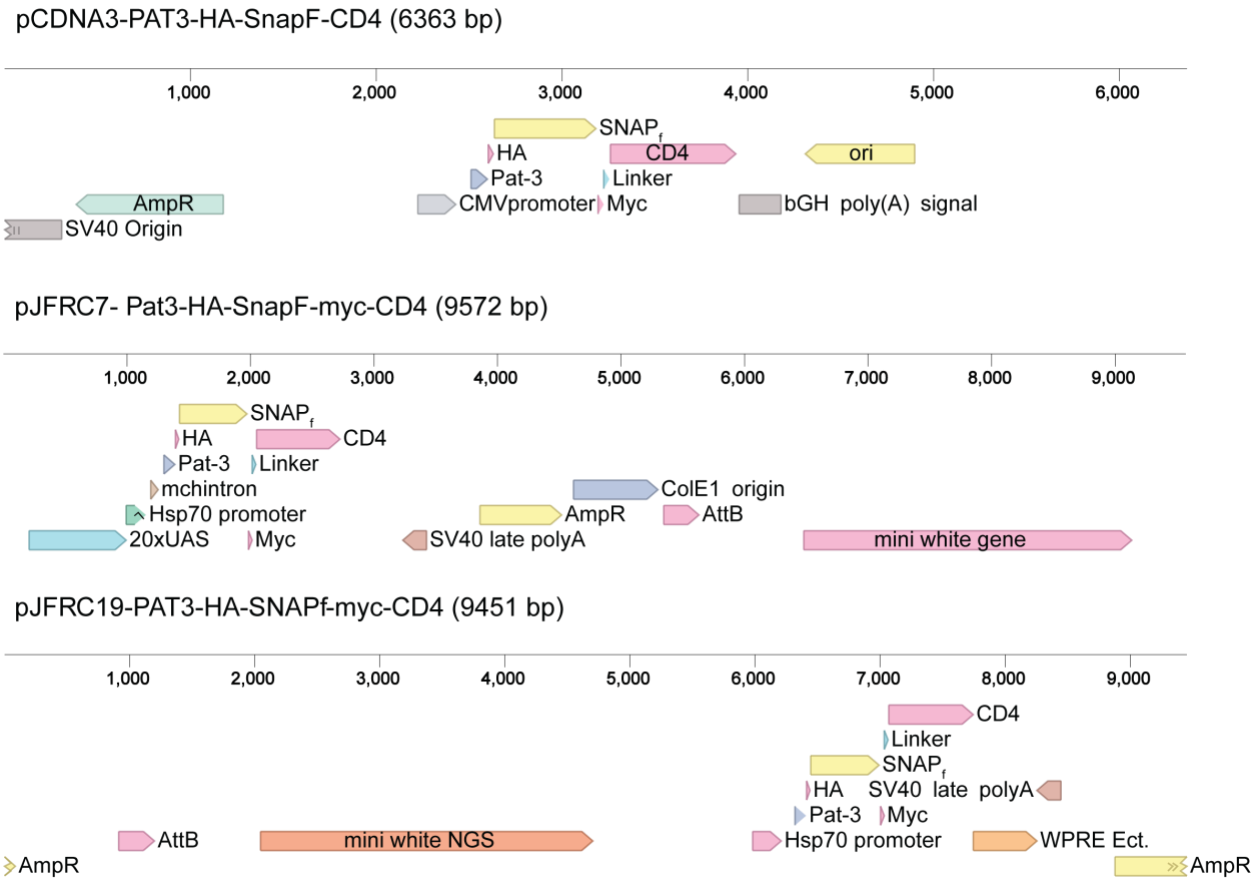

Cell culture and transfection.

We obtained all cell lines from the UCB Cell Culture Facility. Human embryonic kidney 293T (HEK) cells were maintained in Dulbecco's modified eagle medium (DMEM) supplemented with 1 g/L D-glucose, 10% fetal bovine serum (FBS; Thermo Scientific), and 1% GlutaMax (Invitrogen) at 37 °C in a humidified incubator with 5 % CO2. Cells were passaged and plated in DMEM (as above) at a density of 50,000 cells onto 12 mm coverslips pre-treated with Poly-D-lysine (PDL;1mg/ml; Sigma-Aldrich). Plasmid transfection was carried out using Lipofectamine 3000 (Invitrogen) 12 hours after plating. Imaging was performed 36 hours after plating.
S2 Cells were maintained in Schneider's *Drosophila* media (Thermo Fisher Scientific) supplemented with 10% FBS at 28°C in a non-humidified incubator under atmospheric conditions. Cells were passaged and plated at 500,000 cells per well in a 24 well plate. Six hours after plating, Tubulin Gal4 pCaSper (Addgene #17747)[30] was cotransfected with pJFRC7 constructs using a modified Lipofectamine 3000 (Life Technologies) protocol. This protocol included a 20-minute preincubation of lipofectamine and DNA in Opti-MEM (Life Technologies) and no p3000 reagent. Forty-eight hours after transfection, S2 cells were transferred onto PDL (1 mg/mL) treated 12 mm coverslips and allowed to adhere for 30 minutes before dye loading and imaging.

Dye loading.

We maintained DMSO stock solutions (100 µM) of all dyes at -80 °C in single-use aliquots. Aliquots were further diluted to a working concentration of 100nM in HBSS and incubated with cells for 30 minutes at 37 °C for HEK cells and room temperature for S2 cells. We then replaced all dye-containing HBSS with fresh HBSS and imaged in HBSS at room temperature.

Epifluorescence microscopy.

Imaging was performed on an AxioExaminer Z-1 (Zeiss) equipped with a Spectra-X Light engine LED light (Lumencor), controlled with Slidebook (v6, Intelligent Imaging Innovations). Images were acquired with a W-Plan-Apo 20x/1.0 water objective (20x; Zeiss) and focused onto an OrcaFlash4.0 sCMOS camera (sCMOS; Hamamatsu). The optical setup for imaging with each dye is described below.

Table 3-1. Optical filter sets for epifluorescence microscopy

Dye	Excitation	Emission	Dichroic
mSNAP2, SS-A488	475/34 nm BP	540/50 nm BP	510 nm LP
A647	542/33 nm BP	650/60 BP	594 nm LP
Hoechst 33342	375-400nm	405/40 BP	415 LP

Epifluorescent image analysis.

For fluorescence intensity measurements, regions of interest were drawn around cell bodies, and fluorescence was calculated in ImageJ (FIJI), NIH). We identified transfected cells by setting a threshold that excluded all cells in the non-transfected controls. We calculated the fold change between non-transfected and transfected cells by taking the ratio of transfected cells fluorescence and non-transfected cell fluorescence. For each condition, at least 100 cells were circled across three to five individual coverslips.

Immunocytochemistry.

Immediately following live-cell dye loading experiments, cells were fixed for 20 minutes at room temperature with 4% formaldehyde in PBS. Cells were washed in PBS (3x 5-minute washes) and treated with either 0.3% Triton X-100 in PBS for the permeabilized condition or PBS for the non-permeabilized condition. Cells were again washed in PBS and blocked for at least 45 minutes in 0.1% NGS in PBS. Cells were then incubated overnight at 4 °C with 1:500 mouse anti CD4 (OKT4; Thermo Fisher Scientific). We then washed each sample in PBS and stained with a spectrally compatible mouse secondary Goat anti-Mouse A488 (Life Technologies) or Goat anti-Mouse A594 (Life Technologies) 1:1000 in 0.1%NGS for 2hrs at room temperature. We added Hoechst 33342 (10mg/mL, -20 stock) 1:1000 for the last 15 minutes of this incubation period. Cells were washed (3 x 5-minute washes) in PBS and mounted onto glass slides using Fluoromount Mounting Media (VWR International) before imaging.

Transgenic generation.

pJFRC7-Pat3-SNAP$_f$-CD4 were sent to Best Gene Inc. for injection into the following genomic sites via phi-C31 integration.

Table 3-2. Injection phi C31 site and stock line

Construct	Injection Site	Injection Stock
pJFRC7-Pat3-SNAP$_F$-CD4	VK05	#9725

Immunohistochemistry.

Fly brains were dissected in calcium magnesium-free artificial hemolymph (AHL-/-; NaCl 108.0 mM, KCl 5.0 mM, $NaHCO_3$ 4.0 mM, $NaH_2PO_4 \cdot H_2O$ 1.0 mM, Trehalose· 2 H_2O 5.0 mM, Sucrose 10.0 mM, HEPES 5.0 mM and adjusted to pH 7.5 with NaOH) and fixed for 20 minutes in 4% formaldehyde in PBS. Brains were then washed in PBS (3x 5-minute washes) and treated with either 0.3% Triton x -100 in PBS for the permeabilized condition or PBS for the non-permeabilized condition. Brains were again washed in PBS and blocked for at least 45 minutes in 0.1% NGS in PBS. Cells were incubated for 5 days in block containing 1:50 RT anti HA (Sigma Aldrich) and 1:100 mouse anti CD4 at 4 °C. Brains were then washed in PBS (3 x 5-minute washes) and stained with Goat anti-Rat A488 (Life Technologies) 1:1000 and Goat anti-Mouse A594 (Life Technologies) in block for 4 hours at room temperature shaking. We added Hoechst 33342 (10 mg/mL) 1:1000 for the last 15 minutes of this incubation. Brains were then washed and mounted onto glass slides using Vectashield mounting media (Vector Laboratories) before imaging using confocal microscopy.

PLL Coverslips.

PLL was prepared using the FlyLight recipe. (https://www.janelia.org/sites/default/files/FL%20Recipe%20-%20Poly-L-Lysine%20.pdf). Briefly, PLL (Sigma Aldrich. # P1524-25MG) was thawed to room temperature and diluted with 2mL of double-distilled water, transferred to a 50 ml conical vial, and further diluted with 30mL of double-distilled water. 64uL Photo-Flo (Electron Microscopy Sciences. # 74257) was added to this mixture and vortexed. Coverslips were then dipped into PLL and placed on a Kim wipe while drying overnight. Once dried, coverslips were stored at -20 until use.

Dye loading and imaging for expression patterns

Flies aged 10 days post eclosion were dissected in ice-cold AHL-/-. Brains were stored on ice in calcium magnesium-free AHL during the remainder of the dissections (no longer than 20 minutes) before loading with 1 µM Surface Snap DY-549, SS-A488 or SS-A647 in AHL-/- for 15 minutes at room temperature. Brains were then mounted onto PLL coated coverslips and covered with AHL-/- for imaging. Imaging was performed with an LSM 880 scanning confocal microscope under a 20x objective water immersion objective (W Plan-Apochromat 20x/1.0 DIC Vis-IR M27 75mm). Z-stacks were taken under the following settings for 3 µm z-step size, 1024 x 1024 pixels, 0.59 µm x 0.59 µm pixel size, and 1.37

µs pixel dwell time. For deeper samples, the laser power was increased gradually as the focal plane depth increased to reduce the effect of light scattering.

Table S3-3. Confocal microscopy settings for brain registration

Dye	Excitation	Emission
SS-A488	488 nm	490-650 nm
SS-DY549	561 nm	564 –739 nm
SS-A647	633 nm	638-755 nm

Dye loading and imaging for registered brains

Flies aged 10 days post eclosion were dissected in ice-cold AHL-/-. Brains were stored on ice in AHL-/- during the remainder of the dissections (no longer than 20 minutes) before being loaded for 15 minutes with 10 µM Surface Snap A647 in AHL-/- containing 0.2% Pluronic F127 (resuspended in DMSO). Brains were then mounted onto PLL coated coverslips and covered with AHL-/- for imaging. Imaging was performed with an LSM 880 scanning confocal microscope under a 20x objective water immersion objective (Type). Z-stacks were taken under the following settings for 1 µm z-step size, 1024x 1024 pixels, 0.59 x0.59 µm pixel size, and 1.03 µs pixel dwell time . For deeper samples, the laser power was increased gradually as the focal plane depth increased to reduce the effect of light scattering.

Table S3-4. Confocal microscopy settings for brain registration

Dye	Excitation	Emission
SS-A647	633 nm	638-755 nm

Image analysis.

Each confocal stack was collapsed into a maximum intensity projection (Gal4 expression patterns) or average intensity projection (LexA>CD8::GFP expression patterns). For segmented images, projections were traced and filled using Simple Neurite Tracer (FIJI), and all regions not in that projection fill were removed from the image. This was performed to remove autofluorescence background in LexA>CD8::GFP flies which can be high in regions such as the optic lobes.

Registration.

Confocal stacks were registered using the method described in Cachero et al. 2010[14]. Briefly, confocal stacks were reoriented manually in FIJI to best match template orientation and resized to 0.62µm x 0.62µm x 1µm pixel size. Brains were then registered to JFRC2010 using the FIJI CMTK Registration GUI[14] run directly through terminal. Quality was then assessed manually by assuring that the brain structures were not warped or oddly shaped due to the reformatting. We also overlaid the template brain and the registered brain to assure that brain structures were maintained in shape and structure. Finally, each brain was then cropped at a distinct anatomical landmark where

the mushroom bodies end in the brain, and the z- plane was resliced so that each stack was 116 individual images. This final step was required to assure good alignment in the z-plane as only the first half of the brain accurately registers using our technique.

Dice Coefficient Analysis.

A Dice Coefficient defined areal overlaps between our registered brains and the template brains. Each region was then compared to the Ito region from that z-plane slice, and the Dice Coefficient was calculated using the following equation.

Where is the area of the Ito ROI and is the area of the experimenter drawn ROI.

Neuron fill generation.

Registered LexA>CD8::GFP expressing lines were traced and filled using Simple Neurite Tracer. These fills were converted to binary images and overlaid in 3D space using the plot3d function in Natverse [28] (R).

Symmetric Euclidean Distance.

Symmetric Euclidean Distance was measured using the ROIs drawn for Dice Coefficient and the original Ito ROIs. The symmetric Euclidean distance was defined as:

Where is the shortest distance from one point on the raw data to any point on the template data, and is the shortest distance from one point on the template data to any point on the raw data set.

NBLAST search.

NBLAST search was queried against 12,000 neurons of the FlyCircuit[15] database and all of the Janelia Gal4[21] database. The resulting query list contained approximately 15,500 neurons and was seeded with a trace of the interoceptive neurons from immunohistochemistry. The target consisted of a single traced neurite (Simple Neurite Tracer, FIJI) from a live brain registered to JFRC2010. The seed and live brain ISN data were transformed from JFRC2010 template space to FCWB via a bridging registration. NBLAST similarity search was performed using mean normalized comparisons, which compares the neurons bi-directionally to ensure a good match. Neurons selected as positive hits by this search were defined as those with a positive mean normalized similarity score.

Figures

Figure 3-1.

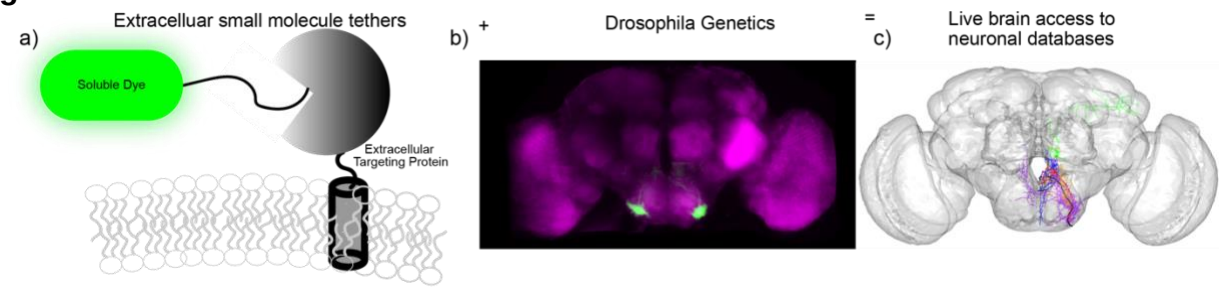

Figure 3-1. Chemical-genetic hybrids for neuron identification in live *Drosophila* brains. Commercially available Snap Tag reactive AlexaFluor and other soluble dyes with Benzyl-guanine reactive moieties will form covalent adducts with extracellularly targeted $SNAP_f$-CD4 or HaloTag-CD4 molecules. The use of GAL4-UAS and LexA/LexA-op fly lines enable selective expression of $SNAP_f$-CD4 fusions in genetically defined populations of neurons in the fly brain. The extracellular location of these tethering enzymes permits the use of commercially available, water-soluble dyes across the visual spectrum and the registration of live brains to template space giving access from light level data to Gal4 expression pattern anatomical databases.

Figure 3-2.

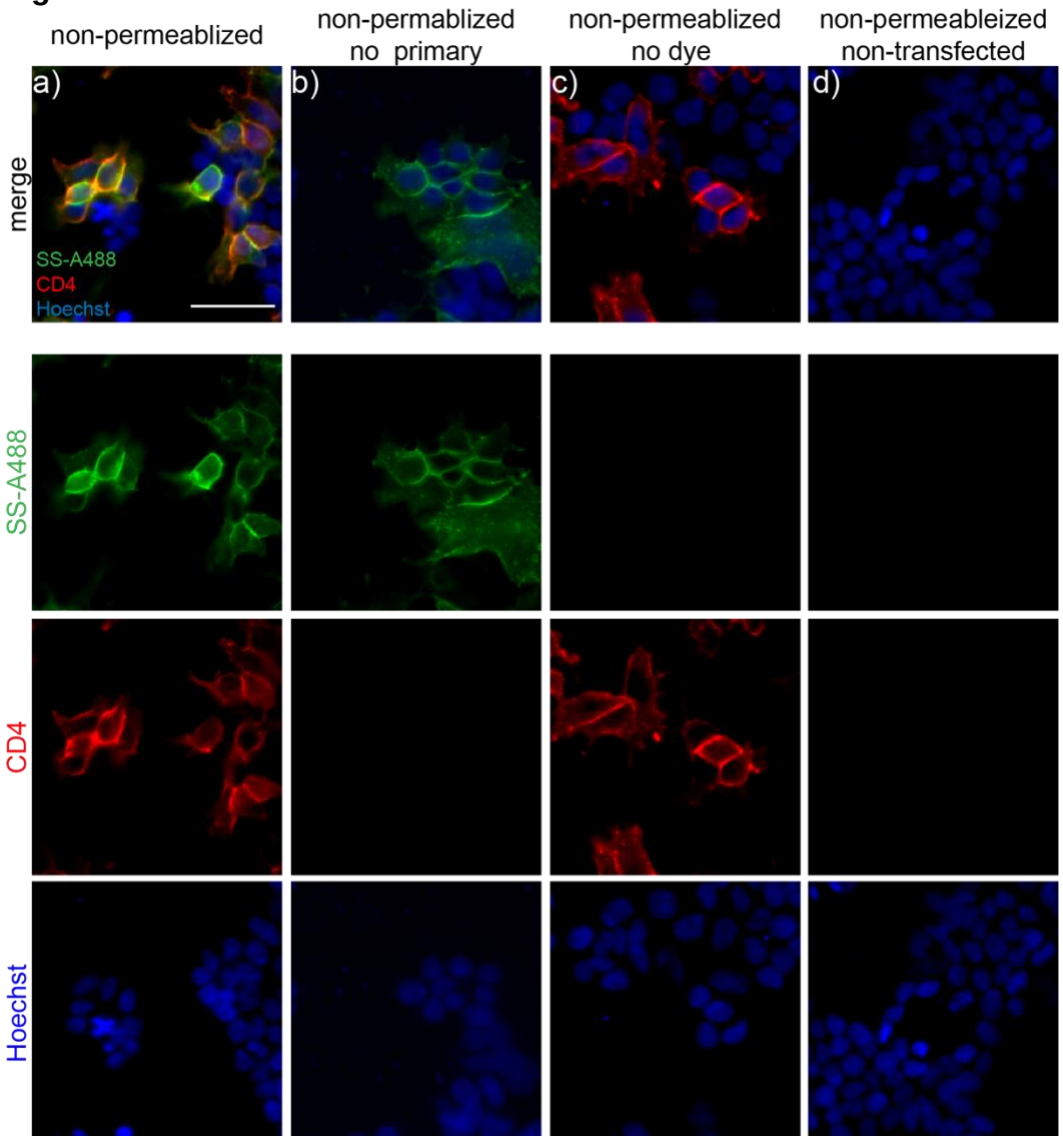

Figure 3-2. Immunocytochemistry of $SNAP_f$-CD4 expression in HEK293T cells. Epifluorescence images of HEK293T cells expressing $SNAP_f$-CD4 (CMV promotor) and stained with SS-A488 (100 nM, green). Cells were then fixed and stained under non-permeabilizing conditions for CD4 (red), and nuclear counterstained using Hoechst 33342 (at a concentration of 10 µg/ul, equivalent to 16 µM) **(a).** Controls were treated with **b)** dye but no primary CD4 antibody, **c)** primary antibody but no dye, and **d)** with dye and primary antibody but without transfection. Scale bar is 50 µm.

Figure 3-3.

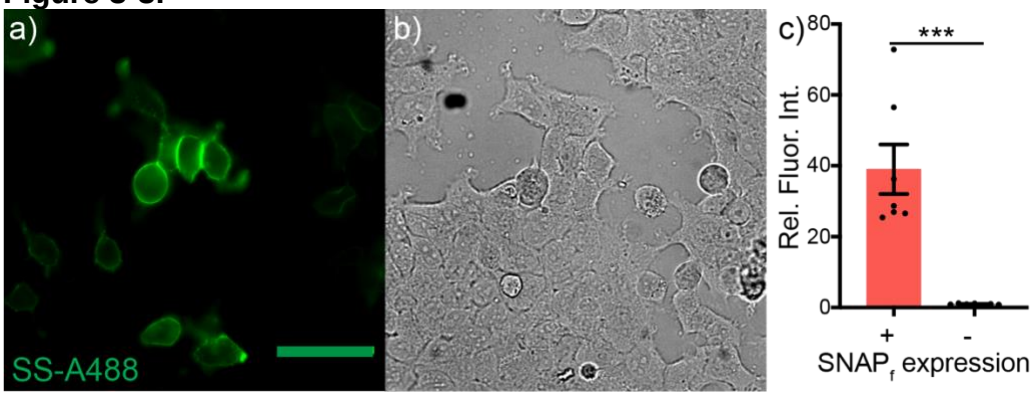

Figure 3-3. Live-cell staining with SS-A488 in HEK293T cells expressing SNAP$_f$-CD4. Epifluorescence images of HEK293T cells expressing SNAP$_f$-CD4 under the CMV promotor and **a)** stained with SS-A488 (100 nM, green). **b)** Transmitted light image of cells in panel **(a)** Scale bar is 20 µm. **c)** Plot of relative fluorescence intensity cells expressing and not expressing SNAP$_f$-CD4. SNAP$_f$ (+) cells were assigned based on a threshold obtained from a non-transfected control. Data are mean ± SEM for n = 6 different coverslips of cells. Data points represent mean fluorescence intensity of 20-30 cells. (t-test, $p < 0.0001$)

Figure 3-4.

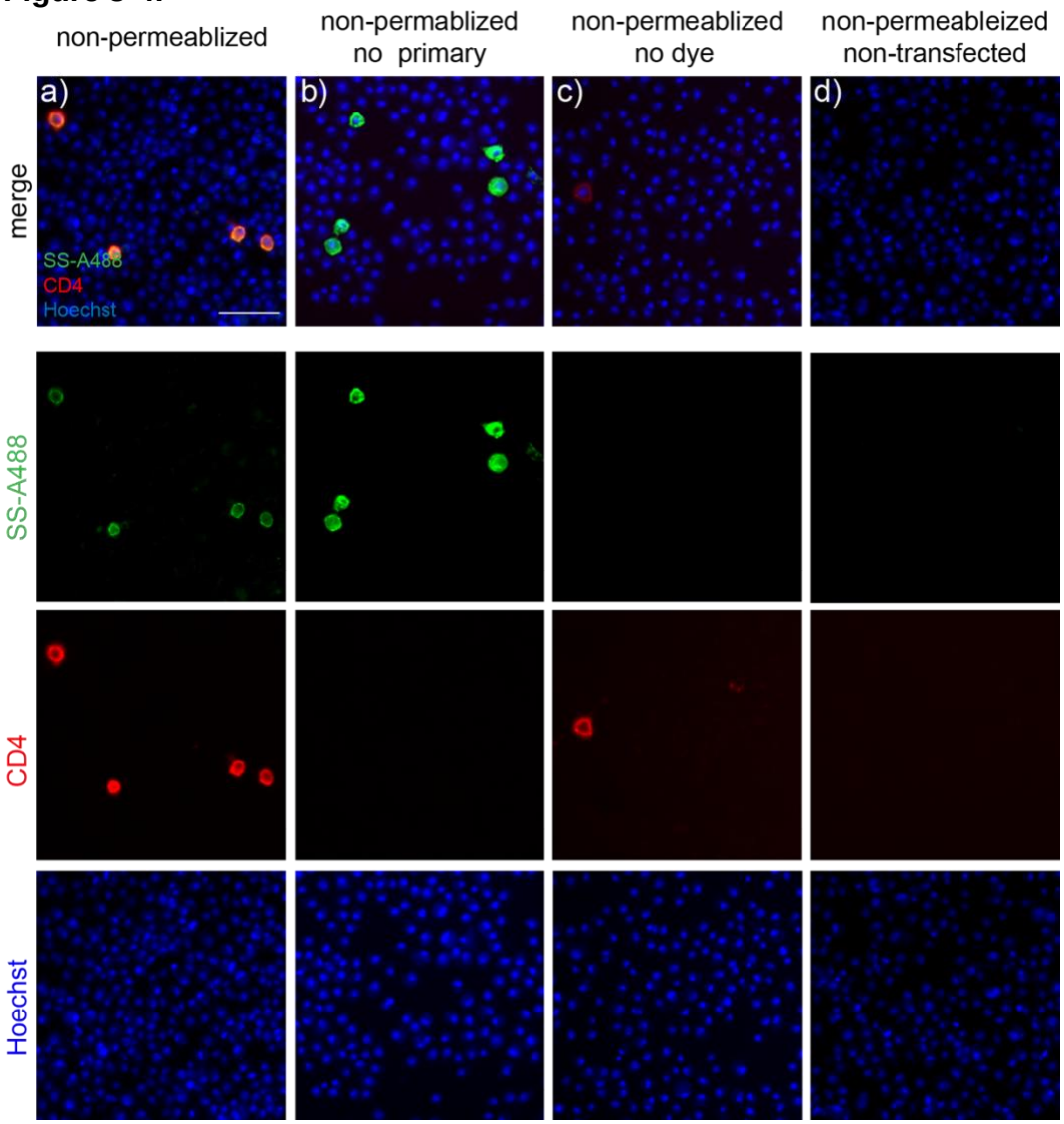

Figure 3-4. Immunocytochemistry in *Drosophila* S2 cells expressing $SNAP_f$-CD4. Confocal images of post hoc immunocytochemistry of *Drosophila* S2 cells expressing $SNAP_f$-CD4 (cotransfection with driver pTubulin Gal4 and UAS-$SNAP_f$-CD4) stained with SS-A488 (100 nM) fixed and stained for CD4 (red) under non-permeabilizing conditions **(a)**. Cells were nuclear counterstained using Hoechst 33342 (at a concentration of 10 µg/ul, equivalent to 16µM). Controls were treated with **b)** dye but no primary CD4 antibody, **c)** primary antibody but no dye, and **d)** with dye and primary antibody but without transfection. Scale bar is 50 µm.

Figure 3-5.

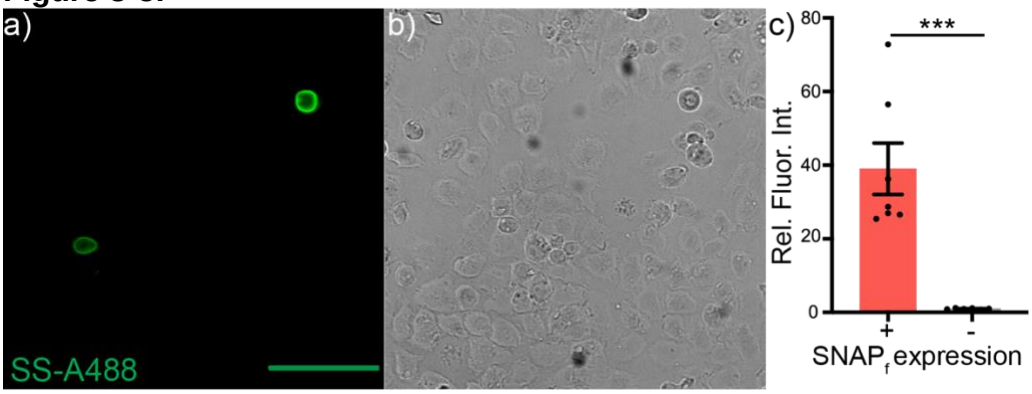

Figure 3-5. Live-cell staining in *Drosophila* S2 cells with SS-A488. Live-cell staining with SS-A488 in *Drosophila* S2 cells expressing $SNAP_f$-CD4. Epifluorescence micrographs of S2 cells expressing $SNAP_f$-CD4 under cotransfected pTubulin-Gal4 and **a)** treated with SS-A488 (100 nM). **b)** transmitted light image of panel **(a)**. Scale bar is 20 µm. **c)** Relative fluorescence intensities of $SNAP_f$-CD4 expressing cells and cells that do not express $SNAP_f$-CD4 from the same culture. $SNAP_f$ (+) cells were assigned based on a threshold obtained from a non-transfected control. Data are the SEM for n=7 cultures; data points represent the average fluorescence intensity of 20-30 cells. (t-test, $p < 0.0001$)

Figure 3-6.

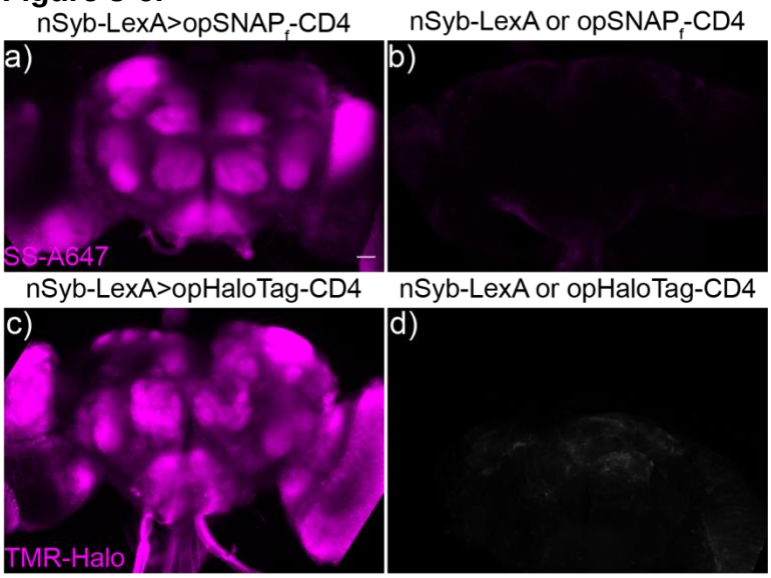

Figure 3-6. Dye loading in pan-neuronal op-SNAP$_f$-CD4 and op-HaloTag-CD4 LexA lines. Average confocal z- projection of **a)** nSyb-LexA>op-SNAP$_f$-CD4 brain or **b)** nSyb-LexA or op-SNAPf-CD4 genetic control brain loaded with SS-A647(10 µM). Confocal average z-projection of **c)** nSyb-LexA>op-HaloTag-CD4 brain or **d)** nSyb-LexA or op-HaloTag-CD4 brain loaded with TMR-Halo (10 µM). Scale for all images is 50 µm.

Figure 3-7.

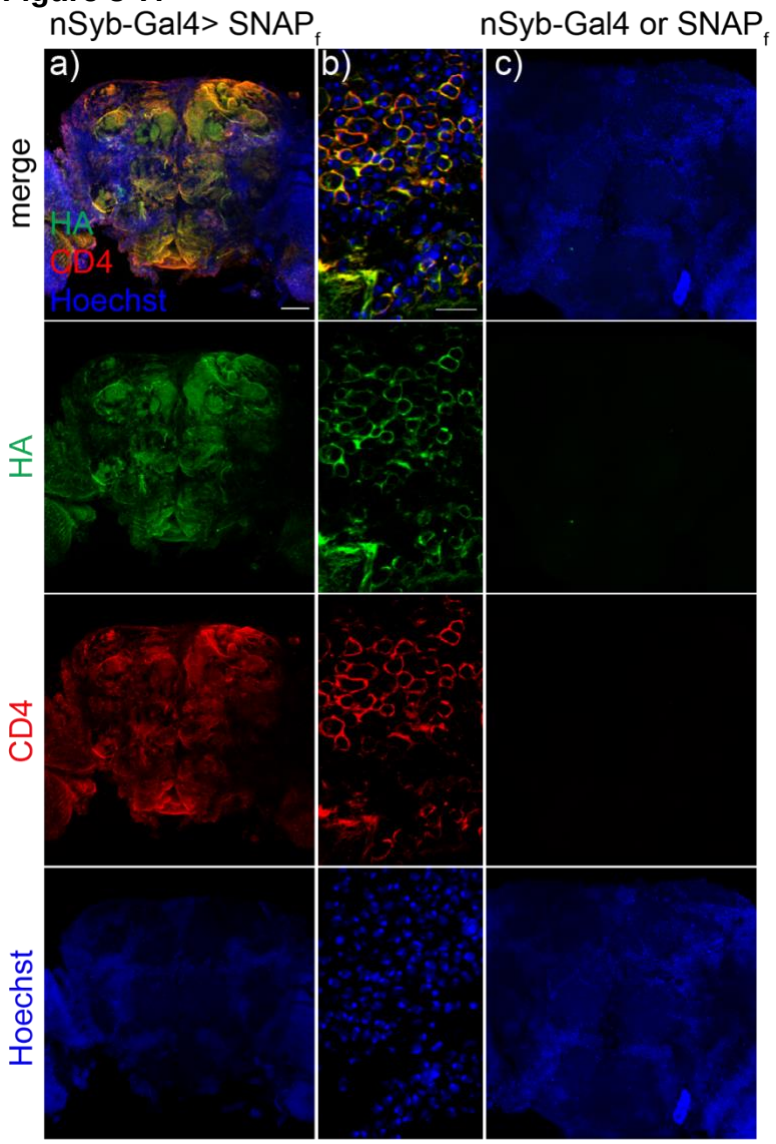

Figure 3-7. Immunohistochemistry of pan-neuronal SNAP$_f$-CD4 expression and trafficking in *Drosophila* brain. **a)** Maximum confocal z-projection of a fixed nSyb-Gal4, SNAP$_f$-CD4 brain stained under non-permeabilizing conditions for HA (green), CD4 (red) and nuclear counterstained using Hoechst 33342 (at a concentration of 10 µg/µL, equivalent to 16 µM) **b)** 63x single confocal plane of cells expressing SNAP$_f$-CD4 under the nSyb-Gal4 driver line as shown in panel **(a)**. **c)** maximum confocal z-projection of either nSyb-Gal4 or SNAP$_f$-CD4 brain, which does not express the SNAP$_f$-CD4 protein. Scale for all images is 50 µm.

Figure 3-8.

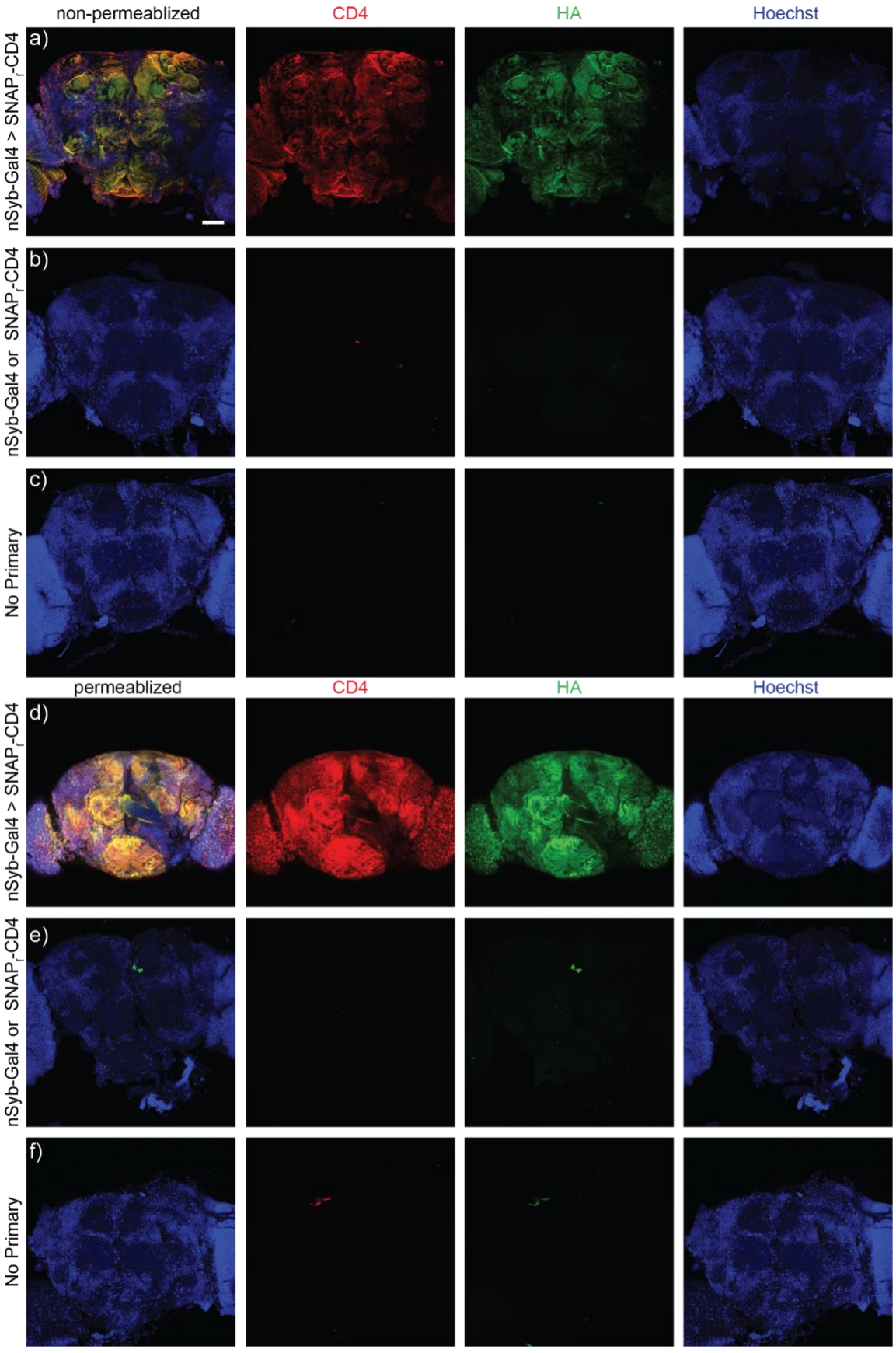
non-permeablized
CD4
HA
Hoechst
a)
nSyb-Gal4 > SNAP$_f$-CD4
b)
nSyb-Gal4 or SNAP$_f$-CD4
c)
No Primary
permeablized
CD4
HA
Hoechst
d)
nSyb-Gal4 > SNAP$_f$-CD4
e)
nSyb-Gal4 or SNAP$_f$-CD4
f)
No Primary

Figure 3-8. Permeabilized and non-permeabilized immunohistochemistry for $SNAP_f$-CD4 in pan-neuronal expressing nSyb-Gal4>$SNAP_f$-CD4 *Drosophila* brains. **a)** Maximum confocal z-projection of a fixed nSyb-Gal4, $SNAP_f$-CD4 brain stained under non-permeabilizing conditions for HA (green), CD4 (red), and nuclear counterstained using Hoechst 33342 (at a concentration of 10 µg/µL, equivalent to 16 µM). Controls were treated under non-permeabilized conditions in the **b)** absence of transgene expression ($SNAP_f$-CD4 or nSyb-Gal4) or **c)** absence of primary antibody. **d)** Maximum confocal projection of nSyb-Gal4, $SNAP_f$-CD4 brain treated with Triton x-100 before immunostaining for HA (green), CD4 (red), and nuclear counterstaining using Hoechst 33342. Controls were treated under permeabilizing conditions in the **e)** absence of transgene expression ($SNAP_f$-CD4 or nSyb-Gal4) or **f)** absence of primary antibody. Scale is 50 µm.

Figure 3-9.

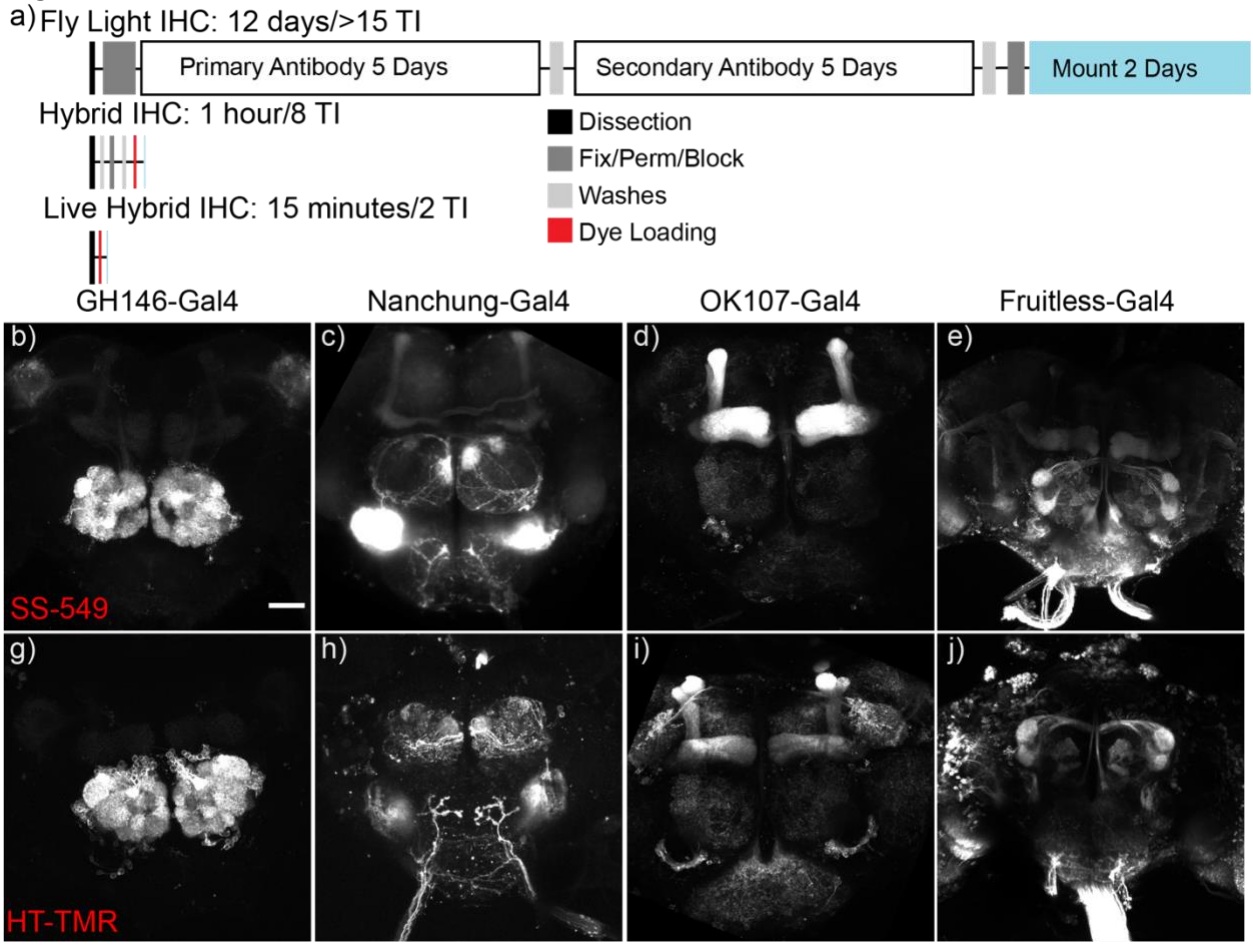

Figure 3-9. Dye loading of Gal4 expression patterns in explant brains. **a)** timeline comparing time required for common immunohistochemistry protocol from Fly Light (top), Hybrid IHC (middle), and live Hybrid IHC (bottom). Timeline includes total time required for each technique and the breakdown of each technical step and number of tissue interactions. Diagram is not to scale. Maximum confocal z-projection of live SS-549 dye (1 µM) loading in *Drosophila* explant brains expressing $SNAP_f$-CD4 under **b)** GH146-Gal4, **c)** Nanchung-Gal4, **d)** OK107-Gal4, and **e)** Fruitless-Gal4. Maximum confocal z-projection of live HT-TMR dye (1 µM) loading in explant brains expressing HaloTag-CD4 under **g)** GH146-Gal4, **h)** Nanchung-Gal4, **i)** OK107-Gal4, and **j)** Fruitless-Gal4. Scale for all images is 50 µm.

Figure 3-10.

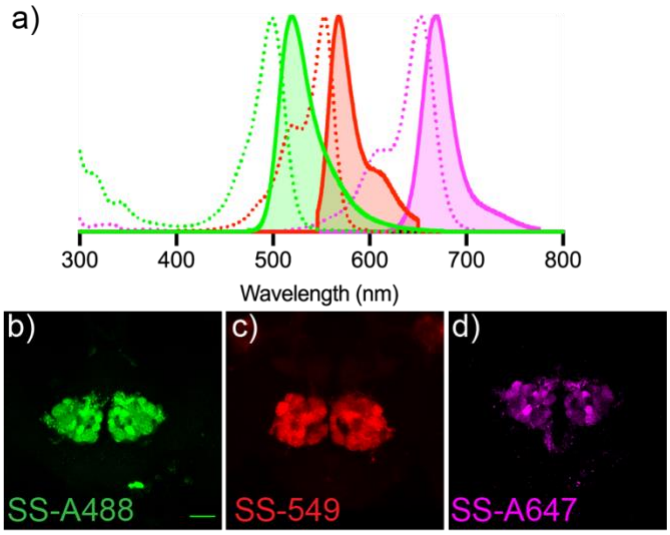

Figure 3-10. Multicolor dye loading in *Drosophila* explant brains. **a)** excitation (dotted lines) and emission (solid lines) spectrum for commercially available SS-A488 (green), SS-549 (red), SS-A647 (magenta). GH146-Gal4, $SNAP_f$-CD4 flies express $SNAP_f$ on the surface of a subset of olfactory projection neurons and can be labeled in live brain explants using **b)** SS-A488 (1 µM), **c)** SS-549 (1 µM) and **d)** SS-A647 (1 µM). Images are displayed as maximum z-projections and pseudo-colored to match the spectra displayed in panel (**a**). Scale is 50 µm.

Figure 3-11.

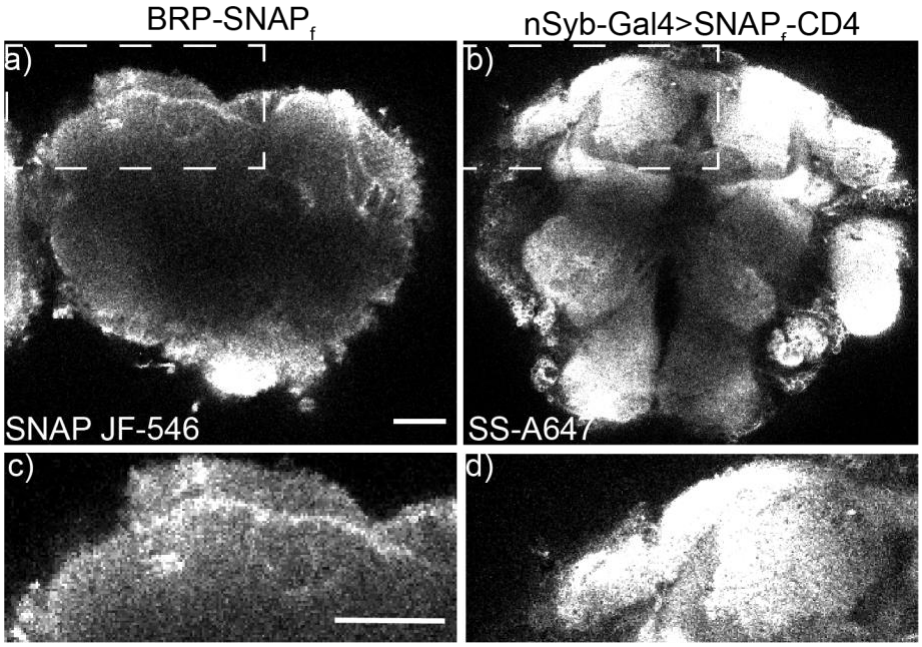

Figure 3-11. Genetic targeting of dye molecules in *Drosophila* brain using intracellularly targeted BRP-SNAP$_f$ and extracellularly targeted SNAP$_f$-CD4. **a)** Single plane confocal image of brain expressing BRP-SNAP$_f$ on the intracellular surface loaded with SNAP JF-546 cell-permeant dye. White box denotes region of protocerebrum selected for zoomed-in inlay in panel **c). b)** Single plane confocal image of brain expressing pan-neuronal SNAP$_f$-CD4 on the extracellular surface loaded with SS-A647 (10 µM). **d)** Zoomed-in region of protocerebrum from panel **b)** (denoted by white box). Scale for all images is 50 µm.

Figure 3-12.

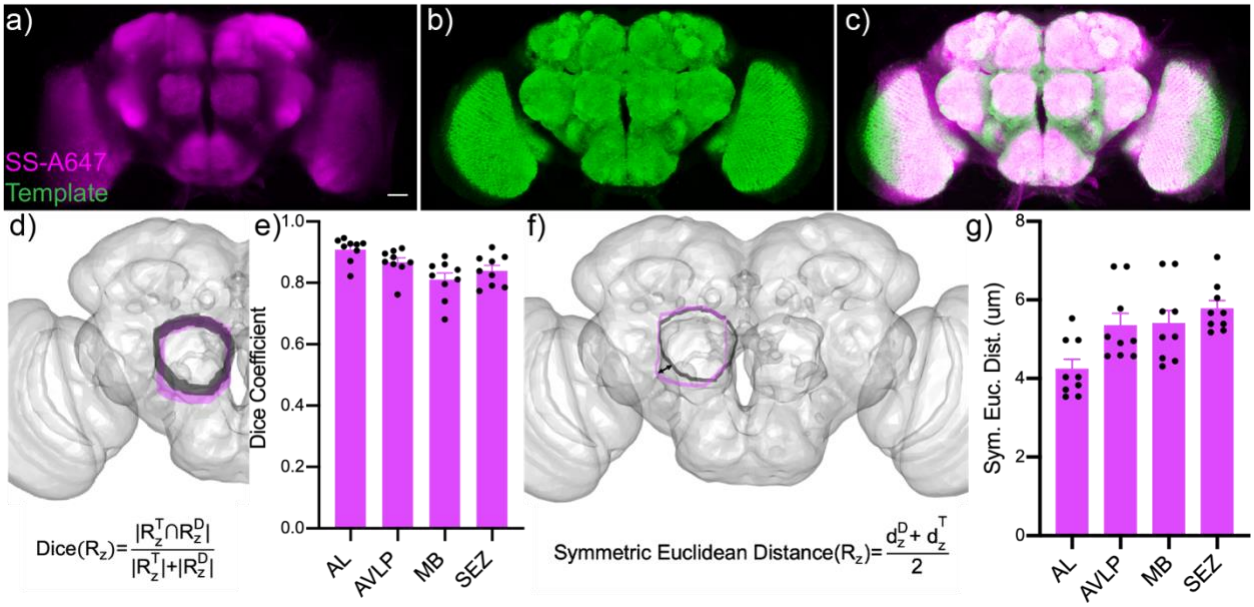

Figure 3-12. Live brain registration using SS-A647 and quantification of registration quality. Explant nSyb-Gal4>SNAP$_f$-CD4 brains were loaded with SS-A647 (10 µM) then registered to JFRC2010 template space using CMTK registration algorithm. **a)** Average z-projection of mean live brain data, constructed from the pixel-wise average of 10 individual confocal stacks of live brains stained with SS-A647 (5 male and 5 female) all registered to JFRC2010. **b)** Average z-projection of JFRC2010 template brain confocal image. **c)** 3D rendering of merged template (green) and mean live brain data (magenta). Scale for all images is 50 µm. **d)** Visual schematic of Dice Coefficient measure of areal overlap, where area of the Ito ROI (Grey) is compared to the area of the experimenter drawn ROI (magenta) using the equation depicted below. R^T is the area of the Ito ROI, and R^D is the area of the drawn ROI. **e)** Average Dice Coefficient ± SEM of the best-registered slice from each region. Each data point represents the Dice Coefficient from one slice of an individual brain registered to JFRC2010 (n=10, 5 male, 5 female). **f)** Schematic of the measurement obtained by Symmetric Euclidean Distance where the shortest distance from one ROI to another is averaged (d^D is shortest distance from Ito ROI to the drawn ROI and d^T is the shortest distance from the drawn ROI to the Ito ROI). **g)** Plot of average Symmetric Euclidean Distance for each individual brain (n=10, 5 female and 5 male) across all z planes for a specific region.

Figure 3-13.

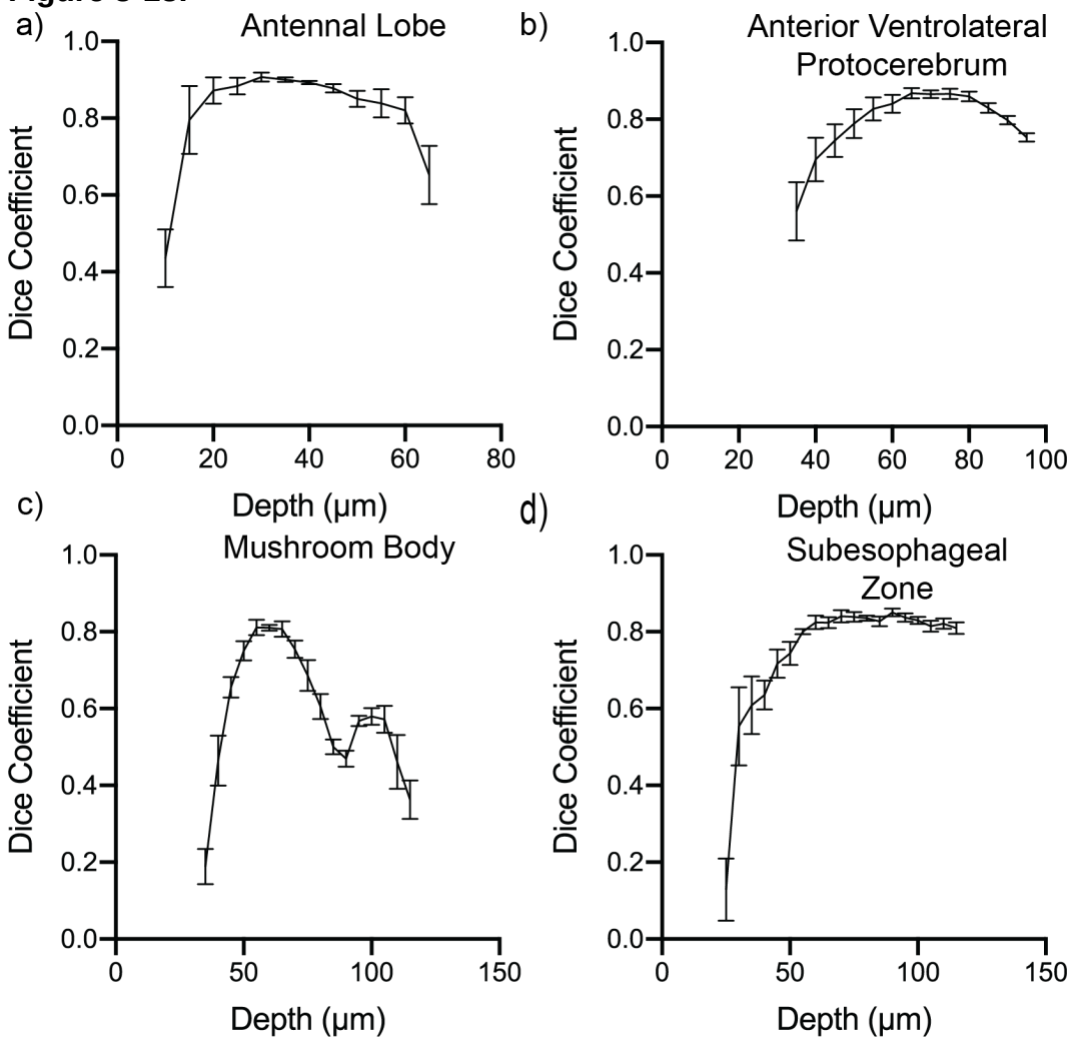

Figure 3-13. Dice coefficient across z planes at 5 μm steps throughout each anatomical structure. Average dice coefficient ± SEM for each individual plane taken at 5 μm steps through the first half of the brain or to the end of the structure for **a)** Antennal Lobe, **b)** Anterior Ventrolateral Protocerebrum, **c)** Mushroom Body, or **d)** Suboesophageal Zone. Data represent the average Dice coefficient ± SEM across 10 individual registered brains (5 male and 5 female).

Figure 3-14.

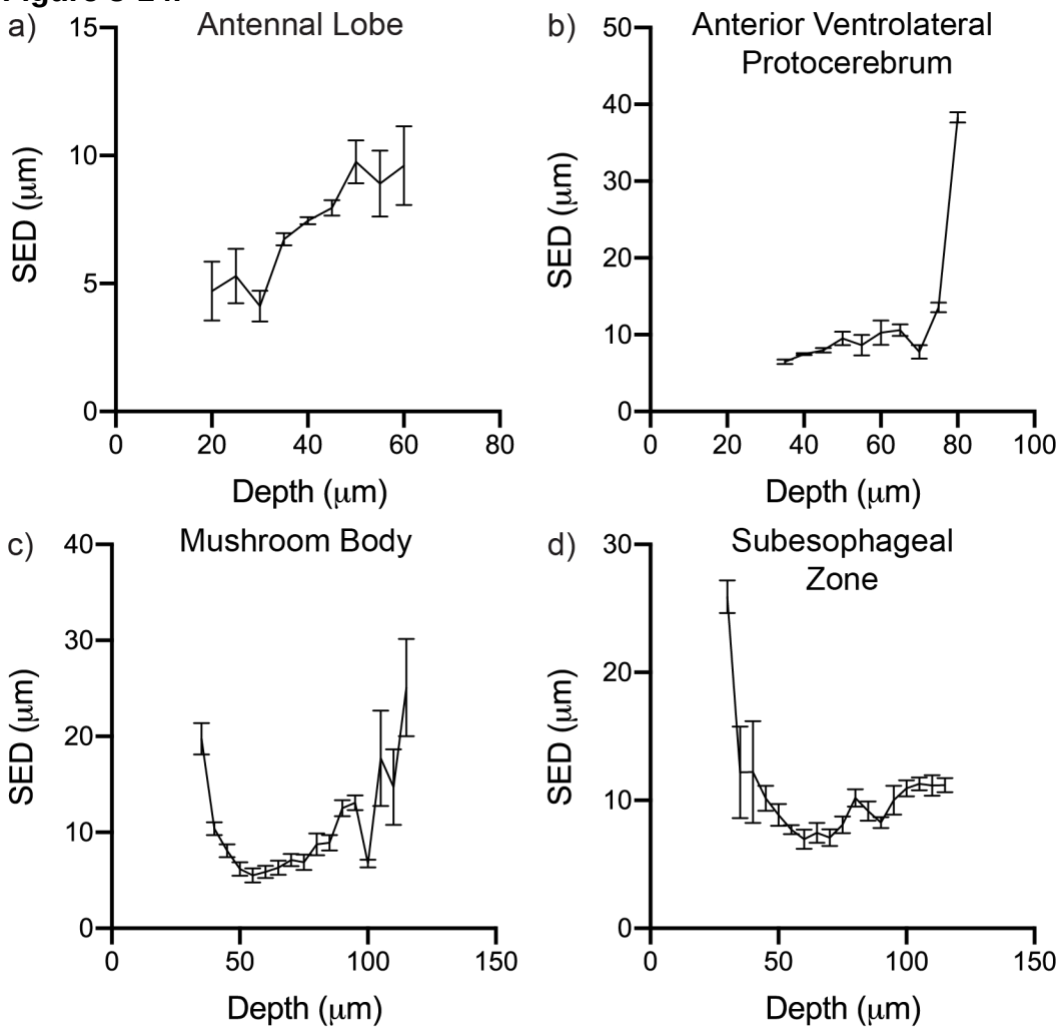

Figure 3-14. Average Symmetric Euclidean Distance across z planes at 5 µm steps throughout each anatomical structure. Average Symmetric Euclidean Distance across z planes ± SEM for each individual plane taken at 5 µm steps through the first half of the brain or to the end of the structure for **a)** Antennal Lobe, **b)** Anterior Ventrolateral Protocerebrum, **c)** Mushroom body, or **d)** Suboesophageal Zone. Data represent the average Symmetric Euclidean Distance for that z plane ± SEM across 10 individual registered brains (5 male and 5 female).

Figure 3-15.

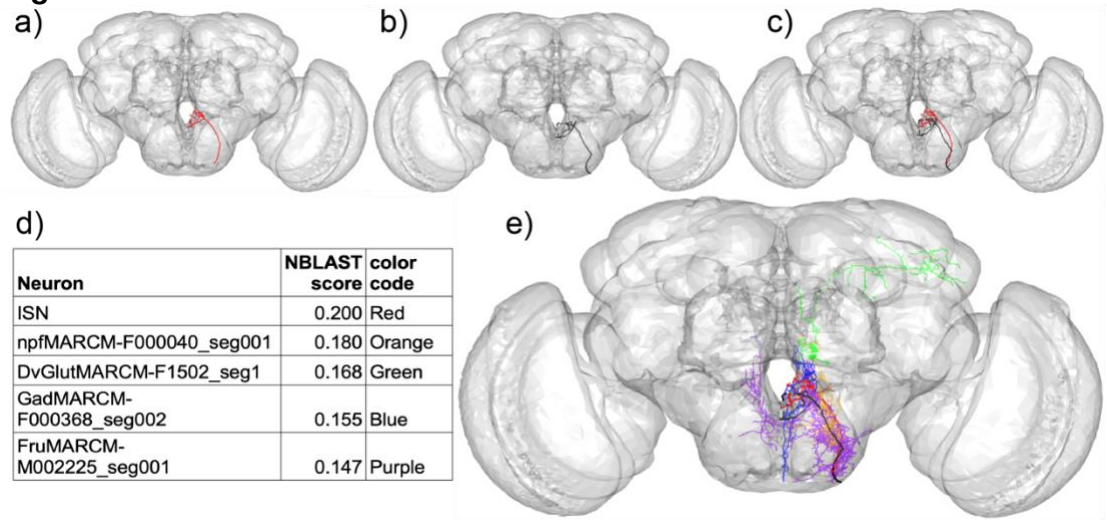

Neuron	NBLAST score	color code
ISN	0.200	Red
npfMARCM-F000040_seg001	0.180	Orange
DvGlutMARCM-F1502_seg1	0.168	Green
GadMARCM-F000368_seg002	0.155	Blue
FruMARCM-M002225_seg001	0.147	Purple

Figure 3-15. NBLAST search using live registered brain samples. The target ISN neuron manually traced expression pattern of R34G02-LexA>CD8::GFP and registered to JFRC2 using $SNAP_f$-CD4 tethered SS-A647 **(a,** black**).** Data was further bridged to FCWB template space for analysis. **b)** Query database seed for the ISN neuron generated from fixed and immunostained ISN neuron sample registered to JFRC2 and bridged to FCWB (red). **c)** Overlay of live brain ISN neuron (black) and fixed brain ISN neuron (red) registered to JFRC2 and bridged to FCWB. **d)** Table summarizing top 5 hits from NBLAST search, showing name of neuron fragment, mean normalized NBLAST score and color-code for panel **(e)**. Overlay of top five hits and their morphology traces overlaid and color-coded according to table in panel **(d).**

References

1. Kirk, M. J. *et al.* Voltage imaging in Drosophila using a hybrid chemical-genetic rhodamine voltage reporter. (2021).
2. Costa, M., Manton, J. D., Ostrovsky, A. D., Prohaska, S. & Jefferis, G. S. X. E. NBLAST: Rapid, Sensitive Comparison of Neuronal Structure and Construction of Neuron Family Databases. *Neuron* **91**, 293–311 (2016).
3. Coons, A. H., Creech, H. J. & Jones, R. N. Immunological Properties of an Antibody Containing a Fluorescent Group. *Proc. Soc. Exp. Biol. Med.* **47**, 200–202 (1941).
4. Kohl, J. *et al.* Ultrafast tissue staining with chemical tags. *Proc. Natl. Acad. Sci.* **111**, E3805–E3814 (2014).
5. Sutcliffe, B. *et al.* Second-generation Drosophila chemical tags: Sensitivity, versatility, and speed. *Genetics* **205**, 1399–1408 (2017).
6. Meissner, G. W. *et al.* Optimization of fluorophores for chemical tagging and immunohistochemistry of Drosophila neurons. *PLoS One* **13**, e0200759 (2018).
7. Los, G. V. *et al.* HaloTag: A novel protein labeling technology for cell imaging and protein analysis. *ACS Chem. Biol.* **3**, 373–382 (2008).
8. Keppler, A. *et al.* Labeling of fusion proteins of O6-alkylguanine-DNA alkyltransferase with small molecules in vivo and in vitro. *Methods* **32**, 437–444 (2004).
9. Sun, X. *et al.* Development of SNAP-tag fluorogenic probes for wash-free fluorescence imaging. *ChemBioChem* **12**, 2217–2226 (2011).
10. Hoelzel, C. A. & Zhang, X. Visualizing and Manipulating Biological Processes Using HaloTag and SNAP-Tag Technologies. *ChemBioChem* **16802**, 1–13 (2020).
11. Yang, G. *et al.* Genetic targeting of chemical indicators in vivo. *Nat. Methods* **12**, 137–139 (2014).
12. DiAntonio, A. *et al.* Identification and characterization of Drosophila genes for synaptic vesicle proteins. *J. Neurosci.* **13**, 4924–4935 (1993).
13. Jefferis, G. S. X. E. *et al.* Comprehensive Maps of Drosophila Higher Olfactory Centers: Spatially Segregated Fruit and Pheromone Representation. *Cell* **128**, 1187–1203 (2007).
14. Cachero, S., Ostrovsky, A. D., Yu, J. Y., Dickson, B. J. & Jefferis, G. S. X. E. Sexual dimorphism in the fly brain. *Curr. Biol.* **20**, 1589–1601 (2010).
15. Chiang, A.-S. *et al.* Three-dimensional reconstruction of brain-wide wiring networks in Drosophila at single-cell resolution. *Curr. Biol.* **21**, 1–11 (2011).
16. Jefferis, G. S. X. E. & Cachero, S. Second-Generation Drosophila Chemical Tags : *Genetics* **205**, 1399–1408 (2017).
17. Grimm, J. B., Brown, T. A., English, B. P., Lionnet, T. & Lavis, L. D. Synthesis of Janelia Fluor HaloTag and SNAP-tag ligands and their use in cellular imaging experiments. in *Methods in Molecular Biology* (2017). doi:10.1007/978-1-4939-7265-4_15
18. Rohlfing, T. & Maurer, C. R. Nonrigid image registration in shared-memory multiprocessor environments with application to brains, breasts, and bees. *IEEE Trans. Inf. Technol. Biomed.* **7**, 16–25 (2003).

19. Ito, K. *et al.* A systematic nomenclature for the insect brain. *Neuron* **81**, 755–765 (2014).
20. Jourjine, N., Mullaney, B. C., Mann, K. & Scott, K. Coupled Sensing of Hunger and Thirst Signals Balances Sugar and Water Consumption. *Cell* (2016). doi:10.1016/j.cell.2016.06.046
21. Jenett, A. *et al.* A {GAL4-driver} line resource for Drosophila neurobiology. *Cell Rep.* **2**, 991–1001 (2012).
22. Mütze, J. *et al.* Excitation spectra and brightness optimization of two-photon excited probes. *Biophys. J.* **102**, 934–944 (2012).
23. Arganda-Carreras, I. *et al.* A statistically representative atlas for mapping neuronal circuits in the drosophila adult brain. *Front. Neuroinform.* **12**, (2018).
24. Bogovic, J. A. *et al.* An unbiased template of the Drosophila brain and ventral nerve cord. *PLoS One* **15**, 1–24 (2020).
25. Mann, K., Gallen, C. L., Clandinin, T. R. & Francisco, S. network in Drosophila. **27**, 2389–2396 (2018).
26. Mann, K., Deny, S., Ganguli, S. & Clandinin, T. R. Coupling of activity, metabolism and behaviour across the Drosophila brain. *Nature* **593**, 244–248 (2021).
27. Pacheco, D. A., Thiberge, S. Y., Pnevmatikakis, E. & Murthy, M. Auditory activity is diverse and widespread throughout the central brain of Drosophila. *Nat. Neurosci.* **24**, 93–104 (2021).
28. Bates, A. S. *et al.* The natverse, a versatile toolbox for combining and analyzing neuroanatomical data. *Elife* **9**, 1–35 (2020).

Chapter 4: Monitoring neuronal activity using PeT Voltage-sensitive Dyes

Portions of this work have been published in “Kirk, M. J., Raliski, B. K. & Miller, E. W. in *Methods in Enzymology* **640,** 185–204 (Academic Press Inc., 2020).”

Portions of this work were completed in collaboration with others: Ben Ralinski assisted in manuscript preparation.

Abstract

Voltage imaging in living cells offers the tantalizing possibility of combining the temporal resolution of electrode-based methods with the spatial resolution of imaging techniques. Our lab has been developing voltage-sensitive fluorophores, or VoltageFluors, that respond to changes in cellular and neuronal membrane potential via a photoinduced electron transfer (PeT)-based mechanism. This unique mechanism enables both the fast response kinetics and high sensitivity required to record action potentials in single trials, across multiple cells without the need for stimuli-triggered averaging.

In this chapter, we present a methodology for imaging membrane potential dynamics from dozens of neurons simultaneously in-vitro. Using simple, commercially available cameras, illumination sources, and microscope optics in combination with the far-red synthetic voltage-sensitive fluorophore BeRST-1 (**B**erkeley **R**ed **S**ensor of **T**ransmembrane potential) provides a readily applied method for monitoring neuronal activity in cultured neurons. We discuss different types of voltage-sensitive dyes, considerations for selecting imaging modalities, and outline procedures for the culture of rat hippocampal neurons and performing voltage imaging experiments with these samples. Finally, we provide an example of how changes to the metabolic input to cultured hippocampal neurons can alter their activity profile.

Keywords

voltage imaging, neurobiology, fluorescent dyes, action potential, membrane potential

Introduction

Action potentials are the basis of neural signaling. These rapid changes in membrane potential underlie the vast array of computations, perceptions, and outputs of the human brain. Disruption to the coordinated firing of neurons within the brain has profound detrimental effects on human health. For example, epilepsy is characterized by excessive rhythmic activity of susceptible neuronal populations and can result in hyperexcitability and excitotoxic death in affected neural circuits[1]. In order to prevent such outcomes, neuronal activity is highly regulated by circuit-based feedback mechanisms, intracellular signaling pathways, and the overall metabolic state of the cell. To obtain deeper insight into neuronal activity and its regulation, it is required to monitor activity while simultaneously perturbing these relevant regulatory systems.

To this end, many techniques have been developed to record action potentials in a high throughput manner. Multi-electrode arrays (MEA), for example, record activity of large populations of neurons via extracellular electrodes with excellent temporal resolution[2]. However, this technique lacks spatial resolution. It records the local field potential and local spike activity but gives little information about which specific neuron exhibited which electrical activity. Calcium imaging on the other hand can be used to record from large numbers of neurons simultaneously with both genetic and spatial specificity[3–5]. However,

calcium imaging measures a secondary response to action potentials, which is an order of magnitude slower than the electrical signal and is liable to confounds such as calcium release from internal stores. An attractive alternative to these two approaches is voltage imaging, which combines the spatial resolution of an imaging technique with the temporal resolution and direct measurement of electrode recordings.

In this chapter, we will discuss the use of voltage-sensitive fluorophores for directly imaging voltage changes in neurons in vitro. We provide an over-view of voltage-sensing approaches and introduce our method of monitoring voltage changes via indicators that we propose operate via a photoinduced electron transfer (PeT) method (**Figure 3-1a**). We then discuss considerations for performing voltage imaging, including methods of detection and choice of filter sets.

To illustrate the PeT voltage-sensitive dye imaging technique, we will explore the effect of the cellular metabolic state on neuronal firing rate. Recent studies have shown that switching the fuel source from glucose to ketone body β-hydroxybutyrate (βHB) causes a dramatic decrease in neuronal activity, which is mediated by the opening of K-ATP channel[6,7]. The K-ATP channel conducts a large potassium selective current, and its open probability is gated by the absence of adenosine triphosphate (ATP). This leads ultimately to a decrease of neuronal activity during times of starvation. Using beta hydroxybutyrate as a model for pharmacological perturbations of neuronal activity, we will describe how to use voltage-sensitive dyes to monitor neuronal activity and its perturbations from a mechanistic perspective.

Voltage Imaging with Voltage-sensitive Fluorophores

Voltage imaging emerged as a method with the discovery of voltage-sensitive dyes. Synthetic voltage indicators have traditionally been divided into in two classes: electrochromic (fast) voltage-sensitive dyes, and Nernstian (slow) voltage-sensitive dyes. Electrochromic dyes show sub-millisecond temporal resolution but exhibit extremely small signal amplitudes. Slow voltage-sensitive dyes on the other hand have a higher fractional fluorescence change per millivolt but exhibit slow dynamics, as well as capacitive loading. For a more comprehensive review of voltage-sensitive dyes, we direct readers to previous reviews on the subject [8].

Our group has initiated a program to develop synthetic voltage-sensitive indicators that can provide large changes in fluorescence in response to membrane potential changes while maintaining the rapid response kinetics needed to monitor action potentials in a single trial[9]. We hypothesize that PeT-based voltage-sensitive fluorophores utilize a photoinduced electron transfer mechanism to sense the potential difference across the membrane (**Figure 4-1a**). At rest, PeT holds the fluorophore in a quenched state, but upon depolarization, the rate of electron transfer is diminished, and the fluorophore becomes unquenched and bright. This results in an increased fluorescence in response to neuronal activity (**Figure 4-1a**). Ultimately, PeT-based voltage-sensitive dyes are a noninvasive and readily applicable method for monitoring neuronal activity in vitro. A

number of voltage-sensitive fluorophores, or VoltageFluors, are available in a range of wavelengths spanning most of the visible spectrum. (**Figure 4-1b**).

Despite the recent emergence of a variety of genetically encoded and genetically-encoded/small molecule hybrid voltage indicators [10,11], voltage-sensitive dyes remain one of the most commonly used methods for in vitro studies of neuronal activity. This is in part because they do not require genetic transfection or transduction and thus are readily applicable to any culture of interest—especially those model systems without a well-developed complement of genetic tools[12]. Because the PeT-based VoltageFluor-style indicators developed in our lab maintain rapid response kinetics and high signal to noise ratios, they are a powerful method for monitoring neuronal activity in vitro.

Challenges and pitfalls often encountered in voltage imaging.

Voltage imaging has been a long standing goal in the neuroscience community yet has remained difficult to implement compared to techniques such as calcium imaging[13] This is in part due to the complex challenges of acquiring, detecting and processing voltage imaging data. The aim of this section will be to directly address the challenges often encountered when using this technique and to demonstrate how to resolve them in functional imaging studies.

Detector Selection and Sampling Rates

A critical challenge in the application of voltage imaging is obtaining sufficient temporal resolution to detect action potentials, while simultaneously collecting enough photons to resolve signals from noise[14]. This balancing act depends on the type of experiments in question, but some overarching principles can be useful for determining the optimal sampling rate. According to Nyquist sampling theory, in order to accurately detect events within a signal, one must sample at a rate two times faster than the fastest event[14,15]. This would require a 1 to 2 kHz sampling rate to reliably detect action potentials with their characteristic 1- 2 ms duration.

For the protocols described here, we are concerned with detecting spikes across multiple neurons, and so a sampling rate of 500 Hz represents a reasonable compromise between spike detection and photon collection. Under-sampling at 500 Hz increase photon integration time and improves the spike detection by enhancing the signal-to-noise ratio (SNR), thus permitting high fidelity action potential detection. Although under-sampling is acceptable for spike detection, the data shows mild aliasing, which can result in variations in spike height. For this reason, if the aim is to collect data concerning spike amplitude, waveform characteristics, or rise and decay kinetics, higher sampling rates may be required.

To achieve the high sampling rates required by voltage imaging, we find it most convenient to utilize standard wide-field epifluorescence microscopy with LED illumination. Although functional imaging methods like Ca^{2+} imaging often rely on confocal or two-photon (2P) microscopy, for voltage imaging, these raster scanning microscopies

cannot achieve fast frame rates. Due to these limitations, the current standard for imaging of voltage transients is wide field epifluorescence coupled with a cooled fast EMCCD or CMOS camera. This allows for rapid acquisition of data with commercially available components, although new methods are improving the frame rates that can be obtained using 2P illumination[16,17].

Maintenance of cell health prevents unwanted erosion of SNR:

Voltage imaging is a highly photon-limited imaging modality. A number of factors influence the scarcity of photons for voltage imaging [13]. First, the event kinetics of action potentials are at least an order of magnitude faster than transient increases in cytosolic Ca^{2+}. Second, for voltage imaging, only dye that is properly localized to the cellular membrane actually reports voltage changes. As a result, compared to cytosolic Ca^{2+} indicators, there is a small pool of voltage indicators that can contribute to the voltage-sensitive fluorescence response. This restriction requires that the fractional change in fluorescence and brightness of each molecule be very large in comparison to a cytosolic indicator, whose bulk concentration can overcome a smaller fractional change. Any dye molecule not localized to the extracellular surface will erode the SNR by increasing the background of the sample. PeT-based voltage indicators localize to the plasma membrane of healthy cells, while unhealthy and dying cells take up PeT voltage-sensitive dyes, resulting in cytosolic labeling, dramatically increasing the background. For this reason, controlling cell health and integrity throughout an experiment is crucial. In order to maintain cellular health and prevent dye internalization, we keep neuron cultures at 37 °C and 5% CO_2 until immediately before imaging. This preserves the integrity of the cells and allows for extended imaging of neuronal activity. Heated and oxygenated stage inserts may also improve cell health, but we have not found it necessary for experimental success. We next turn our attention to the neuron cultures.

Primary hippocampal cell culture

We have optimized a cell culture protocol for primary hippocampal neuron preparation, which both minimizes variability when performed in a stereotyped manner and maintains the sample under metabolically relevant conditions. To this end, we used BrainPhys as our culture media for these experiments. BrainPhys mimics physiologically relevant glucose levels found in the brain: 2.5 mM glucose as opposed to the 10 mM-25 mM glucose found in most neuronal media[18]. It should be noted however that if your experiment does not depend on the metabolic state of the cell, you can also use Neurobasal media with little effect on neuronal health or activity.

Finally, controlling for variation is of utmost importance to reduce variability in cell health. Small variations in cell density and dissection quality can affect the basal activity rates of the cultured neurons. As a result, we have found it useful to have one or two members of our lab perform the dissections and culturing for all of our experiments in order to reduce individual variation between preps. When this protocol is performed in a very standardized manner it will permit stable, reproducible recordings over multiple preparations.

Materials
0.2 µm Sterile filter, 50 mL (VWR 82027-592)
Cell culture plates 24 wells (VWR 62406-183)
12 mm round German glass coverslips (VWR 100499-634)
Glass petri dishes (VWR 75845-542)
Synergy Water Purification System (Millipore Sigma Synergy W-R)
General purpose heating and drying oven (Fisher Scientific 15-103-0503)
Incubator (ThermoFisher Scientific Heracell VIOS 160i)
Dissection microscope (Olympus SZ40 Stereo Zoom)
Tissue culture hood (Baker SterilGARD e3)
Forceps, Dumont #5 for rat dissection, fine tips (Fine Science Tools 11251-20)
Scissors, curved, for rat dissection (VWR 25608-225)
Dissecting Scissors, Sharp Tip, 6 1/2" (VWR 82027-592)
Positive action tweezers, Style 5 (Electron Microscopy Services 72706-01)
50 mL centrifuge tubes, Corning (VWR 21008-725)
15 mL centrifuge tubes, Corning (VWR 21008-673)
Aspirator pipettes 2 mL, Falcon (VWR 53106-450)
Serological pipettes , 1 mL (VWR 29443-041)
Pipets, serological, 5 mL (VWR 29443-045)
Pipets, serological, 10 mL (VWR 29443-047)
Pasteur pipets (FisherScientific 13-678-20C)
Hemocytometer (VWR 15170-089)

Reagents
Hydrochloric acid (CAS; 7647-01-0)
Ethanol (CAS: 64-17-5)
Sodium Borate Buffer (PB, see recipe in Solutions section)
Poly-d-Lysine (Sigma-Aldrich P7280 – 5 mg)
Culture media MEM++++ (see recipe in Solutions section)
Brain Phys media (see recipe in Solution section)
Calcium/Magnesium Free Hanks Balanced Salt Solution with Phenol Red (HBSS, Invitrogen 14170-16)
Dulbecco's phosphate buffered saline (DPBS, Gibco 14200-075)
Timed pregnant Sprague Dawley rat (Charles River Laboratories)
Trypsin, 2.5%, for neuron dissection (Invitrogen 15090-046)

Optional:
Neurobasal media ++ (see recipe in Solutions section)

Protocol for primary culture
1. 1) Two weeks prior to dissection, acid wash 12mm coverslips to prepare and sterilize the plating surface.

    - a. Place 12 mm coverslips in a clean glass petri dish and cover with a solution of 1M HCl. Shake at 90 RPM for 3-5 hours at room temperature.

All wash steps throughout the protocol are performed at room temperature.

- b. Remove the acid solution and replace it with 100% ethanol shaking at 100 RPM overnight. Wash two more times for a total of three overnight washes.

- c. Remove the final ethanol wash and replace it with double distilled water. Wash a total of three times overnight at 100 RPM.

- d. Remove the water and place the dish into a glassware oven (150 °C) for 2-5 hours or until completely dry. Once these cool you can store them at room temperature and use them as needed.

In order to maintain sterility, we have found it best to leave the cleaned coverslips in the petri dish with the lid sealed with parafilm or taped shut to prevent accidental contamination.

- 2) One day prior to tissue collection, make a fresh 1:10 dilution of PDL (stock: 1 mg/mL in PB) in sterile DPBS.

Final concentration is 0.1 mg/mL PDL

- 3) Using sterile forceps place acid washed coverslips into the tissue culture plate and cover each coverslip with the PDL solution incubating them overnight at 37° C in a culture incubator.

For a 24 well plate containing 12 mm coverslips we use 250 µL per well to ensure even coating of the glass.

- 4) On the day of the prep, aspirate the PDL. Wash two times with sterile double distilled water and two times with sterile DPBS.

- 5) Add half of the plating volume (400 µL per 24 well) of MEM++++ to each well and allow the plate to equilibrate to the CO2 in the incubator.

For 24 well plates 12 mm coverslips we plate in a total volume of 750 µL per well, adding 400 µL for equilibration and 350 µL for plating cells.

- 6) Euthanize a timed pregnant female Sprawgue Dawley rat at E17-19 in accordance with IACUC approved protocols.

- 7) Make a caudal to rostral cut along the ventral side of the abdomen, remove the embryonic sac and subsequently the embryos. Decapitate the embryos using sterile technique and place the heads in ice cold HBSS.

- 8) Puncture through the most rostral portion of the cranium with fine forceps. In a rostral to caudal fashion remove skin and skull cutting along the longitudinal fissure using forceps or scissors. Pull away the remaining skull and meninges using fine forceps being careful not to puncture or damage the brain as you extract it. Bisecting the brain along the longitudinal fissure, expose the hippocampi on either side and dissect them away using fine forceps. Place them into fresh ice cold HBSS. Discard all carcasses, blood, and tissue as medical waste in accordance with regulations.

For more details see Figure 3-2 and[19]*.*

- 9) Transfer the hippocampi to 1 mL of 2.5% trypsin and incubate for 15 minutes at 37°C.

- 10) Remove the trypsin and wash hippocampi three times in fresh HBSS being careful each time not to aspirate the tissue. Finally replace the media with 1 mL of MEM++++.

- 11) Triturate three times with increasingly smaller flame polished sterile glass pipettes until the solution appears homogenous and then add 2 mL of MEM++++.

- 12) Measure cell density using a hemocytometer and plate neurons onto the equilibrated dish at the appropriate density

30,000 cells per 12 mm coverslip in a 24 well plate is a good density for most functional imaging experiments.

- 13) At 1 day in vitro (DIV), change half of the plating media to Brain Phys ++ media and at 7 DIV, add 500 µL of Brain Phys++ media to the cells.

Functional voltage imaging of cultured neurons

We have established a functional imaging protocol which allows recording of action potential and subsequent calculation of firing frequency in dissociated hippocampal cultures under varying conditions. First, select healthy cultures aged 14-16 DIV, this is done to ensure that the neurons will fire action potentials, have developed fully functioning synapses, and have integrated into circuits. Cells are then loaded for 30 minutes with 500 nM Berkeley Red Sensor of Transmembrane potential (BeRST1), a far-red PeT voltage-sensitive dye which is excited at 658 nm and emits at 683 nm. Due to the photon starved nature of voltage imaging, it is important to select filters and dichroic mirrors which permit the on peak excitation and collection of fluorescent signals. Near optimal filter sets and dichroics are shown in (**Figure 4-2a**); filter sets optimized for Cy5 are usually fairly close to optimal for BeRST imaging. This technique is amenable for use with any of the PeT-based VoltageFluors[8,20,21], but BeRST 1 was selected for its photostability and robust SNR[22].

The cells are then transferred to the microscope and a field of view (FOV) containing healthy cells (**Figure 4-2b and c**) is selected via differential interference microscopy (DIC) or brightfield imaging. In order to assess cell health, we suggest looking for four different characteristics: an even dispersion of cells lacking neurosphere formation (**Figure 4-2d**), a lack of blebbing on the plasma membrane (**Figure 4-2e**), a distinct nucleus in large diameter cells (**Figure 4-2f**), and lack of dye internalization (**Figure 4-2g**). These are outlined visually in (**Figure 4-3b-g**). Once having selected a region of interest for imaging, focus the sample under fluorescent light and begin recording. Two 10 second recordings are taken per field of view and 4 fields are taken per sample to allow for detection of unhealthy cells and outlier data points. Overall, recording should take less than 20 minutes per sample permitting rapid data acquisition and preventing the deterioration of cell health by minimizing exposure to light and ambient temperature. The protocol below outlines 1) software and hardware configuration for fast functional imaging 2) functional imaging protocol for single perturbations and 3) functional imaging protocols for repeat measures in both pretreatment and rescue experiments.

Materials

50 mL centrifuge tubes, Corning (VWR 21008-725)
Aspirator pipettes 2 mL, Falcon (VWR 53106-450)
0.2 µm Sterile filter, 50 mL (VWR 82027-592)50 mL falcon tubes
Incubator (ThermoFisher Scientific Heracell VIOS 160i)
Fine Forceps #5 (Fine Science Tools 11251-20)
1.5 Eppendorf tubes (Fisher Scientific 14222155)
Imaging Chamber (Warner RC-26 or VWR 25382-348)
Inverted or upright epifluorescence microscope (AxioExaminer Z-1 Zeiss)
20x objective
Filter set compatible with BeRST1 spectrum
LED or Epifluorescence lamp
Dichroic compatible with filter sets for BeRST1
Fast sCMOS or EMCCD camera (Orca flash 4.0 v2, Hamamatsu)
Software to control image capture (we have used both MicroManger and Slidebook)

Optional:
Gridded coverslip

Reagents

BeRST dye (250 µM in DMSO, available from the corresponding author upon request)
Metabolic Saline Solution (MSS, see recipe in Solutions section)
Day 14-16 DIV dissociated cultures

Optional:

If cultures are maintained in Neurobasal we suggest using HBSS as an imaging solution to maintain similar levels of glucose between culture conditions and imaging conditions.

Calcium/Magnesium Free Hanks Balanced Salt Solution without Phenol Red (HBSS, Invitrogen 14170-16)

Detector configuration

- 1) See that the computer has been recently restarted and has plenty of space on the hard drive. This will ensure that the rate of data acquisition will not be slowed down by storage constraints.

Tip: If the acquisition rate decreases throughout a recording, hard drive space is often the issue. We have found it optimal to have two times as much space on the hard drive as the data to be collected.

- 2) Select an imaging field of view (FOV) that is centered at the chip readout point for your camera. The largest FOV on the Orca Flash 4.0-v2 (Hamamatsu) is 2048 pixels x 400 pixels.

- 3) Determine the minimum binning permitted while maintaining fidelity and speed of FOV acquisition.

We have found that 4x4 binning resulting in a 512x100 pixel FOV is optimal for the Orca Flash 4.0, but you will need to determine the binning value empirically for each different detector by referring to the metadata frame rate and number of frames.

Finally, if possible, stream data acquisition directly to the disk, this protects against dropped frames or slowing as your data size increases.

- 4) Once the acquisition has been fully optimized, acquire two ten second test videos and verify via frame rate and number of frames that the detector accurately tracks at 500 Hz. The optimization of your imaging FOV should only need to be performed once and can be reused for future experiments.

Functional imaging and data acquisition

- 1) At 14 -16 DIV cells are ready to perform functional imaging.

- 2) Warm the imaging solutions to 37°C prior to beginning the experiment to prevent temperature shock to the cells.

- 3) Take 1 µL of 250 µM BeRST1 solution and dilute it to 500 nM in 499 µL of MSS solution containing pharmacological agent or a vehicle control. Mix thoroughly.

- 4) Gently, aspirate the media from one well and replace it with the dye solution. Return the culture plate immediately to the incubator and incubate for 30 minutes.

Depending on the drug/perturbation time course, this incubation period may vary. However, around 20 minutes provides good membrane staining of neurons. Longer incubation times are fine.

- 5) Remove the culture from the incubator. Using fine forceps move the coverslip to the imaging chamber and immediately cover with 1 mL of the warm vehicle or experimental imaging solution. Make sure the cells are completely covered.

- 6) Transfer the cells to the microscope and scan for a healthy region of cells using DIC or brightfield microscopy under the 20x objective. Please refer to **Figure 4-2** for examples of healthy and unhealthy cells.

- 7) Obtain a DIC image of the selected imaging FOV using the optimized FOV size, location and binning previously determined in step 4.3. step 3, above. This will be used to generate cellular ROIs in the analysis.

This image must be taken at the exact same spatial resolution and imaging FOV size as the voltage imaging recordings.

- 8) Focus your cells in low intensity red light before data acquisition. This will be slightly different from the DIC images focus point. Confirm cell health by noting the dye location. In healthy cells the dye will localize to the extracellular surface creating a halo while unhealthy cells will show internalized dye in the cytosol. Please refer to **Figure 4-2** for examples of dye internalization.

- 9) Switch to a higher intensity and record two ten second videos at 500 Hz.

- 10) This process can be repeated across multiple, separate fields on the same coverslip (we typically collect 4). Be sure to move each time to a new area to prevent over exposure of the cells to light. If the cells have been over exposed, the firing frequency will decrease from one video to the next across all cells.

- 11) Repeat steps 1-9 for the remaining coverslips under your perturbation and control conditions.

- 12) When acquisition is complete export all of your data as .tiff files for analysis.

Organize the data into separate folders for each FOV containing the DIC image and voltage recording videos. This will expedite the analysis process significantly.

Analysis and interpretation of functional imaging data

Materials
Computer
External hard drive
Image analysis software (for example, MATLAB or ImageJ)

Analysis pipeline

- 1) Import voltage imaging data into an image analysis software system (ImageJ, for example). Custom imaging routines specifically designed for extracting voltage imaging data are available upon request from the authors.
- 2) Using the DIC image as a guide, create regions of interest (ROIs) over the cells of interest.
- 3) Plot the fluorescence grey values in these ROIs vs. time (see **Figure 4-3d**)
- 4) To determine the firing frequency, count the number of spikes within the recording window (in this example, 10 seconds).

Representation and interpretation of data

Voltage imaging data can provide a snapshot of the activity with a neuronal culture. In particular, the enhanced temporal resolution of voltage imaging with BeRST allows interrogation of changes in firing frequency – difficult or impossible to do with traditional Ca^{2+} imaging. Spike frequencies can be represented in a multitude of ways which can offer unique perspectives on the spiking activity under perturbed and unperturbed conditions. For example, in neurons treated with βHB, we see an overall decrease in the average firing rate compared to neurons maintained in glucose solution (**Figure 4-4a**). Examining the activity data as a cumulative frequency plot reveals that greatest changes in firing frequency take place in cells with relatively lower intrinsic firing rates (<2 Hz or so), suggesting that the effects of βHB may be primarily isolated to excitatory, rather than inhibitory, neuronal subtypes (**Figure 4-4b**).

Summary

In this chapter we outlined a protocol for the use of Berkeley Red Sensor of Transmembrane potential (BeRST 1) in cultured neurons isolated from the hippocampus. The use of BeRST 1 – and Voltage-sensitive Fluorophores, or VoltageFluors, more generally – enables rapid assessment of neuronal activity using readily available, commercial cameras, illumination sources, and microscope optics. We envision that BeRST 1, and related indicators will be of use in a number of applications, and we hope

this chapter provides a starting point for others to perform voltage imaging measurements in their own laboratories.

Solutions

Use sterile double distilled water in all recipes and protocol steps

Culture media (MEM++++)
10 mL B27 (Invitrogen 17504-044)
5 mL GlutaMAX (Invitrogen 35050-061)
25 mL fetal bovine serum (VWR 89510-186)
10 mL 1 M dextrose (FischerScientific D16-500; sterile filtered)
500 mL Media, MEM, for rat dissection (Invitrogen 11090-081)
Combine all components, sterile filter, and aliquot into 50 mL tubes. Store at 4 °C for up to 6 months.

Brain Phys media (BP+)
10mL NeuroCult SM1 (Stem Cell 05711)
5 mL GlutaMAX (Invitrogen 35050-061)
500 mL Media, BrainPhys (Stem Cell 05790)
Combine all components, sterile filter, and aliquot into 50 mL tubes. Store at 4 °C for up to 6 months

Neurobasal media (NB++)
10 mL B27 (Invitrogen 17504-044)
5 mL GlutaMAX (Invitrogen 35050-061)
500 mL Media, Neurobasal (Invitrogen 21103-049)
Combine all components, sterile filter, and aliquot into 50 mL tubes. Store at 4 °C for up to 6 months.

Sodium borate buffer
1.55 g Boric acid
4.50 g Sodium tetraborate decahydrate
500 mL sterile double distilled water
Combine all components, bring the pH to 8.5, and sterile filter. Store at room temperature indefinitely.

Metabolic Salt Solution:
135.43 mM sodium Chloride
5.33 mM potassium chloride
4.17 mM sodium bicarbonate
2.5 mM D-Glucose
1.25 mM calcium chloride
0.49 mM magnesium chloride
0.41 mM magnesium sulfate
0.44 mM potassium phosphate monobasic

0.34 mM sodium phosphate dibasic
290 mOsmols
Combine all materials, bring the pH to 7.3, measure osmolarity, sterile filter and store at 4 °C.

Figures.

Figure 4-1.

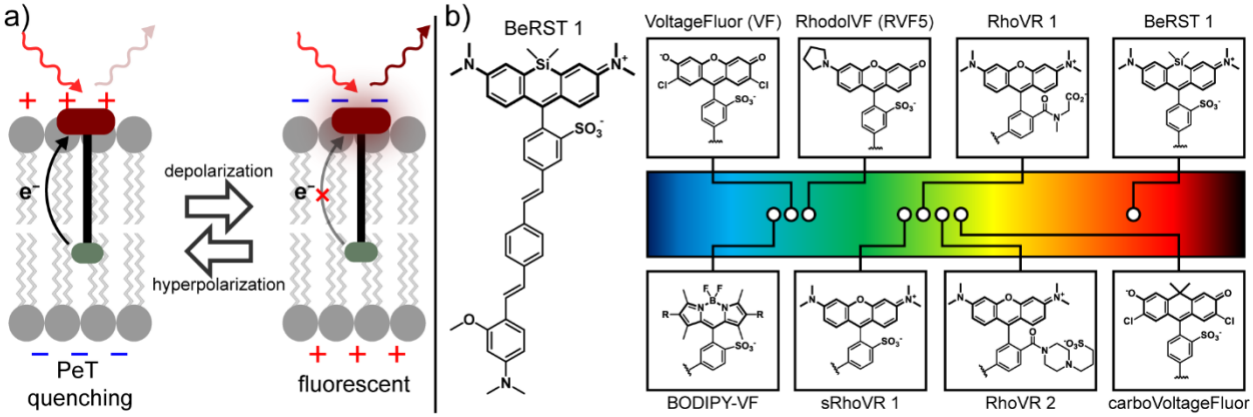

Figure 4-1. Voltage-sensitive Fluorophores sense membrane potential via photoinduced electron transfer (PeT). **a)** Proposed mechanism of voltage sensing via PeT. At rest, electron transfer from an electron rich aniline (green) to the fluorophore (red) quenches fluorescence. Upon depolarization of the plasma membrane, the transmembrane potential inhibits electron transfer and fluorescence increases. **b)** (*left*) The structure of BeRST 1 and (*right*) other Voltage-sensitive Fluorophores (VoltageFluors). The location of the circle in the rainbow spectrum indicates the approximate excitation wavelength required for the dye. Abbreviations: RhoVR = Rhodamine Voltage Reporter; BeRST = Berkeley Red Sensor of Transmembrane potential. sRhoVR is sulfonated RhoVR. Adapted with permission from *Acc. Chem. Res.* **2020**, *53*, 11-19. Copyright 2020 American Chemical Society."

Figure 4-2.

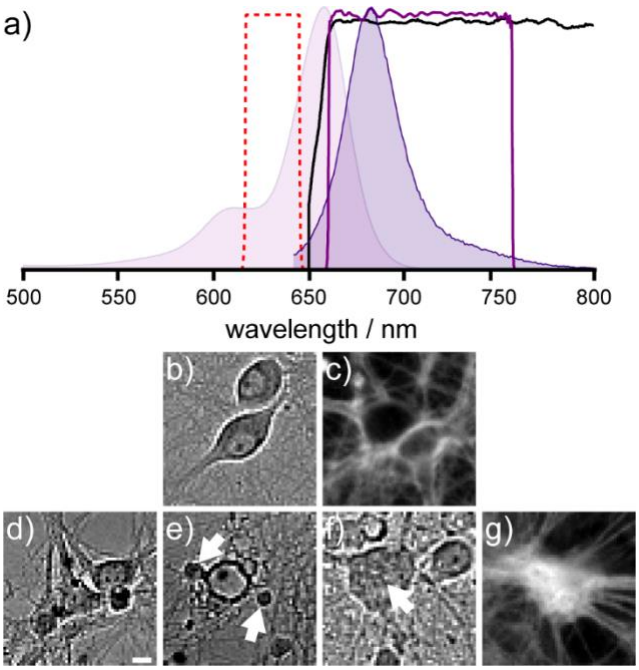

Figure 4-2. Evaluating optics and cellular health for voltage imaging with BeRST 1. **a)** Graphical representation of absorption (light purple) and emission (dark purple) spectra for BeRST 1. Overlaid are the excitation band from the LED light source (red), dichroic mirror (black) and emission bandpass filter (dark purple line). **b and c)** Example of healthy hippocampal neurons.
b) Representative DIC image of healthy hippocampal neurons, with robust halos around their membranes, no blebbing, and clear nuclear compartments. **c)** Representative epifluorescence micrograph of healthy neurons in which BeRST 1 is localized to the extracellular surface forming a halo-like structure around each cell body. **d-g)** Examples of unhealthy neurons. **d)** DIC micrograph of cells forming a neurosphere structure, where cells overlap significantly in a central sphere and projections radiate outward. This structure indicates unhealthy neurons. **e)** DIC micrograph of blebbing of a cell membrane. The membrane of the central large cell shows a large amount of deterioration forming bubbles or blebs at the surface of the cell, indicated by the white arrow. **f)** DIC micrograph of a singular large cell with no defined nucleus. Expected location of the nuclear membrane is indicated by the white arrow. **g)** Epifluorescence image of an unhealthy neurosphere structure which has taken up dye molecules and is thus fluorescent throughout the intracellular space. Scale bar is 10 μm.

Figure 4-3.

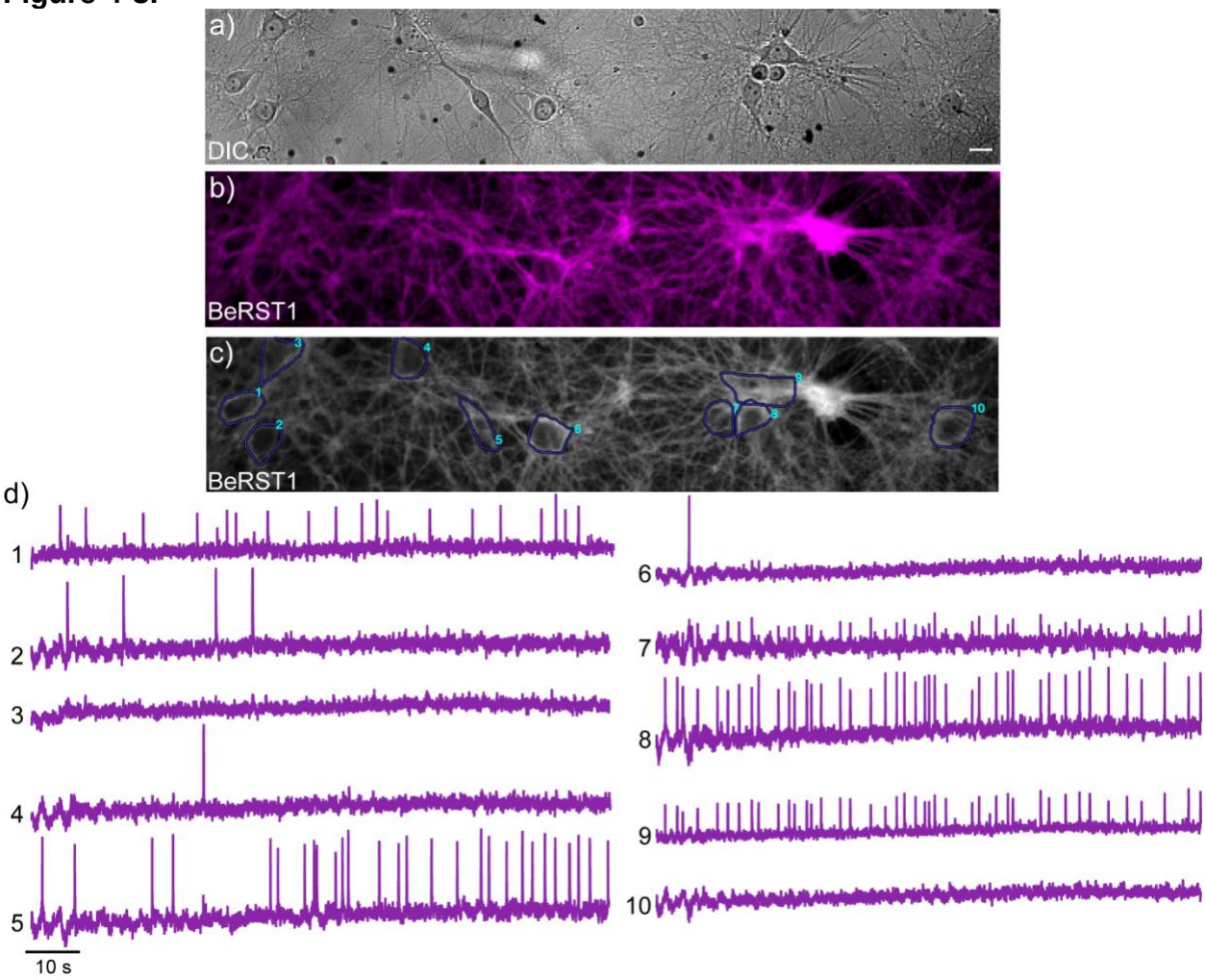

Figure 4-3. Example data from a single ten second recording of 10 dissociated neurons in culture as reported by BeRST 1. **a)** DIC micrograph of 512 x 100 imaging field of view (FOV) region showing 10 healthy cell bodies. Scale bar is 20 μm. **b)** Fluorescent microscopy image of the same 512x100 imaging FOV stained with 500 nM BeRST1. **c)** fluorescent micrograph showing selected cellular ROI for analysis. **d)** Representative fractional change in fluorescence (ΔF/F) traces extracted from the ten second video of cellular ROIs 1-10. Here each trace represents the fluorescent responses indicated cell from panel **(c)** as reported by BeRST1.

Figure 4-4.

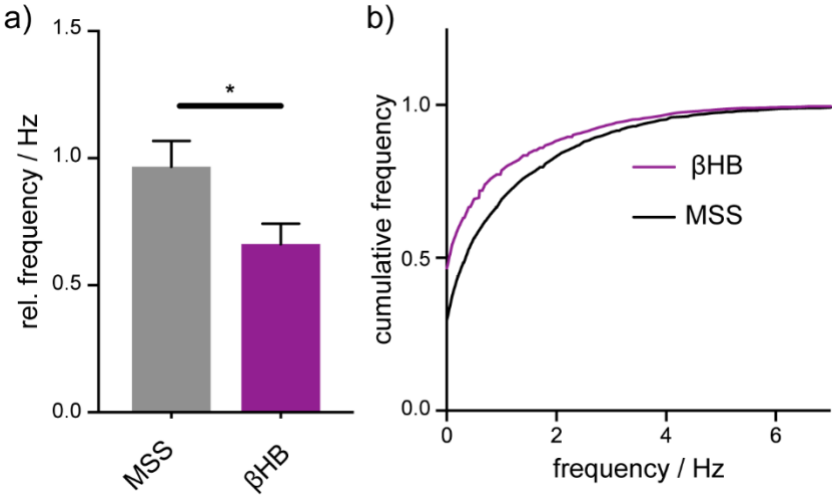

Figure 4-4. Representative data set showing comparison of spike frequency differences under glucose-treated and β-hydroxybutyrate (βHB) treated conditions. **a)** Bar graph depicting mean firing frequency across n=43 coverslips of neurons for βHB and n=36 coverslips for glucose (error bars are standard error of the mean, Mann Whitney test * is p=0.0142). **b)** Cumulative frequency distribution of singular cells frequencies under βHB- and glucose-treated conditions.

References

1. Kawamura, M., Ruskin, D. N., Geiger, J. D., Boison, D. & Masino, S. a. Ketogenic diet sensitizes glucose control of hippocampal excitability. *J. Lipid Res.* (2014). doi:10.1194/jlr.M046755
2. Pine, J. A history of MEA development. *Adv. Netw. Electrophysiol. Using Multi-Electrode Arrays* 3–23 (2006). doi:10.1007/0-387-25858-2_1
3. Chen, T. *et al.* Ultra-sensitive fluorescent proteins for imaging neuronal activity. **499**, 295–300 (2013).
4. Scanziani, M. & Häusser, M. Electrophysiology in the age of light. *Nature* **461**, 930–939 (2009).
5. Sofroniew, N. J., Flickinger, D., King, J. & Svoboda, K. A large field of view two-photon mesoscope with subcellular resolution for in vivo imaging. *Elife* **5**, 1–20 (2016).
6. Ma, W., Berg, J. & Yellen, G. Ketogenic Diet Metabolites Reduce Firing in Central Neurons by Opening KATP Channels. *J. Neurosci.* **27**, 3618–3625 (2007).
7. Sada, N., Lee, S., Katsu, T., Otsuki, T. & Inoue, T. Targeting LDH enzymes with a stiripentol analog to treat epilepsy. *Science (80-.).* **347**, 1362–1367 (2015).
8. Miller, E. W. *et al.* Optically monitoring voltage in neurons by photo-induced electron transfer through molecular wires. *Proc. Natl. Acad. Sci.* **109**, 2114 LP – 2119 (2012).
9. Liu, P. & Miller, E. W. Electrophysiology, Unplugged: Imaging Membrane Potential with Fluorescent Indicators. *Acc. Chem. Res.* **53**, 11–19 (2020).
10. Abdelfattah, A. S. *et al.* Bright and photostable chemigenetic indicators for

extended in vivo voltage imaging. *Science* **365**, 699–704 (2019).
11. Lin, M. Z. & Schnitzer, M. J. Genetically encoded indicators of neuronal activity. *Nat. Neurosci.* (2016). doi:10.1038/nn.4359
12. Tomina, Y. & Wagenaar, D. A. A double-sided microscope to realize whole-ganglion imaging of membrane potential in the medicinal leech. *Elife* **6**, 1–19 (2017).
13. Kulkarni, R. U. & Miller, E. W. Voltage Imaging: Pitfalls and Potential. *Biochemistry* (2017). doi:10.1021/acs.biochem.7b00490
14. Sjulson, L. & Miesenböck, G. Optical recording of action potentials and other discrete physiological events: A perspective from signal detection theory. *Physiology* **22**, 47–55 (2007).
15. Craven, D., McGinley, B., Kilmartin, L., Glavin, M. & Jones, E. Compressed sensing for bioelectric signals: A review. *IEEE J. Biomed. Heal. Informatics* **19**, 529–540 (2015).
16. Kazemipour, A. *et al.* Kilohertz frame-rate two-photon tomography. *Nat. Methods* **16**, 778–786 (2019).
17. Wu, J. *et al.* Kilohertz two-photon fluorescence microscopy imaging of neural activity in vivo. *Nat. Methods* **17**, 287–290 (2020).
18. Bardy, C. *et al.* Neuronal medium that supports basic synaptic functions and activity of human neurons in vitro. *Proc. Natl. Acad. Sci. U. S. A.* **112**, E2725–E2734 (2015).
19. Audesirk, G., Audesirk, T. & Ferguson, C. Culturing Rat Hippocampal Neurons. *Curr. Protoc. Toxicol.* **4**, 1–17 (2000).
20. Deal, P. E. *et al.* Covalently Tethered Rhodamine Voltage Reporters for High Speed Functional Imaging in Brain Tissue. *J. Am. Chem. Soc.* **142**, 614–622 (2020).
21. Ortiz, G., Liu, P., Naing, S. H. H., Muller, V. R. & Miller, E. W. Synthesis of Sulfonated Carbofluoresceins for Voltage Imaging. *J. Am. Chem. Soc.* **141**, 6631–6638 (2019).
22. Huang, Y. L., Walker, A. S. & Miller, E. W. A Photostable Silicon Rhodamine Platform for Optical Voltage Sensing. *J. Am. Chem. Soc.* **137**, 10767–10776 (2015).

Appendix 1: Targeting of porcine liver esterase in *Drosophila melanogaster*.

Portions of this work were completed in collaboration with others: Pei Liu assisted in cloning design.

Background

The brain is an intricate network of cells, or circuits, that communicate via electrical impulses called action potentials. The patterns of these action potentials are fundamental to each circuit's computational and behavioral outputs. Ultimately, these phenomena underlie our cognitive, emotional, and physical capabilities as human beings. Thus, it is a goal in the neuroscience community to record these action potentials with high fidelity across many cells within a circuit simultaneously. To address this aim, the Miller lab has developed a palette of voltage-sensitive dyes, which we hypothesize detect cellular+ transmembrane potentials via a photoinduced electron transfer mechanism[1–6]. Although these voltage-sensitive dyes are well known for their high signal-to-noise reporting of action potentials *in vitro*[2], their application has proven difficult in more complex tissues[4,7]. This difficulty arises from the fact that voltage-sensitive dyes indiscriminately label all membranes. This indiscriminate labeling erodes the signal-to-noise and convolutes somatic voltage signals with the en passant arborizations from other cells[8]. Also, homogenous labeling precludes the genetic identification of cell subtype in complex tissues. For these reasons, a genetically driven mechanism of dye targeting is necessary for applying these voltage-sensitive dyes in complex tissues.

Inspired by work done in the Lavis laboratory, where porcine liver esterase (PLE) was applied to fluorogenically activate cyclopropyl ester quenched fluorescein in mammalian cells[9], we adapted PLE for fluorogenic activation of voltage-sensitive dyes in mammalian cell culture. Here PLE was targeted to the extracellular surface of transfected cells and allowed to react with a voltagefluor containing two cyclopropyl ester caps, one on the phenolic oxygen and the other at the sulfonated pendant ring (VF-EX2). Using the PLE fluorogenic activation mechanism, we were able to monitor neuronal activity in primary hippocampal cell cultures. We also found that VF-EX2 reported membrane potential changes with approximately 21 ± 0.3% $\Delta F/F$ per 100 mV in transfected HEK-293T cells[10].

Having applied the PLE fluorogenic activation in cell culture, we sought to apply this to more complex tissues. Here, we selected *Drosophila* as a platform due to its ease in transgenic generation, low complexity nervous system, and rapid generation times. We first created a transgenic fly lines expressing PLE under the Gal4/UAS enhancer trap system. The Gal4/UAS system utilizes a yeast transcription activator, Gal4, to drive transcription of sequences downstream of the upstream activator sequence (UAS)[11]. Thus, expression of Gal4 in specific cells yields the expression reporter genes in those cells. We used the original mammalian trafficking domains, an IgK secretion signal, and a DAF GPI anchor to traffic the PLE protein to the extracellular surface[10]. Here we found that PLE did not traffic to the extracellular surface in most expected cells. As a result, we redesigned the PLE trafficking system using the PAT-3 secretion signal (from *C. elegans*) and CD4 transmembrane domain[12,13] and found that this system did traffic PLE to the extracellular surface. We then used VF-EX2 to assess the function of the PLE protein in fly brains. We found that PLE did not robustly activate the Voltagefluor in the expected cells suggesting that PLE may either be non-functional or inefficient under conditions

required for *Drosophila* survival. These flies may one day be useful for more reactive substrates or fluorogenic activation of covalently tethered voltagefluor but require further characterization of PLE's efficacy in *Drosophila* as a whole.

Results

We first developed an extracellular trafficking system for PLE using the IgK secretion signal and DAF GPI anchoring domain. This construct was based on the mammalian vector used in the original PLE voltage imaging paper[10] **(Fig. A1-1a).** We then subcloned an IgK-PLE-HA-DAF (PLE-DAF) fragment into a 5x UAS expression vector pUAST and injected this construct for random genomic insertion *Drosophila* embryos **(Fig. A1-2a,** Best Gene Inc.). We began testing PLE-DAF expression under GH146-Gal4[14], which drives PLE-DAF expression in a subset of olfactory projection neurons. Here we found that the protein did not traffic to the extracellular surface, showing only a few positive cells under non-permeabilized immunohistochemistry for the HA epitope **(Figure A1-2 b and c)**. To improve our targeting system, we sought to find an extracellular targeting motif that was confirmed to accurately traffic proteins to the extracellular surface in *Drosophila*.

We thus selected the PAT-3 secretion signal along with the CD4 transmembrane domain [12,13].We first subcloned a PAT-3-PLE-HA-CD4 into a mammalian expression vector pCDNA3.1 **(Figure A1-3a)** and transfected this construct into HEK 293T Cells confirming its expression and dye activation at the cell surface **(Figure A1-3 b-d).** We found that PLE activated dye VF-EX2 with a ~ 2-fold change in fluorescence in transfected cells when compared to non-transfected cells **(Figure A1-3e)**. We then fixed and stained these PLE-CD4 expressing cells for the HA epitope tag under non-permeabilizing conditions, further confirming protein localization at the cells surface (**Figure A1-4**). We then amplified the PAT-3-PLE-HA-CD4 fragment from the mammalian vector and inserted it into the *Drosophila* expression vector pJFRC7(Addgene). We selected this vector due to its high expression rate, which results from the 20 repeats of the upstream activator sequence (UAS) in its promoter region[15] to ensure high PLE-CD4 protein expression, we performed site-specific integration to generate our second group of transgenic animals. Having developed these transgenic lines, we then confirmed their extracellular trafficking via immunohistochemistry under non-permeabilized **(Figure A1-5a)** and permeabilized **(Figure A1-5b)** conditions for the HA epitope in GH146-Gal4>PLE-HA fly brains. We found robust extracellular trafficking of the HA **(Figure A1-5c)**. We next sought to determine if PLE could functionally activate dyes in *Drosophila*. To assess this, we expressed PLE under the GH146-Gal4 driver line and loaded the brain with 20 µM of VF-EX2. However, we found no qualitative difference between brains expressing PLE **(Figure A1-6a)** and brains not expressing PLE **(Figure A1-6b)**. These data suggested two plausible hypotheses 1) the protein is not active in *Drosophila* or 2) the dye is not sensitive enough to reveal the protein function within the sample. To differentiate between these two hypotheses, we ran a series of *in vitro* enzymatic uncaging assays.

The first *in vitro* experiment was to assess whether the isolated PLE (Sigma) protein was capable of fluorogenically activating non-voltage-sensitive F-ex1 *in vitro* (**Figure A1-7a**). We reacted F-EX1 with varying concentrations of the isolated protein and found that F-

EX1 showed a broad dynamic range of fluorogenic activation in PBS(**Figure A1-7b)**. Next, we sought to determine whether the PLE expressed in *Drosophila* brains was functional. To assess this, we used fly lysates from pan-neuronal expressing PLE flies (nSybGal4>PLE-CD4) [16]. F-EX1 fluorescence was not significantly enhanced by the available PLE in solution when compared to Gal4-only controls (**Figure A1-7c)**, suggesting that the fly produced PLE may not be functional. Due to the lack of fluorogenic activation, this project was tabled for more promising small molecule covalent tethering mechanisms such as SNAP Tag and HaloTag.

Conclusion and future directions

We have shown that previously developed IgK-PLE-HA-DAF construct, which readily targets PLE to the extracellular surface in HEK Cells and mammalian neurons, does not function to traffic PLE to the extracellular surface in *Drosophila*. This lack of trafficking may result from a mammalian secretion signal, which may not be recognized by the *Drosophila* secretory system. Since we could not target PLE to the extracellular surface in *Drosophila* using the mammalian domains, we sought to develop a construct that would be compatible with the invertebrate system. We found that we can accurately target PLE to the extracellular surface in HEK cells using a PAT-3 secretion signal and CD4 transmembrane domain adapted from the original *Drosophila* GRASP construct[12,13]. We then used the PAT-3-PLE-HA-CD4 insert to generate a transgenic *Drosophila* reporter line capable of expressing PLE-CD4 under the control of the GAL4/UAS enhancer trap system. We found that PLE trafficked readily to the extracellular surface in *Drosophila*, as confirmed by immunohistochemistry. However, through both live tissue loading experiments and *in vitro* dye activation assays, we found that PLE was not highly reactive in the fly. As a result, we set this project aside for more promising candidates SNAP-Tag and HaloTag. However, through this process, we learned how to traffic proteins accurately in *Drosophila*, a significant step in the direction of the genetic targeting of voltage-sensitive dyes.

If this project were to be resumed, the first thing to assess would be the function of PLE in *Drosophila* – though this was partially determined in lysates, it may be worth-while to evaluate the protein activity in the fly brain using a cell-permeable PLE substrate. The intracellular fluorogenic activation could allow for a more robust signal between PLE positive and PLE negative cellular populations and diminish the effect of dye migration to non-targeted cells after uncaging. It may also be useful to a red-shifted PLE fluorogenic probe such as a cell-permeable carbofluoroscien. We have found that red-shifted dyes show higher contrast overall, due to the lack of autofluorescence at the further red-shifted wavelengths. For this reason, if this project were to be continued, the first step would be to develop a fluorogenic cell-permeable (potential AM-esterified) carbofluoroscien molecule to assess the function of PLE in *Drosophila* as a whole. Next would be to use the carbofluoroscien PLE reactive Voltagefluor[17] to evaluate the PLE protein's activity *in vivo*.

Methods

Plasmid construction.

For the first generation of PLE extracellular trafficking transgenic flies, we subcloned the dual epitope-tagged PLE-HA protein flanked by a 5' IgK secretion signal and 3' DAF sequence into pUAST using the gateway recombination. Sequences for this construct are listed below.

5xUAS:

TCGGAGTACTGTCCTCCGAGCGGAGTACTGTCCTCCGAGCGGAGTACTGTCCTCC
GAGCGGAGTACTGTCCTCCGAGCGGAGTACTGTCCTCCG

HS Promoter:

CGCCGGAGTATAAATAGAGGCGCTTCGTCTACGGAGCGACAATTCAATTCAAACAA
GCAAAGTGAACACGTCGCTAAGCGAAAGCTAAGCAAATAAACAAGCGCAGCTGAA
CAAGCTAAACAATCTGCAGTAAAGTGCAAGTTAAAGTGAATCAATTAAAAGTAACCA
GCAACCAAGTAAATCAACTGCAACTACTGAAATCTGCCAAGAAGTAATTATTGAATA
CAA

IgK:

ATGGAGACAGACACACTCCTGCTATGGGTACTGCTGCTCTGGGTTCCAGGTTCCA
CTGGTGAC

PLE:

ATGGTGTGGCTGCTGCCTCTGGTGCTGACCAGCCTGGCCAGCAGCGCCACCTGG
GCCGGCCAGCCCGCCAGCCCTCCCGTGGTGGACACCGCCCAGGGCAGGGTGCT
GGGCAAGTACGTGAGCCTGGAGGGCCTGGCCCAGCCCGTGGCCGTGTTCCTGGG
CGTGCCCTTCGCCAAGCCTCCCTTGGGCAGCCTGAGGTTCGCTCCTCCTCAGCCT
GCTGAGCCCTGGAGCTTCGTGAAGAACACCACCAGCTACCCTCCCATGTGCTGCC
AGGATCCCGTGGTGGAGCAGATGACCAGCGACCTGTTCACCAACGGCAAGGAGA
GGCTGACCCTGGAGTTCAGCGAGGACTGCCTGTACCTGAACATCTACACACCCGC
CGACCTGACCAAGAGAGGCAGGCTGCCCGTGATGGTGTGGATCCACGGCGGCGG
CCTGGTGCTGGGCGGCGCTCCCATGTACGACGGCGTGGTGCTGGCCGCCCACGA
GAACGTGGTGGTGGTGGCCATCCAGTACAGGCTGGGCATCTGGGGCTTCTTCAGC
ACCGGCGACGAGCACAGCAGgGGCAACTGGGGCCACCTGGACCAGGTGGCCGC
CCTGCACTGGGTGCAGGAGAACATCGCCAACTTCGGCGGCGATCCCGGCAGCGT
GACCATCTTCGGCGAGAGCGCCGGCGGCGAGAGCGTGAGCGTGCTGGTGCTGA
GCCCTCTGGCCAAGAACCTGTTCCACAGGGCCATCAGCGAGAGCGGCGTGGCCC
TGACCGTGGCCCTGGTGAGGAAGGACATGAAGGCCGCCGCCAAGCAGATCGCCG
TGCTGGCCGGCTGCAAGACCACCACCAGCGCCGTGTTCGTGCACTGCCTGAGGC
AGAAGAGCGAGGACGAGCTGCTGGACCTGACCCTGAAGATGAAGTTCCTGACCCT
GGACTTCCACGGCGACCAGAGGGAGAGCCATCCCTTCCTGCCCACCGTGGTGGA
CGGCGTGCTGCTGCCCAAGATGCCCGAGGAGATCCTGGCCGAGAAGGACTTCAA
CACCGTGCCCTACATCGTGGGCATCAACAAGCAGGAGTTCGGCTGGCTGCTGCCC
ACtATGATGGGCTTCCCTCTGAGCGAGGGCAAGtTGGACCAGAAGACCGCCACCAG
CCTGCTGTGGAAGAGCTATCCCATCGCCAACATTCCCGAGGAGCTGACACCCGTG
GCCACCGACAAGTACCTGGGCGGCACCGACGATCCCGTGAAGAAGAAGGACCTG
TTCCTGGACCTGATGGGCGACGTGGTGTTCGGCGTGCCCAGCGTGACCGTGGCC
AGGCAGCACAGGGACaCCGGCGCTCCCACCTACATGTACGAGTTCCAGTACAGGC
CCAGCTTCAGCAGCGACAAGAAGCCCAAGtCCGTGATCGGCGACCACGGCGACGA
GATCTTCAGCGTGTTCGGCTTCCCTCTGCTGAAGGGCGACGCTCCCGAGGAGGAG
GTGAGCCTGAGCAAGACCGTGATGAAGTTCTGGGCCAACTTCGCCAGGAGCGGC

AATCCCAACGGCGAGGGCCTGCCTCACTGGCCCATGTACGACCAGGAGGAGGGC
TACCTGCAGATCGGCGTGAACACCCAGGCCGCCAAGAGGCTGAAGGGCGAGGAG
GTGGCCTTCTGGAACGACCTGCTGAGCAAGGAGGCCGCCAAGAAGCCTCCTAAG
ATCAAG
HA:
TATCCATATGATGTTCCAGATTATGCT
DAF:
CCAAATAAAGGAAGTGGAACCACTTCAGGTACTACCCGTCTTCTATCTGGGCACAC
GTGTTTCACGTTGACAGGTTTGCTTGGGACGCTAGTAACCATGGGCTTGCTGACTT
AG
IRES:
GCCCCTCTCCCTCCCCCCCCCCTAACGTTACTGGCCGAAGCCGCTTGGAATAAGG
CCGGTGTGCGTTTGTCTATATGTTATTTTCCACCATATTGCCGTCTTTTGGCAATGT
GAGGGCCCGGAAACCTGGCCCTGTCTTCTTGACGAGCATTCCTAGGGGTCTTTCC
CCTCTCGCCAAAGGAATGCAAGGTCTGTTGAATGTCGTGAAGGAAGCAGTTCCTCT
GGAAGCTTCTTGAAGACAAACAACGTCTGTAGCGACCCTTTGCAGGCAGCGGAAC
CCCCCACCTGGCGACAGGTGCCTCTGCGGCCAAAAGCCACGTGTATAAGATACAC
CTGCAAAGGCGGCACAACCCCAGTGCCACGTTGTGAGTTGGATAGTTGTGGAAAG
AGTCAAATGGCTCTCCTCAAGCGTATTCAACAAGGGGCTGAAGGATGCCCAGAAG
GCACCCCATTGTATGGGATCTGATCTGGGGCCTCGGTGCACATGCTTTACATGTGT
TTAGTCGAGGTTAAAAAAACGTCTAGGCCCCCCGAACCACGGGGACGTGGTTTTC
CTTTGAAAAACACGATGATAATATGGCCACA
mCherry:
GTGAGCAAGGGCGAGGAGGACAACATGGCCATCATCAAGGAGTTCATGCGCTTCA
AGGTGCACATGGAGGGCTCCGTGAACGGCCACGAGTTCGAGATCGAGGGCGAGG
GCGAGGGCCGCCCCTACGAGGGCACCCAGACCGCCAAGCTGAAGGTGACCAAG
GGCGGCCCCCTGCCCTTCGCCTGGGACATCCTGTCCCCTCAGTTCATGTACGGCT
CCAAGGCCTACGTGAAGCACCCCGCCGACATCCCCGACTACTTGAAGCTGTCCTT
CCCCGAGGGCTTCAAGTGGGAGCGCGTGATGAACTTCGAGGACGGCGGCGTGGT
GACCGTGACCCAGGACTCCTCCCTGCAGGACGGCGAGTTCATCTACAAGGTGAAG
CTGCGCGGCACCAACTTCCCCTCCGACGGCCCCGTAATGCAGAAGAAGACCATG
GGCTGGGAGGCCTCCTCCGAGCGGATGTACCCCGAGGACGGCGCCCTGAAGGG
CGAGATCAAGCAGAGGCTGAAGCTGAAGGACGGCGGCCACTACGACGCCGAGGT
CAAGACCACCTACAAGGCCAAGAAGCCCGTGCAGCTGCCCGGCGCCTACAACGT
CAACATCAAGCTGGACATCACCTCCCACAACGAGGACTACACCATCGTGGAACAG
TACGAGCGCGCCGAGGGCCGCCACTCCACCGGCGGCATGGACGAGCTGTACAAG

To screen our second-generation targeting system in HEK cells, we subcloned PLE via restriction digest (NheI, SalI) and subsequent Gibson Assembly into pCDNA3.1 vector containing a cytomegalovirus (CMV) promoter, a 5' PAT-3secretion signal, and a 3' mouse CD4 transmembrane domain. For expression in *Drosophila*, PAT-3-Targeting Protein-CD4 was inserted into 20X UAS pJFRC7 backbone via restriction digest (XhoI and XbaI) and Gibson assembly (Addgene). All constructs were sequence confirmed by the UCB Sequencing Facility.

CMV enhancer:

GACATTGATTATTGACTAGTTATTAATAGTAATCAATTACGGGGTCATTAGTTCATA
GCCCATATATGGAGTTCCGCGTTACATAACTTACGGTAAATGGCCCGCCTGGCTGA
CCGCCCAACGACCCCCGCCCATTGACGTCAATAATGACGTATGTTCCCATAGTAAC
GCCAATAGGGACTTTCCATTGACGTCAATGGGTGGACTATTTACGGTAAACTGCCC
ACTTGGCAGTACATCAAGTGTATCATATGCCAAGTACGCCCCCTATTGACGTCAAT
GACGGTAAATGGCCCGCCTGGCATTATGCCCAGTACATGACCTTATGGGACTTTCC
TACTTGGCAGTACATCTACGTATTAGTCATCGCTATTACCATG
CMV promotor:
GTGATGCGGTTTTGGCAGTACATCAATGGGCGTGGATAGCGGTTTGACTCACGGG
GATTTCCAAGTCTCCACCCCATTGACGTCAATGGGAGTTTGTTTTGGCACCAAAAT
CAACGGGACTTTCCAAAATGTCGTAACAACTCCGCCCCATTGACGCAAATGGGCG
GTAGGCGTGTACGGTGGGAGGTCTATATAAGCAGAGCT
PAT-3:
ATGCCACCTTCAACATCATTGCTGCTCCTCGCAGCACTTCTTCCATTCGCTTTACCA
GCAAGCGATTGGAAGACTGGAGAAGTCACTG
HA Tag:
TATCCATATGATGTTCCAGATTATGCT
Linker:
GGTGGCGGCGGAAGTGGAGGTGGAGGCTCG
CD4:
TTCCAGAAGGCCTCCAGCATAGTCTATAAGAAAGAGGGGGAACAGGTGGAGTTCT
CCTTCCCACTCGCCTTTACAGTTGAAAAGCTGACGGGCAGTGGCGAGCTGTGGTG
GCAGGCGGAGAGGGCTTCCTCCTCCAAGTCTTGGATCACCTTTGACCTGAAGAAC
AAGGAAGTGTCTGTAAAACGGGTTACCCAGGACCCTAAGCTCCAGATGGGCAAGA
AGCTCCCGCTCCACCTCACCCTGCCCCAGGCCTTGCCTCAGTATGCTGGCTCTGG
AAACCTCACCCTGGCCCTTGAAGCGAAAACAGGAAAGTTGCATCAGGAAGTGAAC
CTGGTGGTGATGAGAGCCACTCAGCTCCAGAAAAATTTGACCTGTGAGGTGTGGG
GACCCACCTCCCCTAAGCTGATGCTGAGCTTGAAACTGGAGAACAAGGAGGCAAA
GGTCTCGAAGCGGGAGAAGGCGGTGTGGGTGCTGAACCCTGAGGCGGGGATGT
GGCAGTGTCTGCTGAGTGACTCGGGACAGGTCCTGCTGGAATCCAACATCAAGGT
TCTGCCCACATGGTCCACCCCGGTGCAGCCAATGGCCCTGATTGTGCTGGGGGG
CGTCGCCGGCCTCCTGCTTTTCATTGGGCTAGGCATCTTCTTCTGTGTCAGGTGCC
GGCACCGAAGGCGCTAG
20xUAS:
TCCGGAACATAATGGTGCAGGGCGCTGACTTCCGCGTTTCCAGACTTTACGAAAC
ACGGAAACCGAAGACCATTCATGTTGTTGCTCAGGTCGCAGACGTTTTGCAGCAG
CAGTCGCTTCACGTTCGCTCGCGTATCGGTGATTCATTCTGCTAACCAGTAAGGCA
ACCCCGCCAGCCTAGCCGGGTCCTCAACGACAGGAGCACGATCATGCGCACCCG
TGGCCAGGGCCGCAAGCTTGCATGCCTGCAGGTCGGAGTACTGTCCTCCGAGCG
GAGTACTGTCCTCCGAGCGGAGTACTGTCCTCCGAGCGGAGTACTGTCCTCCGAG
CGGAGTACTGTCCTCCGAGCGGAGACTCTAGCCCTAGGGCATGCCTGCAGGTCG
GAGTACTGTCCTCCGAGCGGAGTACTGTCCTCCGAGCGGAGTACTGTCCTCCGAG
CGGAGTACTGTCCTCCGAGCGGAGTACTGTCCTCCGAGCGGAGACTCTAGCGCTA
GCGCATGCCTGCAGGTCGGAGTACTGTCCTCCGAGCGGAGTACTGTCCTCCGAG
CGGAGTACTGTCCTCCGAGCGGAGTACTGTCCTCCGAGCGGAGTACTGTCCTCCG
AGCGGAGACTCTAGCACTAGTGCATGCCTGCAGGTCGGAGTACTGTCCTCCGAGC

GGAGTACTGTCCTCCGAGCGGAGTACTGTCCTCCGAGCGGAGTACTGTCCTCCGA
GCGGAGTACTGTCCTCCGAGCGGAGACTCTAGCGACGTCGAGCGCCGGAGTATA
AATAGAGGCGCTTCGTCTAC
HSP70promoter:
GGAGCGACAATTCAATTCAAACAAGCAAAGTGAACACGTCGCTAAGCGAAAGCTAA
GCAAATAAACAAGCGCAGCTGAACAAGCTAAACAATCTGCAGTAAAGTGCAAGTTA
AAGTGAATCAATTAAAAGTAACCAGCAACCAAGTAAATCAACTGCAA

Cell culture and transfection.

We obtained cell lines from the UCB Cell Culture Facility. Human embryonic kidney 293T (HEK) cells were maintained in Dulbecco's modified eagle medium (DMEM) supplemented with 1 g/L D-glucose, 10% fetal bovine serum (FBS; Thermo Scientific) and 1% GlutaMax (Invitrogen) at 37 °C in a humidified incubator with 5 % CO2. Cells were passaged and plated in DMEM (as above) at a density of 50,000 cells onto 12 mm coverslips pre-treated with Poly-D-lysine (PDL;1mg/ml; Sigma-Aldrich). Transfection of plasmids was carried out using Lipofectamine 3000 (Invitrogen) 12 hours after plating. Imaging was performed 36 hours after plating.

Dye Loading.

We maintained DMSO stock solutions (100 µM) of all dyes at -20 °C in single-use aliquots. Aliquots were further diluted to a working concentration of 100 nM or in HBSS (Life Technologies) and incubated on cells for 30 minutes at 37 °C. We then replaced all dye-containing HBSS with fresh HBSS and imaged in at room temperature.

Epifluorescence microscopy.

Imaging was performed on an AxioExaminer Z-1 (Zeiss) equipped with a Spectra-X Light engine LED light (Lumencor), controlled with Slidebook (v6, Intelligent Imaging Innovations). Images were acquired with a W-Plan-Apo 20x/1.0 water objective (20x; Zeiss) and focused onto an OrcaFlash4.0 sCMOS camera (sCMOS; Hamamatsu). The optical set up for imaging with each dye described below.

Table A1-1: Epifluorescence microscopy optics

Dye	Excitation	Emission	Dichroic
VF-Spy	475/34 nm BP	540/50 nm BP	510 nm LP
A647	542/33 nm BP	650/60 BP	594 nm LP
Hoechst 33342	375-400nm	405/40 BP	415 LP

Immunocytochemistry.

Immediately following live-cell dye loading experiments, cells were fixed for 20 minutes at room temperature with 4% formaldehyde in PBS. Cells were then washed in PBS (3x

5-minute washes) and treated with either 0.3% Triton x -100 in PBS for the permeabilized condition or PBS for the nonpermeabilized condition. Cells were again washed in PBS and blocked for at least 45 minutes in 0.1% NGS in PBS. Cells were then incubated overnight at 4 °C with 1:500 Rat anti HA (Sigma Aldrich). We then washed each sample in PBS and stained with a spectrally compatible Goat anti-RT A647 (Life Technologies) 1:1000 in 0.1%NGS for 2hrs at room temperature. We added Hoechst 33342 (10mg/mL -20 stock) 1:1000 for the last 15 minutes of this incubation period. Cells were then washed in PBS and mounted onto glass slides using Fluoramount Mounting Media (VWR International) before imaging.

Transgenic generation.

pUAST-IgK-PLEHA-DAF-IRES-mCherry and pJFRC7-PAT-3 -PLEHA-CD4 were sent to Best Gene Inc. for injection into the following genomic sites via phi C31 integration.

Table A1-2: Injection details

Construct	**Injection Site**	**Injection stock**
pUAST-IgK-PLEHA-DAF-IRES	Random insertion	---
pJFRC7-PAT-3-PLEHA-CD4	VIE260B	VDRC#60100

Immunohistochemistry.

Flies were dissected in calcium-magnesium free artificial hemolymph (AHL-/-; NaCl 108.0mM, KCl 5.0mM, NaHCO3 4.0 mM, NaH2PO4·H2O 1.0 mM, Trehalose· 2 H2O 5.0mM, Sucrose 10.0mM, HEPES 5.0mM and adjusted to pH 7.5 with NaOH) and fixed for 20 minutes in 4% formaldehyde in PBS. Brains were then washed in PBS (Sigma,3x 5-minute washes) and treated with either 0.3% Triton x -100 in PBS for the permeabilized condition or PBS for the non-permeabilized condition. Brains were again washed in PBS (3x 5-minute washes) and blocked for at least 45 minutes in 0.1% NGS in PBS. Cells were incubated overnight in block containing 1:50 RT anti HA (Sigma Aldrich) and nc82 anti-mouse (DSHB) at 4 °C for 48 hours while gently spinning. Brains were then washed in PBS and stained with Goat anti-Rat A488 (Life Technologies) 1:1000 and Goat anti-Mouse A647 (Life Technologies) in block for 2-4 hours at room temperature shaking. We added Hoechst 33342 1:1000 for the last 15 minutes of this incubation. Brains were then washed and mounted onto glass slides using vectashield mounting media (Life Technologies) before imaging using confocal microscopy.

Confocal Microscopy.

Imaging was performed using an LSM710 upright confocal microscope.

Table A1-3: Confocal microscopy optics

Dye	Excitation	Emission	Dichroic
A488	488	505-530 BP	488/543/633
A647	633	635 LP	488/543/633
Hoechst 33342	405	493-557 BP	405

Images were taken as 3 µm step z stacks through the entirety of the brain. Using the following settings 3.20 µs dwell time and pinhole size between 80 µm and 108 µm. For display, each z-stack was displayed as a summed or maximum z-projection of the first 15 frames of the image stack.

Invitro Assay.

For the control assay 1µM Fex-1 was placed PBS and reacted with varying concentrations of isolated PLE (Sigma-Aldrich). Each sample reaction was run in triplicate in black corning 96 well assay plates and 37°C for 1 hour. Fluorescence emission spectra were collected across 300 -700 nm wavelengths using a Tecan plate reader. Data was background subtracted and displayed as fluorescent counts per wavelength.

Lysate assay.

Whole flies were squished in RIPA buffer containing both DTT and protease inhibitor cocktail. Brains were then mechanically dissociated via mortar and pestle until the solution was homogeneous. Solutions were then spun down, and the supernatant was collected and stored on ice. A BCA assay was used to determine protein concentration (Thermo Fisher Scientific). Samples were then stored overnight at -80°C. Samples were thawed on ice and diluted with PBS to 0.32ug/ul total protein in each solution and allowed to react with PLE substrate F-ex1 for 1 hour at 37°C.

Figures.

Figure A1-1.

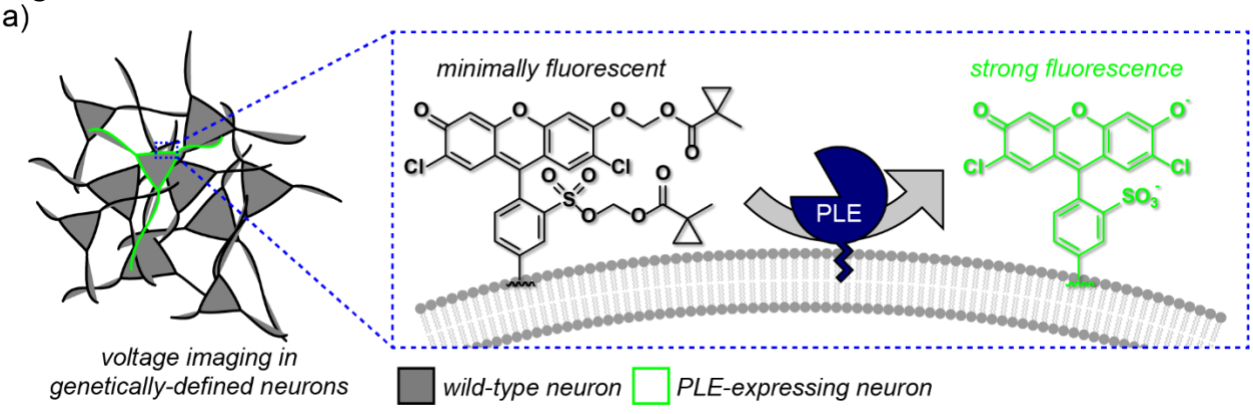

Figure A1-1. Schematic of fluorogenic targeting using PLE. Neurons when loaded with fluorogenic activated dye VF-EX1 and VF-EX2 remain dark until they interact with extracellularly targeted PLE protein which uncages the fluorophore resulting in a fluorescence increase in intensity.

Figure A1-2.

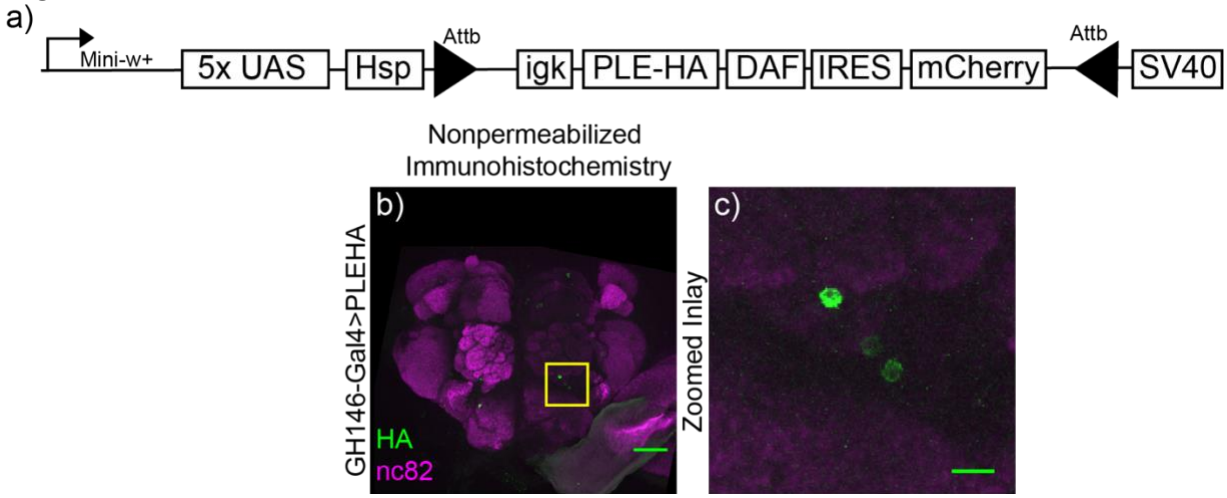

Figure A1-2. First generation PLE for expression in *Drosophila* **a)** pUAST *Drosophila* expression vector design containing IgK secretion signal PLE-HA protein and DAF GPI anchor motif for extracellular plasma membrane trafficking. Maximum z-project confocal image of immunostained GH146-Gal4 driven PLE-DAF expression under non-permeabilizing conditions (**b)**. HA epitope (green) and nc82 counterstain (magenta). Yellow box denotes region displayed in panel **(c)**. The scale is 50 µm. **c)** Zoomed image of cells from the yellow box in panel c showing a small number of HA immunopositive cells in the expected region. HA epitope (green) and nc82 counterstain (magenta). The scale is 10 µm.

Figure A1-3.

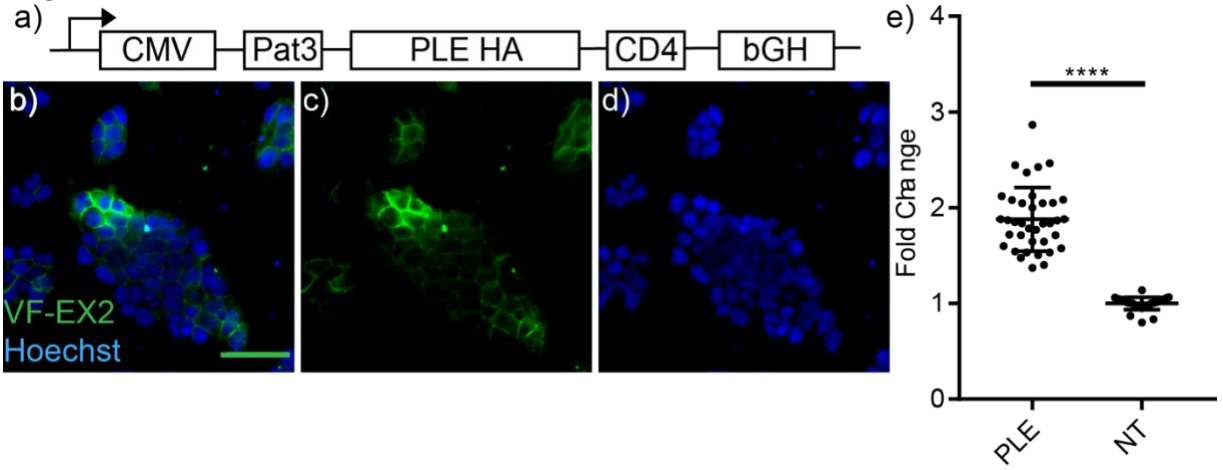

Figure A1-3. Second generation mammalian PLE expression vector in HEK293T cells. **a)** Schematic of pCDNA3.1 mammalian expression vector containing PAT-3-PLE-HA-CD4 expressed under the CMV promotor. **b-d**) Live cell loading of PLE-CD4 transfected

HEK cells with 100 nM VF-EX2 **(c)** and nuclear counterstained using Hoechst 33342 (at a concentration of 10 µg/ul, equivalent to 16 µM **(d)** The scale bar is 50 µM. **e)** Quantification of normalized fluorescence intensity in PLE-CD4 transfected HEK cells treated with 100 nM VF-EX2. Each data point represents one cell across three independent coverslips (t-test, **** $p<0.001$)

Figure A1-4.

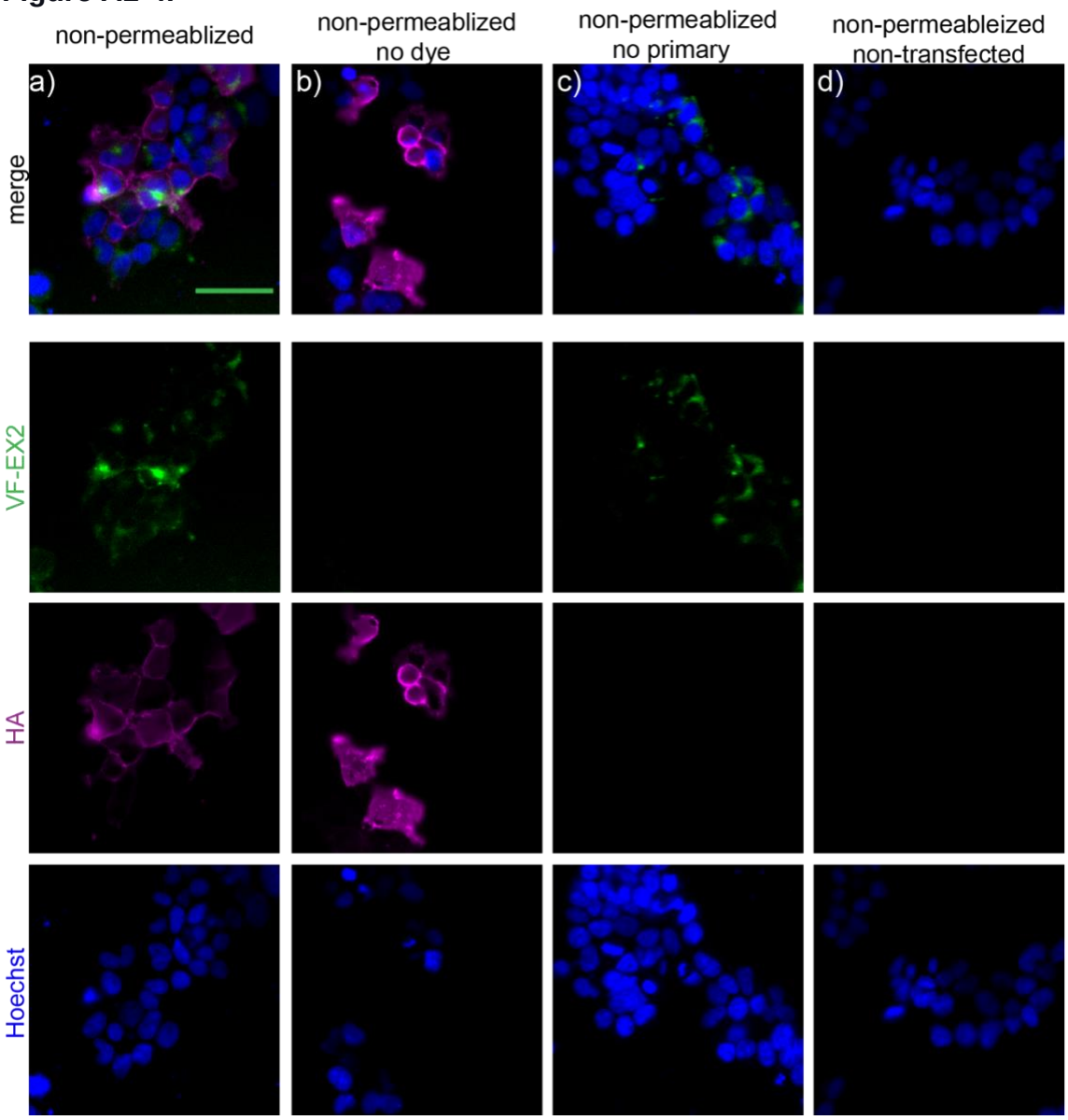

Figure A1-4. Immunocytochemistry in HEK293T cells. Epifluorescence images of HEK293T cells expressing PLE-CD4 and stained with VF-EX2 (100 nm, green). Cells were then fixed and stained under non-permeabilizing conditions for HA (magenta) and nuclear counterstained using Hoechst 33342 (at a concentration of 10 µg/ul, equivalent to 16 µM) **(a).** Controls were treated with **b)** primary antibody but no dye, **c)** dye but no primary CD4 antibody and **d)** with dye and primary antibody but without transfection. Scale bar is 50 µm.

Figure A1-5.

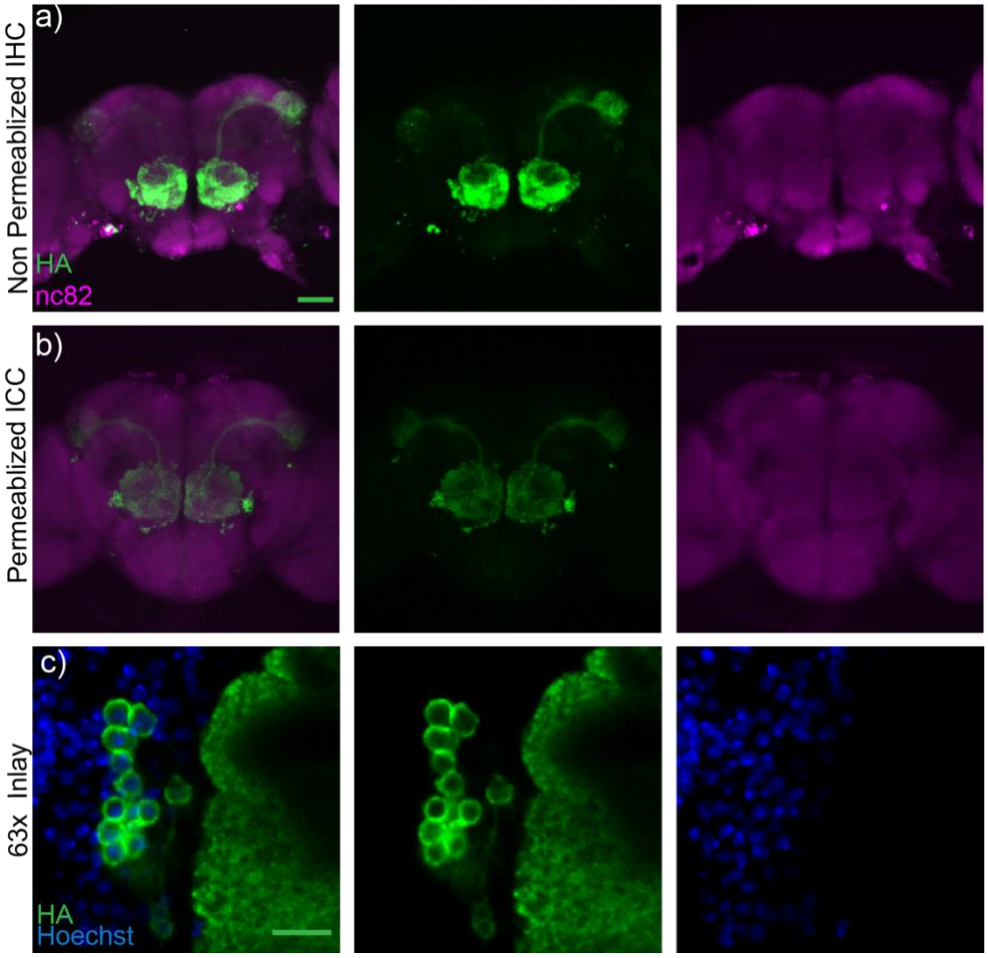

Figure A1-5. Permeabilized and non-permeabilized immunohistochemistry for PLE-CD4 in GH146-Gal4>PLE-CD4 *Drosophila* brains. Confocal summed z-projection of GH146-Gal4 > PLE-CD4 fly immunostained under **a)** non-permeabilizing conditions and **b)** permeabilizing for HA (green) and nc82 (magenta). The scale is 50 µm. **c)** 63x magnification single confocal slice of lateral antennal lobe projection neurons stained for HA (green) and nuclear counterstained using Hoechst 33342 (at a concentration of 10 µg/µL, equivalent to 16 µM). Scale is 10 µm.

Figure A1-6.

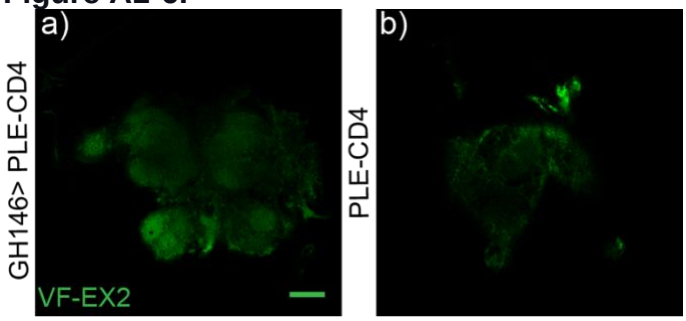

Figure A1-6. Voltage sensitive dye loading in PLE expressing *Drosophila* brains. Single confocal z-slice of **a)** GH146 Gal4>PLE-CD4 or **b)** PLE-CD4 live tissue loaded with 20 µM of VF-EX2 (green). The scale is 50 µm.

Figure A1-7.

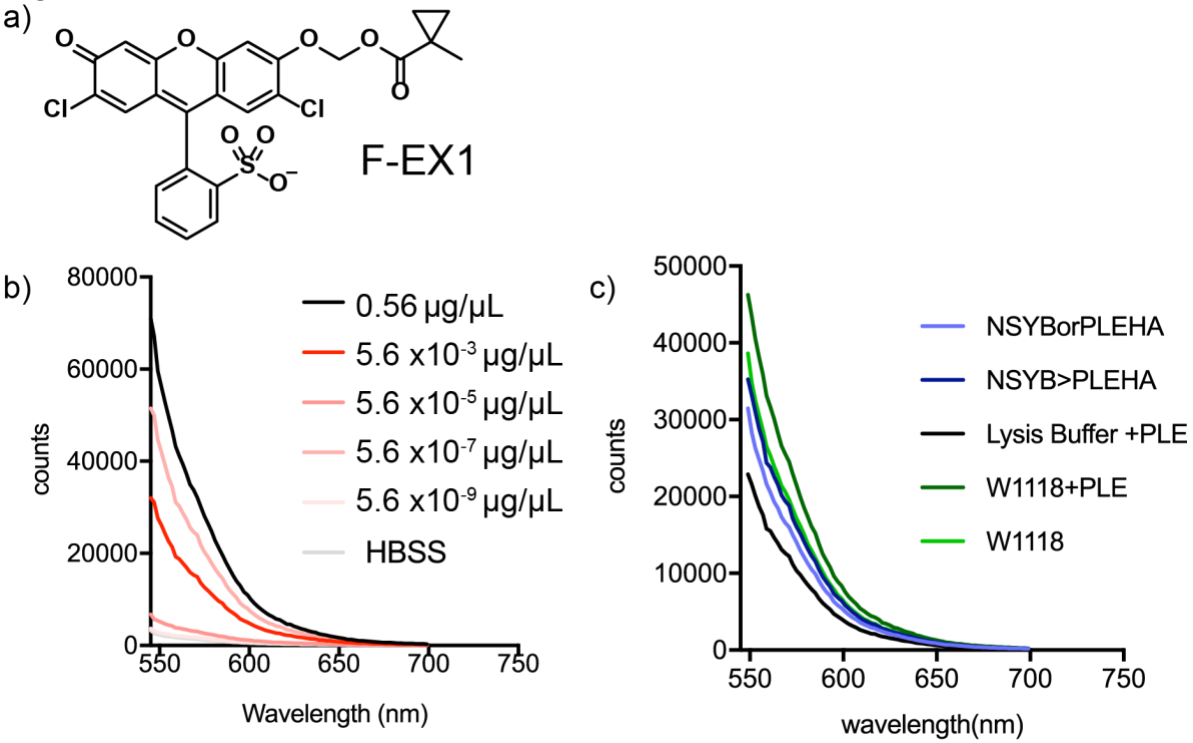

Figure A1-7. In cuvette activity characterization of isolated PLE and PLE expressing *Drosophila* lysate. **a)** Structure of F-ex1 showing single ester capping of the phenolic oxygen of a sulfonated fluorescein dye head. **b)** Fluorescence counts of F-EX1 reacted with a range of PLE concentrations. Each trace represents the average across three individual wells. **c)** Fluorescence spectra of F-EX1 reacted with nSyb-Gal4 or PLE-HA genetic control lysate (light blue), nSyb-Gal4 > PLE-CD4 experimental lysate(dark blue), lysis buffer + PLE(black), W1118 lysate +PLE (dark green) and W1118 lysate alone (light green). Each trace represents the average of three trials.

References

1. Janigro, D., Ikeda, A., Lin, C. K., Jiruska, P. & Aristea, S. Translational Task Force of the ILAE. **58**, 40–52 (2018).
2. Miller, E. W. *et al.* Optically monitoring voltage in neurons by photo-induced electron transfer through molecular wires. *Proc. Natl. Acad. Sci.* **109**, 2114 LP – 2119 (2012).
3. Huang, Y. L., Walker, A. S. & Miller, E. W. A Photostable Silicon Rhodamine Platform for Optical Voltage Sensing. *J. Am. Chem. Soc.* **137**, 10767–10776 (2015).
4. Kulkarni, R. U. *et al.* A Rationally Designed, General Strategy for Membrane Orientation of Photoinduced Electron Transfer-Based Voltage-Sensitive Dyes. *ACS Chem. Biol.* (2017). doi:10.1021/acschembio.6b00981
5. Deal, P. E., Kulkarni, R. U., Al-abdullatif, S. H., Miller, E. W. & Biology, C. Isomerically Pure Tetramethylrhodamine Voltage Reporters. *JACS* **138**, 9085–9088 (2017).
6. Ortiz, G., Liu, P., Naing, S. H. H., Muller, V. R. & Miller, E. W. Synthesis of Sulfonated Carbofluoresceins for Voltage Imaging. *J. Am. Chem. Soc.* **141**, 6631–6638 (2019).
7. Kulkarni, R. U. *et al.* In Vivo Two-Photon Voltage Imaging with Sulfonated Rhodamine Dyes. *ACS Cent. Sci.* (2018). doi:10.1021/acscentsci.8b00422
8. Kulkarni, R. U. & Miller, E. W. Voltage Imaging: Pitfalls and Potential. *Biochemistry* (2017).
9. Tian, L. *et al.* Selective esterase-ester pair for targeting small molecules with cellular specificity. *Proc. Natl. Acad. Sci.* **109**, 4756–4761 (2012).
10. Liu, P., Grenier, V., Hong, W., Muller, V. R. & Miller, E. W. Fluorogenic Targeting of {Voltage-Sensitive} Dyes to Neurons. *J. Am. Chem. Soc.* jacs.7b07047 (2017).
11. Brand, A. H. & Perrimon, N. Targeted gene expression as a means of altering cell fates and generating dominant phenotypes. *Development* **118**, 289–295 (1993).
12. Feinberg, E. H. *et al.* GFP Reconstitution Across Synaptic Partners (GRASP) Defines Cell Contacts and Synapses in Living Nervous Systems. *Neuron* **57**, 353–363 (2008).
13. Gordon, M. D. & Scott, K. NIH Public Access. **61**, 373–384 (2010).
14. Stocker, R. F., Heimbeck, G., Gendre, N. & de Belle, J. S. Neuroblast ablation in Drosophila P[GAL4] lines reveals origins of olfactory interneurons. *J. Neurobiol.* **32**, 443–456 (1997).
15. Pfeiffer, B. D. *et al.* Refinement of tools for targeted gene expression in Drosophila. *Genetics* **186**, 735–755 (2010).
16. DiAntonio, A. *et al.* Identification and characterization of Drosophila genes for synaptic vesicle proteins. *J. Neurosci.* **13**, 4924–4935 (1993).
17. Ortiz, G., Liu, P., Naing, S. H. H., Muller, V. R. & Miller, E. W. Synthesis of Sulfonated Carbofluoresceins for Voltage Imaging. *J. Am. Chem. Soc.* **141**, 6631–6638 (2019)

Appendix 2: Extracellular trafficking of SpyCatcher in *Drosophila melanogaster*.

Portions of this work were completed in collaboration with others: Vincent Grenier generated VF-Spy dyes

Background

The brain is an organ of interconnected cells that utilize electrochemical signals called action potentials to communicate. It is the action potential frequency and pattern from these cells which drives neural computation and output. However, to accurately interpret these events, we must be able to monitor them across multiple neurons simultaneously. One method which has proven successful at monitoring neuronal activity in primary neuronal culture[1–4] and mouse brain slice[5] are Photo-induced electron Transfer Voltage Sensitive Dyes (PeT Dyes). PeT Dyes sit on the extracellular surface of the membrane and sense the transmembrane potential via a photoinduced electron transfer mechanism revealing high fidelity tracking of action potentials across many cells[1]. Unfortunately, PeT dyes have been challenging to apply in complex tissues as they label all available membranes indiscriminately. This indiscriminate labeling significantly reduces the signal to noise ratio and precludes genetic identification of cell subtypes during experimentation[5]. For this reason, we sought to tether the voltage-sensitive dyes to specific genetically defined cell populations. In light of this aim, our group recently reported that voltage-sensitive dyes could be genetically targeted in cultured mammalian cells using a protein and small peptide pair called SpyCatcher and SpyTag, respectively[6,7]. The SpyCatcher protein, an engineered cell adhesion molecule from *Streptococcus pyogenes*, which reacts with the 13 amino acid peptide tag coupled voltage-sensitive dye forming a stable covalent bond between the dye and the extracellularly trafficked SpyCatcher protein. We found that SpyCatcher reactive PeT dyes are voltage-sensitive (12.7 ± 0.1 % $\Delta F/F$ per 100 mV) in HEK 293T cells and report somatic and axonal action potentials in primary hippocampal cell culture with high signal to noise[7].

Due to the success of SpyCatcher *in vitro*, we sought to transition this technology to more complex tissues. We chose *Drosophila* due to their rapid generation times and ease of transgenic development, which made this model organism an ideal platform for testing the voltage-sensitive dye tethering system *in vivo*. As a result of previous experiments targeting Porcine Liver Esterase (Appendix 1) to the extracellular surface, we utilized the *Drosophila* tested PAT-3 secretion signal and CD4 transmembrane domain to traffic SpyCatcher to the extracellular surface in *Drosophila*[8,9]. In this appendix, we will outline the generation and characterization of mammalian SpyCatcher expression vectors in HEK 293T cells as well as the generation and preliminary assessment of SpyCatcher's extracellular expression and trafficking in *Drosophila* nervous tissue. Ultimately, although SpyCatcher expressed intracellularly, it was not readily trafficked to the cell surface in *Drosophila*. The lack of trafficking may result from an unexpected interaction of the protein with the *Drosophila* secretory pathway; however, this remains to be determined. Due to the lack of trafficking, we set this project aside for other covalent tethering systems. We suggest that further characterization of the SpyCatcher protein expression in S2 cells would be required to explicitly determine what hinders the trafficking of this construct in *Drosophila* tissue samples.

Results

To target SpyCatcher to the extracellular surface in mammalian cells (**Figure A2-1**), we first subcloned a Pat3-HA-Spycatcher-Myc-CD4 (SpyCatcher-CD4) fragment into a CMV promoted pCDNA3.1 mammalian expression vector(**Figure A2-2a**). We then confirmed SpyCatcher-CD4 trafficking and protein function by loading transfected HEK 293T cells with 5 nM of Spy reactive voltage-sensitive dye VF-Spy(**Figure A2-2b**). VF-Spy tethered to the SpyCatcher positive cells with an increased fluorescence intensity of approximately 1.5-fold above non-transfected cells (**Figure A2-2e**)**.** To confirm the protein expression on the extracellular surface in HEK293T cells, we performed immunocytochemistry against the HA epitope under non-permeabilized conditions (**Figure A2-2c and d**). We found that the protein was accurately trafficked to the extracellular surface. We next sought to express the SpyCatcher-HA protein in *Drosophila* under the Gal4/UAS enhancer trap system[10]

To drive expression of SpyCatcher-CD4 in *Drosophila*, we first subcloned Pat3-HA-SpyCatcher-Myc-CD4 into a 20x UAS pJFRC7 expression vector (**Figure A2-3a**)[11] We then injected this construct for site-specific genomic integration at the attP3 site due to reported high expression levels and x chromosome location[11]. Having generated the SpyCatcher-CD4 transgenic line, we then crossed it to the pan-neuronal Gal4 driver line nSyb-Gal4[12].To assess the expression and trafficking of the SpyCatcher protein, we performed immunohistochemistry (IHC) against HA and CD4 under non-permeabilizing conditions (**Figure A2-3b**)**,** and permeabilizing conditions (**Figure A2-3c**). IHC revealed that SpyCatcher-CD4 was readily expressed but did not traffic well to the extracellular surface in *Drosophila* nerve cells. Ultimately, further characterization of SpyCatcher trafficking should be performed in an invertebrate cell line such as S2 cells.

Conclusion and future steps

We found that SpyCatcher is functional and capable of targeting voltage-sensitive dyes when expressed at the cell surface in HEK 293T cells using a Pat3 Secretion signal and CD4 transmembrane anchoring domain. We generated a transgenic *Drosophila* UAS reporter line that robustly expresses SpyCatcher when driven under the pan-neuronal driver line nSyb-Gal4. However, the Pat3-Spycatcher-HA-CD4 construct does not traffic well to the extracellular surface in *Drosophila*, a finding confirmed by multiple rounds of non-permeabilized IHC. Having found that SpyCatcher did not traffic well, we tabled this project for other covalent tethering platforms such as HaloTag and SNAP-Tag.

Future efforts for SpyCatcher based targeting of voltage-sensitive dyes should involve the optimization of extracellular trafficking in *Drosophila* S2 cells. These lines will more accurately represent the invertebrate secretory pathway and its interaction with the protein construct. The first experiment would be to examine the current Pat3-Ha-SpyCatcher-Myc-CD4 construct in S2 cells monitoring expression and trafficking using immunocytochemistry for both the HA and CD4. Assuming this will also not traffic to the extracellular surface in S2 cells as expected, the protein sequence should be examined via BLAST search for potential retention signals or other features that could hinder the expression of the protein on the cell surface. Finally, a screen should be run for protein

trafficking using immunocytochemistry as a readout. Here it will be essential to assess three features: 1) epitope tag presence and its effect on extracellular trafficking 2) removal of any potential retention signals within the protein and 3) a series of other *Drosophila* secretion signals and anchoring domains to determine the optimal targeting system for SpyCatcher in *Drosophila*. Ultimately, this project may be of interest as an orthogonal method for the currently functional voltage-sensitive dye tethering platform HaloTag but would require some effort to get to a point where we can assess its potential as a targeting system.

Methods

Plasmid construction.

To target SpyCatcher to the extracellular surface in HEK 293T cells, we subcloned SpyCatcher via restriction digest (NheI, SalI) and subsequent Gibson Assembly into pCDNA3.1 vector containing a cytomegalovirus (CMV) promoter, a 5' Pat3 secretion signal, and a 3' mouse CD4 transmembrane domain. For expression in *Drosophila*, we inserted the Pat3-Targeting Protein-CD4 into the pJFRC7 backbone via restriction digest (XhoI and XbaI) and Gibson assembly (Addgene). All constructs were sequence confirmed by the UCB Sequencing Facility.

CMV enhancer:
GACATTGATTATTGACTAGTTATTAATAGTAATCAATTACGGGGTCATTAGTTCATA
GCCCATATATGGAGTTCCGCGTTACATAACTTACGGTAAATGGCCCGCCTGGCTGA
CCGCCCAACGACCCCCGCCCATTGACGTCAATAATGACGTATGTTCCCATAGTAAC
GCCAATAGGGACTTTCCATTGACGTCAATGGGTGGACTATTTACGGTAAACTGCCC
ACTTGGCAGTACATCAAGTGTATCATATGCCAAGTACGCCCCCTATTGACGTCAAT
GACGGTAAATGGCCCGCCTGGCATTATGCCCAGTACATGACCTTATGGGACTTTCC
TACTTGGCAGTACATCTACGTATTAGTCATCGCTATTACCATG
CMV promotor:
GTGATGCGGTTTTGGCAGTACATCAATGGGCGTGGATAGCGGTTTGACTCACGGG
GATTTCCAAGTCTCCACCCCATTGACGTCAATGGGAGTTTGTTTTGGCACCAAAAT
CAACGGGACTTTCCAAAATGTCGTAACAACTCCGCCCCATTGACGCAAATGGGCG
GTAGGCGTGTACGGTGGGAGGTCTATATAAGCAGAGCT
Pat3:
ATGCCACCTTCAACATCATTGCTGCTCCTCGCAGCACTTCTTCCATTCGCTTTACCA
GCAAGCGATTGGAAGACTGGAGAAGTCACTG
HA Tag:
TATCCATATGATGTTCCAGATTATGCT
Spycatcher:
ATGTCGTACTACCATCACCATCACCATCACGATTACGACATCCCAACGACCGAAAA
CCTGTATTTTCAGGGCGCCATGGTTGATACCTTATCAGGTTTATCAAGTGAGCAAG
GTCAGTCCGGTGATATGACAATTGAAGAAGATAGTGCTACCCATATTAAATTCTCAA
AACGTGATGAGGACGGCAAAGAGTTAGCTGGTGCAACTATGGAGTTGCGTGATTC
ATCTGGTAAAACTATTAGTACATGGATTTCAGATGGACAAGTGAAAGATTTCTACCT
GTATCCAGGAAAATATACATTTGTCGAAACCGCAGCACCAGACGGTTATGAGGTAG

CAACTGCTATTACCTTTACAGTTAATGAGCAAGGTCAGGTTACTGTAAATGGCAAA
GCAACTAAAGGTGACGCTCATATT
Myc:
GAACAAAAACTCATCTCAGAAGAGGATCTG
Linker:
GGTGGCGGCGGAAGTGGAGGTGGAGGCTCG
CD4:
TTCCAGAAGGCCTCCAGCATAGTCTATAAGAAAGAGGGGGAACAGGTGGAGTTCT
CCTTCCCACTCGCCTTTACAGTTGAAAAGCTGACGGGCAGTGGCGAGCTGTGGTG
GCAGGCGGAGAGGGCTTCCTCCTCCAAGTCTTGGATCACCTTTGACCTGAAGAAC
AAGGAAGTGTCTGTAAAACGGGTTACCCAGGACCCTAAGCTCCAGATGGGCAAGA
AGCTCCCGCTCCACCTCACCCTGCCCCAGGCCTTGCCTCAGTATGCTGGCTCTGG
AAACCTCACCCTGGCCCTTGAAGCGAAAACAGGAAAGTTGCATCAGGAAGTGAAC
CTGGTGGTGATGAGAGCCACTCAGCTCCAGAAAAATTTGACCTGTGAGGTGTGGG
GACCCACCTCCCCTAAGCTGATGCTGAGCTTGAAACTGGAGAACAAGGAGGCAAA
GGTCTCGAAGCGGGAGAAGGCGGTGTGGGTGCTGAACCCTGAGGCGGGGATGT
GGCAGTGTCTGCTGAGTGACTCGGGACAGGTCCTGCTGGAATCCAACATCAAGGT
TCTGCCCACATGGTCCACCCCGGTGCAGCCAATGGCCCTGATTGTGCTGGGGGG
CGTCGCCGGCCTCCTGCTTTTCATTGGGCTAGGCATCTTCTTCTGTGTCAGGTGCC
GGCACCGAAGGCGCTAG
20xUAS:
TCCGGAACATAATGGTGCAGGGCGCTGACTTCCGCGTTTCCAGACTTTACGAAAC
ACGGAAACCGAAGACCATTCATGTTGTTGCTCAGGTCGCAGACGTTTTGCAGCAG
CAGTCGCTTCACGTTCGCTCGCGTATCGGTGATTCATTCTGCTAACCAGTAAGGCA
ACCCCGCCAGCCTAGCCGGGTCCTCAACGACAGGAGCACGATCATGCGCACCCG
TGGCCAGGGCCGCAAGCTTGCATGCCTGCAGGTCGGAGTACTGTCCTCCGAGCG
GAGTACTGTCCTCCGAGCGGAGTACTGTCCTCCGAGCGGAGTACTGT-
CCTCCGAGCGGAGTACTGTCCTCCGAGCGGAGACTCTAGCCCTAGGGCATGCCT
GCAGGTCGGAGTACTGTCCTCCGAGCGGAGTACTGTCCTCCGAGCGGAGTACTGT
CCTCCGAGCGGAGTACTGTCCTCCGAGCGGAGTACTGTCCTCCGAGCGGAGACT
CTAGCGCTAGCGCATGCCTGCAGGTCGGAGTACTGTCCTCCGAGCGGAGTACTGT
CCTCCGAGCGGAGTACTGTCCTCCGAGCGGAGTACTGTCCTCCGAGCGGAGTACT
GTCCTCCGAGCGGAGACTCTAGCACTAGTGCATGCCTGCAGGTCGGAGTACTGTC
CTCCGAGCGGAGTACTGTCCTCCGAGCGGAGTACTGTCCTCCGAGCGGAGTACTG
TCCTCCGAGCGGAGTACTGTCCTCCGAGCGGAGACTCTAGCGACGTCGAGCGCC
GGAGTATAAATAGAGGCGCTTCGTCTAC
HSP70promoter:
GGAGCGACAATTCAATTCAAACAAGCAAAGTGAACACGTCGCTAAGCGAAAGCTAA
GCAAATAAACAAGCGCAGCTGAACAAGCTAAACAATCTGCAGTAAAGTGCAAGTTA
AAGTGAATCAATTAAAAGTAACCAGCAACCAAGTAAATCAACTGCAA

Cell culture and transfection.

We obtained all cell lines from the UCB Cell Culture Facility. We maintained Human embryonic kidney 293T (HEK) cells in Dulbecco's modified eagle medium (DMEM) supplemented with 1 g/L D-glucose, 10% fetal bovine serum (FBS; Thermo Scientific)

and 1% GlutaMax (Invitrogen) at 37 °C in a humidified incubator with 5 % CO2. Cells were passaged and plated in DMEM (as above) at a density of 50,000 cells onto 12 mm coverslips pre-treated with Poly-D-lysine (PDL;1mg/ml; Sigma-Aldrich). Cells were transfected using Lipofectamine 3000 (Invitrogen) 12 hours after plating. Imaging was performed 36 hours after plating.

Dye loading.

We maintained DMSO stock solutions (100 µM) of all dyes at -80°C in single-use aliquots. Aliquots were further diluted to a working concentration of 50 nM in HBSS and incubated on cells for 30 minutes at 37 °C. We then replaced all dye-containing HBSS with fresh HBSS and imaged in HBSS at room temperature.

Epifluorescence microscopy.

We performed epifluorescence imaging on an AxioExaminer Z-1 (Zeiss) equipped with a Spectra-X Light engine LED light (Lumencor), controlled with Slidebook (v6, Intelligent Imaging Innovations). Images were acquired with a W-Plan-Apo 20x/1.0 water objective (20x; Zeiss) and focused onto an OrcaFlash4.0 sCMOS camera (sCMOS; Hamamatsu). The optical set up for imaging with each dye described below.

Table A2-1: Epifluorescent microscopy optics

Dye	Excitation	Emission	Dichroic
VF-Spy	475/34 nm BP	540/50 nm BP	510 nm LP
A647	542/33 nm BP	650/60 BP	594 nm LP
Hoechst 33342	375-400nm	405/40 BP	415 LP

Image Analysis.

For fluorescence intensity measurements, regions of interest were drawn around cell bodies, and fluorescence was calculated in ImageJ (FIJI), NIH). We identified transfected cells by setting a threshold that excluded all cells in the non-transfected controls. We calculated the fold change between non-transfected and transfected cells by taking the ratio of transfected cells fluorescence and untransfected cell fluorescence. For each condition, approximately 50 cells were circled across three individual coverslips.

Immunocytochemistry.

Immediately following live-cell dye loading experiments, cells were fixed for 20 minutes at room temperature with 4% formaldehyde in PBS. Cells were then washed in PBS (3x 5-minute washes) and treated with either 0.3% Triton x -100 in PBS for the permeabilized condition or PBS for the non-permeabilized condition. Cells were again washed in PBS and blocked for at least 45 minutes in 0.1% NGS in PBS. Cells were then incubated overnight at 4 °C with 1:500 Rat anti HA (Sigma Aldrich). We then washed each sample in PBS and stained with a spectrally compatible mouse secondary Goat anti-Mouse A488

(Life Technologies) or Goat anti-RT A647 (Life Technologies) 1:1000 in 0.1%NGS for 2hrs at room temperature. We added Hoechst 33342 (10mg/mL -20 stock) 1:1000 for the last 15 minutes of this incubation period. Cells were then washed in PBS and mounted onto glass slides using Fluoramount Mounting Media (VWR International) before imaging.

Transgenic generation.

pJFRC7-Pat3-SpyCatcher-CD4 was sent to Best Gene Inc. for injection into the following genomic sites via phi C31 integration.

Table A1-2: Injection details

Construct	**Injection Site**	**Injection stock**
pJFRC7-HA-SpyCatcher-Myc-CD4	attP3	32230

Immunohistochemistry.

Flies were dissected in calcium-magnesium free artificial hemolymph (AHL-/-; NaCl 108.0 mM, KCl 5.0 mM, $NaHCO_3$ 4.0 mM, $NaH_2PO_4 \cdot H_2O$ 1.0 mM, Trehalose· 2 H_2O 5.0 mM, Sucrose 10.0 mM, HEPES 5.0 mM and adjusted to pH 7.5 with NaOH) and fixed for 20 minutes in 4% formaldehyde in PBS. Brains were then washed in PBS (3x 5-minute washes) and treated with either 0.3% Triton x -100 in PBS for the permeabilized condition or PBS for the non-permeabilized condition. Brains were again washed in PBS and blocked for at least 45 minutes in 0.1% NGS in PBS. Cells were incubated overnight in block containing 1:50 RT anti HA (Sigma Aldrich) or 1:100 mouse anti CD4 at 4 °C for 48 hours while gently spinning. Brains were then washed in PBS and stained with Goat anti-Rat A488 (Life Technologies) 1:1000 and Goat anti-Mouse A594 (Life Technologies) in block for 2-4 hours at room temperature shaking. We added Hoechst 33342 1:1000 for the last 15 minutes of this incubation. Brains were then washed and mounted onto glass slides using vectashield mounting media before imaging using confocal microscopy.

Confocal Microscopy.

Imaging was performed using an LSM 710 upright confocal microscope.

Table A2-3: Confocal microscopy optics

Dye	Excitation	Emission
A488	488	599-639
A647	633	638-755
Hoechst 33342	405	426-643

Images were taken as 1 µm step z stacks through the entirety of the brain. Using the following settings 1.58 µs pixel dwell time and pinhole size 90 µm.

Figures.

Figure A2-1.

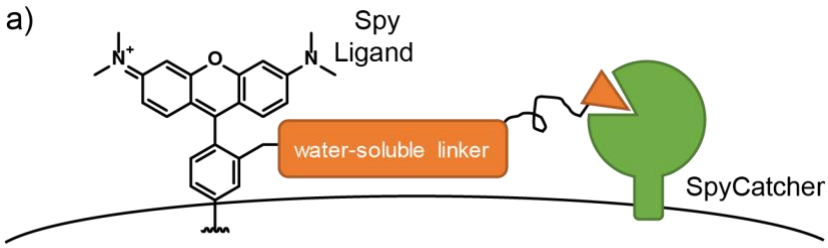

Figure A2-1. Schema depicting the covalent tethering of bath applied Spy-Tagged dye molecules to the extracellular surface via the formation of an isopeptide bond with the extracellular SpyCatcher tethering protein.

Figure A2-2.

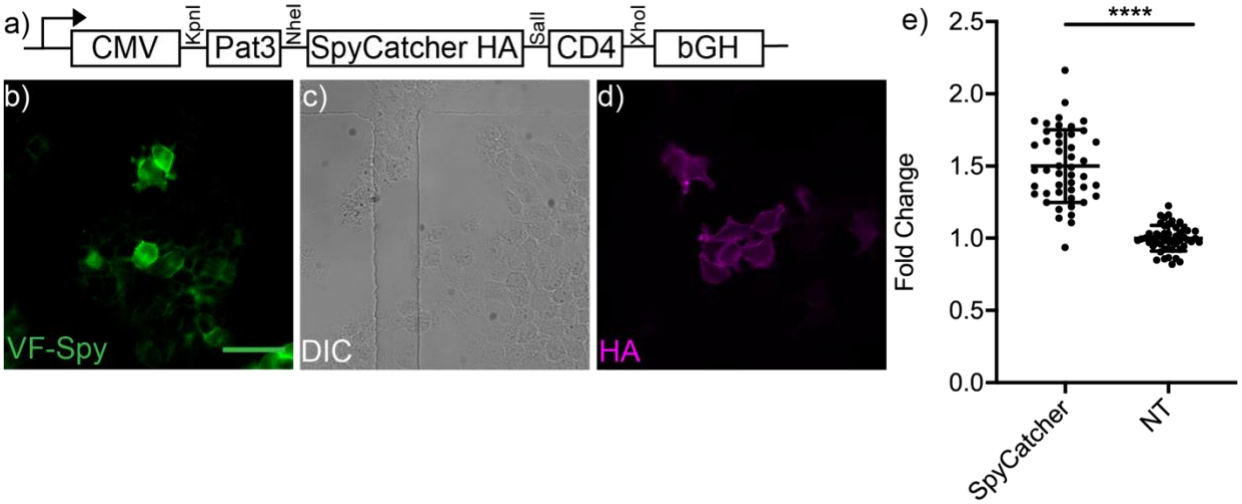

Figure A2-2. Live cell dye loading and immunocytochemistry in SpyCatcher-CD4 expressing HEK293T cells. **a)** pCDNA3.1 mammalian expression vector for SpyCatcher-CD4 fusion protein extracellular trafficking under the control of the CMV promoter. SpyCatcher-CD4 is targeted for secretion by Pat3 and then anchored into the plasma membrane by the CD4 domain-containing. Epifluorescent micrograph of **b)** live HEK 293T cells transfected with SpyCatcher-CD4 and reacted with 5nM VF-Spy (Green). **d)** Epifluorescent image of non-permeabilized immunocytochemistry, against HA (magenta), in HEK293T cells transfected with SpyCatcher-CD4. **c)** DIC image of cells contained in panel **(d)**. Scale for all images is 50 µm. **e)** Quantification of HEK293T cells expressing SpyCatcher-CD4 reacted with 5 nM VF-Spy voltage-sensitive dye. Data represents normalized fluorescence intensity of single HEK cells, revealing an approximately 1.5-fold fluorescence increase in targeted cells as compared to non-targeted cells (student t-test across three biological repeats $p<0.001$).

Figure A2-3.

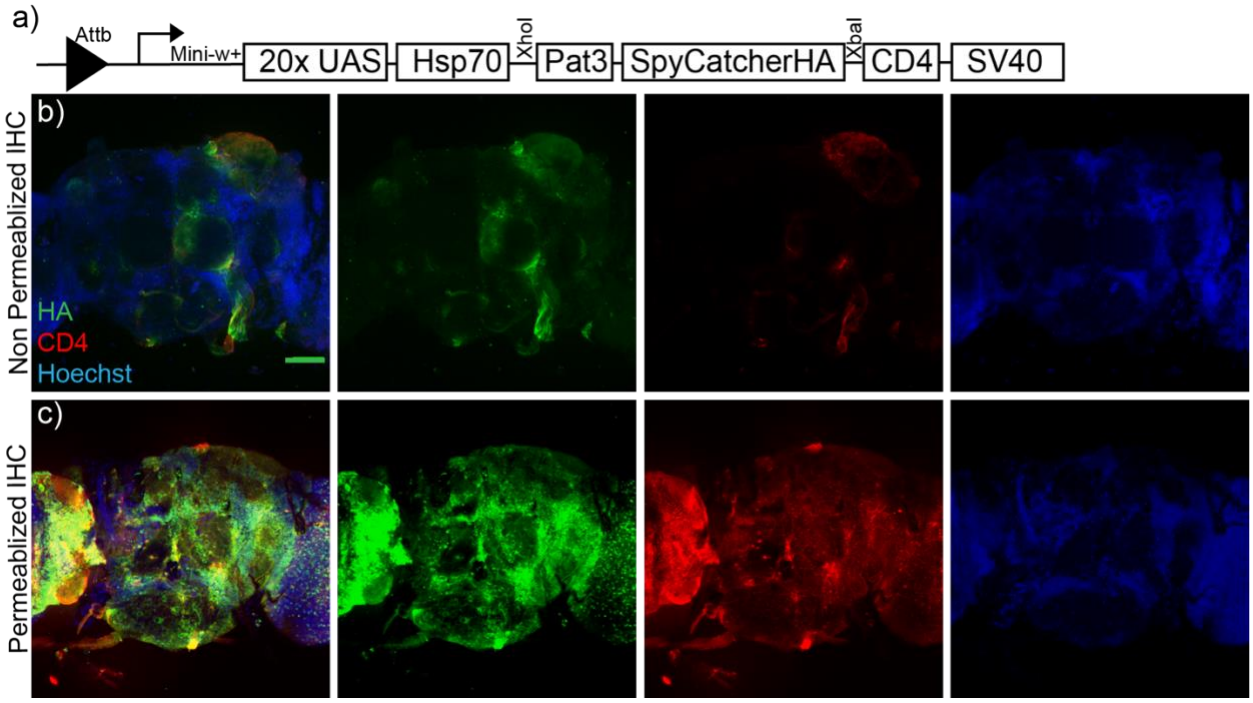

Figure A2-3. Immunohistochemistry in pan-neuronal SpyCatcher-CD4 expressing *Drosophila* brains. **a)** Schema for extracellularly trafficked SpyCatcher fusion protein driven under 20xUAS expression vector pJFRC7. Pat3 secretion signal targets SpyCatcher for secretion and the CD4 transmembrane domain anchors it at the cell surface. **b)** Maximum z-confocal projection of fixed **b)** non-permeabilized or **c)** permeabilized immunohistochemistry in nSyb-Gal4> SpyCatcher-CD4 *Drosophila* brain tissue. Immunostained for HA (green), CD4 (red), and nuclear counterstained with Hoechst (Hoechst 33342, 10 µg/ml, blue). Scale bar is 50 µm.

References

1. Miller, E. W. *et al.* Optically monitoring voltage in neurons by photo-induced electron transfer through molecular wires. *Proc. Natl. Acad. Sci.* **109**, 2114 LP – 2119 (2012).
2. Huang, Y. L., Walker, A. S. & Miller, E. W. A Photostable Silicon Rhodamine Platform for Optical Voltage Sensing. *J. Am. Chem. Soc.* **137**, 10767–10776 (2015).
3. Deal, P. E., Kulkarni, R. U., Al-abdullatif, S. H., Miller, E. W. & Biology, C. Isomerically Pure Tetramethylrhodamine Voltage Reporters. *JACS* **138**, 9085–9088 (2017).
4. Ortiz, G., Liu, P., Naing, S. H. H., Muller, V. R. & Miller, E. W. Synthesis of Sulfonated Carbofluoresceins for Voltage Imaging. *J. Am. Chem. Soc.* **141**, 6631–6638 (2019).
5. Kulkarni, R. U. *et al.* Voltage-sensitive rhodol with enhanced two-photon brightness. *Proc. Natl. Acad. Sci.* **114**, 2813–2818 (2017).
6. Zakeri, B. *et al.* Peptide tag forming a rapid covalent bond to a protein, through engineering a bacterial adhesin. *Proc. Natl. Acad. Sci.* **109**, E690–E697 (2012).

7. Grenier, V., Liu, P., Miller, E. W. & Daws, B. R. Spying on Neuronal Membrane Potential with Genetically Targetable Voltage Indicators. *J. Am. Chem. Soc.* (2019).
8. Feinberg, E. H. *et al.* {GFP} Reconstitution Across Synaptic Partners ({GRASP}) Defines Cell Contacts and Synapses in Living Nervous Systems. *Neuron* **57**, 353–363 (2008).
9. Gordon, M. D. & Scott, K. NIH Public Access. **61**, 373–384 (2010).
10. Brand, A. H. & Perrimon, N. Targeted gene expression as a means of altering cell fates and generating dominant phenotypes. *Development* **118**, 289–295 (1993).
11. Pfeiffer, B. D. *et al.* Refinement of tools for targeted gene expression in Drosophila. *Genetics* **186**, 735–755 (2010).
12. Stocker, R. F., Heimbeck, G., Gendre, N. & de Belle, J. S. Neuroblast ablation in Drosophila P[GAL4] lines reveals origins of olfactory interneurons. *J. Neurobiol.* **32**, 443–456 (1997).

Appendix 3: SNAP-CD4 Characterization, Comparison with $SNAP_f$ and functional imaging with mSNAP2

Portions of this work were completed in collaboration with others: Brittany R. Benlian who generated the mSNAP2 and RhoVR-SNAP dyes.

Background

Voltage imaging offers a unique prospect of watching neuronal activity as it occurs; however, techniques for visualizing these phenomena are still being developed. Currently, there are two main classes of voltage sensors which can be genetically encoded and targeted to genetically defined cell populations *in vivo*[1]. First, is the purely protein based sensors. These sensors utilize a voltage sensitive domain[2] or a voltage sensitive opsin[3] to sense the voltage across the membrane and through protein movements[4] or Förster Resonance Energy Transfer (FRET) translates the voltage into fluorescence changes in an attached fluorescent protein. The second class is the chemi-genetic hybrid systems which use a voltage sensitive FRET opsins and transfers that voltage sensitivity into fluorescence changes in a genetically tethered fluorescent dye molecule[5,6].

Both of these systems offer great strides toward the development of voltage indicators; however, there are still some issues with those that are available. Namely that they struggle with sensitivity, speed, linearity of voltage to fluorescence relationship and in some cases multiphoton sensitivity[7]. For this reason, our team has developed a series of photo-induced electron transfer voltage-sensitive dyes which complement existing probes with high speed, good signal to noise and a linear voltage to fluorescence relationship[8–13]. We hypothesize that these probes function via PeT mechanism where an electron dense aniline is integrated into the membrane via a hydrophobic phenylene-vinylene wire. Once integrated the aniline acts as a charge sensor, while at rest the voltage-sensitive dye is held in a quenched state via electron transfer from the aniline. However, upon depolarization this quenching is diminished resulting in a fluorescence increase in response to neuronal activity[8].

Although these PeT voltage sensitive dyes function very well *in vitro* their transition to more complex tissues has proven difficult as they indiscriminately label all membranes making genetic identification difficult and diminishing the signal to noise ratio[12]. For this reason, it is necessary that some sort of genetic targeting be employed. Our group has previously characterized many of these systems including Porcine liver esterase[14,15](Appendix 1), SpyCatcher[16] (Appendix 2) and HaloTag[17,18](Chapter 2). Another method we have used to attain this goal is the extracellular expression of a small molecule tethering proteins such as SNAP Tag or $SNAP_f$. SNAP Tag is a monomeric O^6-alkylguanine-DNA alkyltransferase which catalyzes the formation covalent bond between a O^6-*benzyl*guanine appended substrates and a SNAP-Tag derived cystieic acid residue[19]. $SNAP_f$ is a modified SNAP Tag protein which carries 10 point mutations compared to the original SNAP Tag. These mutations strongly increased the reactivity of these $SNAP_f$ molecules to a variety of O^6-benzylguanine derivatives. Having shown in previous work (unpublished, Brittany Benlian) that we could target voltage-sensitive dyes using both SNAP Tag and $SNAP_f$ *in vitro*, we sought to establish a method by which we can target voltage-sensitive dyes in vivo. For this we selected *Drosophila* melanogaster, due to its genetic tractability and relatively small nervous system. Here we present the development of novel extracellular SNAP Tag for the genetic targeting of dyes in

Drosophila, the comparison of the SNAP Tag system with previously characterized $SNAP_f$ in live brain samples, and finally characterize the voltage-sensitivity of voltage sensitive dye mSNAP2 tethered to $SNAP_f$-CD4 in live explant *Drosophila* brains.

Results

Generation of SNAP Tag constructs for expression in flies

SNAP Tag has been expressed successfully under the Gal4/UAS in *Drosophila*[20–22]. However, all of these tethers have been expressed intracellularly where our voltage sensitive dyes cannot reach. As a result, we first developed an extracellularly trafficked SNAP Tag molecule. This appendix may seem redundant with Chapter 3 of this thesis, however, here we are describing the development of SNAP Tag targeting systems not $SNAP_f$. Previous chemical-genetic hybrids deployed in mammalian cells used a 3' transmembrane domain from the platelet-derived growth factor receptor (PDGFR) to localize SNAP Tag to the extracellular surface and a 5' secretion signal peptide from immunoglobulin K (IgK) (unpublished, Brittany Benlian). Adapting SNAP-Tag for expression in *Drosophila*, we used a 3' CD4 transmembrane anchor, fusing it to the C-Terminus of SNAP-Tag, in conjunction with a 5' invertebrate PAT-3 secretion signal on account of their robust extracellular trafficking of other proteins in *Drosophila*[23,24]*.* We then subcloned with PAT-3-HA-SNAP Tag-CD4 (SNAP-CD4) into mammalian (pcDNA3.1) and insect (pJFRC7) expression vectors. When expressed in HEK293T cells our mammalian vector robustly targeted water-soluble SNAP-Surface-A488 (NEB, SS-A488) dye to the cell surface in transfected cell populations (**Figure A3-2 a**) but not dye-treated untransfected cell populations (**Figure A3-2 b**). The construct is non-fluorescent on its own and shows no fluorescence in the absence of dye loading (**Figure A3-2 c**). HEK cells expressing SNAP-CD4 and treated with SS-A488 (100 nM) show good membrane localization (**Figure A3-2 a**), while cells that do not express SNAP-CD4 in the same cultures show approximately 3.5-fold lower fluorescence levels (**Figure A3-2 d**). Following live cell staining, cells can be fixed and retain their SS-A488 fluorescence which can then be compared to CD4 immunofluorescence to confirm extracellular localization of the protein and colocalization with the dye (**Figure A3-3**).

In *Drosophila* S2 cells, we find that SNAP-CD4 also localizes to the extracellular surface **(Figure A3-4)** as shown by anti CD4 immunocytochemistry. The addition of the SNAP-CD4 tag allows not only for the localization but the functional characterization of the dye tethering platform in S2 cells by treating the cells with SS-A488. Here, we find that dyes are readily targeted to transfected cells (**Figure A3-5 a)** and do not strongly label non transfected cells **(Figure A3-5 b)**. Live cell staining is also retained post fixation serving as a useful counterstain for anti CD4 immunocytochemistry.

Validation of SNAP Tag-expressing flies

To evaluate the extracellular localization and function of cell surface expressed SNAP-CD4 in vivo, we generated transgenic flies (BestGene Inc.). To express SNAP-CD4 in all neurons throughout the brain, we crossed the UAS-SNAP-CD4 generated lines with

panneuronal expression driver nSyb-Gal4. nSyb-Gal4>SNAP-CD4 flies show strong and uniform neuronal expression of both the 5' HA epitope as well as the 3' CD4 epitope on the extracellular surface as shown by nonpermeabilizing immunohistochemistry (**Figure A3-6 a)**. These data suggest that the entire fusion protein has been secreted to the extracellular surface. At higher magnification we can see that the HA and CD4 immunofluorescence is localized well to the extracellular surface and remains isolated from the Hoechst nuclear counter stain(**Figure A3-6b)**. Finally, a driver only or reporter only control, which does not express SNAP-CD4 reveals no anti HA or anti CD4 fluorescence present in the non-transgenic expressing brain (**Figure A3-6c).**

To assess the functional ability of SNAP-CD4 to tether dyes to the extracellular surface we expressed it in a small population of neurons. Crossing UAS-SNAP-CD4 to the GH146-Gal4 driver line, expressed SNAP-CD4 in a subpopulation of olfactory projection neurons in the antennal lobe. When loaded with SS-A488 in live brain tissue the antennal lobe projection neurons: glomeruli, cell bodies and axonal projections were visible and SS-A488 staining localized well to the extracellular surface (**Figure A3-7 a and b**). However, when compared to previously characterized $SNAP_f$-CD4 (unpublished Molly Kirk, Chapter 3), GH146-Gal4>$SNAP_f$-CD4 tethered SS-A488 (**Figure A3-7 c and d)** significantly better with a 4-fold greater fluorescence intensity in antennal lobe regions than GH146-Gal4>SNAP-CD4 brains (**Figure A3-7 e**). For this reason, we halted experiments on SNAP-CD4 and continued experiments with $SNAP_f$-CD4.

Having selected $SNAP_f$-CD4 as our best option for SNAP Tag based voltage imaging, we evaluated the ability of $SNAP_f$-CD4 to target mSNAP2 voltage sensitive dye. Using GH146-Gal4> $SNAP_f$-CD4 we again expressed $SNAP_f$-CD4 in a subset of olfactory projection neurons. We then loaded brains with mSNAP2 (100nM) and found that it labeled the expected expression pattern in the antennal lobe(**Figure A3-8a**).

Functional imaging

To evaluate the voltage-sensitivity of mSNAP2 in vivo, we again expressed $SNAP_f$-CD4 in olfactory projection neurons. Our group had previously shown that olfactory projection neurons can be readily and robustly stimulated with carbachol (CCH), a non-hydrolysable acetylcholine mimic. Loading mSNAP2 (500 nM) in live flies, we then removed the brain and imaged in explants using epifluorescence microscopy. We imaged mSNAP2 responses to three individual carbachol stimuli and found that mSNAP2 showed robust voltage responses in the positive direction as expected for these turn-on probes **(Figure A3-9c, green).** The chemical-genetic hybrid approach of mSNAP2 enables additional controls to be carried out using the same transgenic flies. Loading brains with non-voltage-sensitive SS-A488 and stimulating with carbachol yielded little to no response. (**Figure A3-9c, blue)**. The use of a non-voltage-sensitive dye allows for experiments to be run in the same transgenic animals, eliminating unwanted confounds from the use of various transgenes. If the same control was attempted in a non-chemigenetic probe we would have been required to generate a novel sensor with an inactivating mutation.

RhoVR-Snap dye loading in vivo

During the beginning of this project, we had a red-shifted voltage-sensitive dye RhoVR-SNAP. Unfortunately, this dye was found to be highly unstable for somewhat unclear reasons. As a result, we did not pursue voltage-sensitive measurements or dye loading of this species into $SNAP_f$-CD4. I have included the SNAP-CD4 characterization of dye loading in *Drosophila* for future reference (**Figure A3-10**). Here, we again used GH146-Gal4>SNAP-CD4 flies and loaded them under various condition to fully optimize loading for the RhoVR dye. We first began by loading the dye at 100 nM in AHL-/- in the presence(**Figure A3-10a**) or absence(**Figure A3-10b**) of an FBS preincubation. Here it was found that FBS preincubation greatly increase the dye penetration most likely due to it hydrophobicity assisting in the permeation of the dye into the tissue. Second, we loaded the dye at varying concentrations and found here that the dye loaded with the highest targeted to background intensity ratio at 750 nM (**Figure A3-10c**). Having loaded at 750 nM we next sought to determine if washing had an impact on the contrast between targeted and non-targeted regions of the brain. We found that had no impact on dye loading (Data not shown). To evaluate if Pluronic F127 concentration affected dye loading in the brain, we loaded brains with 750 nM in the presence of either 0.02% or 0.2% Pluronic F127. Here, we found that higher concentrations of Pluronic F127 resulted in higher intensity dye loading as compared to background fluorescence intensity(**Figure A3-10d**). We then compared variations in the time course 30' FBS pretreatment – 15' dye loading vs. 15' FBS pretreatment and 30' dye loading vs. 45' dye loading (Data not shown). Here we found little to no difference between the latter two suggesting that at high concentrations the FBS pretreatment may not have a large effect(**Figure A3-10e**). I have included this data to assist future students in their application of red-shifted voltage sensitive dyes in vivo.

Conclusion and future steps

In summary, we have generated a novel extracellular SNAP Tag construct for expression both in vitro and in vivo. We have characterized its effectiveness at tethering dyes to the extracellular surface in both mammalian and *Drosophila* S2 cells. Generating a novel UAS-SNAP-CD4 transgenic reporter line we have expressed SNAP-CD4 on the extracellular surface of defined neuronal populations. We then compared the ability of SNAP-CD4 and $SNAP_f$-CD4 (characterized in Chapter 3) to target non-voltage-sensitive dyes in live Drosophila brain tissue and found that $SNAP_f$-CD4 was capable of targeting dyes with a much higher intensity than the original SNAP Tag construct. Finally expressing $SNAP_f$-CD4 in *Drosophila* olfactory projection neurons and stimulating with acetylcholine mimic carbachol we were able to drive robust voltage responses as reported by $SNAP_f$-CD4 targeted mSNAP2 voltage sensitive dye.

Although these systems present the generation of a novel transgenic targeting mechanisms for PeT voltage-sensitive dyes, there are some drawbacks to the methodology as it is currently employed. First, mSNAP2 is a green voltage sensitive dye which limits its spectral compatibility with popular GFP based probes as well as decreasing its effectiveness in deeper complex tissues. As a result, the first future direction for this project would be te develop a stable, red-shifted voltage-sensitive dye

which is SNAP reactive. This is especially of importance as we have previously seen that red voltage sensitive dyes which are targeted to the extracellular surface show very high contrast between targeted and untargeted regions suggesting that they may give much bigger voltage responses than their green counter parts. Secondly, these targeting mechanisms seem to be less effective than HaloTag based targeting mechanisms thus it would be ideal to generate mechanisms to increase the extracellular export of these fusion proteins. This innovation coupled with a red shifted dye may generate an even more voltage sensitive probe in general. Third, using the current experiment, does not actually push this voltage sensor in terms of kinetics which will be a very important aspect to assess in live tissue. My first suggestion to assess this via patch-clamp electrophysiology in larval muscle tissue as we have previously done with RhoVR-Halo. This is a good method to assess the functional capabilities of these probes to detect phenomena such as action potentials, EPSPs or IPSPs in vivo. Finally, there is a voltage imaging avenue which I believe is yet to be explored. As we now have both the LexA and Gal4 genetic targeting mechanisms for HaloTag and $SNAP_f$-CD4. We can begin to do dual color voltage imaging. Expressing HaloTag-CD4 in first order sensory neuron and expressing $SNAP_f$-CD4 in a second order sensory neurons we should be able to simultaneously report the activity of both neurons essentially watching in real time the process of sensory transduction through to sensory relay in live or explant brains. Ultimately our novel voltage sensors may permit the interrogation of voltage in complex systems in two colors throughout the brain.

Methods

Drosophila DNA constructs

Transgenic generation, the insert Pat3-SNAP Tag-CD4 was assembled into pJFRC7[29] backbone via restriction digest (CD8::GFP was removed by XhoI and XbaI) and Gibson assembly (Addgene). All constructs were sequence confirmed by the UCB Sequencing Facility. Sequences used for all constructs can be found below.

Pat3
ATGCCACCTTCAACATCATTGCTGCTCCTCGCAGCACTTCTTCCATTCGCTTTACCA
GCAAGCGATTGGAAGACTGGAGAAGTCACTG
HA epitope tag
TATCCATATGATGTTCCAGATTATGCT
$SNAP_f$-CD4
ATGGACAAAGACTGCGAAATGAAGCGCACCACCCTGGATAGCCCTCTGGGCAAGC
TGGAACTGTCTGGGTGCGAACAGGGCCTGCACCGTATCATCTTCCTGGGCAAAGG
AACATCTGCCGCCGACGCCGTGGAAGTGCCTGCCCCAGCCGCCGTGCTGGGCGG
ACCAGAGCCACTGATGCAGGCCACCGCCTGGCTCAACGCCTACTTTCACCAGCCT
GAGGCCATCGAGGAGTTCCCTGTGCCAGCCCTGCACCACCCAGTGTTCCAGCAG
GAGAGCTTTACCCGCCAGGTGCTGTGGAAACTGCTGAAAGTGGTGAAGTTCGGAG
AGGTCATCAGCTACAGCCACCTGGCCGCCCTGGCCGGCAATCCCGCCGCCACCG
CCGCCGTGAAAACCGCCCTGAGCGGAAATCCCGTGCCCATTCTGATCCCCTGCCA
CCGGGTGGTGCAGGGCGACCTGGACGTGGGGGGCTACGAGGGCGGGCTCGCCG

TGAAAGAGTGGCTGCTGGCCCACGAGGGCCACAGACTGGGCAAGCCTGGGCTGG
GT
SNAP Tag
GGGGCCCAGCCGGCCAGATCTGCTGGGCAAAGGAACATCATGAAGCGCACCACC
CTGGATAGCCCTCTGGGCAAGCTGGAACTGTCTGGGTGCGAACAGGGCCTGCAC
GAGATCAAGCTGCTGGGCAAAGGAACATCTGCCGCCGACGCCGTGGAAGTGCCT
GCCCCAGCCGCCGTGCTGGGCGGACCAGAGCCACTGATGCAGGCCACCGCCTG
GCTCAACGCCTACTTTCACCAGCCTGAGGCCATCGAGGAGTTCCCTGTGCCAGCC
CTGCACCACCCAGTGTTCCAGCAGGAGAGCTTTACCCGCCAGGTGCTGTGGAAAC
TGCTGAAAGTGGTGAAGTTCGGAGAGGTCATCAGCTACCAGCAGCTGGCCGCCCT
GGCCGGCAATCCCGCCGCCACCGCCGCCGTGAAAACCGCCCTGAGCGGAAATCC
CGTGCCCATTCTGATCCCCTGCCACCGGGTGGTGTCTAGCTCTGGCGCCGTGGG
GGGCTACGAGGGCGGGCTCGCCGTGAAAGAGTGGCTGCTGGCCCACGAGGGCC
ACAGACTGGGCAAGCCTGGGCTGGGTCCTGCAGGTATAGTCGACGAACAAAAACT
CATCTCAGAAGAGGATCTG
Linker
GGTGGCGGCGGAAGTGGAGGTGGAGGCTCG
CD4
TTCCAGAAGGCCTCCAGCATAGTCTATAAGAAAGAGGGGGAACAGGTGGAGTTCT
CCTTCCCACTCGCCTTTACAGTTGAAAAGCTGACGGGCAGTGGCGAGCTGTGGTG
GCAGGCGGAGAGGGCTTCCTCCTCCAAGTCTTGGATCACCTTTGACCTGAAGAAC
AAGGAAGTGTCTGTAAAACGGGTTACCCAGGACCCTAAGCTCCAGATGGGCAAGA
AGCTCCCGCTCCACCTCACCCTGCCCCAGGCCTTGCCTCAGTATGCTGGCTCTGG
AAACCTCACCCTGGCCCTTGAAGCGAAAACAGGAAAGTTGCATCAGGAAGTGAAC
CTGGTGGTGATGAGAGCCACTCAGCTCCAGAAAAATTTGACCTGTGAGGTGTGGG
GACCCACCTCCCCTAAGCTGATGCTGAGCTTGAAACTGGAGAACAAGGAGGCAAA
GGTCTCGAAGCGGGAGAAGGCGGTGTGGGTGCTGAACCCTGAGGCGGGGATGT
GGCAGTGTCTGCTGAGTGACTCGGGACAGGTCCTGCTGGAATCCAACATCAAGGT
TCTGCCCACATGGTCCACCCCGGTGCAGCCAATGGCCCTGATTGTGCTGGGGGG
CGTCGCCGGCCTCCTGCTTTTCATTGGGCTAGGCATCTTCTTCTGTGTCAGGTGCC
GGCACCGAAGGCGCTAG

Cell culture and transfection.

We obtained all cell lines from the UCB Cell Culture Facility. Human embryonic kidney 293T (HEK) cells were maintained in Dulbecco's modified eagle medium (DMEM) supplemented with 1 g/L D-glucose, 10% fetal bovine serum (FBS; Thermo Scientific), and 1% GlutaMax (Invitrogen) at 37 °C in a humidified incubator with 5 % CO2. Cells were passaged and plated in DMEM (as above) at a density of 50,000 cells onto 12 mm coverslips pre-treated with Poly-D-lysine (PDL;1mg/ml; Sigma-Aldrich). Transfection of plasmids was carried out using Lipofectamine 3000 (Invitrogen) 12 hours after plating. Imaging was performed 36 hours after plating.

S2 Cells were maintained in Schneider's Drosophila media (Thermo Fisher Scientific) supplemented with 10% FBS at 28°C in a non-humidified incubator under atmospheric conditions. Cells were passaged and plated at 500,000 cells per well in a 24 well plate.

Six hours after plating, promotor Tubulin Gal4 pCaSper (Addgene #17747)[42] was cotransfected with pJFRC7 constructs using a modified Lipofectamine 3000 (Life Technologies) protocol. This protocol included a 20-minute preincubation of lipofectamine and DNA in Opti-MEM (Life Technologies) and no p3000 reagent. Forty-eight hours after transfection, S2 cells were transferred onto PDL-treated (1 mg/mL) 12 mm coverslips and allowed to adhere for 30 minutes before dye loading and imaging.

Dye loading.

We maintained DMSO stock solutions (100 µM) of all dyes at -80 °C in single-use aliquots. Aliquots were further diluted to a working concentration of 100 nM in HBSS and incubated on cells for 30 minutes at 37 °C for HEK cells and room temperature for S2 cells. We then replaced all dye-containing HBSS with fresh HBSS and imaged in HBSS at room temperature.

Epifluorescent microscopy.

We performed epifluorescent microscopy on varying concentrations of the mSNAP2 voltage sensitive dye in live loaded *Drosophila* brains. Epifluorescence microscopy. Imaging was performed on an AxioExaminer Z-1 (Zeiss) equipped with a Spectra-X Light engine LED light (Lumencor), controlled with Slidebook (v6, Intelligent Imaging Innovations). Images were acquired with a W-Plan-Apo 20x/1.0 water objective (20x; Zeiss) and focused onto an OrcaFlash4.0 sCMOS camera (sCMOS; Hamamatsu). The optical setup for imaging with each dye is described below.

Table A3-1. Optical filter sets for epifluorescence microscopy

Dye	Excitation	Emission	Dichroic
mSNAP2, SS-A488	475/34 nm BP	540/50 nm BP	510 nm LP
A647	542/33 nm BP	650/60 BP	594 nm LP
Hoechst 33342	375-400nm	405/40 BP	415 LP

Epifluorescent image analysis.

Epifluorescent images from live loaded brain samples focused on the middle of the antennal lobes were analyzed in the following way. Fluorescence intensity was measured for the antennal lobe and a region of non-labeled protocerebrum from each brain. The ratio of the AL region's intensity and the nontargeted protocerebrum was then calculated and displayed as fold change above background.

Immunocytochemistry.

Immediately following live-cell dye loading experiments, cells were fixed for 20 minutes at room temperature with 4% formaldehyde in PBS. Cells were then washed in PBS (3x 5-minute washes) and treated with either 0.3% Triton X-100 in PBS for the permeabilized condition or PBS for the nonpermeabilized condition. Cells were again washed in PBS and blocked for at least 45 minutes in 0.1% NGS in PBS. Cells were then incubated overnight at 4 °C with 1:500 mouse anti CD4 (OKT4; Thermo Fisher Scientific). We then washed each sample in PBS and stained with a spectrally compatible mouse secondary Goat anti-Mouse A488 (Life Technologies) or Goat anti-Mouse A647 (Life Technologies) 1:1000 in 0.1%NGS for 2hrs at room temperature. We added Hoechst 33342 (10mg/mL -20 stock) 1:1000 for the last 15 minutes of this incubation period. Cells were then washed (3 x 5-minute washes) in PBS and mounted onto glass slides using Fluoramount Mounting Media (VWR International) before imaging.

Transgenic generation.

pJFRC7-Pat3-Snap Tag-CD4 were sent to Best Gene Inc. for injection into the following genomic sites via phi-C31 integration.

Table A3-2. Injection phi C31 site and stock line

Construct	Injection Site	Injection Stock
pJFRC7-Pat3-SNAP Tag-CD4	VK05	#9725

Immunohistochemistry.

Fly brains were dissected in calcium-magnesium free artificial hemolymph (AHL-/-; NaCl 108.0 mM, KCl 5.0 mM, $NaHCO_3$ 4.0 mM, $NaH_2PO_4 \cdot H_2O$ 1.0 mM, Trehalose· 2 H_2O 5.0 mM, Sucrose 10.0 mM, HEPES 5.0 mM and adjusted to pH 7.5 with NaOH) and fixed for 20 minutes in 4% formaldehyde in PBS. Brains were then washed in PBS (3x 5-minute washes) and treated with either 0.3% Triton x -100 in PBS for the permeabilized condition or PBS for the nonpermeabilized condition. Brains were again washed in PBS and blocked for at least 45 minutes in 0.1% NGS in PBS. Cells were incubated overnight in block containing 1:50 RT anti HA (Sigma Aldrich) or 1:100 or 1:200 mouse anti CD4 at 4 °C for 48 hours. Brains were then washed in PBS (3 x 5-minute washes) and stained with Goat anti-Rat A488 (Life Technologies) 1:1000 and Goat anti-Mouse A594 (Life Technologies) in block for 4 hours at room temperature shaking. We added Hoechst 33342 (10 mg/mL) 1:1000 for the last 15 minutes of this incubation. Brains were then washed and mounted onto glass slides using Vectashield mounting media (Vector Laboratories) before imaging using confocal microscopy.

Live-fly brain dye loading with SS-A488 and voltage-sensitive dyes.

Live-fly preparations were performed in the following way: 10–20-day old flies were briefly anesthetized on ice and placed into a small slit on a custom-built plastic mount at the cervix so that the head was isolated from the rest of the body. The head was then immobilized using clear nail polish, which was allowed to set for 15 minutes. The head cuticle was then removed using sharp forceps in calcium-magnesium free Artificial Hemolymph solution, AHL-/-, (NaCl 108.0 mM, KCl 5.0 mM, $NaHCO_3$ 4.0 mM, $NaH_2PO_4 \cdot H_2O$ 1.0 mM, Trehalose 2 H_2O 5.0 mM, Sucrose 10.0 mM and HEPES 5.0 mM, perfused at 5 mL/min)[25], and the esophagus was cut to eliminate autofluorescence. The AHL was then replaced with calcium-magnesium free AHL containing 0.2% Pluronic F127, and either 500nM mSNAP2 or 1 µM SS-A488 (for functional imaging experiments, this was lowered to 5 nM SS-A488 to match fluorescence intensity with mSNAP2), and the glial sheath was punctured manually over the optic lobes to permit dye access. DMSO concentrations were maintained below 3% vol/vol in the dye loading solutions. Following a 45-minute loading period in the dark at room temperature, the brains were removed and then imaged via confocal or epifluorescent microscopy. When imaged under confocal microscopy, brains were mounted onto glass coverslips with spacers to prevent sample loss and deformation. When imaged under epifluorescent microscopy, brains were adhered to PDL- (Poly-D-Lysine), or PLL- treated (Poly-L-Lysine) coverslips and bathed in AHL-/-.

Confocal microscopy.

We performed confocal imaging using an LSM710 upright confocal microscope maintained by the Biological Imaging Facility at UC Berkeley. Images were acquired under laser illumination focused on the sample using a 20x air objective and collecting at 0.64 µs pixel dwell time through a 39-45 µm pinhole. Brains were scanned in the z-direction beginning at the top of the brain for 15 planes with 3µm steps. Each image totals the first 45 µm of the brain tissue.

Table A3-3. Optical settings for confocal microscopy

Dye	Excitation	Emission
mSNAP2, SS-A488 and A488	488 nm	493-578 nm
A546	594 nm	599-712 nm
Hoechst	405 nm	410-490 nm

Carbachol ArcLight functional imaging.

GH146-Gal4, $SNAP_f$-CD4; Tm2/TM6b flies had their cuticle removed as described in the section above and then loaded with 500 nM mSNAP2 or 5 nM SS-A488 in the presence of 0.2% Pluronic F127 at room temperature for 45 minutes. Post loading, brains were immediately removed from the cuticle placed a perfusion chamber where they were mounted onto a PDL-coated coverslip. Samples were incubated for 3 minutes at room

temperature with constant perfusion of AHL+/+ (NaCl 108.0 mM, KCl 5.0 mM, $NaHCO_3$ 4.0 mM, $NaH_2PO_4 \cdot H_2O$ 1.0 mM, Trehalose 2 H_2O 5.0 mM, Sucrose 10.0 mM, HEPES 5.0 mM, $CaCl_2$ 2 H_2O 2.0 mM, $MgCl_2$ 6 H_2O 8.2 mM, perfused at 5 mL/min) before imaging was performed. Perfusion was maintained throughout the experiment. Imaging was performed on an AxioExaminer Z-1 (Zeiss) equipped with a Spectra-X Light engine LED light (Lumencor), controlled with Slidebook (v6, Intelligent Imaging Innovations). Images were acquired with a W-Plan-Apo 20x/1.0 water objective (20x; Zeiss) and focused onto an OrcaFlash4.0 sCMOS camera (sCMOS; Hamamatsu). The acquisition rate of 1 Hz for each experiment with 250 ms exposure times and light power (19.7 mW/mm^2) were maintained across all experiments independent of acquisition frequency. A baseline was obtained for one minute, and then brains were stimulated for 30 seconds, followed by a 5-minute recovery period between stimulations.

Functional imaging data analysis.

We extracted fluorescence intensity values over time for the antennal lobe using an in-house MATLAB code, and background-subtracted these values. We used these traces to calculate the % $\Delta F/F_0$, where F_0 was defined as the average of frames 2 to 50 from each video. These were then subsequently plotted and displayed using Prism Graph Pad as Mean and Standard Error of the Mean.

Figures.

Figure A3-1.

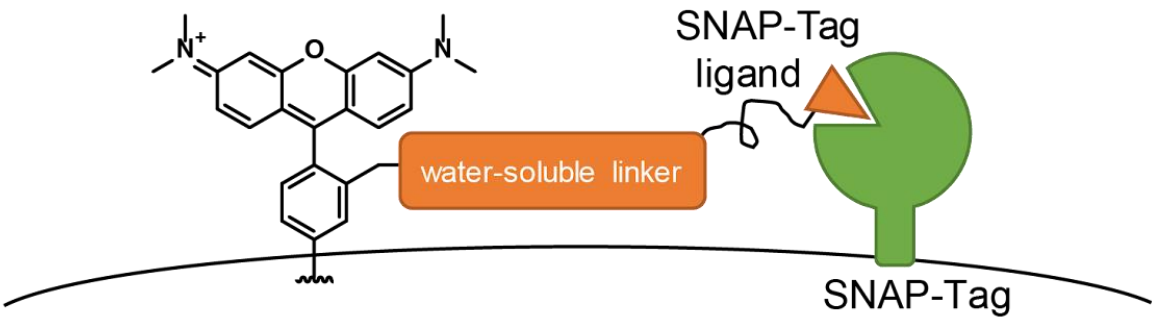

Figure A3-1. Schematic of the covalent tethering of bath applied SNAP Tag reactive dye molecules to the extracellular surface via cell surface expressed SNAP Tag.

Figure A3-2.

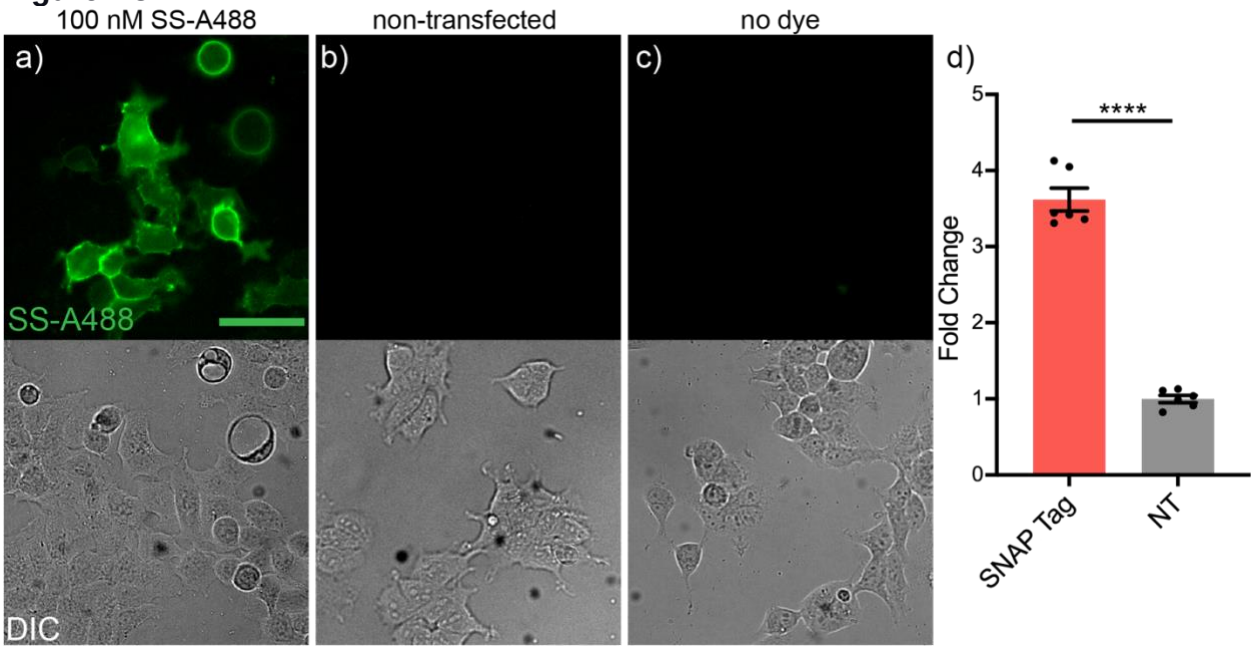

Figure A3-2: Live cell dye loading of SS-A488 (100 nM) in SNAP-CD4 expressing HEK293T cells. **a)** Epifluorescence microscopy images of HEK293T cells transfected with SNAP-CD4 and treated with SS-A488 (10 0nM, green). Controls were treated identically but **b)** were not transfected or **c)** in the absence of SS-A488 dye. DIC images of each area are located directly below the fluorescent images. **d)** Plot of relative fluorescence intensity in cells expressing SNAP Tag vs. cells that do not express Snap Tag. SNAP Tag positive cells were assigned based on a threshold obtained from a non-transfected control**(c)**. Data are mean ± SEM for n = 6 different coverslips of cells. Data points represent average fluorescence intensities of 40 to 50 cells. (Paired t-test, $p<0.0001$)

Figure A3-3.

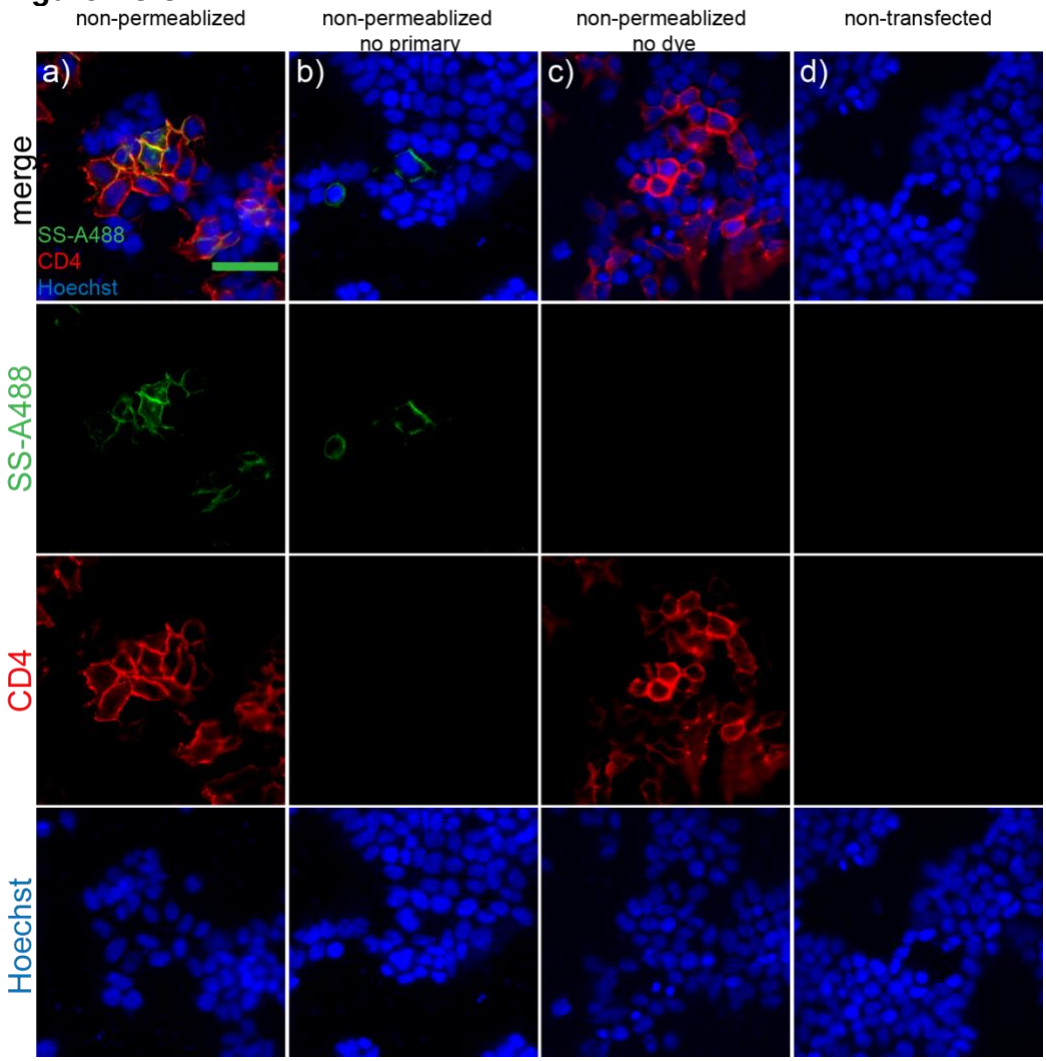

Figure A3-3. Immunocytochemistry of Snap-CD4 in HEK293T cells. Epifluorescence microscopy images of *post hoc* immunocytochemistry of HEK293T cells expressing Snap Tag, stained with SS-A488 (100 nM), and then treated under **a)** non-permeabilizing conditions (no detergent). Control cells were treated under non-permeabilizing conditions and lacked either **c)** primary anti-CD4 antibody, **d)** SS-A488 dye or **e)** were not transfected. Green is SS-A488, red is anti-CD4 (100 nM, during live-cell imaging, prior to fixation), and blue is Hoechst 33342 (at a concentration of 10 µg/mL, equivalent to 16 µM). Scale bar is 50 µm.

Figure A3-4.

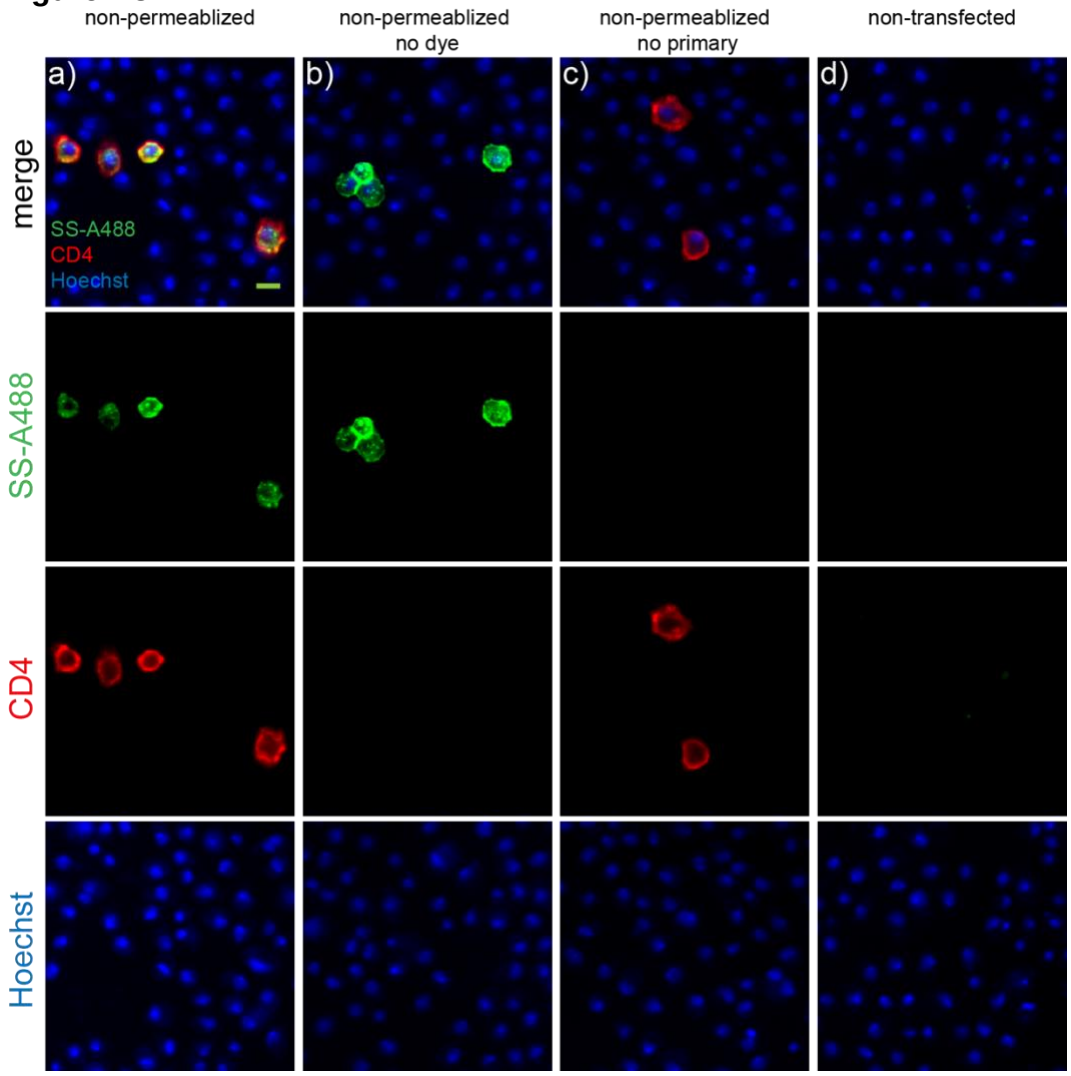

Figure A3-4. Immunocytochemistry in SNAP-CD4 expressing *Drosophila* S2 cells. Epifluorescence images of *post hoc* immunocytochemistry of *Drosophila* S2 cells expressing SNAP-CD4 (co-transfection with tubP-GAL4 and UAS-SNAP-CD4), stained with SS-A488 (100 nM), and fixed under **a)** non-permeabilizing conditions. Before fixation, control cells were treated either **b)** without SS-A488 ("no dye"), **c)** with dye, but without primary anti-CD4 antibody, or **d)** with dye and antibody, but without transfection. Green is SS-A488 (100 nM, during live-cell image, before fixation), red is CD4 and blue is Hoechst 33342 (at a concentration of 10 µg/mL, is equivalent to 16 µM). Scale bar for all images is 10 µm.

Figure A3-5.

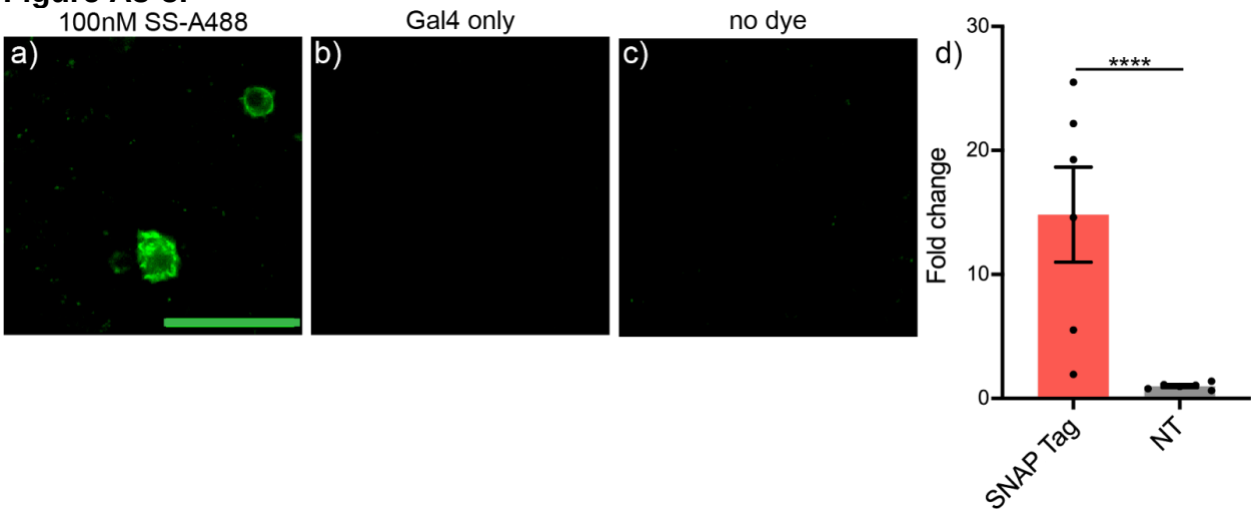

Figure A3-5. Live-cell staining of SNAP-CD4 expressing *Drosophila* S2 cells with SS-A488 (100 nM). Epifluorescent microscopy images of S2 cells expressing SNAP-CD4 under co-transfected tubP-Gal4 treated with **a)** SS-A488 (100 nM). Control cultures were treated identically but lacked either **b)** SNAP-CD4 reporter transfection or **c)** SS-A488 dye. Scale for all images is 50 µm. **d)** Plot of relative fluorescence intensity in cells expressing SNAP-CD4 vs. cells that do not express SNAP-CD4. SNAP Tag positive cells were assigned based on a threshold obtained from a non-expressing control **(c)**. Data are mean ± SEM for n = 6 different coverslips of cells. Data points represent average fluorescence intensities of 20 to 30 cells. (Paired t-test, $p<0.0001$)

Figure A3-6.

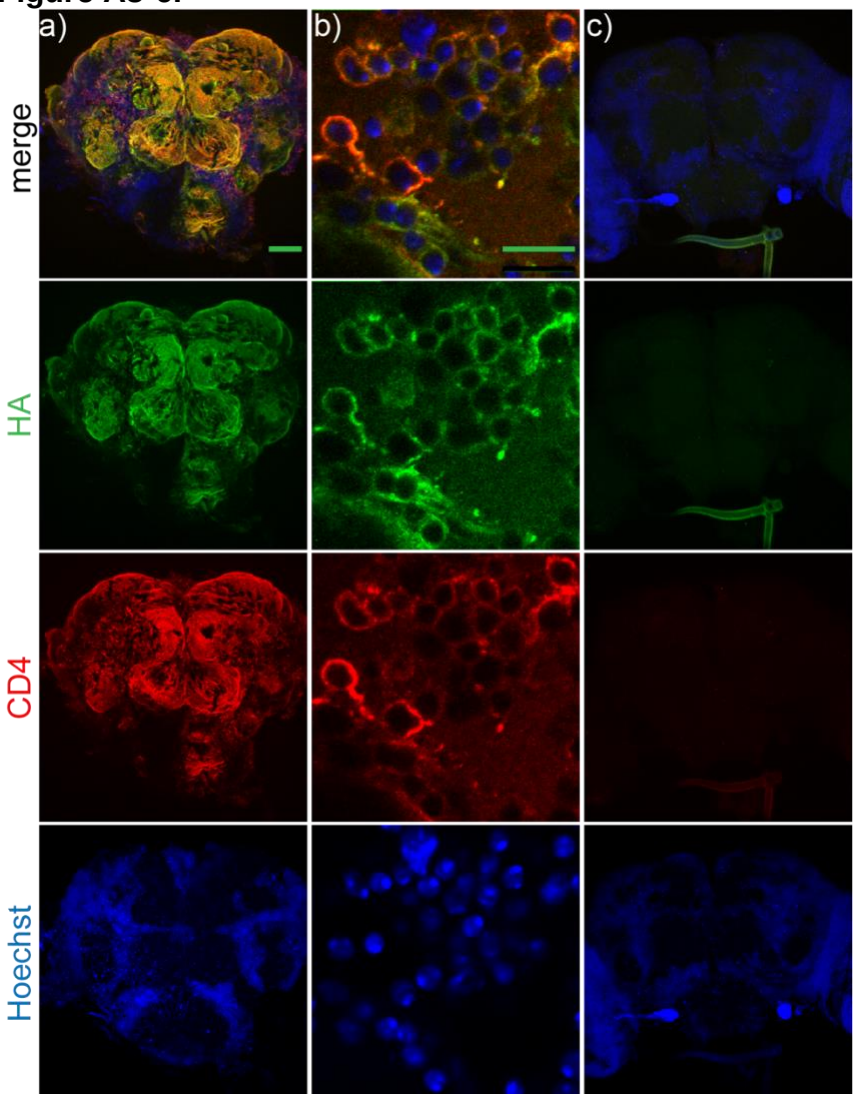

Figure A3-6. Immunohistochemistry of pan-neuronal SNAP-CD4 expression and trafficking in *Drosophila* brain. **a)** Maximum confocal z-projection of a fixed nSyb-Gal4, SNAPTag-CD4 brain stained under non permeabilizing conditions for HA (green), CD4 (red) and nuclear counterstained using Hoechst 33342 (at a concentration of 10 µg/ul, equivalent to 16µM) Scale for this image is 50 µm. **b)** 63x single confocal plane of cells expressing $SNAP_f$-CD4 under the nSyb-Gal4 driver line as shown in panel **(a)**. Scale for this image is 10 µm **c)** Maximum confocal z-projection of either nSyb-Gal4 or SNAP-CD4 brain which does not express the SNAP-CD4 protein. Scale is the same as panel **(a)**.

Figure A3-7

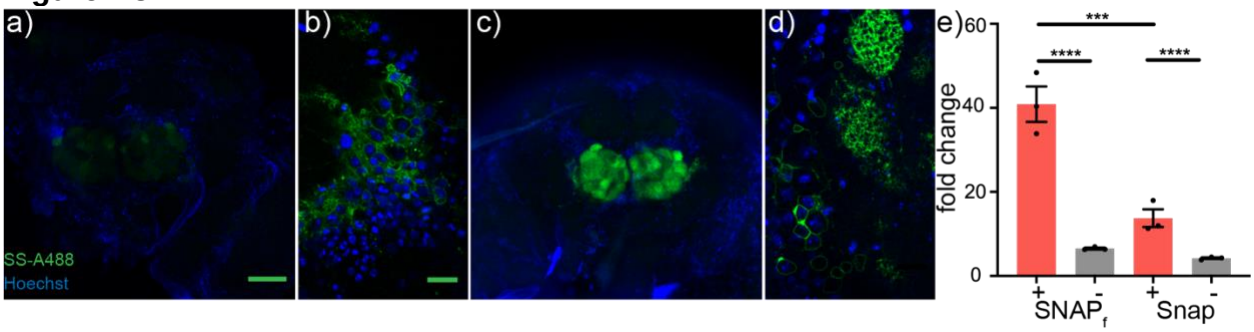

Figure A3-7. Live brain dye loading in *Drosophila*. Confocal maximum z-projection of live brain SS-A488 (1 µM) dye loading in GH146-Gal4 driven **a)** SNAP-CD4 or **c)** SNAP$_f$-CD4 expressing *Drosophila* nervous tissue. Scale bar is 50 µm. High magnification single confocal plane of **b)** SNAP-CD4 or **d)** SNAP$_f$-CD4 expressing olfactory projection neurons treated with SS-A488 (1 µM). Scale is 10 µm. c) Plot of relative fluorescence intensity of antennal lobe region expressing SNAP-CD4 vs. antennal lobe regions expressing SNAP$_f$-CD4. Nontransfected regions were selected as large non-antennal lobe regions of protocerebrum. Data are mean ± SEM for n = 3 individually loaded brains. Data points represent the relative fluorescence intensity of the antennal lobe region or protocerebral region. (One way ANOVA with Tukey's multiple comparisons test, p<0.0001, **** and p=0.0002, ***).

Figure A3-8.

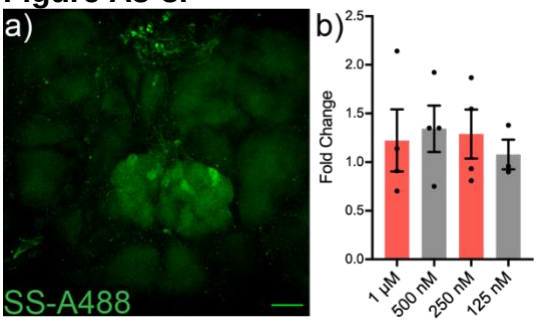

Figure A3-8. Live brain voltage-sensitive dye loading in *Drosophila*. Confocal maximum z-projection of live brain mSNAP2 (100 nM) dye loading in GH146-Gal4 driven **a)** SNAP-CD4 expressing *Drosophila* brains. Scale is 50 µm. **b)** Plot of relative fluorescence intensity of antennal lobe region expressing SNAP$_f$-CD4 vs. non-expressing regions. Non-expressing regions were selected as large non-antennal lobe regions of protocerebrum. Data are mean ± SEM for n = 3 individually loaded brains. Data points represent the relative fluorescence intensity of the antennal lobe region or protocerebral region. (One way ANOVA with Tukey's multiple comparisons test, p= 0.9132)

Figure A3-9.

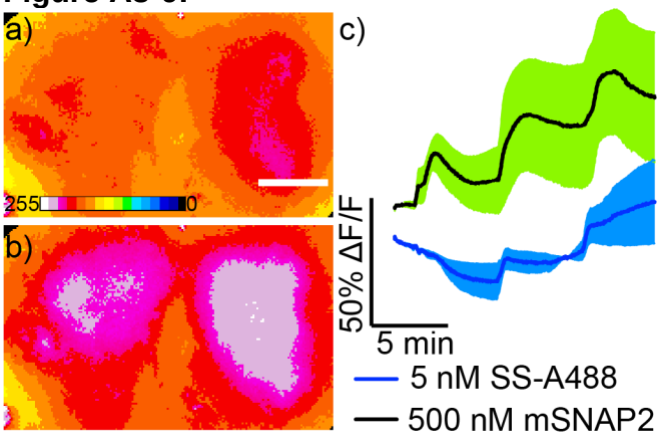

Figure A3-9. mSNAP2 voltage reporting in live *Drosophila* brain tissue Epifluorescence images of explant *Drosophila* brain expressing $SNAP_f$-CD4 in olfactory projection neurons (GH146-GAL4 /CyO>$SNAP_f$-CD4::) **a)** immediately before and **b)** at peak fluorescence response to the carbachol stimulation. Scale bar is 50 µm. Image is pseudo-colored, and the color scale bar indicates 8-bit pixel grey values. **c)** Plot of mSNAP2 (Green, n=3, 500 nM) or SS-A488(blue, n=3, 5 nM) fluorescence (ΔF/F) vs. time for individual fly brains in response to three 100 µM carbachol stimulations. Data are mean ± SEM. Black bars represent the addition of carbachol.

Figure A3-10.

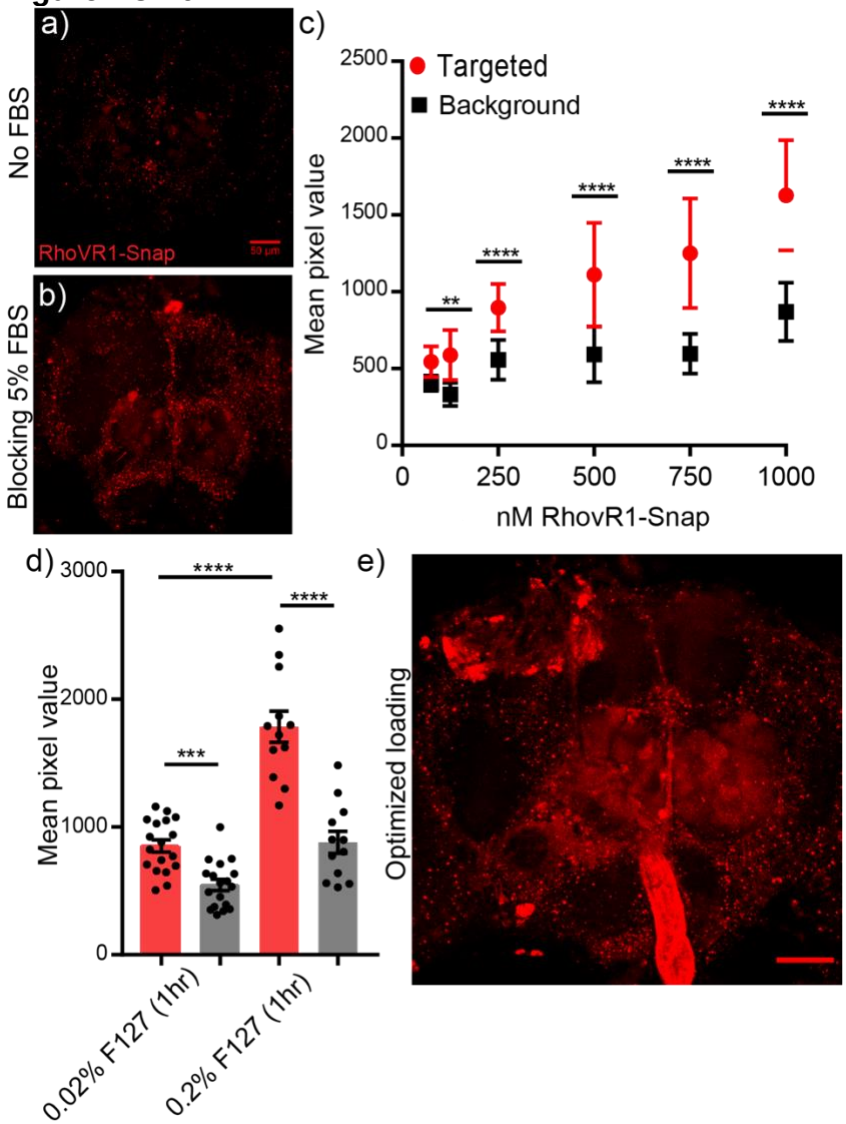

Figure A3-10. Live brain dye loading and optimization of RhoVR1-SNAP in SNAP-CD4 expressing brains. Maximum confocal z-projection of GH146-Gal4, SNAP-CD4 live brains loaded in the **a)** absence or **b)** presence of a 5% FBS pretreatment with RhoVR1-SNAP (100nM). Scale is 50 µm. **c)** Mean pixel values of antennal lobe regions expressing SNAP-CD4 (red) and non-antennal lobe regions (black) across various concentrations of RhoVR1-SNAP. All comparisons are found to be significant with the largest difference at 750 nM (one-way ANOVA, Sidak's multiple comparisons test. $p<0.0001$ across all but the first comparison at $p=0.0039$.) **d)** Plot of mean fluorescence intensity values across targeted (red) and non-targeted (grey) regions of neuropil loaded with 750 nM RhoVR1-SNAP in the presence of 0.02% Pluronic acid F127 or 0.2% Pluronic acid F127(One-way ANOVA with Tukey's multiple comparisons test, $p=0.0001$ for 0.02% and $p<0.0001$ for

0.2%, when comparing the two targeted regions p<0.0001). **e)** Maximum confocal z-projection of fully optimized loading protocol with RhoVR1-SNAP. Scale is 50 µm.

References

1. Bando, Y., Grimm, C., Cornejo, V. H. & Yuste, R. Genetic voltage indicators. *BMC Biol.* **17**, 1–12 (2019).
2. Kohout, S. C. *et al.* Electrochemical coupling in the voltage-dependent phosphatase Ci-VSP. *Nat. Chem. Biol.* (2010). doi:10.1038/nchembio.349
3. Kralj, J. M., Hochbaum, D. R., Douglass, A. D. & Cohen, A. E. Electrical Spiking in Escherichia coli Probed with a Fluorescent Voltage-Indicating Protein. *Science (80-.).* **333**, 345 LP – 348 (2011).
4. Kang, B. E. & Baker, B. J. Pado, a fluorescent protein with proton channel activity can optically monitor membrane potential, intracellular pH, and map gap junctions. *Sci. Rep.* (2016). doi:10.1038/srep23865
5. Abdelfattah, A. S. *et al.* Bright and photostable chemigenetic indicators for extended in vivo voltage imaging. *Science* **365**, 699–704 (2019).
6. Abdelfattah, A. S. *et al.* A general approach to engineer positive-going {eFRET} voltage indicators. *bioRxiv* **14**, 690925 (2019).
7. Kulkarni, R. U. & Miller, E. W. Voltage Imaging: Pitfalls and Potential. *Biochemistry* **56**, 5171–5177 (2017).
8. Miller, E. W. *et al.* Optically monitoring voltage in neurons by photoinduced electron transfer through molecular wires. *Proc. Natl. Acad. Sci. U. S. A.* **109**, 2114–2119 (2012).
9. Huang, Y. L., Walker, A. S. & Miller, E. W. A Photostable Silicon Rhodamine Platform for Optical Voltage Sensing. *J. Am. Chem. Soc.* **137**, 10767–10776 (2015).
10. Grenier, V., Walker, A. S. & Miller, E. W. A Small-Molecule Photoactivatable Optical Sensor of Transmembrane Potential. *J. Am. Chem. Soc.* **137**, (2015).
11. Deal, P. E., Kulkarni, R. U., Al-Abdullatif, S. H. & Miller, E. W. Isomerically Pure Tetramethylrhodamine Voltage Reporters. *J. Am. Chem. Soc.* **138**, (2016).
12. Kulkarni, R. U. *et al.* Voltage-sensitive rhodol with enhanced two-photon brightness. *Proc. Natl. Acad. Sci.* **114**, 2813–2818 (2017).
13. Gonzalez, M. A. *et al.* Voltage Imaging with a NIR-Absorbing Phosphine Oxide Rhodamine Voltage Reporter. *J. Am. Chem. Soc.* **143**, 2304–2314 (2021).
14. Tian, L. *et al.* Selective esterase-ester pair for targeting small molecules with cellular specificity. *Proc. Natl. Acad. Sci.* **109**, 4756–4761 (2012).
15. Liu, P., Grenier, V., Hong, W., Muller, V. R. & Miller, E. W. Fluorogenic Targeting of {Voltage-Sensitive} Dyes to Neurons. *J. Am. Chem. Soc.* jacs.7b07047 (2017).
16. Grenier, V., Liu, P., Miller, E. W. & Daws, B. R. Spying on Neuronal Membrane Potential with Genetically Targetable Voltage Indicators. *J. Am. Chem. Soc.* (2019).
17. Deal, P. E. *et al.* Covalently Tethered Rhodamine Voltage Reporters for High Speed Functional Imaging in Brain Tissue. *J. Am. Chem. Soc.* **142**, 614–622 (2020).
18. Kirk, M. J. *et al.* Voltage imaging in Drosophila using a hybrid chemical-genetic rhodamine voltage reporter. (2021).

19. Keppler, A. *et al.* Labeling of fusion proteins of O6-alkylguanine-DNA alkyltransferase with small molecules in vivo and in vitro. *Methods* **32**, 437–444 (2004).
20. Kohl, J. *et al.* Ultrafast tissue staining with chemical tags. *Proc. Natl. Acad. Sci.* **111**, E3805–E3814 (2014).
21. Sutcliffe, B. *et al.* Second-generation Drosophila chemical tags: Sensitivity, versatility, and speed. *Genetics* **205**, 1399–1408 (2017).
22. Meissner, G. W. *et al.* Optimization of fluorophores for chemical tagging and immunohistochemistry of Drosophila neurons. *PLoS One* **13**, e0200759 (2018).
23. Feinberg, E. H. *et al.* {GFP} Reconstitution Across Synaptic Partners ({GRASP}) Defines Cell Contacts and Synapses in Living Nervous Systems. *Neuron* **57**, 353–363 (2008).
24. Gordon, M. D. & Scott, K. NIH Public Access. **61**, 373–384 (2010).
25. Wang, J. W., Wong, A. M., Flores, J., Vosshall, L. B. & Axel, R. Two-photon calcium imaging reveals an odor-evoked map of activity in the fly brain. *Cell* **112**, 271–282 (2003).